RECYCLABLE THERMOSETS POLYMER MATERIALS BASED ON DYNAMIC COVALENT LINKAGE FOR VARIOUS APPLICATIONS

Thesis submitted in partial fulfillment
for the award of the degree

Doctor of Philosophy

by

SUMAN DEBNATH

BASIC SCIENCES & HUMANITIES

RAJIV GANDHI INSTITUTE OF PETROLEUM TECHNOLOGY

JAIS, – 229304

PC16003 2020

CERTIFICATE

It is certified that the work contained in the thesis titled " **Recyclable Thermosets Polymer Materials Based on Dynamic Covalent Linkage for Various Applications** " by "**Suman Debnath**" has been carried out under my supervision and this work has not been submitted elsewhere for a degree.
It is further certified that the student has fulfilled all the requirements of Comprehensive, Candidacy and SOTA.

_____

(Supervisor)
Dr. Umaprasana Ojha

DECLARATION BY THE CANDIDATE

I, "**Suman Debnath**", certify that the work embodied in this thesis is my own bonafide work and carried out by me under the supervision of "**Dr. Umaprasana Ojha**" from "January 2017" to "October 2020", at the "Basic Sciences & Humanities", Rajiv Gandhi Institute of Petroleum Technology, Jais. The matter embodied in this thesis has not been submitted for the award of any other degree. I declare that I have faithfully acknowledged and given credits to the research workers wherever their works have been cited in my work in this thesis. I further declare that I have not willfully copied any other's work, paragraphs, text, data, results, etc., reported in journals, books, magazines, reports dissertations, theses, etc., or available at websites and have not included them in this thesis and have not cited as my own work.

Date:
Place:

_____

Suman Debnath
Roll No. PC16003

CERTIFICATE BY THE SUPERVISOR(S)

It is certified that the above statement made by the student is correct to the best of my knowledge.

_____

(Supervisor)
Dr. Umaprasana Ojha

_____

Head of Department

CERTIFICATE

CERTIFIED that the work contained in the thesis titled "**Recyclable Thermosets Polymer Materials Based on Dynamic Covalent Linkage for Various Applications**" by **Mr. Suman Debnath** has been carried out under my supervision. It is also certified that he fulfilled the mandatory requirement of TWO quality publications arose out of his thesis work.

It is further certified that the two publications (copies enclosed) of the aforesaid Mr. Suman Debnath have been published in the Journals indexed by –

(a) SCI
(b) SCI Extended
(c) SCOPUS

_____	_____	_____
(Supervisor)	(Head of Department)	(Convener, DPGC)
Dr. Umaprasana Ojha	Dr. Amritanshu Shukla	Dr. Atul Sharma

COPYRIGHT TRANSFER CERTIFICATE

Title of the thesis: Recyclable Thermosets Polymer Materials Based on Dynamic Covalent Linkage for Various Applications
Name of the student: Suman Debnath

Copyright Transfer

The undersigned hereby assigns to the Rajiv Gandhi Institute of Petroleum Technology, Jais all rights under copyright that may exist in and for the above thesis submitted for the award of the "Doctor of Philosophy".

Date:
Place:

Suman Debnath
Roll No. PC16003

Dedicated to my beloved parents ···

Acknowledgement

This thesis is the result of the research work carried out at Rajiv Gandhi Institute of Petroleum Technology, Jais. During this period, I have been associated with many people, whom I would like to express my gratitude for their support and help.

I am deeply grateful to my thesis supervisor Dr. Umaprasana Ojha, for his encouragement and support at all stages of my early research career. I am, of course, indebted to Prof. Ojha for providing me an exciting working environment, many opportunities to develop new ideas, and liberty in research, discussion and expression. I would also like to thank my Research Progress Evaluation Committee (RPEC) members, Dr. A. Aijaz and Dr. M. S. Balathanigaimani for evaluating my work and providing valuable suggestions at all levels of my research work. I sincerely thank Department of Basic Sciences and Humanities, RGIPT, Jais for providing me facilities for carrying out the research work during this course of time.

My acknowledgment goes to the Human Resource Development Group, Council of Scientific and Industrial Research Government of India, for providing me fellowship (CSIR-SRF) to carry out Ph.D. program at RGIPT. I would also like to acknowledge the Bhabha Atomic Research Centre (BARC), Mumbai, India for Junior Research Fellowship 2016-18. I also owe thanks to my senior lab mate Dr. Rewati Raman Ujjwal, who helped me during my research work and understanding the critical concepts and operating various instruments. I also want thank to my fellow lab mates Niharika, Subhankar, Chandan and Arpan for their help and support through various ways in my Ph.D. journey and to make it an unforgettable one.

I would like to thank various institutes in India such as IIT BHU, IIT Kanpur, IIT Guwahati, IISC Bangalore, CBMR Lucknow, CSIR IIP. These institutes allowed me to perform the research work and use their central facilities.

I also would like to extend my acknowledgment to many people from scientific community who helped me about sample charecterization and direct communications at various international conferences. I especially thank Dr. Nagavatla Viswanadham and Dr. Rajaram Bal from the CSIR-Indian Institute of Petroleum.

I want to thank all my friends, Basab, Ramesh, Sayan, Nanigopal, Santanu, Palash,

Chandan, Santu, Monan, Mithun, Sidhu, Anup, Bijoy, Ravishankar, Bijoy Purahit, Vartika, Harsh, Arijit, and my seniors Amitda, Tarunda, Soumenda, Anilda, Soumendra Sir, Belal Sir, Parveen Sir, Milanda, Saurabh Sir, Reena Mam, Tripti Mam, Shyma Mam and my jounoirs Shadab, Gargi, Abhishek, Surja,Suvodeep for making such a stressful journey smooth and memorable one. I have missed few names also but I think all of them whom I have interacted, developed a friendship during my RGIPT days. I would like to thank two special persons in my life Bisumama and Tarashankar Babu throughout my journey.

Most of all, I would like to thank my parents and Sejokaa, Sejokaki, Taradidi, Sukdebda, Biswajitda, Boudi, Bara kaka, Bara kaki, Lakhi, Jhuma, Praddep, Natun kaka, Natun kaki, Santu, Sontu, Additya, Choto kaka, Choto kaki, Preetam, Dada, Boudi, Piru, without their moral support, these few years would have been tough. Especially, my wife Monimala who remain supportive during this period. My parents are my constant source of power and their faith in has propelled me cross all the hurdles swiftly. They deserve all the credits for each success of mine.

Contents

List of Tables

List of Figures

List of Schemes

List of Abbreviations

NMR	Nuclear Magnetic Resonance
TMS	Tetramethylsilane
PMA	Poly(methyl acrylate)
PAH	Polyacryloyl Hydrazide
FT-IR	Fourier Transform-Infrared
DSC	Differential Scanning Calorimetry
Tg	Glass Transition Temperature
GPC	Gel Permeation Chromatography
THF	Tetrahydrofuran
DMSO	Dimethyl sulfoxide
TBAB	Tetra-n-butyl Ammonium Bromide
UTS	Ultimate tensile strength
UTM	Universal Tensile Machine
UV-vis	Ultraviolet-Visible
AFM	Atomic Force Microscopy

Preface

The first chapter summarizes the importance of dynamic covalent networks in current scenario, because the main environmental concern arises with plastic commodities. Covalently cross-linked dynamic polymeric networks showed recyclability, sustainability, mechanical strength, reprocessability and thermal stability. Thus, the main objective of my thesis work is to synthesize recyclable, degradable and reprocessable thermosets based on dynamic covalent linkages with high strength, self-healability, shape memorable and solvent reprocessable properties. Here, I have elaborated the different properties of dynamic covalent networks. I have discussed about the characterization techniques for the evaluation of mechanical properties such as ultimate tensile strength, tensile stress, elongation at break, Young's modulus, frequency sweep, temperature sweep, and stress-relaxation etc. I also have discussed about the different dynamic covalent chemistries such as sulfur related chemistry, Diels-Alder chemistry, transestrification chemistry, imine chemistry, olefin metathesis, transamidation chemistry, transalkylation, silyl ether chemistry, thiol-michael chemisry, boronate ester and thiol-michael chemisry etc.

The second chapter discusses the dynamics of Michael addition reaction between -$CONHNH_2$ moieties of a polymeric network and α,α,-biscarboxylic ester substituted double bonds. Cross-linked networks by using Hydrazide-Michael addition as the simple key reaction is investigated. The model compound study revealed that both the formation of adduct and exchange of donors in the adduct occur readily via a dynamic covalent exchange reaction at room temperature under catalyst-free and ambient conditions. The dynamic covalent polymer networks based on the above hydrazide Michael addition reaction possess Young's modulus value up to $\sim$23.8 MPa and $\sim$2.5 GPa, respectively. The material exhibits stress relaxation behavior in the temperature range of 30-55 °C. This network is thermally stable upto 170 °C and this moderate stability is attributed to the heat-sensitive β -keto ester linkage present in the samples. It also showcase solvent resistance properties. These Michael adduct linkages are spontaneously exchangeable under ambient conditions. At room temperature the material is easily self-healable and recyclable without sacrificing the mechanical properties. Depolymerization of the network is done by using hydrazine. This dynamic Michael addition chemistry is easy to carry out , and applicable both in homogeneous and heterogeneous conditions.

In third chapter, Vitrimers based on polyester linkage is studied for reprocessable and self-healable dynamic covalent networks. Vitrimers are a class of plastics, which are de-

rived from thermosetting polymers (thermosets) and can change their topology by thermally activated bond-exchange reactions. We have synthesized a catalyst free vitrimer based on β-activated ester linkage which is reprocessable and self-heallable at 150 °C. The major ingredients of the system are polyhydroxyethyl methacrylate (a hydroxyl group precursor) and diethyl malonate (an ester precursor), that is cost effective and could be extracted from the bio-source (different fruit juices). These vitrimers show ultimate tensile stress (11.3-33.0 MPa), storage modulus (1112-317 MPa), and elongation (80- 290%) in acceptable range. The networks display vitrimer behavior and exhibited stress relaxation ability in the temperature range of 130 to 170 °C. The relaxation temperature decreases to 110 °C in presence of $Sn(Oct)_2$. The properties of the vitrimers based on catalyst are also similar to that of the catalyst free vitrimers. The materials can be effectively self-healed and reprocessed in the presence of heat without sacrificing the tensile properties. In presence of $Sn(Oct)_2$ catalyst the vitrimers can reprocessed at 100 °C.

In fourth chapter, we have discussed about the synthesis of the covalent adaptable networks by utilizing the trans-esterification of α-substituted β, β'-diesters with multi-hydroxy compounds under moderate temperature conditions (110-140 °C). This material are easily processable, recyclable, and degradable to monomer. The synthesized networks show ultimate tensile strength (UTS) and elongation at break values up to $\sim$1.1MPa and $\sim$595%, respectively. The material show thermal stability up to 215 °C and also exhibited the stablility under acidic as well as basic medium. The dynamic cross-linked networks are reprocessable at 140 °C temperature in n-nutyl Alcohol within 15 h via competitive trans-esterification with the solvent. The films are reformed on evaporation of the solvent followed by curing at 140 °C. After reprocessed, the material have tensile strength and Young's modulus value up to $\sim$1.0 MPa and $\sim$1.81 MPa respectively. Hydrogels and organogels based on dynamic covalent linkages are an important class of materials in material science. The ester based covalent adapted network can selectively absorbed toluene from various organic solvents. This covalent network swell $\sim$750 wt% within 90 min. This important property could be utilized in industry to efficiently separate aromatics from various azeotropic mixtures involving toluene, methanol and water.

Similarly, the last chapter discusses about the dynamic β-carbonyl carboxylate linkage based Polyurethane networks (PUN). We have incorporated the dynamic carboxylate linkage in the main chain of polytetramethylene oxide (PTMO) based segmented PUNs to prepare the dynamic polyurethane networks. In polyurethane network we have used PTMO as the soft segment and combination of pentaerythrotol (PETL) and methyl diphenyl diisocyanate (MDI) as the hard segment. PETL units will also assist in crosslinking of the PU chains. The synthesized Polyurethanes show ultimate tensile strength (UTS) in the range of $\sim$ 8 to 33MPa, elongation at break in the range of $\sim$345-680% and Young's modulus $\sim$19-270

MPa). The samples display typical vitrimer behavior and stress relaxed in the temperature range of 140 to 180 °C. The material reprocessed at 150 °C. The UTS and E' values of the reprocessed samples in the range of 70-80% and 71-88% respectively of the original samples supporting the reprocessability efficiency. This material have excellent creep resistance ability at high stress (20 MPa) and high temperature (140 °C). The materials can be self-healed and re-weld in presence of heat without sacrificing the tensile properties at 150 °C. These materials show stability and swelling properties under different solvents. This PUNs exhibit triple shape memory abilities at inflection temperatures of 60 and 130 °C respectively. Overall, these PUNs with versatile properties are potential candidates for a range of applications.

Overall this dynamic linkage strategy may be extended to develop some other applications like development of coatings, hydrogels, biomaterials, adhesives, controlled release, energy storage, biomedical, sensing and commodity plastics in the future.

Chapter 1

Introduction and Literature Survey

1.1 Background

The synthesis of polymer networks with high performance and recyclability by a simplistic method is a great challenge. The growing concern over global growth of plastic debris has inspired the development of recyclable and degradable plastics having dynamic or labile linkages. Thermosets and elastomers have excellent thermal, chemical, solvent resistance, and mechanical properties but it is very difficult to recycle or reprocess these materials due to its permanent and rigid molecular structure. Throughout the globe, several researchers are working on transformation of the permanent network to dynamic cross-linked networks. Dynamic covalent bonds, reversible covalent bonds, intermolecular interactions play the vital role for the synthesis of dynamic cross-linked networks.[1, 2] Dynamic covalent bond may break and reform by autonomously or in presence of stimuli. This bond breaking and reforming nature has been used in many areas such as material science, organic synthesis, biomedical etc.[3] Rearrangement of reversible covalent bonds occur by external stimuli such as temperature,[4, 5], pH,[6, 7] light,[8, 9] and solvents.[10, 11] Basically, dynamic covalent networks can flow and change their permanent shape.[12] Dynamic polymer materials have some useful properties like self-healing, [13] reprocessing/ recycling, [14, 15] malleability, [16] shape-memory, [17, 18] adaptability,[19]responsiveness,[20, 21]degradability[22] and stress relaxation etc.[23, 24]. Dynamic covalent bonds are formed based on simple or-

ganic click reactions. Recently polymer chemists are focusing on exchange mechanisms of dynamic covalent bonds. There are two types of exchange mechanisms in dynamic covalent networks. The two mechanisms are associative and dissociative mechanisms.[25, 26]In dissociative mechanism, the broken chemical bonds are formed in another place. In dissociate covalent adaptable networks, the networks losses it's integrity but in associative mechanism the cross linked density remains fixed. In case of associative mechanism, exchange happens in polymer chains if a new covalent bond at another position has been formed only if original cross-link is broken. Reversible Diels-Alder reactions are the example of dissociative exchange reactions in covalent adaptable networks. The examples of associative exchange reactions in covalent adaptable networks are the epoxy/acid or epoxy/anhydride polyester based networks as introduced by Leibler and co-workers in 2011. The properties of polyester based networks has been first observed in organic polymer materials and authors introduced the name "Vitrimer". Vitrimers are the thermally malleable materials, swelled but remain unchanged in solvents.[27, 28] Efforts have been made for the synthesis of dynamic materials based on reversible linkages or reactions such as ester linkage,[29] Diels-Alder adducts,[30, 31]imines,[32] hemiaminals,[33] epoxy,[34] Michael adducts,[35] hyrdrazones,[36] disulfide linkages,[37] carbonates, [38] boronate esters,[39] poly urethanes,[40] silyl-ethers,[41] boroxine exchange,[42] siloxanes,[43] transcarbamoylation,[44] urea,[45] transalkylation, [46] diselenide olefin metathesis,[47] thiol-disulfide,[48, 49]vinylogousurethanes,[50] transaminations[51] oximes[52] etc. Here we have studied the properties of the dynamic covalent adaptable networks and also different dynamic covalent linkages and reactions.

1.2 Properties of Dynamic Covalent Adaptable Networks

Here, we have discussed several properties of dynamic covalent adaptable networks, e.g. self-healing, reprocessability, shape memory, responsiveness and stress relaxation.

1.2.1 Self-healing Property of Dynamic Covalent Networks

Now a days self-healing property is very important in material science because it can rebuilt physical damages by avoiding catastrophic failure which increase the working life.[53] The self-healing materials increase the functional lifetimes of the materials, reduce the total cost and improve the reliability. Extrinsic and intrinsic are the two types of self-healing material based on healing mechanism.[54]In extrinsic healing process (e.g. Microcapsules and microvascular networks) the healing agents are released from capsules.[55]

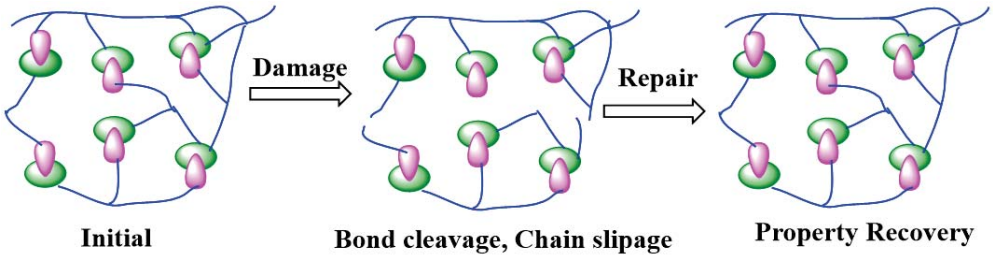

Figure 1.1: Self-healing property of dynamic covalent networks.

The main thing in case of the intrinsic healing process is the dynamic or reversible nature of the material with fabrication behaviour . In this case it repeatedly heals the same position of damage.[56] Now a days intrinsic self-healing materials have scientific interest because of its enhanced reliability and ability to get heal multiple times.[57] The main applications of the intrinsic self-healing materials have been found in thermoplastic elastomers,[58] thermo reversible rubbers,[59] mechanically enhanced hydrogels,[60] electrically conductive materials,[61, 62] electronic skin,[63] organic transistors [64, 65] etc. Not only the experimental but also the theoretical studies have been reported in recent times based on self-healing thermosetting polymers.[66] Self-healing elastomers are very important due to its potential applications. It is used in wearable electronic skin,[67] protective coatings,[68] reversible adhesions,[69] 3D/4D printing, self-healing conductors etc.[70] Mechanical damage in elastomers can be repaired by self-healing process (Fig. 1.1). Self-healing property can be repair the scratch of coating and protect it from the environmental exposure. Viscosity transition mechanism is the important factor for the 3D/4D printing of self-healing elastomer. Self-healing conductors have been made by adding the conducting fillers into self-healing elastomers. Wearable electronic skin and devices are the most important application of self-healing materials. Self-healing functionalized stretchable conductive materials successfully improve the safety reliability and sustainability of electronic devices. Self-healing stretchable material have been used as strain sensing devices and that's why it is used in electronic sensors,[71] electronic skin, human-machine interactions,[72] and supercapacitors.[73]

1.2.2 Reprocessability/ Recyclability or Reversibility Property of Dynamic Covalent Networks

In recent times, the reprocessability or recyclability of dynamic covalent adaptable networks are very important in environmental or economic respective. Hydrogen bonding, ion-metal interactions, supramolecular interactions and reversible covalent bonding are the main player behind the reversible nature of the materials. The reversibly formed covalent bond show high

stability and high mechanical strength in polymeric system. Reversibly formed cross-linked materials containing covalent bonds are known as covalent adaptable networks (CAN). Reversibly formed covalent bonds are knows as dynamic covalent bonds.[74]

Figure 1.2: Reprocessable property of dynamic covalent networks.

1.2.3 Shape memory Property

Shape plays an important role in various applications in polymer science. Shape memory polymers have very important role in scientific and technological applications. It is a smart responsive material. Basically in shape memory polymers, the material is fixed in a permanent shape by programming and can recover its original shape by external stimuli.[75]

Figure 1.3: Shape memory performance of dynamic covalent networks.

The dynamic covalent linkages in shape memory polymers are able to rearrange the topology due to bond exchange in permanent shape reconfigurable in its solid state. The external stimuli such as heat,[76] light,[77] moisture,[78] pH,[79] electricity,[80] or magnetic field,[81] have been used in the study of shape memory effect. One way characterization is not able to recover their original shape under cooling. That's why the reversible bidirectional shape memory effect on heating and cooling is highly desirable.[82] People have reported some experimental strategies based on reversible shape memory effect such as persistent external mechanical forces,[83, 84] chemically heterogeneous structure, a broad

melting transition,[85] and change in crystal structure[86] etc. In one way, triple or multiple shape memory effect, multiple transition points are able to memorize the multiple shapes.[87, 88] Thermoplastic polyurethane show reversible bidirectional shape memory effect. Many dynamic covalent adaptable networks have been used for the shape memory polymers such as reversible TAD Chemistry,[89] transesterification,[90] Diels-Alder reaction,[91] and transcarbamoylation etc.[92] The shape memory effect has very important application in many fields such as soft robotics[93] medical devices,[94] advanced manufacturing,[95] and aerospace structures[96] etc.

1.2.4 Responsiveness Property

In material science the research in fundamental chemistry of the molecular systems which can adapt and reorganize in response to external stimuli is very important thing. We have observed the photo switchable dynamic behavior in molecular machines.[97, 98] Azobenzene, [99] Spiro (thio)-pyran,[100, 101] diarylethene [102, 103] are responsible for photo switches. These photo switches are incorporated in polymeric materials for reversible coloration, [104, 105] repeatable volume contraction/expansion [106, 107] and liquid-gel transitions. [108, 109]

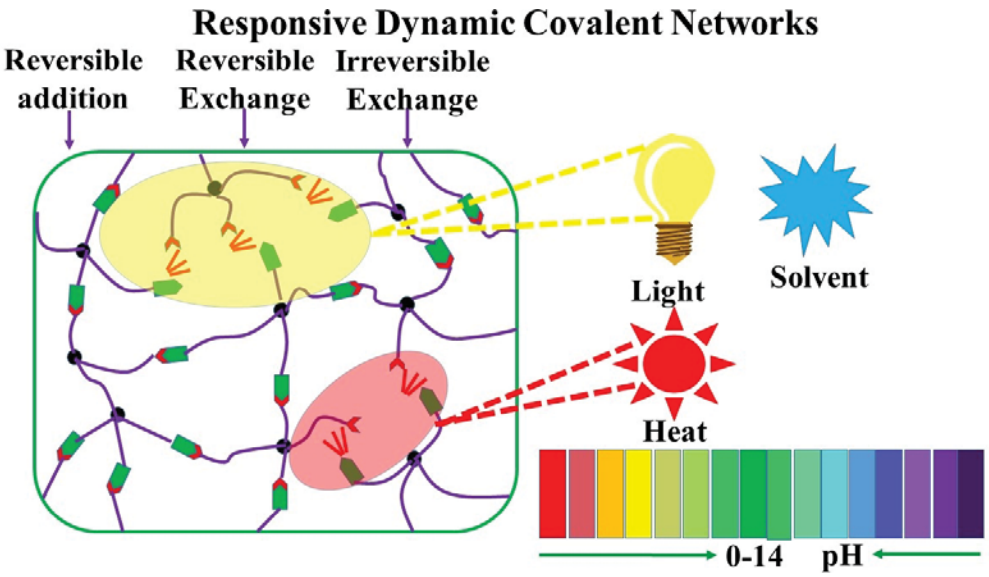

Figure 1.4: Responsive property of dynamic covalent networks.

1.2.5 Stress-relaxation Property

Several methods are available to characterize the dynamic cross-linking network. Temperature dependent stress relaxation experiment is one of them. The capability to relax stress is a unique property of dynamic covalent networks, through the bond exchange in the networks. Stress relaxation seems to be faster at higher temperatures.[110]

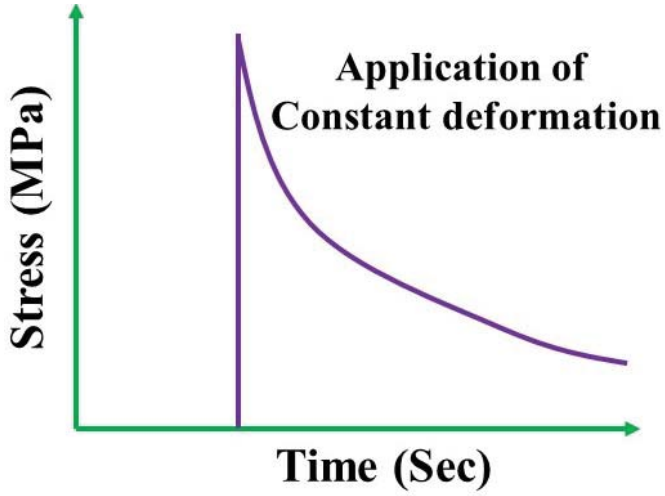

Figure 1.5: Stress relaxation behavior of dynamic covalent networks.

Stress-relaxation property of dynamic networks can be described by the following Maxwell equation (1.1)

$$E = E_0 e^{-t/\tau} \tag{1.1}$$

Where E is the stress relaxation modulus, t is the relaxation time. The relaxation time have determined at E/E_0 = 1/e. The dynamic covalent adaptable network will relax to zero faster than the traditional thermosets. Associative exchange process is the controlling factor in determining the relaxation time. The Arrhenius equation (1.2)

$$\tau(T) = \tau_0 e^{E_{a,r}/RT} \tag{1.2}$$

has been used for the determination of temperature dependence of the relaxation time where $\tau(T)$ = Relaxation time at temperature T, $E_{a,r}$ = Relaxation Activation energy, R = Gas Constant, τ_0 = Constant.

1.3 Characterization of Mechanical Properties

Tensile experiment is the most widely used method for the determination of mechanical properties of a material. We can determine the ultimate tensile stress, tensile strength, elongation at brake, Young's modulus of the materials from the tensile experiment. Materials can be easily processed into suitable shape for the tensile experiments. The recovery of mechanical properties can be measured by the tensile experiments. We can evaluate the self-healing property by resilience. The resilience result can also be obtained from the tensile experiment. We can obtain some mechanical data from Dynamic Mechanical Analyzer (DMA). We can analyze frequency sweep, temperature sweep, stress-relaxation data from DMA. We can obtain the storage modulus, loss modulus, and tanδ data from the DMA. Atomic Force Microscopy (AFM) can be used for the determination of hardness and modulus. Recovery of mechanical property of elastomer coating in self-healing process is very important hurdles in time (Sec) stress (MPa) application of constant deformation in material science. AFM can solve this problem. Zuilhof et al. have developed the method for the determination of macroscopic mechanical properties of original, damaged and repairing coating during self-healing process.[111]

1.4 Dynamic Covalent Chemistry

In dynamic covalent chemistry, the dynamic linkages play an important role. Dynamic covalent bonds in linear polymers have been used for the synthesis of dynamic covalent networks. Here, I have discussed some dynamic covalent networks based on dynamic chemistries.

1.4.1 Sulfur Related Chemistry

Sulfur chemistry has an important role in polymer science from the invention of rubber vulcanization. Disulfide bond is used to recycle the rubber. That's why it has importance in industry and society. Tobolsky et al. have reported the stress-relaxation behavior of polysulfide linkage. They have observed the rapid interchange in presence of catalyst. Oxidation and reduction reactions take place in this system. In reduction, dissociation of disulfide bond into thiols and oxidation can reverse back to the disulfide. These oxidation reduction processes have been utilized in reversible crosslinking nature of hydrogels[112] and epoxy resins.[113]

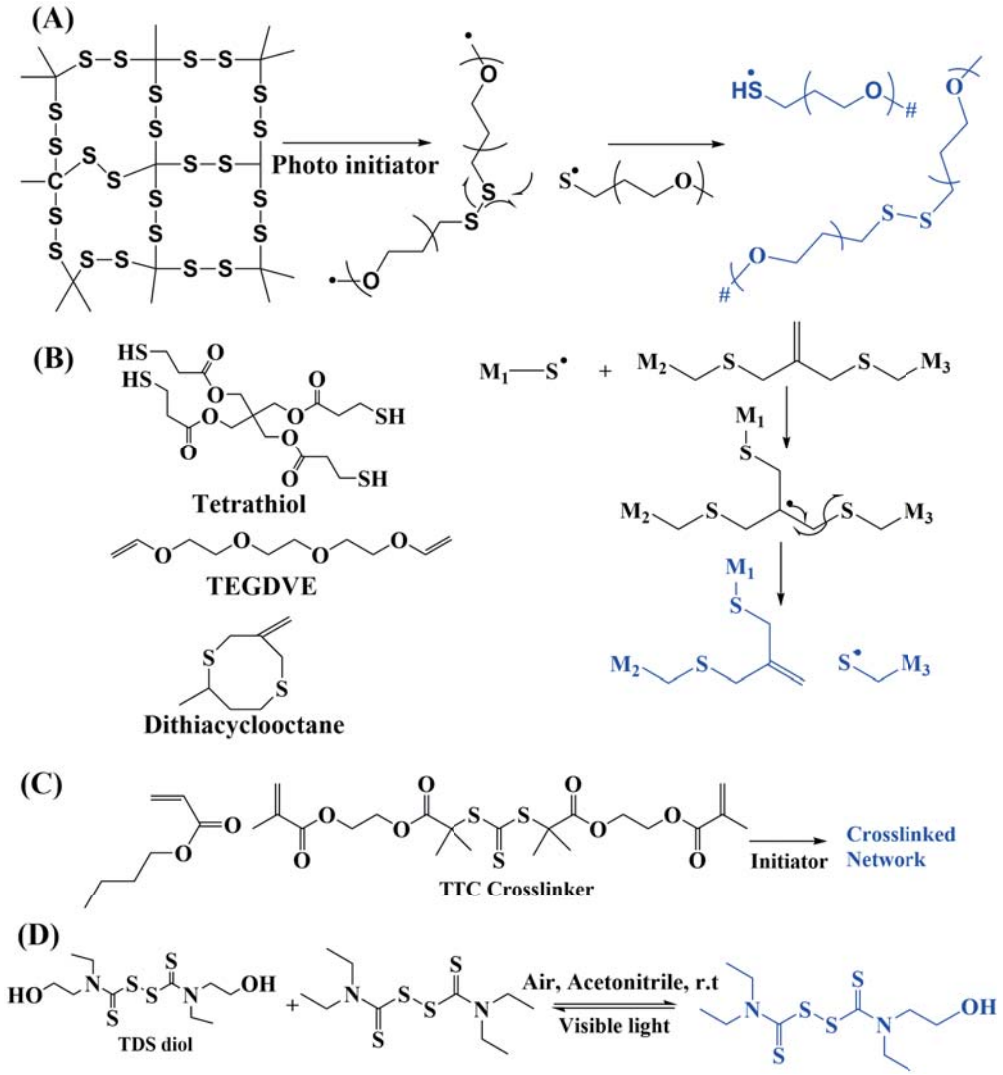

Figure 1.6: (A) disulfide exchange in dynamic polydisulfide hydrogel, (B) thiol-ene chemistry and exchange of allyl sulfide derived from dithiacyclooctane used for the synthesis of Allyl sulfide based network, (C) TTC based, (D) TDS based dynamic network synthesis.

Disulfide based polymer networks show self-healing and reprocessable behavior in presence of external stimuli such as heat, light, catalyst, external radicals etc. Norvez and coworkers have reported the thermally activated reprocessing of natural rubber with disulfide linkages.[114] The degradable property of disulfide based crosslinked epoxy resin has introduced by Takahashi and Otuska.[115] Rowan's group introduced the photo healable polydisulfide network.[116]Room temperature self-healing property of thiol-disulfide linkages have been introduced by Matyjaszewski's group.[117] Photodegradability of disulfide containing polyethylene glycol is introduced by Anseth and Bowman's group.[118] Allyl- sulfide based addition-fragmentation process is very important due to its application in stimuli-

responsive materials.[119] Matyjaszewski's group have reported UV-induced self-healing material based on trithiocarbonate as the RAFT agent for chain shuffling.[120] They also have studied thiuram disulfide (TDS) bond exchange reaction under visible light. This TDS cross-linked polyurethane showed self-healing behavior under table lamp in air.

1.4.2 Diels-Alder Chemistry

Diels-Alder chemistry, proposed by Diels and Alder is very important in dynamic covalent adaptable networks.[121] Electron-rich diene (e.g.furan) and an electron-deficient dienophile (e.g. maleimide) produces cyclohexene in [4 + 2] cycloaddition reaction and this product can reverse back via retro-Diels-Alder in presence of temperature.

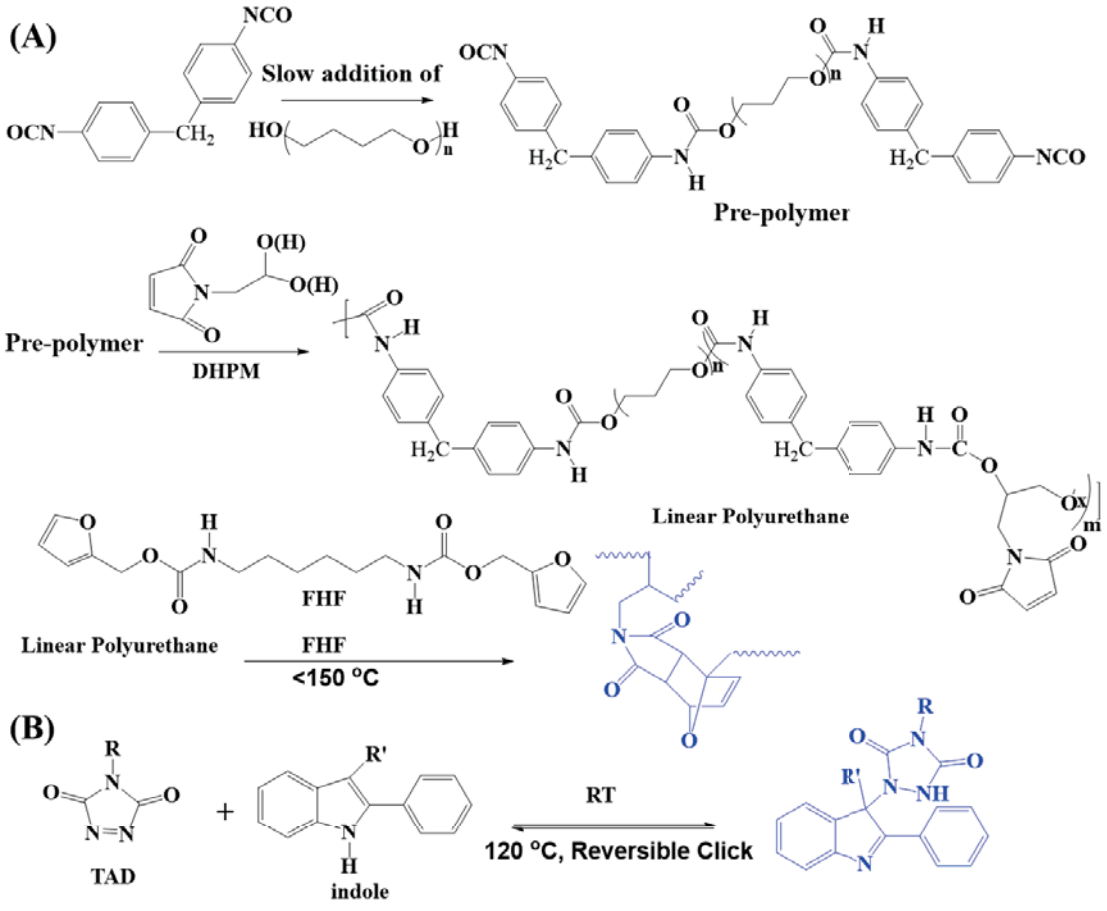

Figure 1.7: Diels-Alder chemistry. (A) polyurethane based dynamic reversible Diels-Alder reaction, (B) TAD-indole based dynamic Diels-Alder reaction.

Crosslinking of polystyrene in pendant furan maleimide group is introduced by Stevens

and Jenkins in 1979.[122] Recyclability of pendant cyclopentadiene crosslinked polyisobutylene is discovered by Kennedy and Castner.[123] Scientists have worked on thermo reversible crosslinking based on DA chemistry between polymer chains, like polyphosphazenes, [124] polyoxazoline hydrogels,[125] polyacylate elastomers,[126] etc. Recently research based on DA chemistry has also expanded to polyurethanes[127], epoxy resins,[128, 129], polyamides,[130] polyketones,[131] ethylene/ propylene/ diene rubb-ers,[132] poly(lactic acid),[133] polycaprolactone[134] etc. Stiffness of dielectric elastomers introduced the fast quenching of a DA networks was discovered by Pei et al.[135] The DA reaction between furan and maleimide has shown reversibility efficiently. 1,2,4-triazoline-3,5-dione (TAD) molecule is introduced as an alternative dienophile in DA reaction by Winne and Du Prez.[136]

1.4.3 Transesterification Chemistry

Transesterification reaction is very important in dynamic covalent adaptable networks. Polyester has been used in various material applications such as transport, construction, packaging, apparel, piping, adhesive, electronic devices, marine, biomedical and aerospace etc.[137, 138] Ester linkages are important due to the biodegradable nature. Recently people have worked on a number of vitrimers based on ester linkages.[139, 140] $Zn(OAc)_2$, $Sn(Oct)_2$, $Ti(OPr)_4$, $Zn(acac)_2$, or an organic base, i.e., DBU and TBD were used as the transesterification catalyst.[141, 142] In 2011 Leibler et al. have worked on recycling and reprocessing of thermosets by taking the transesterificaion reaction as the bond exchange reaction. The hydroxyl groups are essential for the transesterfication reaction. The epoxy material show reprocessability by heat. Hilmyer and coworkers have worked on vitrimers concept to polyesters. Tao Xie and coworkers have showed thermal plasticity nature of polyesters. Generally, transesterification reaction occurs in presence of catalyst or at high temperature but the boronic ester based trans-esterification occurs under mild reaction conditions. Low temperature stress relaxation (35-55 °C) and wide range of tunability of boronic esters are introduced by Guan et al. Recently we have reported thermally reprocessable and self-healable β-activated ester groups.[143] The malonic ester, the starting material of polyester is extracted from the various fruit juices. Poly (hydroxyethyl methacrylate) is used as the hydroxyl starting material. The material has high mechanical strength, Young's modulus, storage modulus. We have synthesized polyester based covalent adaptable network by the α-substituted β, β'-diesters and multi-hydroxy compounds at moderate temperature (110-140 °C). This covalent network has some good properties such as thermally stable, stable in acidic, basic and organic solvents. We have depolymerized the network in alcoholic solvent and reformed the network after evaporating the solvent. The covalent network selectively absorbs toluene from the other organic solvents. This material swells $\sim$750 wt% in toluene within 60 min and thus

it can be used for the separation of aromatics from azeotropic mixture. [144]

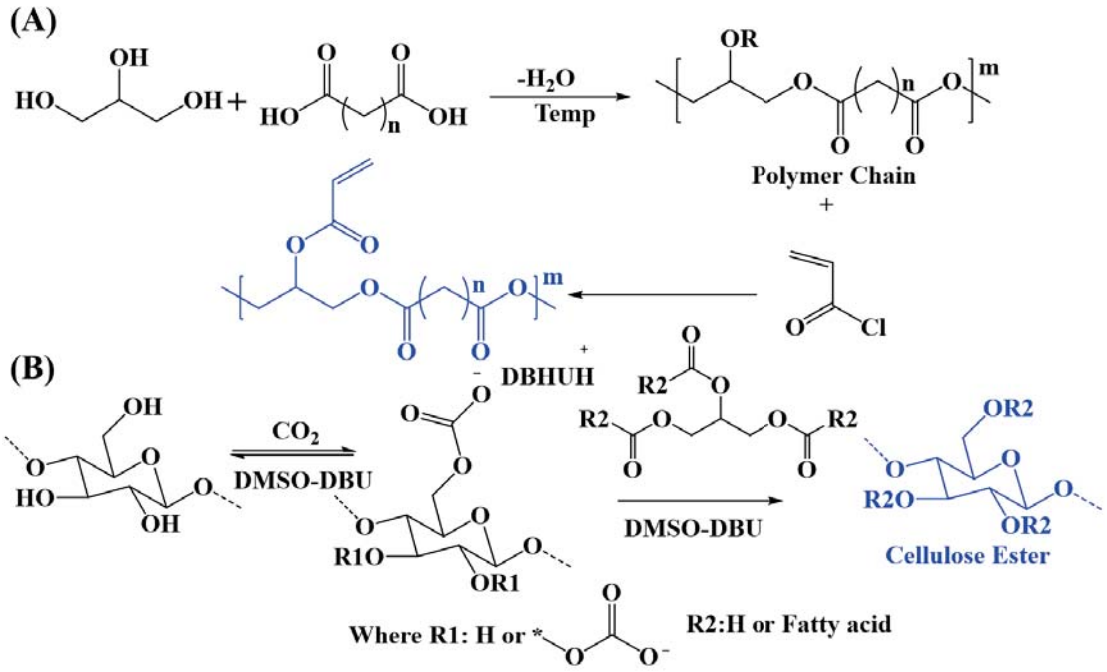

Figure 1.8: (A) Acrylate functionalized polyester based network, (B) fatty acid cellulose ester based network.

1.4.4 Imine Chemistry

Imine chemistry is very important for the synthesis of dynamic covalent adaptable networks. It covers lot of reversible reactions. Carbonyls and amines react to form the imine type (e.g. imine, hydrazones) compound in mild conditions without catalyst and have showed reversible behavior. Deng and Chen have developed the acylhydrazone based crosslinked polymer gel.[145] They have synthesized acylhydrazone crosslinked based polyethylene glycol. This network has self-healable and degradable properties. Zhang and coworkers have reported the thermoset malleability of transamination.[146] Basically C=N bond plays a vital role for imine exchange reaction. This group also have introduced imine based dynamic covalent polymeric networks. Basically they have used condensation polymerization reaction of poly(ethylene glycol) bis(3-aminopropyl) with 1,3,5-triformylbenzene with an equal molar ratio of aldehyde and amine functionalities. The reaction has carried out under organic solvents in different polarity.[147] Jethava's group have synthesized sustainable nitrogen heterocycles by using dynamic imine chemistry.

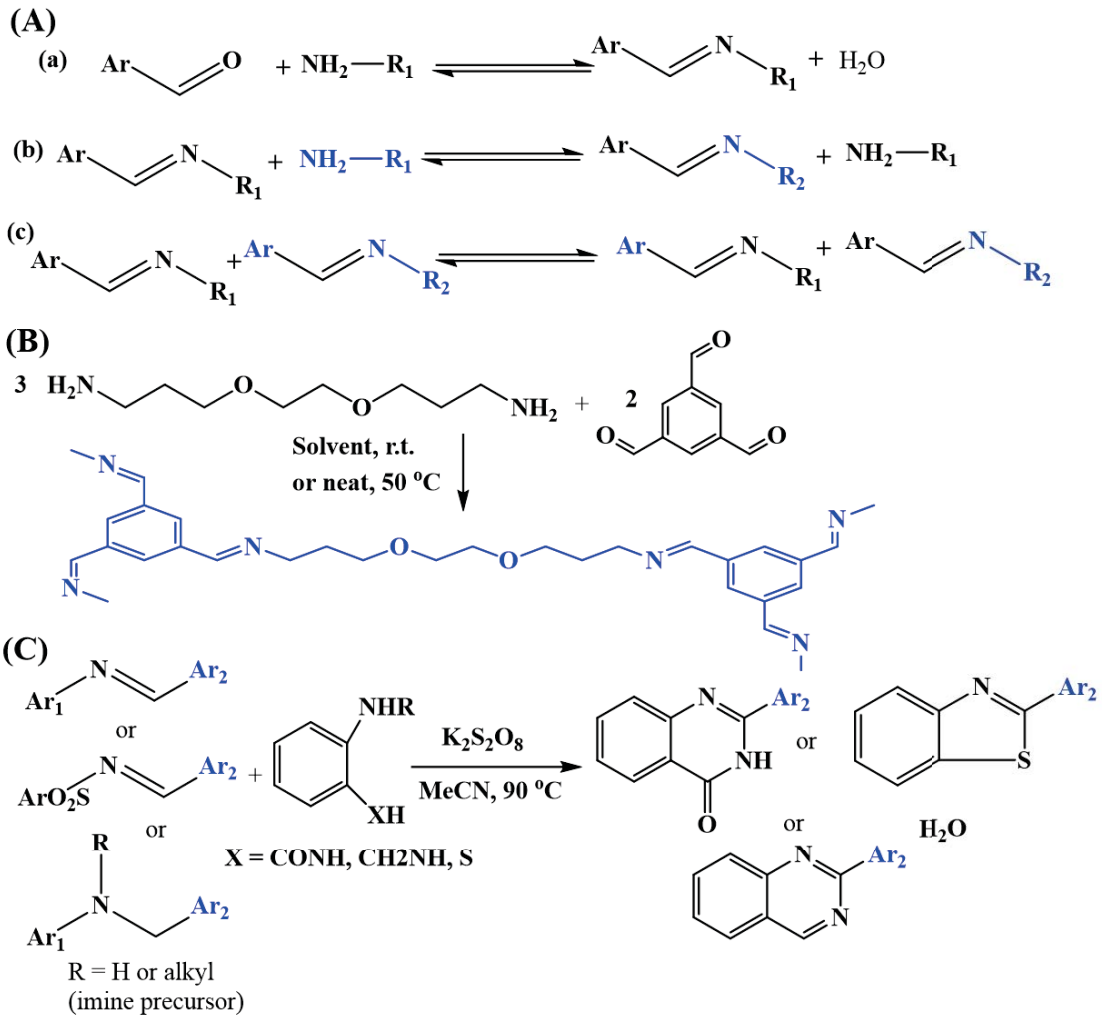

Figure 1.9: (A) (a) Imine formation equilibrium through hemi-aminal, (b) transamination through aminal formation, (c) imine metathesis. (B) imine based dynamic covalent polymeric networks from aldehyde and amine. (C) transimination of imines and its applications.

This nitrogen heterocycle is synthesized via transimination followed by intramolecular cyclisation.[148]

1.4.5 Olefin Metathesis

Olefin metathesis plays an important role for the synthesis of dynamic networks. Unparalleled nature of carbon-carbon bond is used to bring dynamic nature in polymer science. Guan's group have worked on the olefin metathesis.[149] They have achieved the malleabil-

ity of crosslinked polybutadiene in presence of Grubb's catalyst. This network show stress relaxation behavior. The network having carbon-carbon double bonds and amides show self-healing behavior with enhanced mechanical properties.[150] They also reported the dynamic self-healable networks based on olefin metathesis. They have created dynamic energy dissipative hydrogen bonds in covalently crosslinked polymer networks through secondary amide side chains. Leibler, and Guan have worked based on olefin metathesis based dynamic covalent networks. They have developed cross-linked polymer networks through Grubbs' second-generation Ru metathesis catalyst. In this work they showed the room temperature malleable property of chemically cross-linked polybutadiene network.

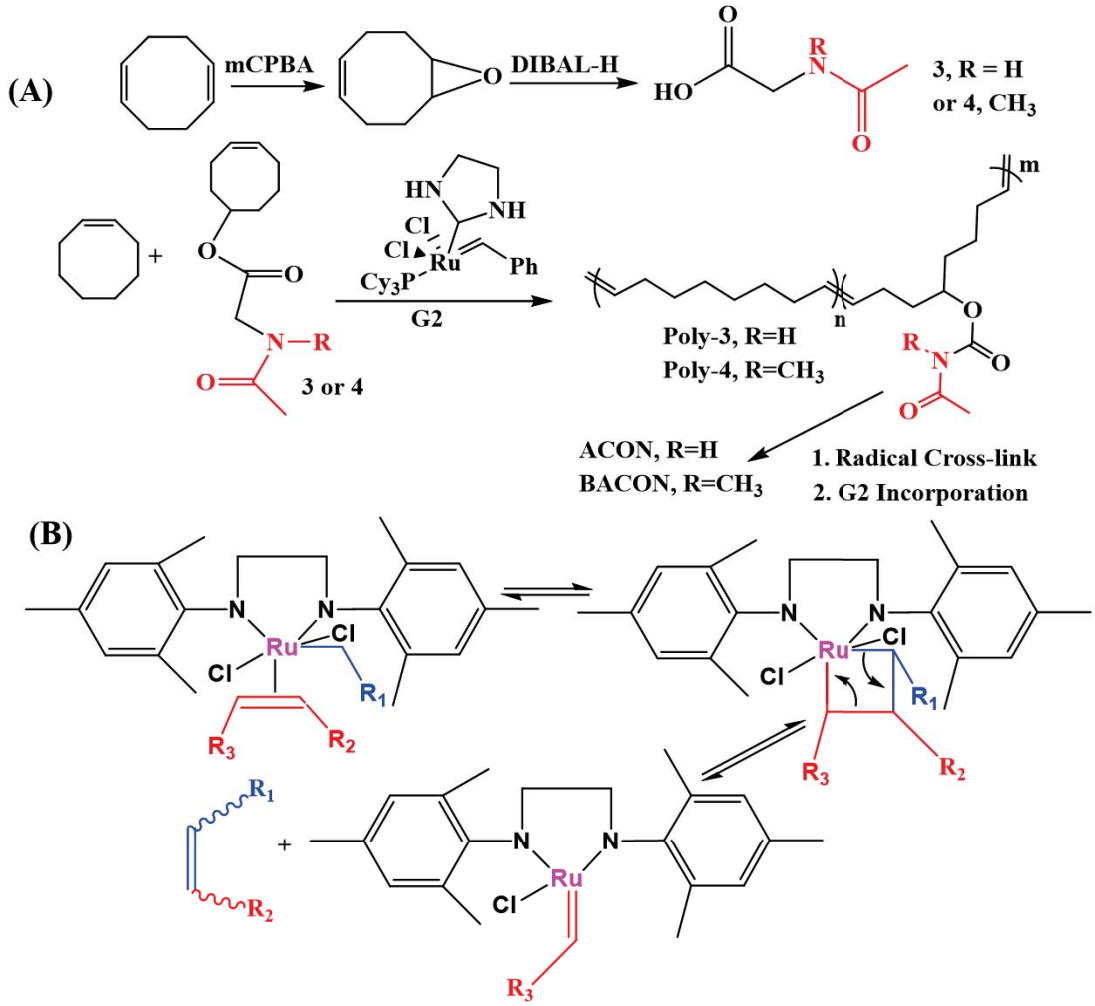

Figure 1.10: (A) Olefin containing dynamic polymeric networks based on cyclooctene derivatives (B) malleable covalently dynamic polymeric network through Ru-catalyzed olefin metathesis.

1.4.6 Transamidation Chemistry

Transamidation is very important for the synthesis of dynamic covalent adaptable networks. Du Prez's group recently have studied on transamidation as an alternative to transesterification. Shi's group have worked on transamidation reaction based malleable crosslinked networks. They have used acetoacetyl chemistry for the synthesis of dynamic covalent linkages of amides. They have described the dynamic transamidation reaction through proton switch mechanism.[151]

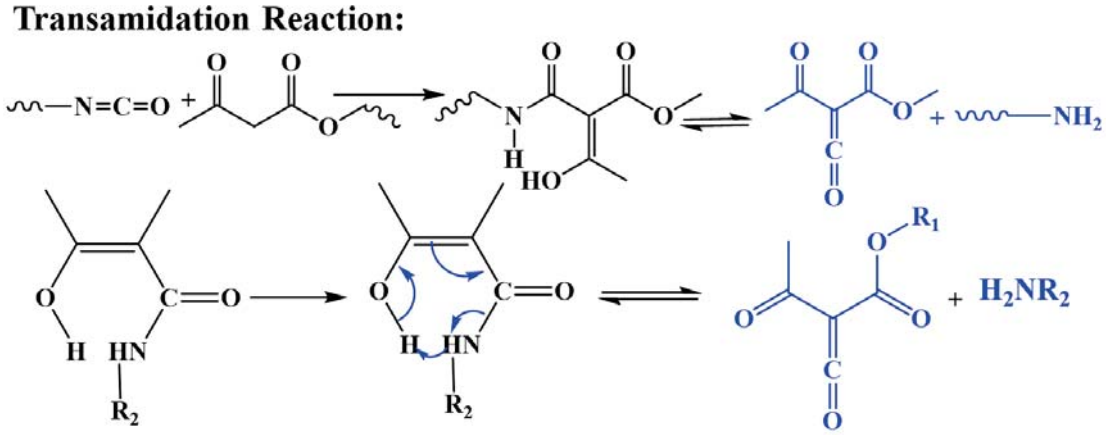

Figure 1.11: Transamidation reaction through proton switch mechanism.

1.4.7 Transalkylation

Drockenmuller and co-workers first have discovered the ion conducting vitrimers based on poly (1, 2, 3-triazolium ionic liquid)s via azide-alkyne cycloaddition.[152] The mechanism lie in the transalkylation between 1,2,3-triazoliums and alkyl halides. This ion conducting material is used for the solid electrolyte. Du Prez and Winne's group have synthesized vitrimers based on transalkylation chemistry. They also have prepared poly(thioester) network through thiol-ene polymerization. They have prepared catalyst free vitrimer materials through partial alkylation of thioesters to trialkylsulfonium salts. They have reformed the trialkylsulfonium salts via transalkylation reaction in the presence of heat.[153] Zhang and Guo's group have developed recycling loop of sulfur-cured rubber through transalkylation exchange chemistry. They have introduced the simple way to recycle sulfur-cured rubber by using transalkylation exchange reaction of C-S bonds. They have showed the cross-linked rubber network rearrangement and reprocessing ability of the material.[154]

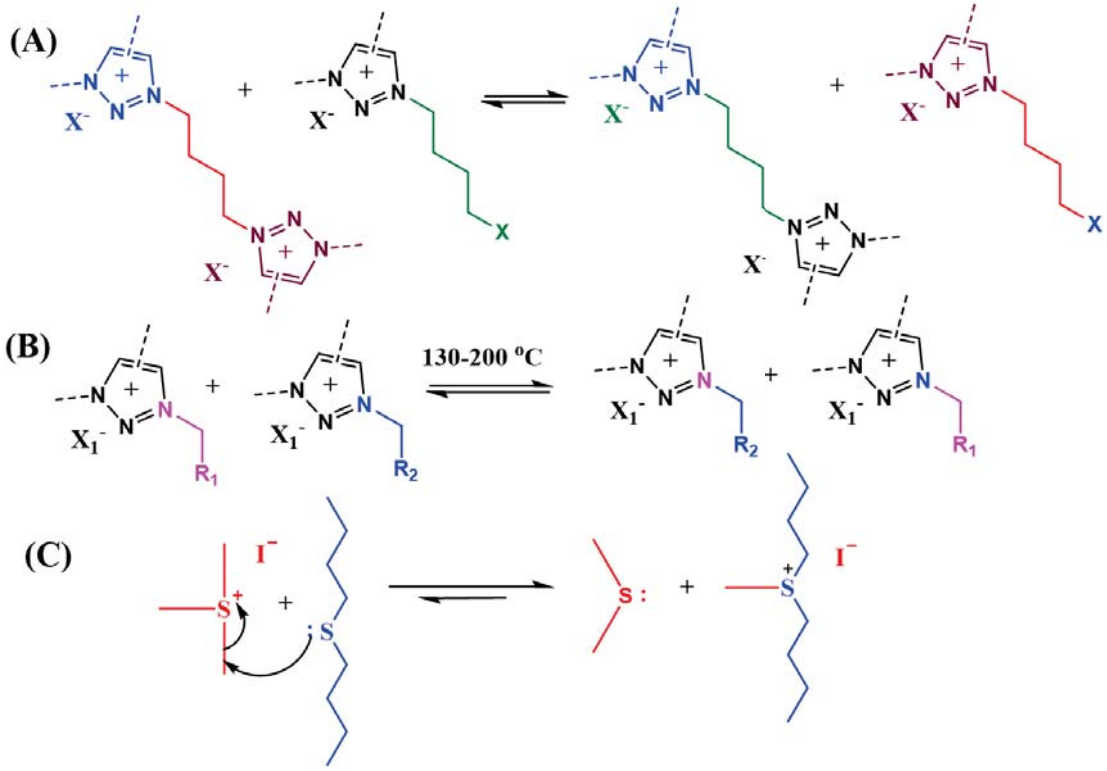

Figure 1.12: (A) Temperature-induced transalkylation exchanges of C-N bonds between 1,2,3- triazolium cross-links and halide-functionalized dangling chains (B) transalkylation of sulfonium salt, (C) TMSI and butyl sulfide based C-S transalkylation reaction.

1.4.8 Silyl Ether Chemistry

Silyl ether, a thermally stable dynamic covalent linkages have been used for the synthesis of dynamic covalent networks in presence of hydroxyl groups.[155] Guozheng Liang and Aijuan Gu have worked on silyl ether based thermally resistant shape memorable crosslinked dynamic covalent linkages. This network is applicable for selffolding and self-deployable smart 3D structures.[156] They have used the epoxy resin, ethanolamine, 4,4′- diaminodiphenylmethane and 3-isocyanatopropyl trimethoxysilane for the synthesis of silyl ether based dynamic network. Zhibin Guan and coworkers have introduced the silyl ether linkage for the synthesis of dynamic covalent adaptable network.[157] This network show malleability, reprocessability and stress relaxation behavior. This material show the chemical and thermal stability. This is the first reported silyl ether based vitrimers. They have prepared the crosslinked network by bis-alkoxysilane and pendant hydroxyl groups functionalized styrene monomer units. Guan's group have reported direct silyl ether metathesis for vitrimer synthesis. They first have silylated poly(ethylene-covinyl alcohol) (PEOH) with trimethylsilyl

(TMS) groups and then cross-linked the material with a bis-silyl ether cross-linker.[158]

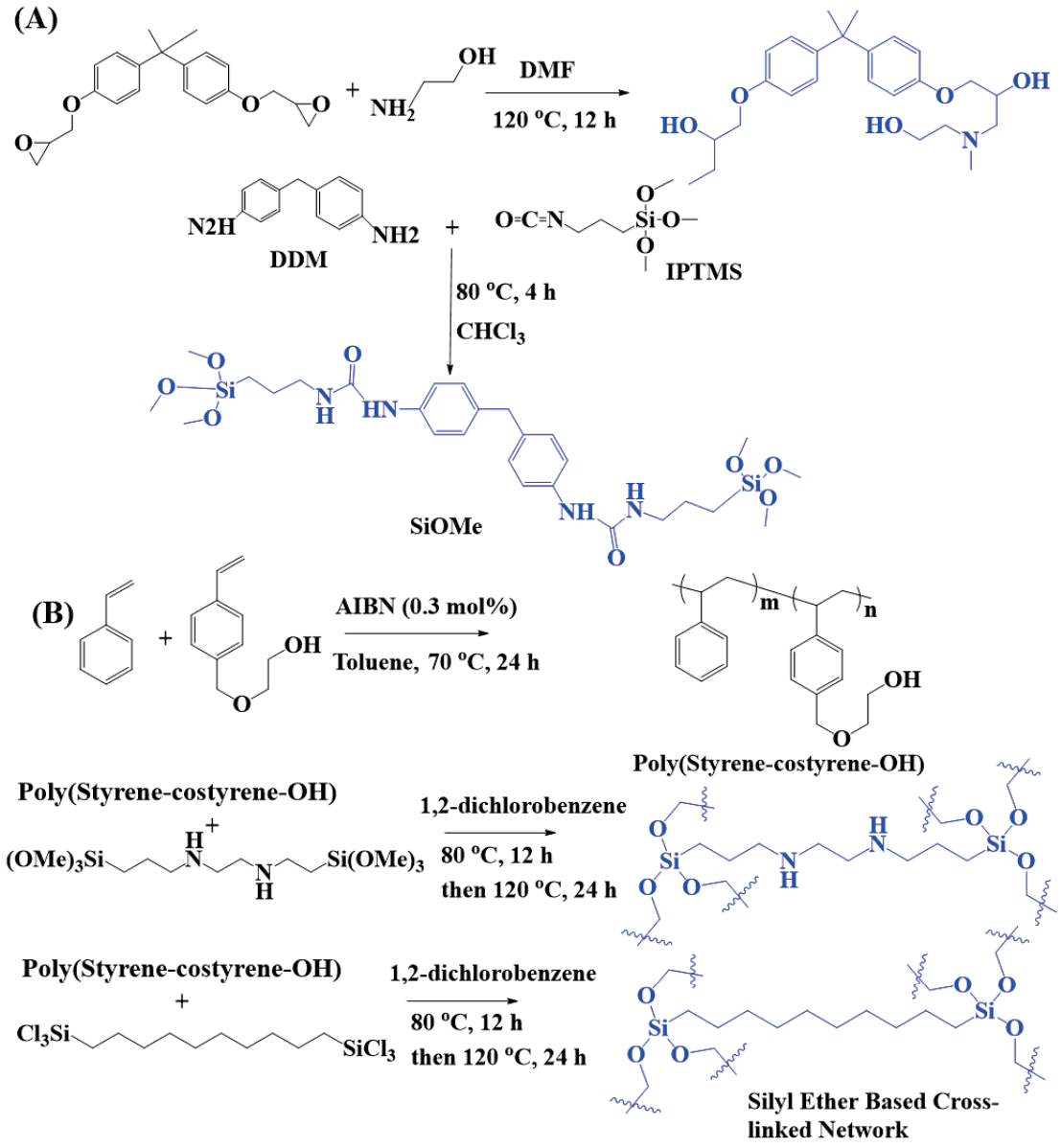

Figure 1.13: (A) Silyl Ether based dynamic covalent polymeric networks, (B) silyl ether based robust and thermally stable dynamic covalent network from poly(styrene-costryrene-OH).

1.4.9 Thiol-Michael Chemisry

Thiol-Michael chemistry is very important for the synthesis of dynamic covalent adaptable network. Thiol-Michael adducts show dynamic behavior at elevated temperature or at elevated pH. Dominik Konkolewicza's group have reported the dual stimuli responsive malleable and self-healing materials based on Thiol-Michael linkages.[159] This linkage show self-healing, malleability and thermally responsive behavior. This material show room temperature creep resistance and creep recovery as mechanical stability. These stimuli responsive self-healing, elastic, malleable, mechanically stable networks, may utilize in coating, elastomers as potential applications. Kevin M. Miller's group has introduced crosslinked Polyester networks attached with thermoreversible Thiol-Michael bond.[160] Thermoreversible Thiol-Michael based crosslinked polyester network have prepared by base-catalyzed Michael addition polymerization.

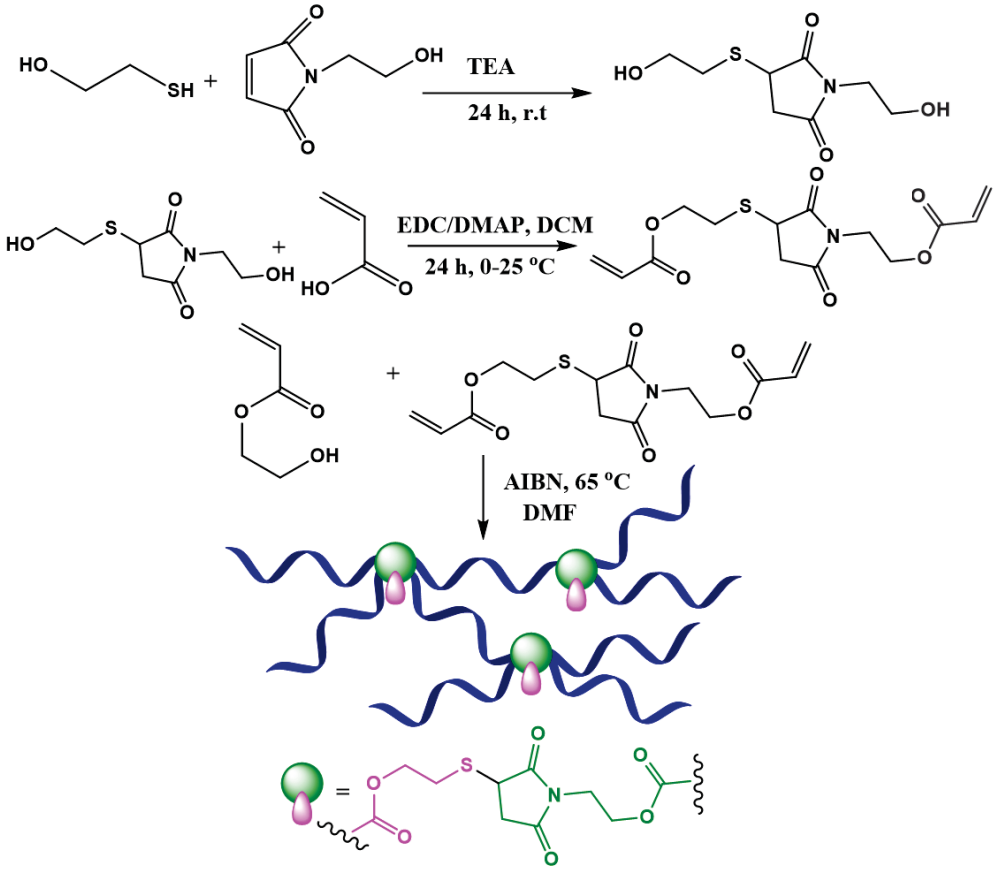

Figure 1.14: Thiol-maleimide crosslinker (TMMDA) based dynamic thiol-michael networks.

1.4.10 Boronate Ester Network

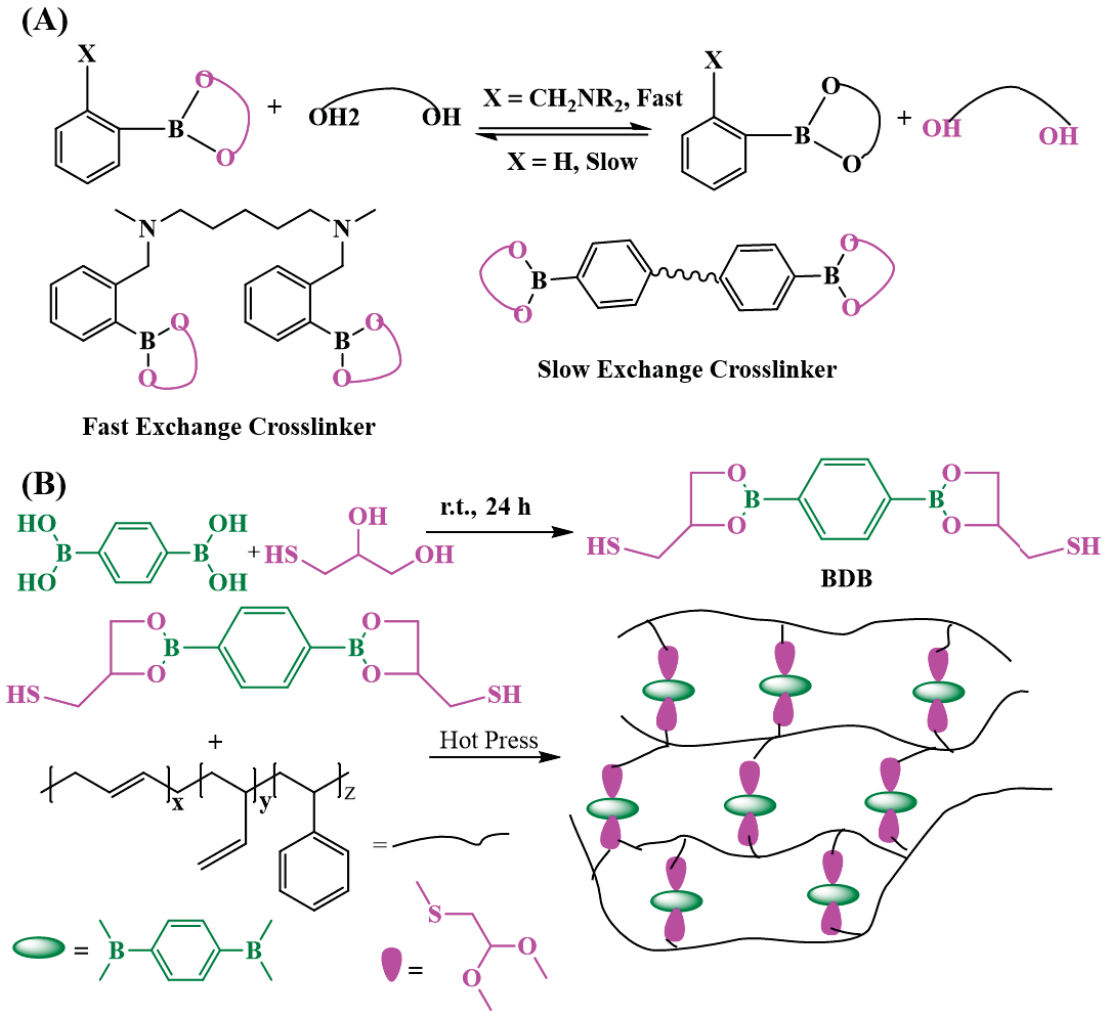

Figure 1.15: (A) Exchange kinetics of boronic ester and diboronic ester crosslinker, (B) dithiolcontaining boronic ester cross-linker and styrene-butadiene rubber based boronate ester network.

Boronate Ester network is very useful for the synthesis of dynamic covalent adaptable networks. Tao Chen and his coworkers have introduced the simple synthesis procedure PAAm/PVA-borate hydrogel system which has borate ester bond to realize shape memory behavior.[161]Yoshie's group has synthesized the boronate ester by catechol functionalized polymers and p-phenyldiboronic acid (PDBA). This material showe self-healing abilities, stability, and transparency under seawater.[162] Auzely-Velty's group have reported self-healing hydrogels based on boronate ester linkages.They have prepared boronate ester linkage from Benzoxaborin derivatives and saccharides.[163] Guan's group also have reported

tunable dynamic covalent boronic ester linkage, which show self-healing and malleable properties.[164] Guo's group also have reported boronic ester based covalently crosslinked elastomers with self-healing and malleable properties. Dithiol-containing boronic ester crosslinker and styrene-butadiene rubber have used for the networks synthesis.[165]

1.5 Summary and Outlook

Polymer network with dynamic covalent linkages are very important in recent academic community. This dynamic covalent network may be useful as an alternative of plastic materials. Development of self-healing and reprocessable material is started from nineteenth century onwards. The dynamic covalent adaptable network is very important with some relevant properties such as malleability, shape memory, adaptability, responsiveness, degradability, and stress relaxation etc. Recently people have developed different dynamic covalent adaptable networks such as sulfur related chemistry, Diels-Alder reaction, transesterification, imine chemistry, olefin Metathesis, transamidation, transalkylation, silyl ether chemistry, thiol-michael chemistry, boronate ester network etc. Scientists are now focusing for the synthesis of dynamic covalent networks based on new organic reactions.

This page was intentionally left blank.

Chapter 2

Self-Healable and Recyclable Dynamic Covalent Networks Based on Room Temperature Exchangeable Hydrazide Michael Adduct Linkages

2.1 Abstract

Covalently cross-linked polymers having characteristics like environmental resistance, recyclability, sustainability, mechanical strength, and thermal stability are very important as we can apply them in various fields. Using Hydrazide-Michael addition as a key reaction, we can form these cross-linked networks. In Michael addition system carbonyl hydrazide is used as a donor and the acceptor we use is α, β-unsaturated double bonds. The formation of adduct and exchange of donors in the adduct both happen quickly under catalyst-free and ambient conditions. Through model compound study we have reached in a conclusion that the reaction is room temperature exchangeable. The dynamic covalent networks based on the above hydrazide michael addition showed Young's modulus value up to $\sim$23.8 MPa and $\sim$2.5 GPa, respectively. In room temperature our material is easily self-healable and recyclable. The depolymerization of the DCNs was done by using NH_2NH_2. This dynamic

Michael addition chemistry is easy to carry, useful both in homogeneous and heterogeneous condition, and room temperature exchangeable may be extended to different application like energy storage, biomedical, sensing etc.

2.2 Introduction

Dynamic covalent networks (DCN) having stimuli-responsive reversible covalent linkages are beneficial due to their significant material properties like healability,[166, 167] stress-relaxation ability,[168] processability,[169] adaptability,[170]and recyclability. [171, 172] Hence, various efforts are currently taken to progress a range of DCNs based on different dynamic covalent motifs.[173, 174]The reversible linkages in these DCNs promptly break and re-form in presence of external stimuli like heat,[175] light,[176] and reagent.[177] These covalent dynamic linkages follow either a dissociative or an associative pathway during bond breaking and reformation. The dissociative pathway follows sequential bond breaking followed by reformation (e.g., oxime-urethane[178] and Diels-Alder adduct[179]), while both the processes occur concurrently in the associative path way, resulting in an exchange reaction (e.g., acyl hydrazone [180] and imine[181]). In the associative pathway, the cross-link density is maintained during the exchange reaction and the exchange rate is influenced by the applied stimulus. The DCNs that undergo exchange reaction at higher temperature are called "vitrimers" [182, 183] and a range of articles centered on this important class of materials having thermo sensitive chemical linkages are available in the literature.[184, 185] Recently, many articles on dynamic covalent linkages such as boronicester,[186]disulfide,[187]and urea-urethane[188] that show dynamic behaviour under moderate temperature conditions are come in the literature.[189] Similarly, materials based on noncovalent linkages such as hydrogen bonding, ionic bonding, and metal on coordination have showed autonomous self-healing characteristic, malleability, and adequate mechanical properties.[190] Therefore, new covalent chemistries capable of ambient condition dynamic behaviour are looked for to develop the field of DCNs.

Aza Michael addition is another useful reaction in this prolonged list of dynamic covalent linkages. Though the forward reaction, i.e., formation of Aza-Michael adduct, is facile and occurs under moderate temperature conditions, the reverse reaction usually requires catalyst and stringent conditions to occur. With amine donors, the retro-Michael addition have occurred in the presence of a specific catalyst and elevated temperature conditions.[191, 192] Likewise, the exchange of donors in aliphatic thiol-based Michael adducts is reagent dependent and progress very slow under ambient conditions.[193, 194] Interestingly, highly activated Michael acceptors based on α, β unsaturated double bonds having two activat-

ing groups (electron-withdrawing groups; e.g., carbonyl and cyano) in the germinal position induced swift reversibility into the corresponding Michael addition reactions.[195, 196] However, the thiol-Michael adduct stayed in dynamic equilibrium with the corresponding precursors under ambient conditions, and the equilibrium depends on the concentration of the reactant species. Similarly, the adduct of 2° amine and highly activated double bond stayed in equilibrium with the reactants under moderate temperature conditions.[197] The facile β-elimination in the above cases was assigned to the greater acidity of the proton, and the reaction continued through the E1 mechanism with the generation of a carbanion intermediate.[198] These observations restricted the possibility of formation of polymers based on the Aza-Michael addition chemistry with activated systems.

The carbonyl hydrazide ($CONHNH_2$) functionality as a Michael donor is already published in the literature.[199, 200] Interestingly, the pKa value of $CONHNH_2$ ($\sim$3-4)[201, 202] is much lower in comparison with the thiols ($\sim$7-11)[203] and amines ($\sim$10-11).[204, 205] Therefore, the conjugate base of $CONHNH_2$, i.e., the leaving group (CONHNH-) in the case of the β-elimination of the corresponding Michael adduct, is weaker in comparison with the thiol (RS-) and amine(R_2N^-). Moreover, the process of α-proton extraction mediated by $CONHNH_2$ as the base is anticipated to be sluggish in comparison with the amines and thiols. This may hinder the rate of β-elimination and enhance the stability of corresponding hydrazide Michael adducts. To examine the above, we have studied the dynamics of Michael addition between $CONHNH_2$ moieties and α, α-biscarboxylic ester substituted double bonds by using suitable model compounds. The possibility of formation of DCNs based on this dynamic covalent linkage was explored, and the self-healing ability along with recyclability has been accessed.

2.3 Experimental Section

2.3.1 Materials

Thiodiglycolic acid (Acros Organics, 98.0%), ethanol (Merck, 99.9%), sulfuric acid (Merck, 98%), ethyl acetate (Merck, $\geq$99.5%), diethyl oxalate (s-dfine chem, 99%), sodium methoxide (NaOMe, s-dfine chem., 98%), benzaldehyde (Qualigens, 98.5%), acetone (s-dfine chem., 99%), methanol (Qualigens, 99.0%), hydrochloric acid (HCl, s-dfine chem., 35-38%), D_2O (Sigma-Aldrich, 99.0%), tetrahydrofuran-d8 (ARMAR Chemicals, 99.5% atom%D), N,N-dimethylformamide (DMF, Merck,$\geq$99.8%), 1-bromobutane (s-dfine chem., 98%), potassium carbonate (Qualigens,98.0%), chloroform ($CHCl_3$, s-dfine chem., 99.5%), sodium chlo-

ride (Qualigens, >99.9%), hydrazine hydrate (s-dfine chem., 99%), diethylmalonate (DEM, s-dfine chem., 98%), terephthalaldehyde (Alfa Aesar, 99%), piperidine (Qualigens, 99.0%), acetic acid (s-dfinechem., 99.5%), lauric acid (Molychem, 99%), 4-hydroxybenzoic acid (Spectrochem, 99%), methyl acrylate (s-dfine chem., >99%), potassium bromate (Merck, >99.0%), sodium hydrogen sulfite (Merck, 58.5-67.4%), sodium chloride (Qualigens, >99.9%), tetra-n-butyl ammonium bromide (TBAB, Merck, $\geq$98.0%), $CHCl_3$-d ($CDCl_3$, Sigma-Aldrich, 99.8 atom % D), acetonitrile (Fisher Sci., 99.8%), tetrahydrofuran (THF)-d8 (Armar Chem., 99.5 atom % D), and Na metal (s-dfine chem., >98%) were used as received. THF (Qualigens, 99.0%) was refluxed over sodium metal and benzophenone overnight and distilled under a nitrogen atmosphere prior to use.

2.3.2 Characterization

^{1}H and ^{13}C NMR spectra were recorded using Bruker AMX-500 or AMX-400 and JEOL-400 spectrometers at probe temperature of 25°C. The ^{1}H and ^{13}C NMR spectra were recorded at 500 or 400 and 125 MHz, respectively. The $CDCl_3$ or THF-d8 was calibrated to tetramethylsilane (TMS) as internal standard (δH 0.00) to record the spectra. The Fourier transform infrared (FTIR) spectra of the samples were recorded as either solid powder or thin film. To record the FTIR spectra, the Perkin Elmer Spectrum PIKE MIRacle single reflection horizontal ATR accessory equipped with a ZnSe ATR crystal was used. Solvent-cast thin films of the polymers and powdered samples of the small molecules were pressed against the ATR crystal to record the spectra. High-resolution mass spectra (HRMS) were recorded on an Agilent Accurate-Mass Q-TOF LC/MS 6520 or a Waters QTOF LC-MSMS single mass analysis was done in tolerance 1 mDa/DBE: minimum = -1.5 and maximum = 50.0, monoisotopic mass, and even electronions. The peaks are specified in m/z (% of basis peak). Thermal gravimetric analysis (TGA) of the samples was performed on a TGAQ500 (TA Instruments) under a N_2 atmosphere (60 mL/min). Approximately 10 mg of finely powdered samples was taken in the platinum pan and heated to 700 °C at a rate of 10°C/min, and the weight loss was measured. A Thermo Scientific κ-Alpha+ X-ray photo electron spectrometer (XPS) was used to determine the surface elemental compositions of thin film samples. All samples were surveyed, and high-resolution XPS data were taken at both 90° and 30° incident angles. The samples were gently cleaned using the MAGCIS (Monatomic and Gas Cluster Ion Source) before recording the spectra. The data were processed using Avantage XPS software. The XPS depth profiling analysis of the samples was performed by etching the samples using an Ar-cluster ion beam (6 keV, 500-atom cluster). The depth was estimated based on the etch rate on an Irganox-1010 standard. The ultimate tensile strength (UTS) were measured using an H25KS UTM Tinius Olsen extensometer following the ASTMD 882 protocol. The tensile

data of samples were recorded as rectangular (width: 4 mm; thickness: 0.8 mm) strips at $\sim$ 25°C using a 1.0 kN load cell at a crosshead speed of 5.0 mm/min unless otherwise mentioned. The data represented here are an average of three specimens. The Young's moduli (E) of the samples were determined from the linear region (Hookean slope) of the tensile stress versus strain plot. Hysteresis studies under tension and compression were performed with rectangular (width: 4 mm; thickness: 0.8 mm) strips and circular (radius: 18 mm; thickness: 5mm) discs, respectively, at $\sim$25°C. The data for tension and compression were recorded at a crosshead speed of 5.0 or 1.0 mm/min, respectively, using a 1.0 kN load cell. Optical microscopic images of the samples were found at 25°C on a LEICA-DM750P instrument. The differential scanning calorimetry (DSC) profiles of the samples were recorded on a DSC Q2000 TA Instruments under a N_2atmosphere (50 mL/min). Finely powdered samples were taken in an aluminium pan for the measurement. The samples were heated from 0 to 100°C, cooled to 0°C, and again heated to 100°C at a rate of 10°C/min. The second heating traces of the samples are reported and used for determination of glass transition temperature (T_g) of the samples. The dynamic mechanical analysis (DMA) was performed on a DMA Q-800 using the tension mode. 50 ASTM D4065-01 norm was followed to record the samples. The specimen samples of 4 mm width and 10 mm length were used for this purpose. The peak of the tan δ trace was considered as the T_g of the samples. TA Instruments DMA Q 800 in compression mode was used for stress relaxation experiments. Rectangular samples (3 mm $\times$ 10 mm) were compressed to a constant strain of 0.1% and equilibrated at a set temperature for 10 min before collecting the data. The storage (E') and loss moduli (E'') were determined from the frequency scans recorded under tension mode. The E' was then normalized, and the corresponding relaxation time was plotted against temperature for elucidating the activation energy (Ea) using standard procedures. A Lab India UV-vis 3200 instrument was used to record the UV-vis spectra of the samples. UV-vis spectra were recorded at a 1 nm/min scan rate. The high performance liquid chromatography (HPLC) data were recorded on a Waters 2414 equipped with an auto sampler and refractive index detector using a solvent combination of 20% H_2O in acetonitrile. We used a C18 column with flow rate of 0.50 mL min^{-1} for the analysis. The column temperature was maintained at 30 $\pm$ 1 °C. The ground-state geometries of the compounds were optimized using the density functional theory (DFT) with the Becke 3LYP functional as implemented in the Gaussian 09W software package. The default options for the self-consistent-field convergence and threshold limits in the optimization were used. Time-dependent DFT (TDDFT) calculations were performed on the gas phase optimized geometry of the ground state.

2.3.3 Synthesis of Polyacryloyl hydrazide (PAHz)

A solution of PMA (20.0 g, 0.3 mmol) in 600 mL of THF was taken in a 1 L round-bottom flask. Hydrazine hydrate (77.6 g, 15.2×10^2 mmol) and TBAB (20.0 g, 62.0 mmol) were added into flask. The mixture was stirred at 60 °C for 12 h until the layers separated out. The reaction was stopped and kept undisturbed till the temperature cooled down to room temperature.[206] The aqueous layer was transferred into methanol to precipitate the product polymer. The precipitate was washed with methanol several times to remove the impurities and dried under reduced pressure at ambient temperature. Yield: 90%. FTIR (thin film, cm^{-1}): 980 (m, C-N), 1447 (m, C-H), 1610 (s, C=O), 2925 (m, C-H), 3261 (m, NH).

2.3.4 Synthesis of Tetraethyl-2,2′-[1,4-phenylenebis (methanylylidene)] dimalonate (TPMD)

Terepthalaldehyde (3.0 g, 22.4 mmol) was dissolved in anhydrous ethanol (50 mL) in a round bottom flask. To it DEM (8.9 g, 55.6 mmol) was added followed by piperidine (0.2 g, 2.3 mmol) and acetic acid (0.2 g, 3.3 mmol). The resulting mixture was refluxed overnight under an inert atmosphere. The solvent was allowed to evaporate slowly to crystallize the product.[207] The final product was obtained as white crystals (4.5 g, 10.8 mmol) in 48.2 % yield. ^{1}H NMR (500 MHz, $CDCl_3$) δ (ppm): 7.7 (s, 2H, C***H***=C−$(COO)_2$), 7.4 (s, 4H, Ar-***H***), 4.2 (q, 8H, -O−C***H***$_2$-), 1.2 (m, 12H, -O−CH_2−C***H***$_3$). ^{13}C NMR (125 MHz, $CDCl_3$) δ (ppm): 164.5 (−***C***$OOCH_2$), 142.7 (−***C***H=C−$(COO)_2$), 132.6 (Ar C), 130.1 (−***C***H=C−$(COO)_2$), 127.4 (Ar ***C***H), 60.2 (−O−***C***H_2−), 14.0 (−O−CH_2−***C***H_3). FTIR (thin film, cm^{-1}): 774 (m, p-substitution), 1200 (s, C-O), 1443 (m, C=C, Ar), 1487 (w, C-H), 1626 (m, C= C), 1718 (s, C=O), 2875 (w, C-H), 2976 (m, C-H).

2.3.5 Synthesis of Benzylcarbonyl hydrazide (BzCH)

A solution of methyl benzoate (8.0 g, 58.8 mmol) and hydrazine hydrate (17.6 g, 352.4 mmol) in THF (50 ml) was refluxed for 6h. The resulting solution was concentrated by rotary evaporation and the residue was poured into distilled water (100 ml). The product obtained was repeatedly washed with distilled water. The white solid obtained was dried under vacuum before characterization. Yield: 85.0% ^{1}H NMR (500 MHz, $CDCl_3$) δ (ppm): 7.9 (s, 1H, -N***H***), 7.7 (d, 2H, Ar ***H***), 7.5 (m, 1H, Ar ***H***), 7.4 (t, 2H, Ar ***H***), 4.1 (s, 2H, -

N*H*2).^{13}C NMR (125 MHz, $CDCl_3$) δ (ppm): 168.7 (-***C***=O), 132.6 (Ar ***C***), 131.8 (Ar ***C***), 128.7 (Ar ***C***), 126.9 (Ar ***C***), FTIR (thin film, cm^{-1}): 751 (m, C-H bend.), 1556 (m, N-H bend), 1612 (m, N-H bend), 1660 (s, C=O).

2.3.6 Synthesis of laurylcarbonyl hydrazide (LCH)

A solution of methyl laurate (1 g, 4.67 mmol) and hydrazine hydrate (1.40 g, 28 mmol) in dry THF (10 ml) were refluxed for 8h. at 60 °C. The product obtained was precipitated and repeatedly washed with distilled water. The white solid obtained was dried under vacuum before characterization. Yield: 84.0% ^{1}H NMR (500 MHz, $CDCl_3$) δ (ppm): 6.75 (s, H, -N***H***), 2.19 (t, 2H, $-C\boldsymbol{H}_2(CO)$), 1.6(m, 2H, $-C\boldsymbol{H}_2-CH_2-(CO-)$), 1.25 (m, 2H, C$H_2$), 0.8 (t, 3H, C$\boldsymbol{H}_3$), ^{13}C NMR (125 MHz, $CDCl_3$): δ (ppm) 174.5 (-***C***O), 35.9 ($-\boldsymbol{C}H_2CO^-$), 32 ($-\boldsymbol{C}H_2-CH_2-CH_3-$), 30 ($-(\boldsymbol{C}H_2)_6-$), 27.1 ($-\boldsymbol{C}H_2-CH_2-CO$), 24.1 ($-\boldsymbol{C}H_2-CH_3-$), 15 (-***C***$H_3$).FTIR (thin film, cm^{-1}): 729, 718 (m, $C-H_2$,bend), 1451 (s, C-H, bend), 1535(s,-NH bend),1626 (s, -C=O str.), 2849, 2919 (m, C-H str.), 3315 (s, -NH). HRMS (ESI-TOF) m/z: [M + H] Calcd for [$C_{12}H_{26}N_2O$] 215.2123. Found 215.2101.

2.3.7 Synthesis of p-butoxy-benzylcarbonyl hydrazide (BCH)

A solution of methyl 4- hydroxy benzoate (5 g, 32.89 mmol), potassium carbonate (45.39 g, 328.94) and 1-bromobutane (11.26 g, 82.18 mmol) in DMF (50ml) were refluxed for 8 h and got methyl 4-butoxybenzoate. Then the solution of 4-butoxybenzoate (2.8 g, 13.46 mmol) and hydrazine hydrate (4.03 g, 80.6 mmol) in THF (50 ml) was refluxed for 6h. The resulting solution was concentrated by rotary evaporation and the residue was taken into distilled water (100 ml). The precipitate settled at the bottom was filtered using Whatman filter paper (pore size = 11 μm and recrystallized from ethanol/water (50:50, v:v) solution to obtain the final product as a pale white solid in 65.0% yield. ^{1}H NMR (500 MHz, $CDCl_3$) δ (ppm): 7.7 (d, 1H, Ar ***H***), 7.5 (d, 1H, Ar ***H***), 6.9 (d, 2H, Ar ***H***) 4.2 (t, 4H, $-O-C\boldsymbol{H}_2-$), 4.1 (br, 2H, $-N\boldsymbol{H}_2$), 3.9 (t, 2H, $(-O-C\boldsymbol{H}_2-$), 1.8 (m, 2H, $-C\boldsymbol{H}_2-$), 1.5 (m, 2H, $-C\boldsymbol{H}_2-$), 0.96 (m, 3H, -C$\boldsymbol{H}_3$). ^{13}C NMR (125 MHz, $CDCl_3$) δ (ppm): 168.0 (-***C***=O), 161.0 (Ar ***C***), 128.0 (Ar ***C***), 124.0 (Ar C), 112.0 (Ar ***C***), 68.0 ($-O-\boldsymbol{C}H_2-$), 31.0 ($-\boldsymbol{C}H_2-CH_2-$), 18.0 ($-CH_2-\boldsymbol{C}H_2-$), 13.8 ($-CH_2-\boldsymbol{C}H_3$), FTIR (thin film, cm^{-1}): 769 (s, C-H bend.), 1504 (s, N-H bend), 1572 (m, N-H bend), 1607 (s, C=O), 2868 (m, C-H str), 2936 (m, C-H), 3343 (m, N-H). HRMS (ESI-TOF) m/z: [M + H] Calcd for [$C_{11}H_{16}N_2O_2$] 209.1245. Found 209.1290.

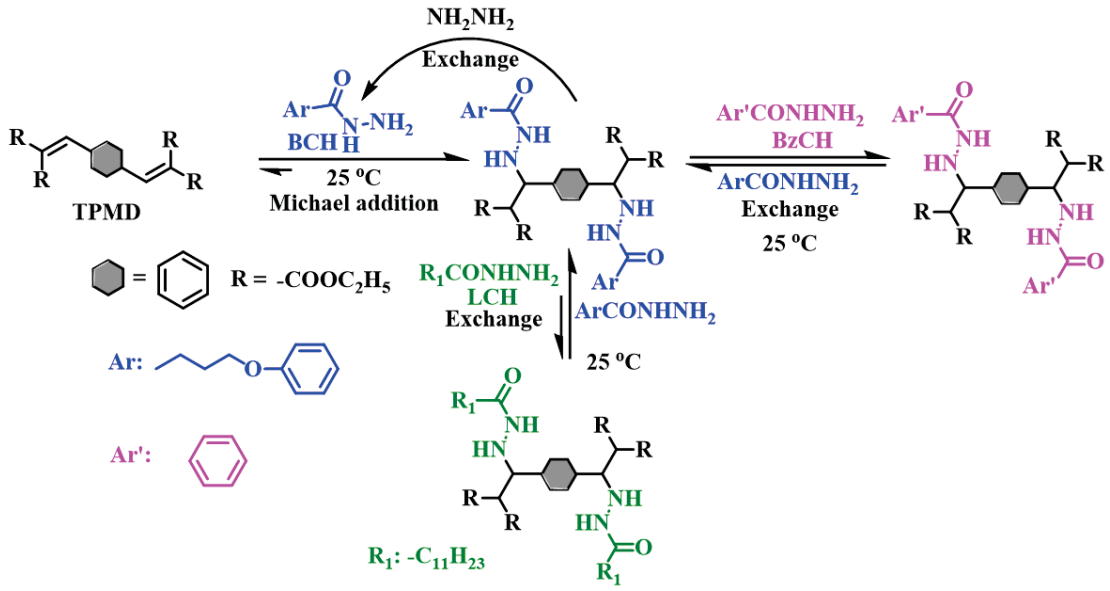

Scheme 2.1: Hydrazide Michael addition of aliphatic and aromatic $CONHNH_2$ with TPMD and dynamics of the exchanges of various donors in the hydrazide Michael adduct

2.3.8 Synthesis of Mono hydrazide Michael Adduct of BCH and DBM (DBM-BCH)

DBM (1.0 g, 4.0 mmol) and BCH (0.9 g, 4.4 mmol) were dissolved in dry THF (10 mL) and stirred for 8 h at 25 °C. The solvent was then evaporated under reduced pressure, and the solid mass obtained was purified by column chromatography using hexanes:ethyl acetate (90:10, vol:vol) mixture as the eluent. Yield: 60%. ^{1}H NMR (500 MHz, $CDCl_3$) δ (ppm): 7.6 (d, 2H, Ar ***H***), 7.4 (d, 2H, Ar ***H***), 7.3 (m, 2H, Ar ***H***), 7.2 (m, 1H, Ar ***H***), 6.8 (d, 2H, Ar ***H***), 5.7 (d, 1H, -C*H*-NH-), 4.8 (s, 1H, -N***H***), 4.1 (m, 4H, -OC***H***$_2-CH_3$), 3.9 (t, 2H, -OC***H***$_2-CH_2$), 3.8 (d, 1H, -C***H***CO-), 1.7 (m, 2H, -CH_2-CH_2O-), 1.4 (m, 2H, -C***H***$_2-CH_3$-), 1.2 (t, 6H, -C***H***3), 0.9 (t, 3H, -C***H***$_3$). ^{13}C NMR (125 MHz, $CDCl_3$): δ (ppm) 168.2 (-***C***OO-), 166.8 (-***C***ONH), 162.3 (-Ar ***C***O-), 148.3 (Ar ***C***), 134.0 (Ar C), 130.1 (Ar ***C***), 128.9 (Ar ***C***), 127.5 (Ar ***C***), 124.8 (Ar ***C***), 114.0 (Ar ***C***), 67.8 (-O***C***H_2), 63.7 (-***C***H-O), 61.6 (***C***H-NH), 57.1 (-***C***$H_2-(COO-)_2$), 31.1 (-***C***H_2-CH_2-), 19.0 (-***C***H_2-CH_2-), 13.9 (-*C*H_3). FTIR (cm^{-1}): 768 (m, C-H), 837 (s, C-H), 1177 (s, C-O), 1573 (m, N-H), 1606 (s, CONH), 1733 (s, -COO-), 2958 (m, C-H), 3299 (m, N-H). HRMS (ESI-TOF) m/z: [M + H] Calcd for [$C_{25}H_{32}N_2O_6$] 457.2339. Found 457.2349.

2.3.9 Synthesis of Bis-Hydrazide Michael Adducts LCH-TPMD-LCH (L-T-L), BCH-TPMD-BCH (B-T-B), and BzCH-TPMD-BzCH (Bz-T-Bz)

A typical procedure for L-T-L is described below. TPMD (1.0 g, 2.3 mmol) and LCH (1.0 g, 4.7 mmol) were dissolved in dry THF (10 mL) and stirred for 8 h at 25 °C. The solvent was evaporated, and the sticky mass obtained was washed with acetonitrile to remove the unreacted starting material. The white solid obtained was dried under vacuum before further characterization. Yield: 65%. ^{1}H NMR (500 MHz, $CDCl_3$) δ (ppm): 7.4 (s, 2H, (-CO-N***H***), 7.3 (s, 4H, Ar ***H***), 4.6 (d, 2H, -C***H*** – NH-), 4.2 (m, 8H, -OC***H***$_2$), 3.9 (d, 2H, -C***H***), 3.7 (s, 2H, -CONH – N***H***), 2.1 (t, 4H, -C***H***$_2$ – CO), 1.5 (m, -4H, -C***H***$_2$ – CH_2 – CO-), 1.2 (m, 44H, C***H***$_3$, -C***H***$_2$), 0.8 (t, 6H, C***H***$_3$ – CH_2-). ^{13}C NMR (125 MHz, $CDCl_3$): δ (ppm) 174.0 (-***C***ONH-), 166.6 (-***C***OO-), 137.92 (Ar ***C***), 128.4 (Ar ***C***), 63.4 (-O – ***C***H_2-), 61.6 (***C***H-NH), 61.1 (-***C***H-COO-), 56.8 (-***C***H_2 – CO), 34.4 (-***C***H_2 – CONH –)$_2$), 31.9 (-***C***H_2 – CH_2 – CH_3), 29.2 (-***C***H_2 – CH_2), 25.4 (-***C***H_2 – CH_2 – CO), 22.6 (-***C***H_2 – CH_3), 13.9 (-***C***H_3). FTIR (cm^{-1}): 859 (w, C-H), 1064 (s, C-N), 1208 (s, C-O), 1465 (m, Ar, C=C), 1660 (m, CONH), 1732 (s, -COO-), 2853 (m, C-H), 2923 (s, C-H), 3287 (m, N-H). HRMS (ESI-TOF) m/z: [M + H] Calcd for [$C_{46}H_{79}N_4O_{10}$] 847.5796. Found 847.5795. Similarly, B-T-B and Bz-T-Bz were synthesized by reacting TPMD and BCH or BzCH in suitable molar proportions in THF.

2.3.10 B-T-B

Yield: 69%. ^{1}H NMR (500 MHz, $CDCl_3$) δ (ppm): 7.6 (d, 4H, Ar H), 7.3 (s, 4H, Ar ***H***), 6.8 (d, 4H, Ar ***H***), 5.7 (d, 2H, -C***H***-NH-), 4.8 (s, 2H, -N***H***), 4.2 (m, 8H, (-OC***H***$_2$ – CH_3), 3.9 (t, 4H,-OC***H***$_2$ – CH_2), 3.8 (d, 2H, -C***H***CO), 1.7 (m, 4H, -C***H***$_2$ – CH_2O), 1.4 (m, 4H,-C*H*$_2$ – CH_3), 1.2 (t, 12H, -C***H***$_3$), 0.9 (t, 6H, -C***H***$_3$). ^{13}C NMR (125 MHz, $CDCl_3$): δ (ppm) 167.8 (-***C***OO-), 166.8 (-***C***ONH), 162.1 (-Ar ***C***-O), 138.2 (Ar ***C***), 128.7 (Ar ***C***), 124.4 (Ar ***C***), 114.2 (Ar ***C***), 67.8 (-O – ***C***H_2), 62.0 (***C***H-NH), 61.3 (-***C***H-COO-), 56.9 (-***C***H_2 – $(COO)_2$), 30.9 (-***C***H_2 – CH_2-), 19.1 (-***C***H_2 – CH_2-), 13.7 (-***C***H_3). FTIR (cm^{-1}): 780 (m, C-H), 840 (s, C-H), 1195 (s, C-O), 1556 (m, N-H), 1607 (s, CONH), 1747 (s, -COO-), 2956 (m, C-H), 3285 (m, N-H). HRMS (ESI-TOF) m/z: [M + H] Calcd for [$C_{44}H_{59}N_4O_{12}$] 835.4129. Found 835.4131.

2.3.11 Bz-T-Bz

Yield: 67%. ^{1}H NMR (400 MHz, THF-d8) δ (ppm): 8.8 (s, 2H, -CON***H***), 7.7 (d, 4H, Ar *H*), 7.5 (d, 2H, Ar ***H***), 7.2 (m, 4H, Ar ***H***), 7.1 (s, 4H, Ar ***H***), 4.6 (d, 2H, -C***H***-NH), 4.1 (m, 8H,OC$\boldsymbol{H}_2$), 3.7 (d, 2H, -C***H***-CO-), 1.1 (t, 6H, -C$\boldsymbol{H}_3$), 0.9 (t, 6H, -C$\boldsymbol{H}_3$). ^{13}C NMR (125 MHz, $CDCl_3$) δ (ppm): 167.5 (-***C***OO-), 166.4 (-***C***ONH-), 138.5 (Ar ***C***), 132.5 (Ar ***C***), 131.6 (Ar ***C***), 128.6 (Ar *C*), 126.5 (Ar *C*), 62.2 (-O−***C***H_2-), 61.6 (***C***H-NH), 57.0 (-***C***H-COO-), 13.9 (-***C***H_3). FTIR (cm^{-1}): 695 (s, C-H), 804 (m, C-H), 1233 (s, C-O), 1467 (s, N-H), 1651 (s, Ar, C=C), 1719 (s, -COO-), 3304 (m, N-H). HRMS (ESI-TOF) m/z: [M + H] Calcd for [$C_{36}H_{43}N_4O_{10}$] 691.2979. Found 691.2982.

2.3.12 Synthesis of Cross-Linked Networks of PAHz and TPMD (PAHTD)

Thin uniform films of PAHz (∼0.5 g) were dipped in THF:H_2O mixture of a particular proportion (10.5 mL, 97:3 or 95:5 vol:vol) containing a certain amount of TPMD (5–10 wt %). The cross-linking under heterogeneous conditions was performed at 25 °C for a specific time period (6 or 12 h). The cross-linked films were then removed from solution and washed repeatedly in THF to remove unreacted TPMD from the network surface. Subsequently, the films were dried at 50 °C for 24 h before measuring the mechanical properties. FTIR (thin film, cm^{-1}): 1017 (s, C-C), 1262 (s, C-O), 1466 (s, C=C), 1725 (s, C=O), 2982 (m, C-H), 3263 (s, NH).

2.3.13 Synthesis of DBM Functionalized PAHz (PAHz-DBM)

A thin uniform film of PAHz (0.5 g) was dipped in THF:H_2O mixture (10.5 mL, 95:5, vol:vol) containing 10 wt % of DBM. The reaction was performed under heterogeneous conditions at 25 °C for 12 h. The resulting film was removed from solution, washed repeatedly with THF, and dried under vacuum at 50 °C for 24 h. FTIR (thin film, cm^{-1}): 1006 (s, C-C), 1262 (s, C-O), 1450 (s, C=C), 1643 (m, C=C), 1738 (s, C=O), 2922 (m, C-H), 3276 (m, -NH-).

2.3.14 Determination of TPMD mol % in DCNs

The amount of TPMD in DCNs was calculated by comparing the concentrations of TPMD in THF:H_2O mixture before and after cross-linking reaction. The TPMD concentration was determined by recording the absorbance value of cross-linking solution at 320 nm using the UV-vis spectroscopic technique. To maintain the accuracy of calculation, the DCN films after cross-linking reaction were washed with THF to collect any unreacted TPMD adsorbed on the film surface, the washings were included in the resulting cross-linking solution, and subsequently the volume was adjusted by evaporating excess THF under ambient conditions before recording the UV-vis spectra. The cross-linker mol % values reported are an average of three experiments.

2.3.15 Reprocessing of DCN Samples

Typical PAHTD strips were dipped in a THF:H_2O (95:5, vol:vol) mixture for 3 h. The softened strips were removed from the liquid mixture, and excess water was removed from film surface by using tissue paper. The soft DCN strips (water content ≈4.0 wt %) were cut into small pieces. The cut pieces were assembled in an aluminum foil and pressed under a load of 1 kg for 48 h at 25 °C. The remolded samples were dried at 50 °C for 12 h and used for mechanical analysis.

2.4 Results and Discussion

To investigate the Michael addition reaction of $CONHNH_2$ (donor) with highly activated double bond (acceptor) and factors that govern the exchange dynamics of donors in adduct, suitable low molecular weight model compounds were synthesized and studied (Scheme2.1). Both LCH and BCH were reacted with TPMD at 25 °C to form the corresponding adducts (L-T-L and B-T-B). The disappearance of the FTIR band at 1626 cm^{-1} (C=C of TPMD) and shifting of C=O (-$COOC_2H_5$) peak to 1747 cm^{-1} supported the formation of B-T-B (Figure2.1). The peak at 7.7 ppm assigned to the C=C-H of TPMD disappeared, and the aromatic peak at 7.4 ppm shifted upfield (∼7.3 ppm) in the product (Figure2.2). Likewise, the peak at 7.7 ppm assigned to the aromatic proton of BCH shifted to 7.6 ppm, and new peaks at 5.7 ppm (-NHNHCH) and 3.8 ppm (-CHCO) appeared supporting formation of B-T-B (Figure2.2).

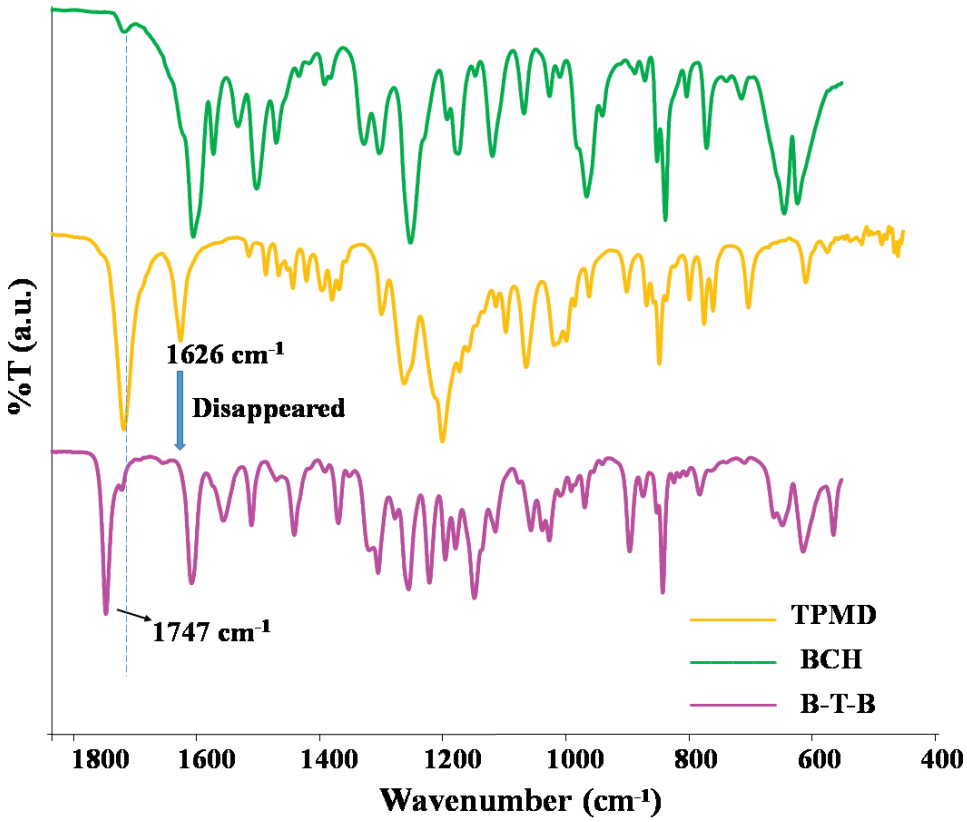

Figure 2.1: ATR FTIR spectra of BCH, TPMD and B-T-B networks.

In HRMS, the principal peak at 835.4131 accountable to the M + H ion of B-T-B was found. Likewise, various spectroscopic data supported the formation of hydrazide Michael adducts (B-T-B and L-T-L). The mono hydrazide Michael adduct (DBM-BCH) was synthesized by reacting DBM with BCH under ambient conditions. Hydrazide Michael addition of aromatic $CONHNH_2$ with mono substituted ester DBM and the exchange of hydrazide donor in the hydrazide Michael adduct (Scheme2.2). The FTIR band at 1630 cm^{-1} accountable to the C=C of DBM disappeared in the product, and the HRMS data showed a new peak at 457.2349 for the M + H ion of DBM-BCH (Figure2.3). The ^1H NMR spectrum displayed new resonances at 3.8, 4.8, and 5.7 ppm for the $-CH(CO)_2$, -CHNHNH-, and -NHCHCH- protons present in DBM-BCH. The rate of hydrazide Michael addition was tracked spectrophotometrically by periodically recording the concentration of TPMD in the reaction mixture. TPMD in THF exhibited an absorption maximum at 320 nm, and upon Michael addition the peak became blue-shifted due to removal of double bonds. These hydrazide Michael additions fitted well within the third-order model. The Arrhenius plots of these hydrazide Michael additions were created by comparing the conversion with reaction time at various temperatures and fitting the data as per third-order kinetics (Figure2.4).

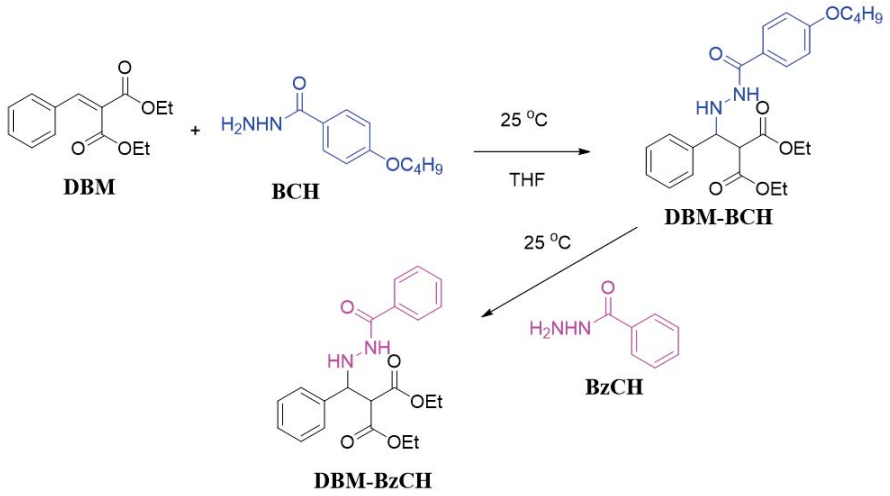

Scheme 2.2: Hydrazide Michael addition of aromatic $CONHNH_2$ with mono substituted ester DBM and the exchange of hydrazide donor in the hydrazide Michael adduct.

Table 2.1: The Ea and ΔG^0 data of the hydrazide Michael addition and exchange reactions

Reaction type (method)	Reactants	Ea^a (kJ/mol)	$\Delta G^{0a,b}$ (kJ/mol)	ΔG^{0c} (kJ/mol)
Michael addition	RCH + TPMD	39.7	-29.7	-23.8
(spectroscopic)	BCH + TPMD	45.2	-40.2	-44.3
Exchange Reaction	BzCH + B-T-B	93.3	-3.8	-0.8
(chromatographic)	BzCH + R-T-R	86.1	-17.6	-21.8

[a]The values were determined by monitoring the reaction rate experimentally using UV-vis spectroscopic or HPLC analysis. [b]The value was determined from the equilibrium concentrations of the products and reactants. [c]Determined theoretically from DFT analysis. RCH = n-hexyl or lauryl -$CONHNH_2$

The Ea of the hydrazide Michael additions involving BCH and RCH was calculated to be 45.2 and 39.7 kJ/mol, respectively (Table2.1). The marginally higher Ea value in the case of the former may be assigned to the ground-state stability of the aromatic $CONHNH_2$ precursor. Intuitively, the Ea values were lower compared to that of the conventional aza Michael addition (96.0 kJ/mol) system[208] and comparable to that of the system based on activated acceptors (32.2 kJ/mol) reported earlier.[209] The hydrazide Michael addition of BCH with monofunctional double bond compound (DBM) was somewhat sluggish (half-life $\approx$175 min), and the Ea value (53.4 kJ/mol) was marginally higher compared to that of the TPMD-BCH system (half-life $\approx$120 min, Ea = 45.2 kJ/mol) . For exchange reaction; this minor difference in reactivity of TPMD compared to that of the DBM may be assigned to the activating effect of para-substituted electron-withdrawing group (-CH=$C(COOEt)_2$) present in the system.

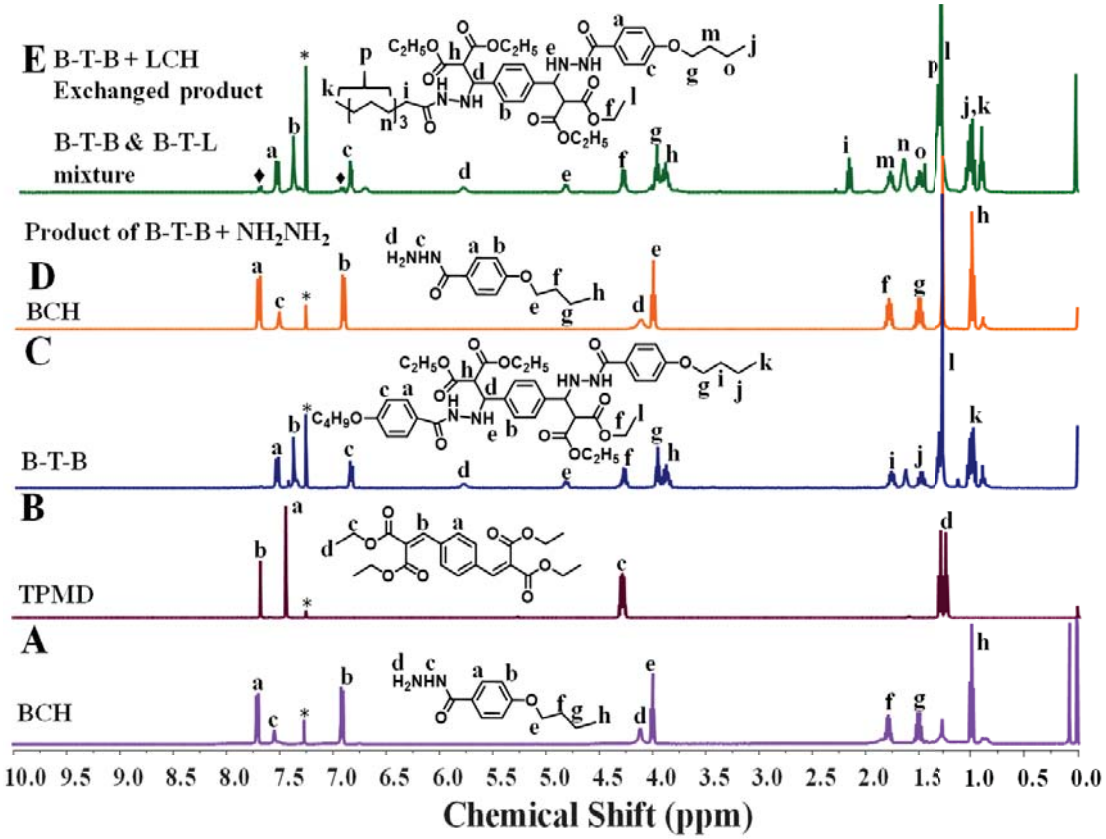

Figure 2.2: ^{1}H NMR spectra of (A) BCH, (B) TPMD, (C) hydrazide Michael adduct (B-T-B) of TPMD and BCH, (D) the product formed after treatment of B-T-B with NH_2NH_2 at 25 °C, and (E) the exchanged product formed after reacting B-T-B with LCH at 25 °C. The peaks marked with "♦" represent the trace amount of BCH released due to the exchange of BCH with LCH in B-T-B.

The standard free energy change (ΔG^0) for the reactions was calculated experimentally from equilibrium concentrations and theoretically from DFT calculations (Table2.1). The experimental ΔG^0 value of B-T-B (-40.2 kJ/mol) was higher in comparison with the the R-T-R (-29.7 kJ/mol) (Table2.1). A relatively higher ΔG^0 value of B-T-B recommended that the possibility of formation of stable adducts with aromatic $CONHNH_2$ is higher in comparison with the aliphatic analogues. The theoretical ΔG^0 (kJ/mol) values (B-T-B = -44.3 and R-T-R = -23.8) supported the experimental data. The exchangeability of these adducts were studied by treating B-T-B with competitive donors (BzCH or LCH) at 25 °C (Scheme2.3).

NH_2NH_2 was chosen as one of the competitive donors as the reagent is easy to separate. NH_2NH_2 replaced BCH in B-T-B within 3 h (Figure2.2D). HRMS data of the exchanged product extracted in ethyl acetate showed the most abundant peak at 209.1297 (M + H), supporting the release of BCH (Figure 2.5).

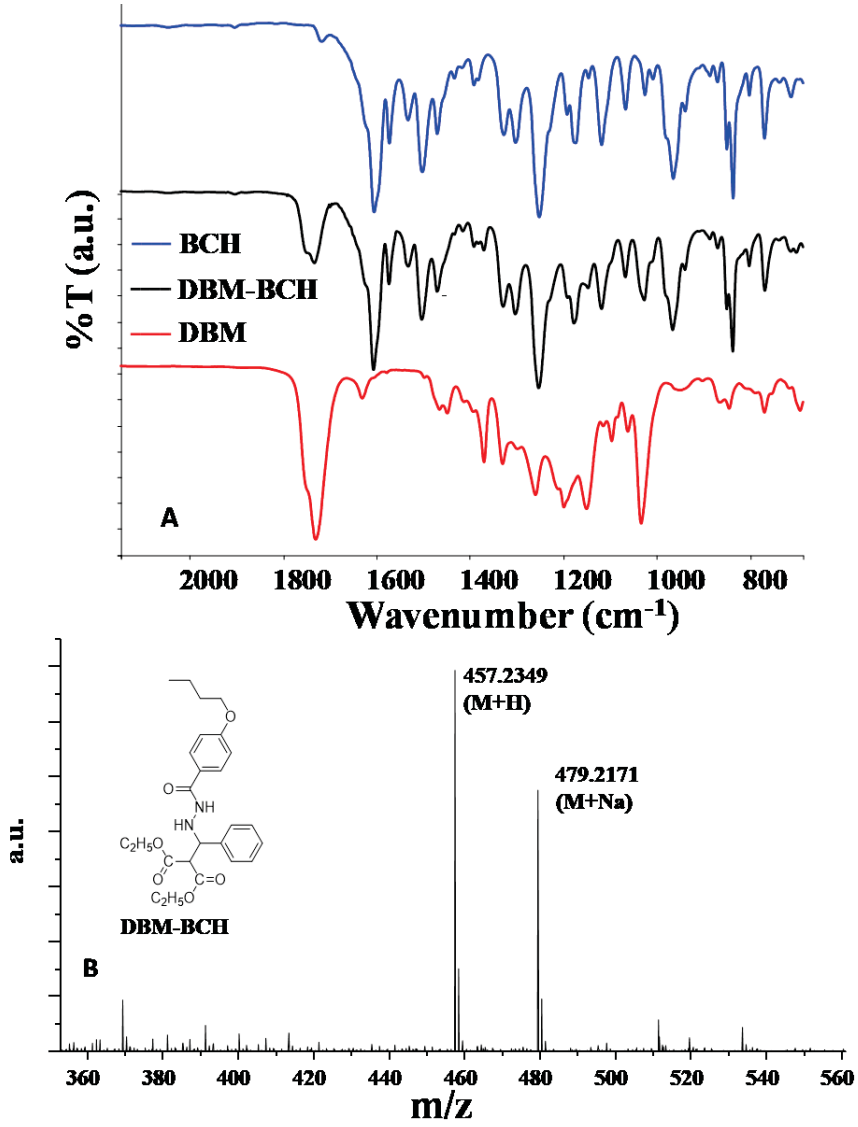

Figure 2.3: (A) ATR FTIR spectra of BCH, DBM-BCH and DBM, (B) HRMS trace of DBM-BCH.

The arrival of peak traces at 7.7 and 6.9 ppm in ^{1}H NMR spectroscopic analysis supported the release of BCH and successful exchange (Figure2.2E). Likewise, new signals at 4.1, 6.8, and 7.7 ppm seemed in the ^{1}H NMR spectra of BzCH and the B-T-B mixture, and the intensity of the signals gradually increased, suggesting gradual formation of -T-Bz linkage and release of BCH with time (Figure2.6). As anticipated, the product of trans-Michael addition of BCH with L-T-L consisted of a major fraction of -T-B linkages, whereas no selectivity was found during the exchange of BzCH with B-T-B. This could be assigned to the higher ΔG^{0} value of -T-B in comparison with the -T-L linkage (Table2.1).

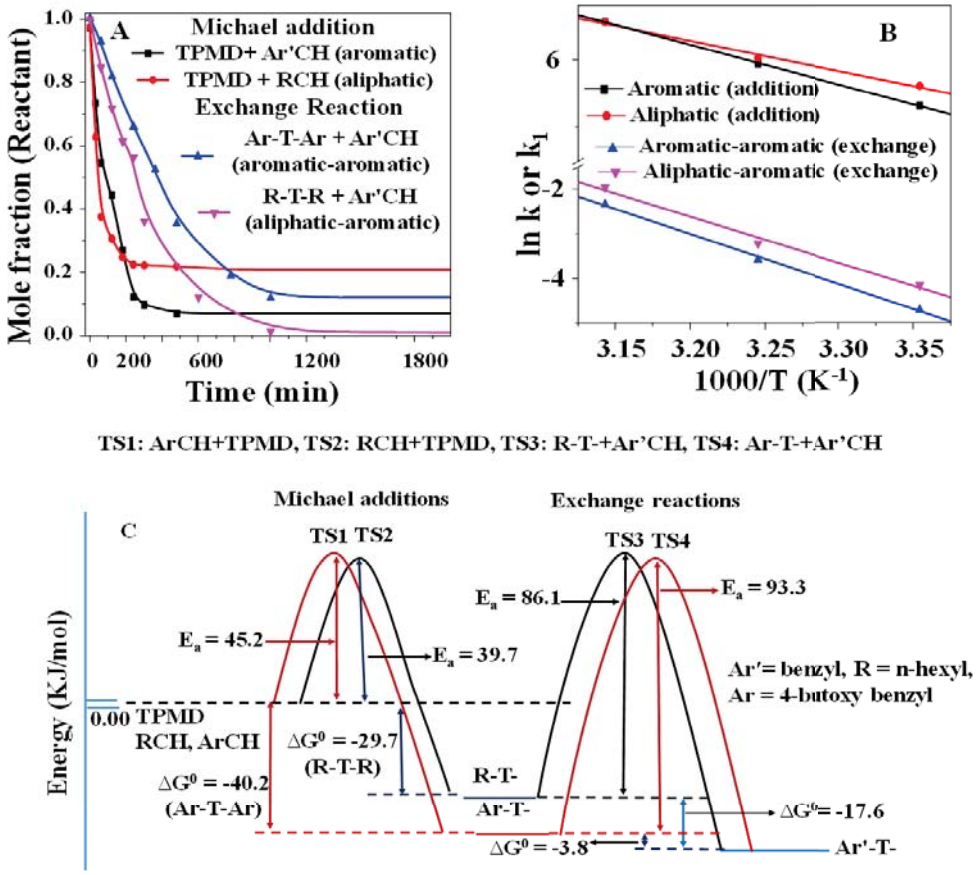

Figure 2.4: (A) The conversion plots of the Michael addition of TPMD with BCH or RCH and exchange reactions at 25 °C. The ratio between double bond and $CONHNH_2$ was maintained at 1:1 (mol:mol) for the hydrazide Michael addition. The ratio between $CONHNH_2$ and B-T-B/H-T-H was maintained at 4:1 (mol:mol) for the exchange reactions. (B) The Arrhenius plots of various hydrazide Michael and trans-Michael (exchange) additions, (C) the energy profile diagram of the hydrazide Michael additions and various trans-Michael additions. The Ea and ΔG^0 values were determined experimentally from UV-Vis and HPLC analysis

The rates of these exchange reactions were anlyzed by HPLC and ^{1}H NMR analysis, and the Ea values were found by plotting the data as per reversible pseudo-second-order kinetics. β-Elimination is probably the rate-determining step in these exchange reactions, since the ΔG^0 values for these hydrazide Michael adducts formation were negative (-29.7 to -40.2 kJ/mol) (Table2.1,Figures2.6, 2.7, 2.8). Intuitively, the Ea values (aromatic-aromatic exchange: 93.3 kJ/mol; aromatic-aliphatic exchange: 86.1 kJ/mol) of these exchange reactions supported the above (Table2.1 & Figure2.5).

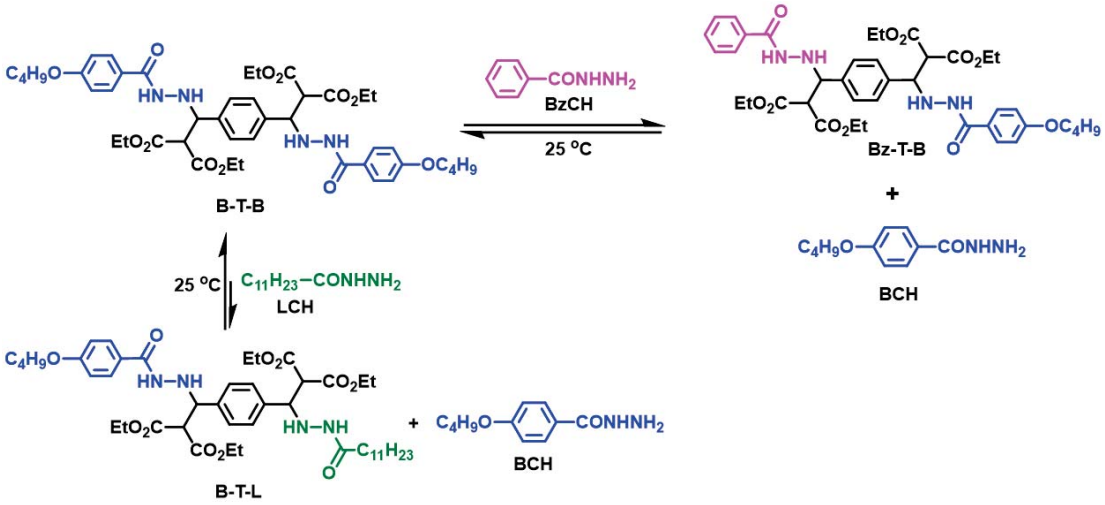

Scheme 2.3: Carbonyl hydrazide exchange reactions of BzCH and LCH with B-T-B.

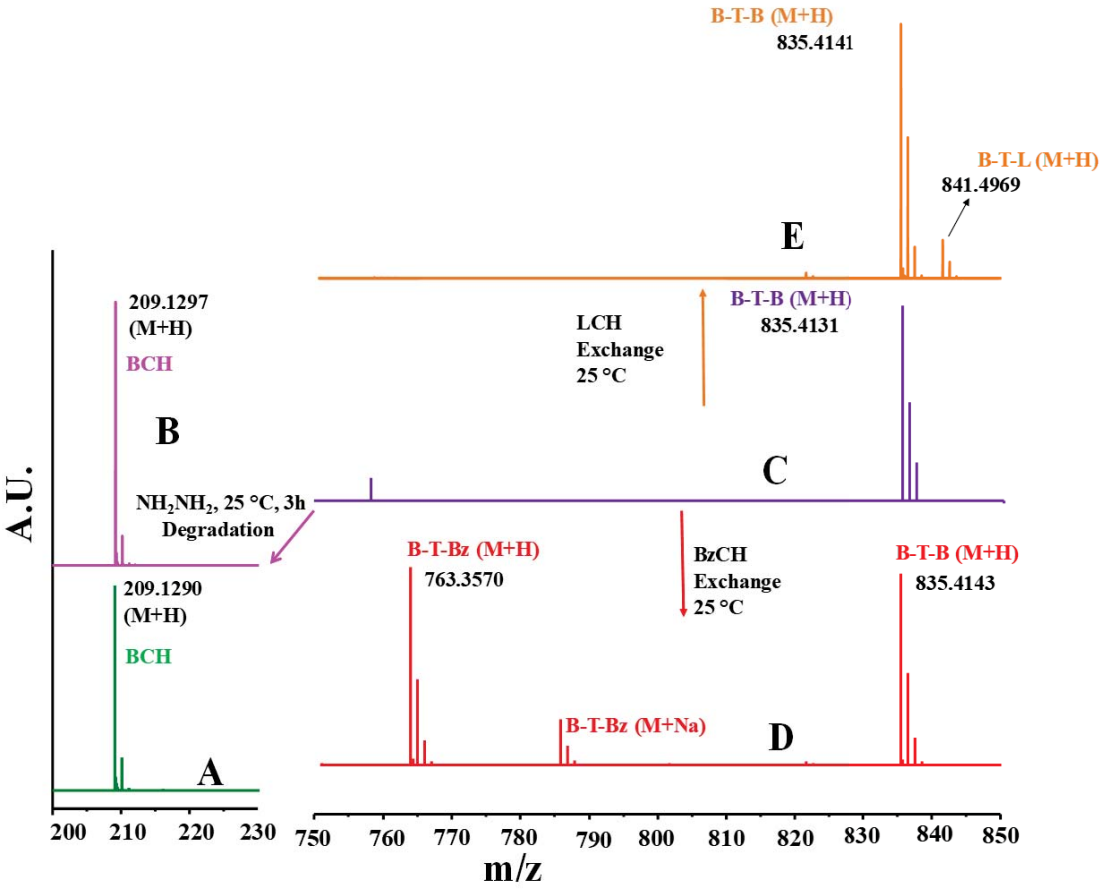

Figure 2.5: HRMS traces of (A) BCH, (C) B-T-B and exchange products of B-T-B with (D) BzCH, (B) NH_2NH_2 and (E) LCH.

The experimental Ea value for the exchange reaction of BzCH with monohydrazide Michael adduct (DBM-BCH) (91.4 kJ/mol) was analogous to that of the BzCH and bis-hydrazide Michael adduct (B-T–B) (93.3 kJ/mol) (Table2.1).

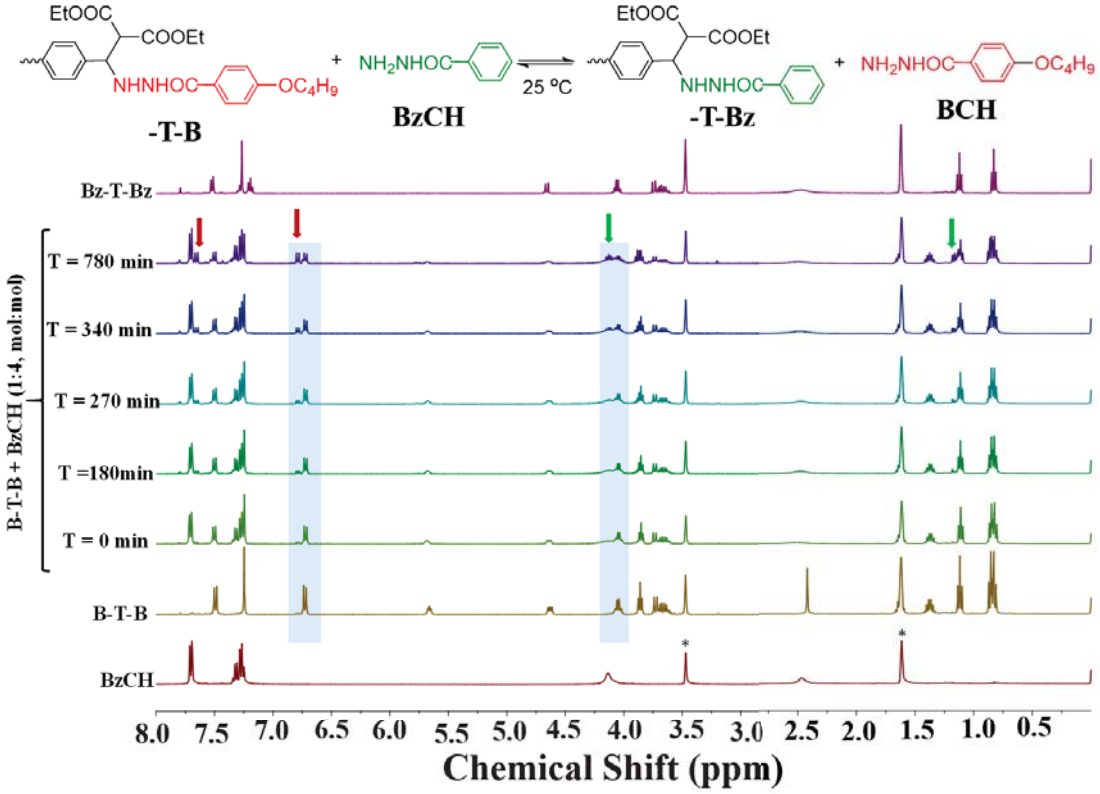

Figure 2.6: ^{1}H NMR spectra of BzCH, B-T-B, Bz-T-Bz, and mixture of B-T-B and BzCH in 1:4 molar ratio recorded after different time intervals in THF-d8 solvent. The peaks marked with "$*$" is assigned to the solvent. The red and green arrows suggest the release of BCH from B-T-B and formation of Bz-T linkage in situ, respectively. The schematics above shows the exchange of aromatic donors in the Michael adduct.

2.4.1 DCNs Based on Poly hydrazide Michael Adducts

The model compound study highlighted that the exchangeability rate of hydrazide Michael adducts based on aliphatic donors (half-life $\approx$ 275 min at 25 °C) is somewhat faster in comparison with the aromatic donors (half-life $\approx$ 370 min at 25 °C). Therefore, PAHz having aliphatic $CONHNH_2$ groups was chosen as the polymeric system to synthesize DCNs with quick self-healing ability (Scheme2.4).

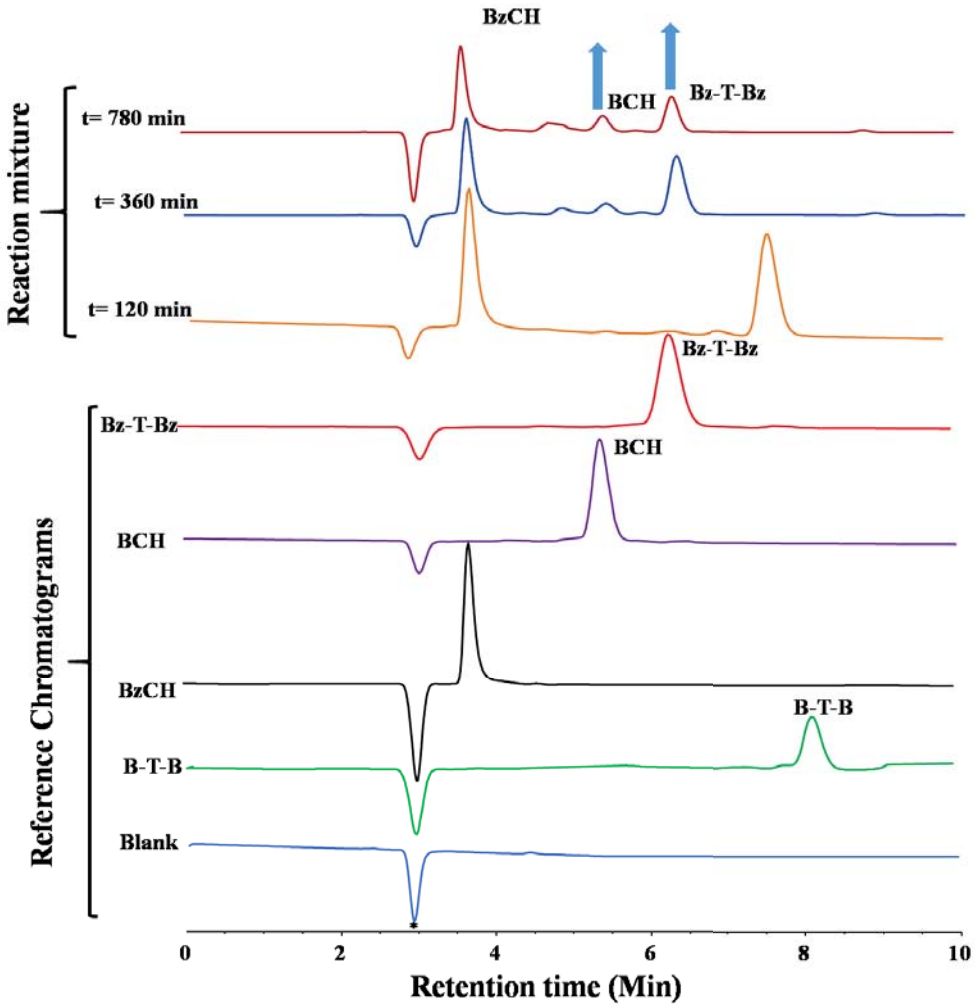

Figure 2.7: HPLC traces of B-T-B, BzCH and the products obtained after exchange reaction of B-T-B with BzCH recorded using 20% H2O in acetonitrile as eluent.

Facile synthesis of PAHz from economic starting materials also prompted the use of this polymer as precursor for DCNs. TPMD was used as the cross-linker for this purpose. The cross-linking under homogeneous condition in solution was not possible due to the solubility difference between PAHz and TPMD. PAHz is only soluble in water, whereas TPMD is insoluble. Efforts to create a homogeneous solution of PAHz and TPMD in binary solvent mixtures (methanol-water and THF-water) were fruitless. Hence, the cross-linking was achieved under heterogeneous conditions by dipping thin uniform films of PAHz in a THF:water mixture containing a fixed amount of TPMD. PAHz was solvent casted from aqueous solution into uniform thin films. The films were dipped in a THF:water mixture containing a certain amount of TPMD (5-10 wt %) to achieve the cross-linking under heterogeneous conditions (Table2.2).

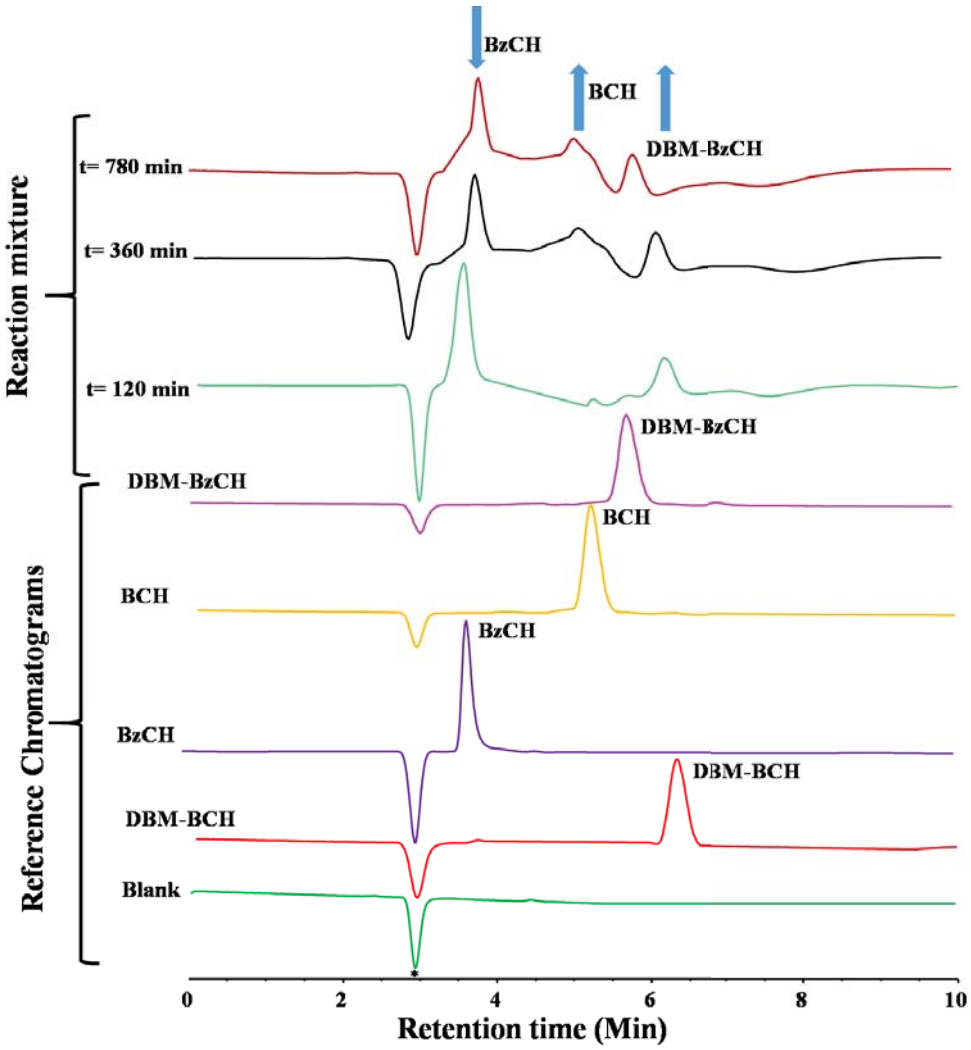

Figure 2.8: HPLC traces of blank, DBM-BCH, BzCH, BCH, DBM-BzCH and the products obtained after exchange reaction of DBM-BCH with BzCH recorded using 20% H_2O in acetonitrile as eluent.

The cross-linking was successful at 25 °C, and the appearance of the FTIR band at $\sim$1725 cm^{-1} (C=O, ester) supported incorporation of TPMD into the PAHz film. The C=O band in DCN shifted up field by 7 cm^{-1} in comparison with the TPMD, and the C=C band at 1626 cm^{-1} disappeared, telling formation of the hydrazide Michael adduct (Figure2.9A). XPS analyses of the PAHz and resulting DCNs were performed at 90° and 30° incident angles to gain insight into the cross-linking chemistry (Figure2.9B). New peaks at 289 and 533 eV accountable to C 1s and O 1s, respectively, of the -COO- functionality of TPMD appeared in the XPS spectrum of PAHTD-4, supporting the incorporation of TPMD moieties into the network (Figure2.9B).

Table 2.2: Reaction Condition, Mechanical Properties and Cross-Link Density (d_c) Data of PAHTD DCNs

code[a]	TPMD[f] (mol %)	UTS[b] (MPa)	ε^b (%)	E^b (GPa)	E'^c (GPa)	$d_c \times 10^3$ [c,d] (mol/cm^3)	TGA[e] (°C)
PAHTD-1	1.2	10.4 ± 0.5	1.7 ± 0.1	1.0 ± 0.1	1.6 ± 0.1	8.0 ± 0.4	170
PAHTD-2	1.9	13.0 ± 0.7	2.0 ± 0.1	1.3 ± 0.1	2.5 ± 0.0	25.7 ± 1.0	160
PAHTD-3	2.6	15.6 ± 0.9	1.7 ± 0.1	1.9 ± 0.1	3.4 ± 0.1	62.8 ± 1.8	-
PAHTD-4	3.2	23.8 ± 1.0	1.6 ± 0.1	2.5 ± 0.2	4.4 ± 0.1	113.5 ± 5.6	170
PAHz	-	7.8 ± 0.4	1.9 ± 0.1	0.7 ± 0.1	1.5 ± 0.0	-	100

[a] For PAHTD-1 and 2, THF:H2O = 1:0.03 vol:vol; for PAHTD-3 and 4 THF:H2O = 1:0.05 vol:vol; the TPMD wt % in solution was maintained at 5 for PAHTD-1 and 10 for other networks.[b] The UTS, ε (elongation at break), and E values were obtained from tensile analysis. [c]The values were obtained from DMTA analysis. dThe value was obtained from the rubbery modulus data at 100 °C. [e]Represents the onset of mass loss in TGA analysis, and E' represents the storage modulus value at 30 °C. The reaction time was 6 h for PAHTD-3 and 12 h for other networks. [f]The mol% of TPMD was calculated with respect to the PAHz repeating units (mol) in the DCNs.

The intensity of the above peaks gradually increased with increase in extent of cross-linking. Importantly, the intensities of C 1s at 289 eV and O 1s at 533 eV were higher in the spectra recorded at 90° compared to that of the 30°, suggesting that the TPMD cross-linkers are present more toward the bulk than the surface of the films (Figure2.9B). Hence, the cross-linking reaction was not only limited to the surface of the film, but also occurred in bulk through swelling of the PAHz film. It is worthwhile to mention that the depth covered for the data collected at 30° is lower compared to that of the 90°. Likewise, the peak at 402 eV assigned to the N 1s of $CONHNH_2$ notably decreased in PAHTD-4, supporting attachment of TPMD to $CONHNH_2$ and suggesting that the surface is mainly occupied with the TPMD modified -CONHNH– groups (Figure2.9B). The XPS data are known to provide information about the surface atomic composition of the samples, and at 90° takeoff angle, most of the XPS signal originates from a depth up to 7 nm.[210] To further investigate the distribution of -$CONHNH_2$ groups in the DCN films, the atom % of PAHz and the PAHTD DCNs were analyzed. The calculated N 1s atom % with respect to the peak at 402 eV (-$CONHNH_2$) in the 30° data (0.6) was lower compared to that of the 90° (Figure2.10). This suggested that the concentration of free $CONHNH_2$ groups increased with the depth of the film. The XPS data recorded at different depths of a typical PAHTD-4 film by controlled etching of the film showed a gradual increase in intensity of the N 1s peak at ∼402 eV with depth further supporting the above (Figure2.10). The amounts of TPMD cross-linker (1.2-3.2 mol % of -$CONHNH_2$) in the DCNs were calculated from the change in concentration of TPMD in cross-linking solution after reaction (Table2.2). The absorbance of the peak maximum at 320 nm were equated to determine the amount of TPMD consumption.

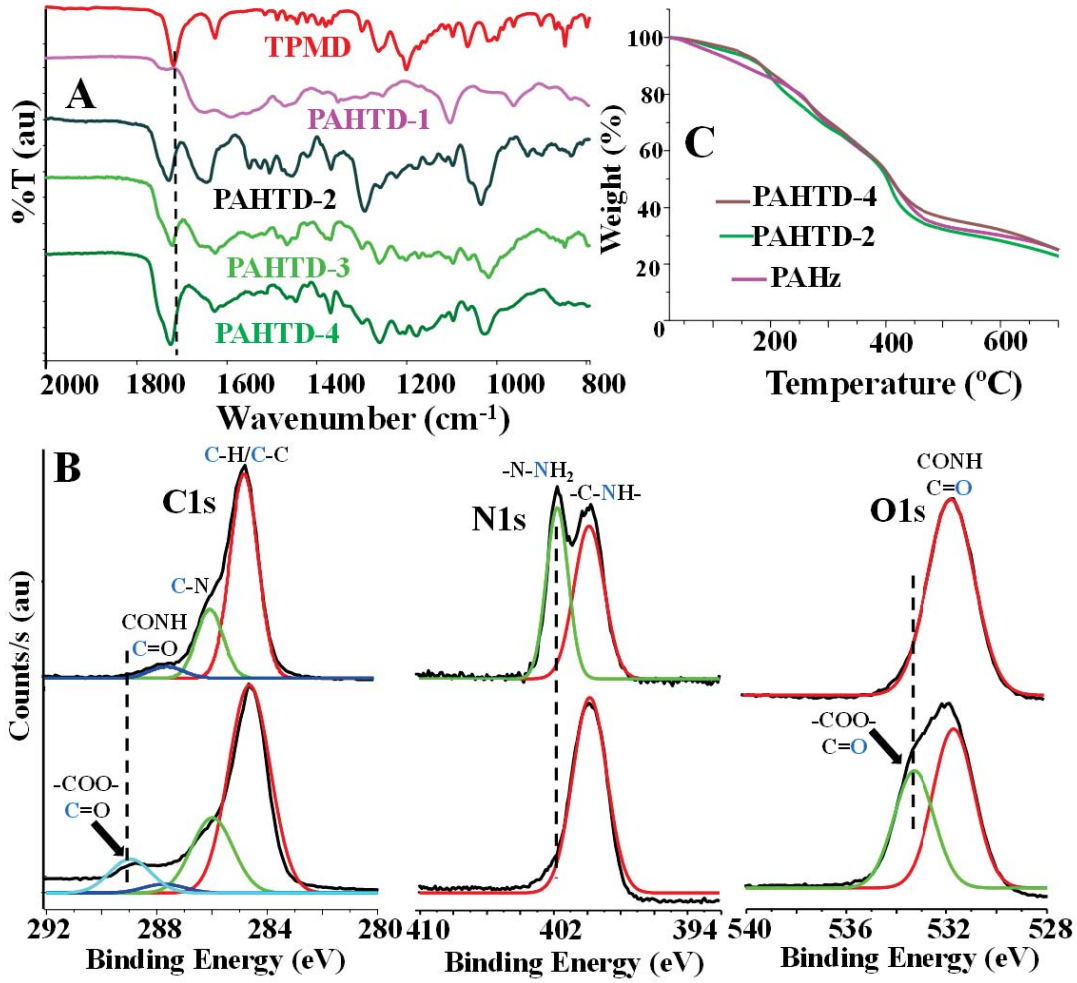

Figure 2.9: (A) FTIR and (C) TGA traces of PAHz and the DCNs synthesized under different crosslinking conditions, (B) The C1s, N1s and O1s XPS spectra of PAHz and PAHTD-4 films recorded at 90° incident angle.

The average enhancement in weight of the films by ∼10 wt % after cross-linking further supported the quantification data from UV-vis spectroscopy. The mechanical properties of the PAHTD DCNs were measured, and the effect of d_c on tensile data was investigated. The d_c of the PAHTD films was calculated from the rubbery plateau modulus data of the DMTA analysis using the expression[211]

$$d_c(mol/cm^3) = E'/RT \tag{2.1}$$

where ER' is the relaxed rubbery modulus in MPa, R is the universal gas constant in MPa, R is the universal gas constant in J/(mol K), and T is the temperature in K.

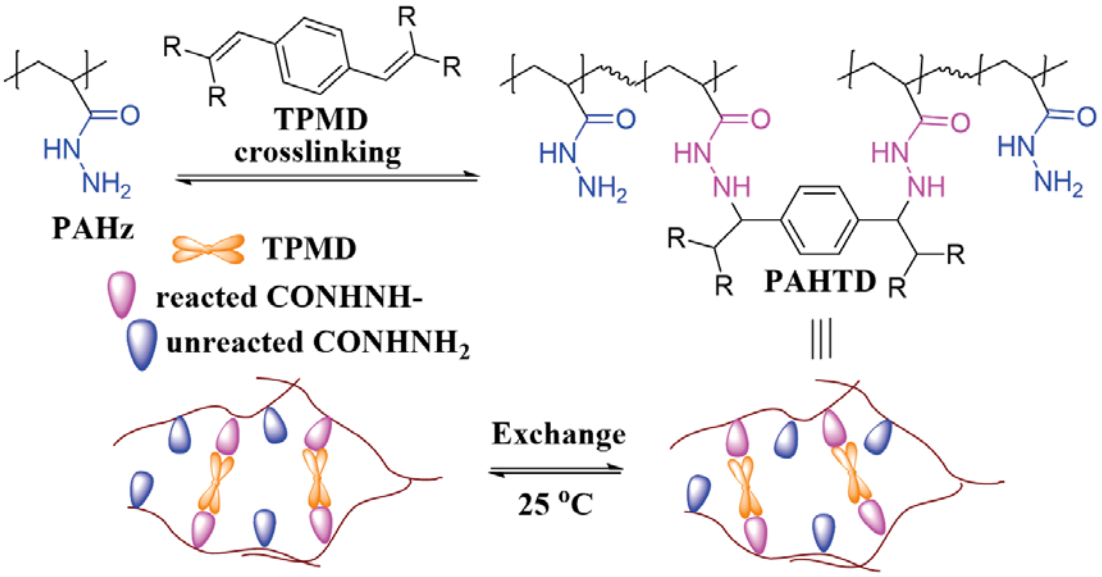

Scheme 2.4: Synthesis of DCNs (PAHTD) based on hydrazide Michael Addition and autonomous exchange of the $CONHNH_2$ donors in the Michael adduct linkages present in the DCN.

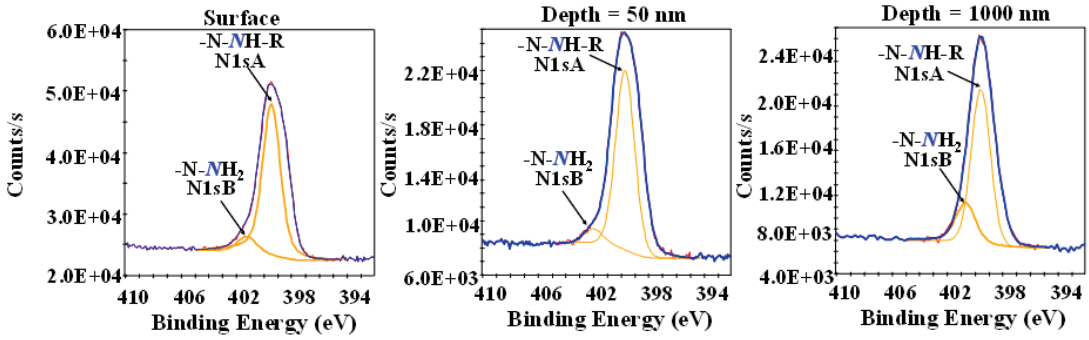

Figure 2.10: The depth profiling XPS data of the PAHTD-4 film recorded at different depths from the surface. The depths were created by controlled etching of the films using Ar-cluster ion beam in K-Alpha+ XPS. The atomic % of the N1s peaks at 400.0 and 402.0 eV are assigned as A and B respectively.

The d_c value increased from 0.008 mol/cm^3 (PAHTD-1) to 0.113 mol/cm^3 (PAHTD-4) on optimization of the cross-linking condition (Table2.2). The E' values in the frequency scans were $\sim$1 order higher compared to the corresponding E'' values supporting the strongly cross-linked nature of the networks (Figure2.11A). The water content in THF-water mixture was limited to 5 vol %, since further increase in water amount precipitated the TPMD. The DCN (PAHTD-4) synthesized in a solution of THF:water (95:5, vol:vol) and 10 wt % TPMD exhibited a E' value of $\sim$4.4 GPa after 12 h of reaction time (Figure2.11B).

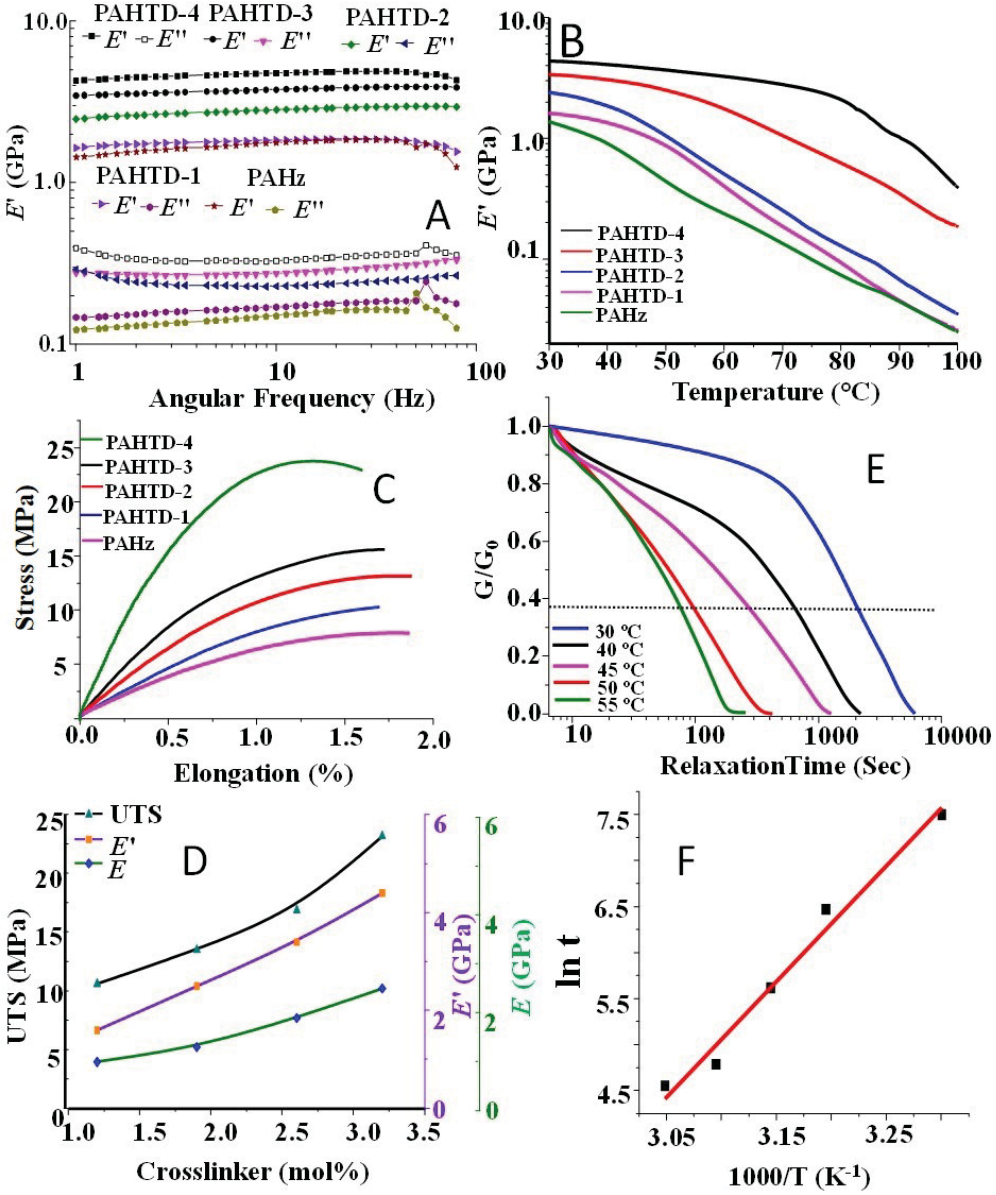

Figure 2.11: (A) Frequency sweep data, (B) DMTA traces and (C) tensile plots of the PAHTD networks, (D) Effect of crosslinker content on the UTS, E and E′ of PAHTD, (E) the stress relaxation data and (F) Arrhenius plot of PAHTD-4 created from stress relaxation data. The tensile data in C were recorded at 5 mm/min strain rate.

The UTS and E values gradually increased with the increase in TPMD mol % in DCNs (Figure2.11D). The UTS ($\sim$23.8 MPa) and E(2.5 GPa) values of PAHTD-4 were $\sim$3 times higher compared to that of the PAHz (UTS $\approx$ 7.8 MPa, $E \approx$ 0.7 GPa) (Figure2.11D and Table2.2). To further support the cross-linked nature of the PAHTD DCNs, the PAHz film was functionalized with a suitable mono functional control molecule (DBM) possessing one

activated double bond. The reaction was performed using conditions similar to that of the synthesis of PAHTD-4 .The FTIR band assigned to C=O stretching of DBM shifted from 1730 to 1738 cm^{-1}, and the C=C band at 1630 cm^{-1} disappeared, supporting the functionalization through hydrazide Michael addition. The amount of DBM in the PAHz film was quantified based on the UV-vis spectroscopic analysis and determined to be 3.7 mol % of $CONHNH_2$ groups in the system. The E (0.7 GPa) and UTS values (7.5 MPa) of the DBM attached PAHz (PAHz-DBM) film were comparable to that of the PAHz precursor ($E \approx 0.7$ GPa, UTS $\approx$ 7.8 MPa) and reasonably lower in comparison with the PAHTD-4 ($E \approx 2.5$ GPa, UTS $\approx$ 23.8 MPa) (Figure2.11C). Furthermore, PAHz-DBM sample disintegrated on dipping in water for 5 min only, whereas the PAHTD-4 softened on dipping in water for 12 h with no observable cracks on the surface of the film. This observation supported the cross-linked nature of the PAHTD-4. The T_g values of PAHz and the PAHTD DCNs (60-67 °C) were obtained from the tan δ traces (Figure2.12A-E). The T_g value of PAHTD-1 (60 °C) increased by 14 °C in comparison with the PAHz precursor (46 °C). The T_g value of the DCNs gradually increased to 67 °C with the increase in dc value from 0.008 to 0.11 mol/cm^3. The T_g values of PAHz (50 °C) and PAHTD DCNs (56-60 °C) obtained from the DSC analysis supported the DMTA data (Figure2.12F). The stress relaxation data of PAHTD-4 were recorded under variable temperature conditions (Figure2.11E). The Arrhenius plot obtained from the relaxation times at normalized stress value of 0.37 was linear, suggesting typical vitrimer behavior (Figure2.11F). The Ea value (109.5 $\pm$ 10.9 kJ/mol) obtained from stress relaxation data was higher in comparison with the model compound ($\sim$86.1 kJ/mol) studies (Table2.1). The difference between these two data may be attributed to the fact that the stress relaxation studies were performed in the solid state under a restricted environment, whereas the model reactions were performed with small molecules in diluted solution.[212] Interestingly, the nature of stress relaxation curve changed for temperature scans of 50 °C and above (Figure2.11E). Because the onset of T_g peak for PAHTD-4 was observed at $\sim$50 °C, the above change in stress relaxation behavior may be attributed to the combined effect of exchange reaction and softening of the sample (Figure2.12).

The freezing transition temperature was calculated by extrapolating the viscosity value up to 10^{12} Pa·s as reported earlier.[213, 214] The value was found to be -9.2 °C (Figure2.13) Both the stress relaxation and freezing transition temperature data suggested that this hydrazide Michael addition chemistry based thermoset is highly malleable at 30 °C. Importantly, the DCNs maintained high structural integrity under ambient conditions, and no visible change in sample configuration of PAHTD-4 was noticeable over 3 months of study period. The tensile properties also remained unchanged after 3 months of sample preparation. Several strong DCNs possessing room temperature malleability are already reported in the literature.[215, 216] The hysteresis behavior of PAHTD-4 under both tension and compression was monitored to understand the performance under load.

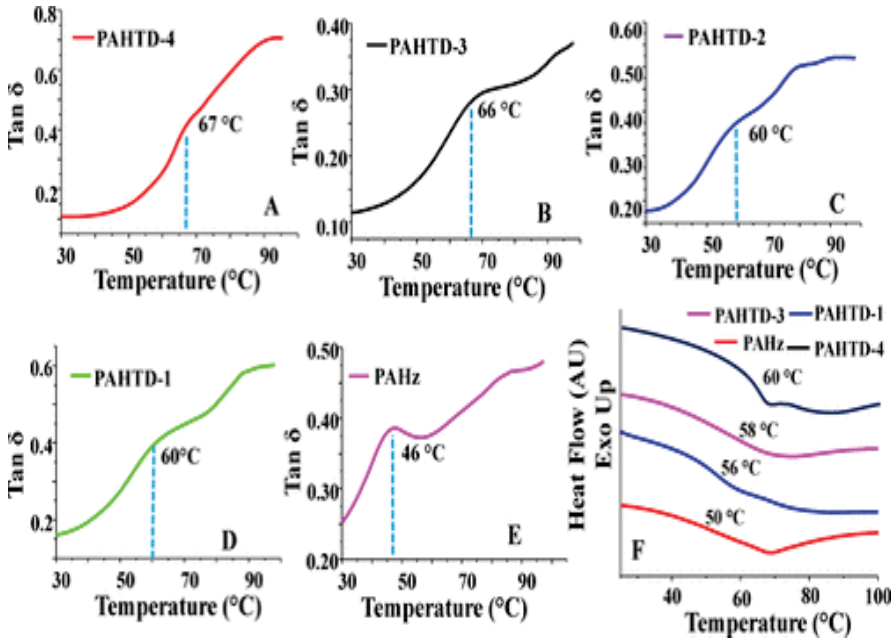

Figure 2.12: Tan δ versus temperature traces of (A) PAHTD-4, (B) PAHTD-3, (C) PAHTD-2, (D) PAHTD-1, and (E) PAHz films obtained from DMTA analysis, (F) The second heating DSC traces of PAHz and PAHTD DCNs recorded under a N_2 atmosphere at a heating rate of 10 °C/min.

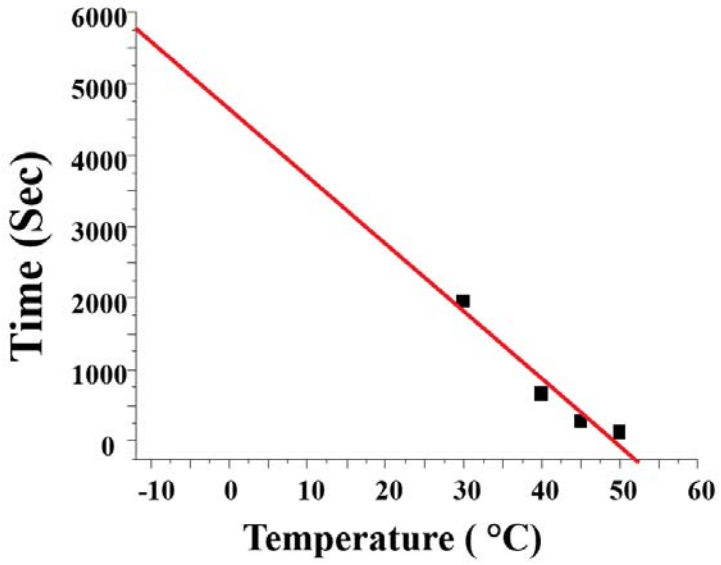

Figure 2.13: Freezing transition temperature calculation by extrapolating of viscosity value. The plot corresponds to the relaxation time and temperature values of the stress relaxation curve of PAHTD-4 at G/G° = 0.37.

Both the tensile and compressive hysteresis cycles were recorded under similar stress (∼20 MPa) and strain (∼0.8-1.0%) conditions (Figure2.14A-B). The loading curves of tensile stress-strain loop revealed a compliant behavior until limiting stress value (20 MPa) (Figure2.14A).

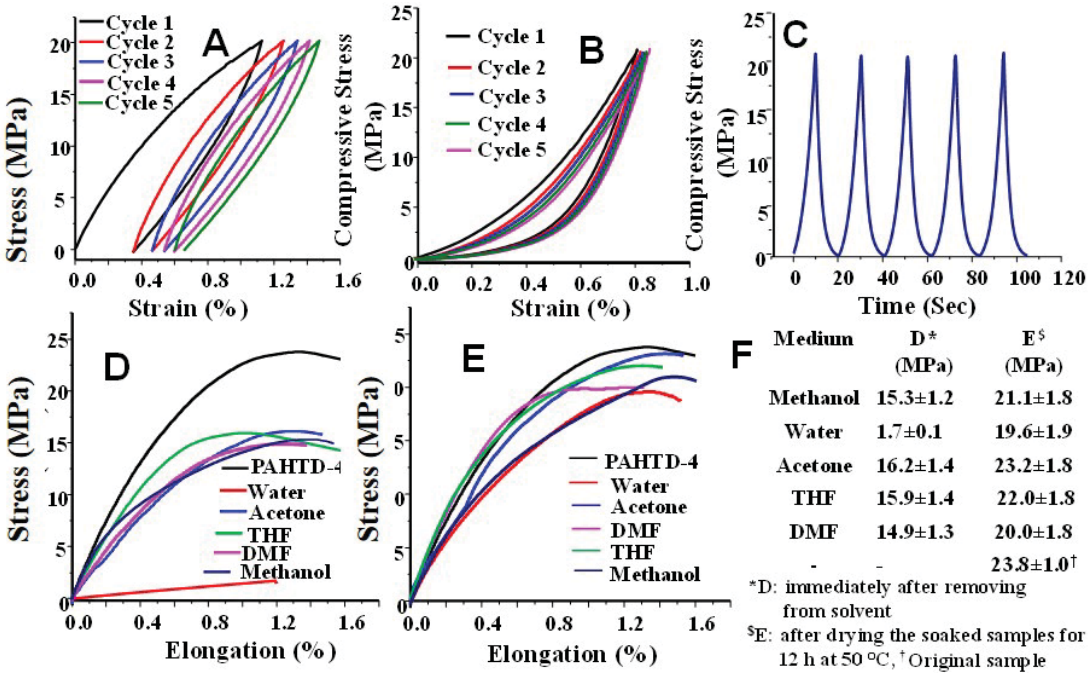

Figure 2.14: Hysteresis curves for PAHTD-4 from uniaxial (A) tension and (B) compression cycles recorded under control stress (20 MPa) mode, (C) compressive stress versus time profile data of PAHTD-4 for five continuous cycles, the tensile plots of PAHTD-4 after, (D) immediately removing from the solvent, (E) drying the soaked samples at 50 °C for 12 h, (F) the UTS values of solvent treated PAHTD-4 samples.

Each loading-unloading cycle was associated with a hysteresis loop and residual strain up to 0.3%. This trend recommended that the recovery of PAHTD-4 from tensile load is not quantitative. The residual strain value was maximum for first cycle, and gradually decreased with the number of cycles. The dissipation energy was calculated from the area under hysteresis loop of each cycle. Under tension, the dissipation energy observed for the first cycle was 71.1 kJ/m^3, which subsequently decreased to 41.3 kJ/m^3 for the second cycle. The higher loss in the first cycle in comparison with the subsequent cycles could be attributed to the change in morphology of the samples under deformation[217] The stress-strain cycles under compression showed a viscoelastic behavior with significant hysteresis during each cycle (Figure2.14B). Importantly, the residual strain at the end of each cycle was negligible unlike the tension data and the unloading cycles almost superimposed upon each other.

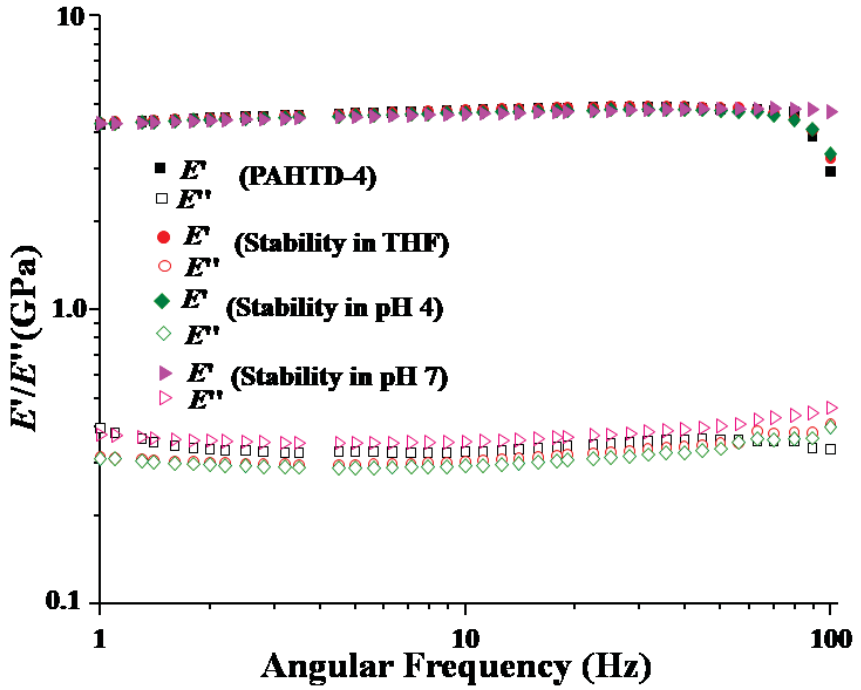

Figure 2.15: The frequency sweep plots of the PAHTD-4 recorded after keeping the network in THF, pH 4 and pH 7 for 12 h. The samples were removed and dried in oven for 12 h at 50 °C before recording the data.

The dissipation energy value for the first cycle (26.2 kJ/m^3) under compression was reasonably lower in comparison with the tensile cycle (71.1 kJ/m^3). This suggested that the recovery of these DCNs from compressive stress may be superior in comparison with the tensile stress. The DCNs softened in water because of the presence of hydrophilic PAHz. A typical PAHTD-4 strip dipped in water for 12 h absorbed up to ∼5 wt % of water and the UTS value (1.7 MPa) decreased by ∼93%. The tensile properties (UTS = 19.7 MPa, *E* = 2.3 GPa) were retrieved up to 83% on drying the wet film at 50 °C, suggesting that the absorption of water minimally affected the internal structure of the DCNs (Figure2.14E). The DCNs exhibited adequate solvent resistance. Typical PAHTD-4 strips were dipped in different solvents for 12 h at 25 °C, and the tensile properties were measured. The UTS values (∼14.9-16.2 MPa) of samples recorded instantly after removing from the solvents were somewhat lower compared to that of the original sample (∼23.8 MPa). This minor decrease in UTS value may be attributed to the presence of moisture in these hygroscopic solvents that softened the PAHTD-4 film. As anticipated, the tensile properties (UTS ≈ 19.6-23.2 MPa) of the solvent-treated samples after drying became comparable to that of the original film (Figure2.14 D-E). The E′ values and nature of the DMTA traces of the solvent treated and subsequently dried films remained identical with that of the original sample (Figure2.14).

These DCNs showed somewhat higher thermal stability (170 °C) compared to that of the PAHz (∼100 °C) (Table2.2 and Figure2.9C). The weight loss in TGA traces occurred in three steps with maximum loss occurring between 250 and 350 °C. The loss around 250 °C could be aasigned to the decomposition of labile β-carbonyl esters present in the TPMD moiety.

2.4.2 Recyclability and Self-Healing of the Network

These DCNs hold a large concentration of free $CONHNH_2$ groups along with the hydrazide Michael adduct linkages. This accelerated the opportunity of self-healing of damages in the samples through spontaneous exchange reactions in the bulk of the PAHTD films (Scheme2.4). To ease the movement of polymer chains and facilitate self-healing, the PAHTD-4 films were softened by dipping in THF:H_2O (95:5, vol:vol) mixture for 3 h.

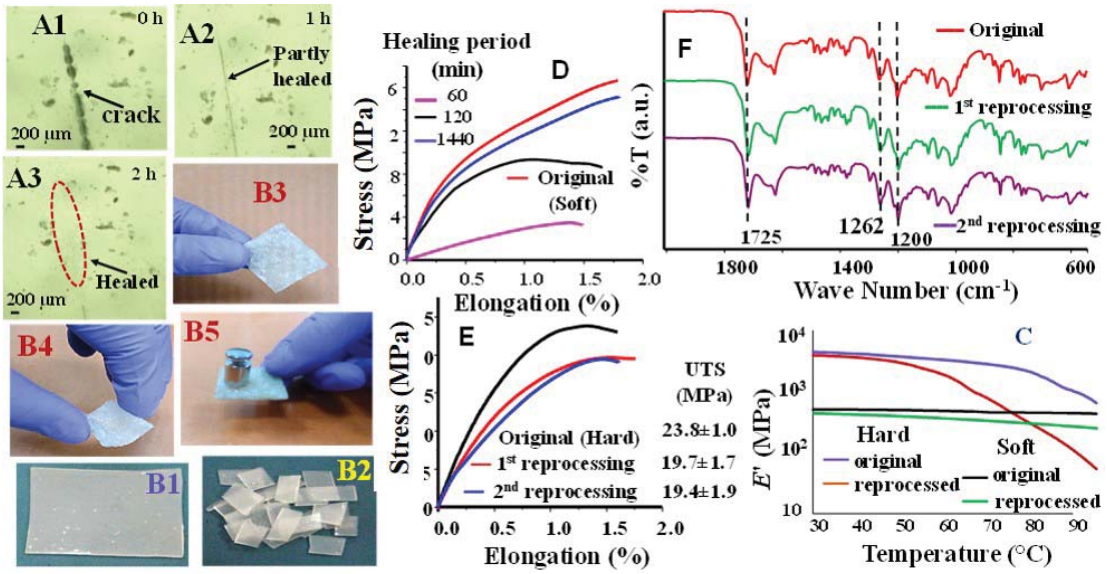

Figure 2.16: (A1) PAHTD-4 soft film with a cut made using razor blade, A1 after (A2) 1 h and (A3) 2 h of self-healing, (B1) as prepared soft PAHTD-4 film, (B2) B1 cut into small pieces, (B3) reprocessed B2 (the cut pieces were assembled in aluminum foil and pressed under 1 kg load for 48 h), (B4) flexibility of B3, (B5) B3 after drying at 50 °C for 12 h, (C) the DMTA data of reprocessed soft and hard PAHTD-4 film, (D) the tensile data of B3 after different self-healing time interval, (E) the tensile data of original and reprocessed hard PAHTD-4 films (the films were reprocessed in soft state and dried subsequently). (F) the FTIR data of original and reprocessed film.

The T_g peak at 67 °C disappeared, and the E′ value decreased by 1 order after soaking PAHTD-4 film with water, suggesting softening of the sample (Figure2.14C). The crack healing of the resulting PAHTD-4 soft thin film (water content ≈4.0 wt %) at ambient conditions was monitored under microscope. A thin cut (width ≈120 μm) created on the surface of the PAHTD-4 using a razor blade quantitatively healed within 2 h and the damage site was unrecognizable after this period (Figure2.16A1-A3). The self-healing efficiency was quantified based on UTS analysis. Two PAHTD-4 soft films were end-on overlapped, pressed under 1 kg load, and allowed to self-heal at room temperature. The UTS value gradually increased with self-healing period and recovered up to 88% of the original value (1.7 MPa) after 24 h, suggesting close to quantitative healing (Figure2.16D).

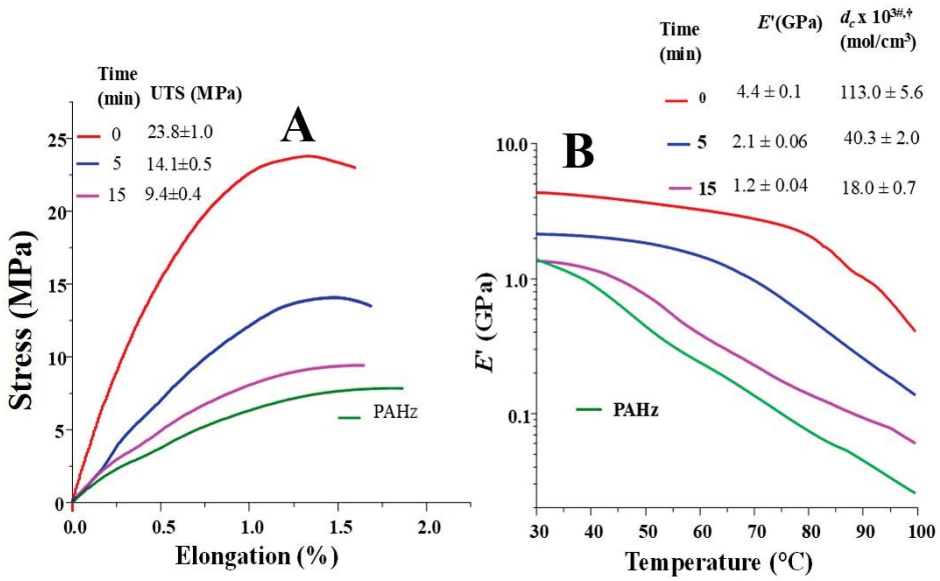

Figure 2.17: (A) Tensile and (B) DMTA traces of the de-crosslinked PAHTD-4 in NH_2NH_2 solution after different time intervals. #the values were obtained from DMTA analysis. †the value was obtained from the rubbery modulus data at 100 °C.

The reprocessability of these DCNs was accessed by cutting a soft PAHTD-4 film into small pieces (Figure2.16B1-B2). The cut pieces were assembled in an aluminum foil and pressed under a nominal 1 kg load at 25 °C. The pieces joined together in 48 h to result in a flexible continuous film. The E' value of the reprocessed soft film (0.4 GPa) was comparable to that of the original soft sample (0.5 GPa) (Figure2.16C).The reprocessed film was subsequently dried at 50 °C for 12 h. Possibly, evaporation of water rebuilt the CO-HN hydrogen-bonding interactions in the system and stiffened the films. The UTS (19.7 MPa) and E (∼1.9 GPa) values of the resulting film were somewhat lower compared to those of the original film (UTS ≈ 23.8 MPa and E = 2.5 GPa) (Figure2.16E). This suggested that the reprocessability of these DCNs is associated with a minor loss in tensile properties. The minor

loss in tensile properties during reprocessing could be assigned to the presence of possible voids created during the molding process by simply assembling the small pieces together.

Importantly, the UTS (19.4 MPa) and E (1.7 GPa) values of the twice reprocessed film were similar to those of the first reprocessed film (Figure2.16E). The E' value (3.8 GPa) of reprocessed and dried PAHTD-4 was comparable to that of the original PAHTD-4 (4.4 GPa) (Figure2.16C). FTIR traces of the original and reprocessed samples were compared to access possible structural changes occurred during reprocessing (Figure2.16F). The intensity and positions of critical bands at 1725 and 1262 cm^{-13} accountable to C=O and C-O bonds remained unchanged, suggesting the reprocessing has least affected the chemical linkages in the DCN.

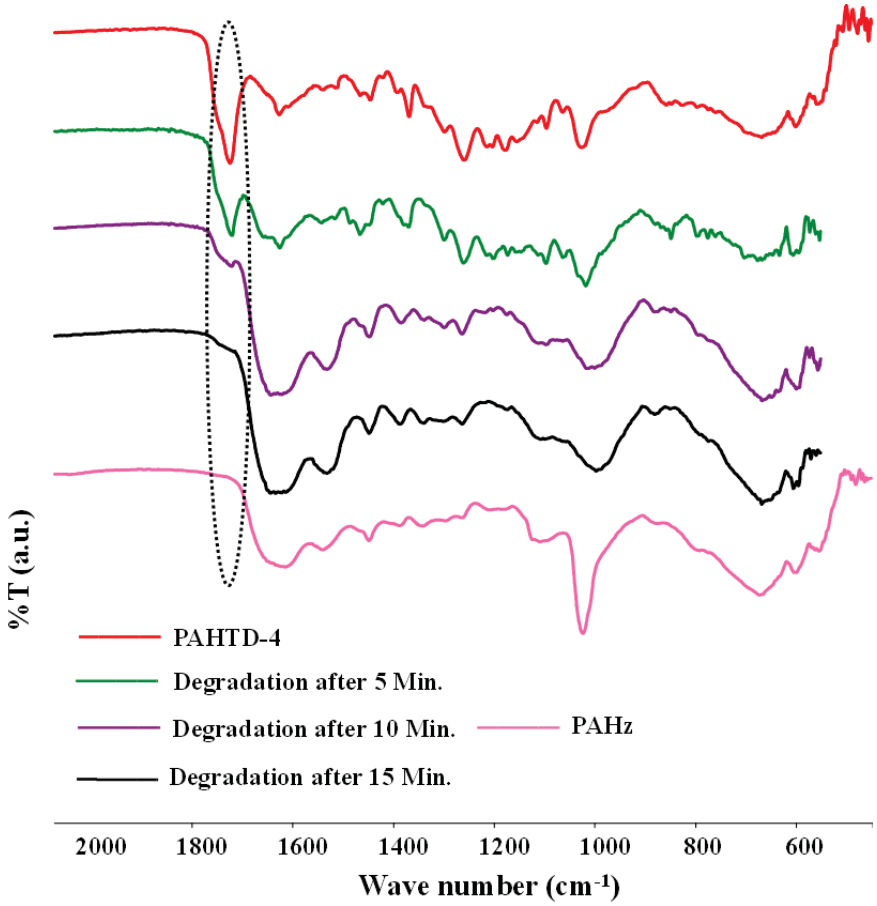

Figure 2.18: ATR FTIR spectroscopic data for the degradation of PAHTD-4. The network thin films were dipped in NH_2NH_2 solution (NH_2NH_2: THF = 1:10, vol:vol) at 25 °C. The samples were removed from the solution at different time intervals, washed repeatedly in water and dried before recording the spectra.

These DCNs were depolymerizable in the presence of NH_2NH_2. The d_c of PAHTD-4

films readily decreased from 0.1 to 0.02 mol/cm^3 within 15 min of dipping in NH_2NH_2 solution at 25 °C, supporting depolymerization of the DCN (Figure2.17). The UTS, E′, and *E* values became comparable to that of the PAHz film, suggesting release of most of the TPMD and retrieval of the PAHz film. The FTIR spectroscopic data revealed gradual decrease in intensity of the C=O band and removal of TPMD from the matrix (Figure2.18). Overall, both hydrazide Michael addition of -$CONHNH_2$ with TPMD and the corresponding exchange reactions are facile under ambient and catalyst-free conditions. The resulting DCNs based on above Michael addition possess adequate tensile properties and display swift recyclability and self-healability at ambient temperature conditions. Due to the above, the DCNs are anticipated to show sustainability and long self-life. In future, this hydrazide Michael addition chemistry we may use to develop various dynamic thermoplastic elastomers by suitably designing the precursors. This autonomously exchangeable covalent chemistry offers a discrete advantage over a range of conventional dynamic covalent linkages those typically require catalyst or external stimuli in form of heat or light energy to exhibit dynamic behavior. The fast exchange dynamics of covalent linkages have already shown promises in various areas like controlled release,[218] 3D cell encapsulation,[219] biomedical implants,[220]sensing,[221] and energy storage applications.[222] The swift exchangeability of reported dynamic hydrazide Michael adducts may be utilized in future for similar applications.

2.5 Conclusions

The $CONHNH_2$ functionality is a suitable donor to form stable Michael adducts with highly activated double bonds under ambient and catalyst-free conditions. As per the kinetic data, the adducts based on aromatic $CONHNH_2$ are more stable compared to that of aliphatic analogues. These Michael adduct linkages are spontaneously exchangeable under ambient conditions. The DCNs derived based on this Michael addition chemistry are cost-effective, possess adequate strength and modulus, and exhibit recyclability along with self-healing ability. Advantageously, the cross-linking is effective both under homogeneous and heterogeneous conditions. The thermal stability of these networks is up to 170 °C, and this moderate stability is assigned to the heat-sensitive β-keto ester linkage present in the samples. These DCNs display adequate solvent tolerance. NH_2NH_2 may also be used to depolymerize these polyhydrazide Michael adducts. This dynamic Michael addition chemistry is swift, easy to carry out both under homogeneous and heterogeneous conditions, and may be extended to develop dynamic polymers targeting controlled release, biomedical, sensing, and energy storage applications.

Chapter 3

Catalyst Free Partially Bio-Based Polyester Vitrimers

3.1 Abstract

Most of the vitrimers based on ester linkages reported so far contain a Lewis acid or a strong organic base as the trans-esterification catalyst. The recyclability and reusability of these vitrimers is dependent on the catalyst retention, stability and sintering issues. Herewith, a set of β-activated ester based vitrimers are described that can be thermally reprocessed at $\sim$150 °C under catalyst free conditions. The relaxation temperature decreases to 110 °C in presence of $Sn(Oct)_2$. Importantly, the precursor of these vitrimers; malonic ester is a cost effective naturally occurring ester and can be extracted from various fruit juices. As a proof of concept, polyhydroxyethyl methacrylate is used as the hydroxyl precursor for the synthesis of vitrimers. These vitrimers show adequate tensile strength (11.3 to 33.0 MPa), elongation (80 to 290%) and resilience. The materials can be successfully self-healed and reprocessed in presence of heat without sacrificing the tensile properties. The vitrimers based on $Sn(Oct)_2$ show mechanical properties similar to that of the catalyst free analogs and reprocess at $\sim$110 °C. These vitrimers may potentially be utilized for the development of biomaterials, coatings, hydrogels, adhesives commodity and adhesives plastics in the future.

3.2 Introduction

Polyester resins are one of the significant industrially important versatile materials owing to their uses in packaging, apparel, transport, construction, piping, adhesive, marine, biomedical, electronic devices and aerospace applications.[223, 224] The polyester networks are beneficial compared to other conventional thermosets due to the biodegradable nature of ester linkage.[225]However, the inability of conventional polymer networks to reprocess have so far restricted their commercial usability. Especially, the recent environmental concerns related to the accumulation of plastic wastes on the planet have delayed their further development and utilization. The recent prominent discovery of vitrimer have obtainable the possibility of developing thermally processable and recyclable covalent networks based on ester linkages.[226]These materials combine excellent mechanical properties of conventional thermosets and high temperature malleability of thermoplastics.[227] The chemical crosslink in vitrimers undergoes exchange reaction at elevated temperature that permits topology change of the materials leading to processability, reshapability and remoldability. In addition to the above, the vitrimers are known to display important material properties such as self-healability,[228] shape memory ability,[229] adhesiveness[230] and stimuli-responsibility.[231] Vitrimers based on boronic ester,[232] silyl ether,[233] hindered urea,[234] aminal transamination,[235] dioxa-borolane,[236] carbonate,[237] amine-urea,[238] oxime-ester[239] and enamine[240] dynamic linkages are described in literature. Recently, the type and mechanism of bond exchange, mechanical properties, their usefulness and different functionalities used for vitrimer development are thoroughly elaborated in recently published reviews.[241, 242] Vitrimers have shown potential in the area of adhesive,[243] tissue engineering,[244] actuator,[245] nanolithography,[246] and coating[247] for future applications.

A number of vitrimers based on various ester linkages are recently described in literature. [248, 249] Typically, vitrimers based on dynamic ester linkages possess a transesterification catalyst, such as $Ti(OPr)_4$, $Zn(Ac)_2$, $Sn(Oct)_2$, and $Zn(acac)_2$ or an organic base, i.e.TBD, DBU, .[250, 251] The temperature of relaxation is maintained above 200 °C to achieve swift processability.[252, 253] Recently, several activated precursors are designed and studied to lower the processing temperature of the polyester vitrimers. For example, lactide based polyesters showed very fast relaxation time under moderate temperature condition of 140 °C in presence of $Sn(Oct)_2$.[254] Similarly, the transesterification of β-hydroxy esters were quantitative within one hour at 150 °C under 5 mol% catalyst loading.[255] In some cases, the stoichiometry between ester and hydroxyl groups was used as the tool to facilitate the trans-esterification.[256] However, repeated recyclability of these catalyst based polyester vitrimers is dependent on the catalyst retention, stability and sintering issues. Addi-

tionally, some of the trans-esterification catalysts used for these vitrimer synthesis, gradually evaporate or decompose on heating above 200 °C. Therefore, catalyst free vitrimers based on ester linkages are necessary for long self-life and potential commercial applications.

Nucleophilic substitution reactions of activated esters possessing a keto or cyano group at β position are known to freely occur compared to that of the conventional esters.[257] For example, the β-keto esters readily underwent amidation under room temperature conditions in a fairly short time period.[258, 259] Similarly, the reaction of β-cyano esters with primary amines was quantitative overnight at moderate temperature (50 °C) conditions.[260] Importantly, the trans-esterification of β-keto esters with primary alcohols are described to occur at $\sim$110 °C under catalyst free conditions.[261, 262] Recently, we have displayed that amidation of β, β'-diester compound is rapid under ambient conditions.[263] We assumed, the trans-esterification of β, β'-diesters to be facile and occur under moderate temperature conditions in presence or absence of a typical trans-esterification catalyst. Diethyl malonate (DEM) is a low cost β, β'-diester and present in various fruit juices such as pineapple, guava, and blackberry etc. DEM is already used as a precursor for synthesis of polyesters in literature.[264, 265] However, vitrimers based on this β activated ester have up to now not been explored in literature to the best of our knowledge. In this report, we have studied the rate of trans-esterification using DEM as the model compounds under catalyst free conditions. Subsequently, the trans-esterification is observed in presence of β, β' under mild temperature conditions. Several vitrimers based on diethyl malonate are designed and manufactured using the above trans-esterification reaction as key reaction and polyhydroxyethyl methacrylate (PHEMA) as the hydroxyl precursor. The mechanical and thermal properties of the resulting vitrimers are studied. The processability and recyclability of these vitrimers are analyzed.

3.3 Experimental

3.3.1 Materials

DEM (SD Fine Chem., 98.0%), n-hexanol (Alfa Aesar, 98.0%), Tin (II) 2-Ethylhexanoate ($Sn(Oct)_2$, >85.0%), 2-Hydroxyethyl Methacrylate (TCI Chemicals, >95.0%), α, α-Azoisobutyronitrile (AIBN, Spectrochem, 98.0%), THF (Qualigens, 99.0%), Methanol (SD Fine Chem., 99.0%), $CDCl_3$ (Sigma Aldrich, 99.8 atom %D) were used as received.

3.3.2 Characterization

All ^{1}H and ^{13}C NMR spectroscopic data were recorded in JEOL-400 YH NMR Spectrometer at 25 °C probe temperature using $CDCl_3$ solvent. Agilent Accurate-Mass Q-TOF LC/MS 6520 was used to record mass spectra MS (ESI-HRMS) and peaks were given in m/z (% of basis peak). The FTIR spectra was recorded in ATR mode using Perkin Elmer Spectrum Two. H5KL UTM (Tinius Olsen) was used to measure the ultimate tensile strength (UTS) following Generic Tensile mode at a machine speed of 5.0 mm/min. The samples of width ∼4 mm and thickness ∼0.8 mm were used during measurements and the average of three measurements were taken for data representation. The Young's moduli (E) of the specimens were calculated from the Hookean region of the tensile trace. DMA Q-800 TA instrument was used for dynamic mechanical analysis using tension mode and 50 ASTM D4065-01 norm. The rectangular samples of width ∼4.5 mm and thickness ∼1.0 mm were used for analysis. For stress relaxation experiment, we have used DMA Q800 under compression mode. The samples (dimension 10 x 10 x 3 mm^3) were compressed at constant strain of 0.5% and the data was collected after 10 min of temperature equilibration. During data analysis, the E' value was normalized first and the activation energy (Ea) was calculated from the temperature versus relaxation time plot using standard procedure.

3.3.3 Synthesis of hexylmalonate (Exchange Product)

Diethylmalonate (DEM) (0.5 g, 3.1 mmol) and n-hexanol (1.3 g, 12.5 mmol) were taken in a Round Bottomed Flask for trans-esterification reaction without catalyst at 150 °C for 3 h or in presence of $Sn(Oct)_2$ (62.3 mg, 0.16 mmol) at 100 °C under solvent free conditions for 5 h. ^{1}H NMR (400 MHz, $CDCl_3$) δ (ppm): 4.1 (t, 4H, -COOC$\boldsymbol{H}_2$CH$_2$-), 3.3 (s, 2H, -C$\boldsymbol{H}$(COO)$_2$-), 1.6 (m, 4H, -CH$_2-$C$\boldsymbol{H}_2-$CH-), 1.3 (m, 12H, -C$\boldsymbol{H}_2-$C$\boldsymbol{H}_2-$C$\boldsymbol{H}_2-$CH$_2$-), 0.9 (t, 6H, -C$\boldsymbol{H}$3). ^{13}C NMR (100 MHz, $CDCl_3$): δ (ppm) 167.1 (-$\boldsymbol{C}$OO-), 65.8 (-O$-\boldsymbol{C}$H$_2$), 41.8 (-$\boldsymbol{C}$H$-$(COO$-$)$_2$), 31.5 (-$\boldsymbol{C}$H$_2$-), 28.3 (-$\boldsymbol{C}$H$_2$-), 22.7 (-$\boldsymbol{C}$H$_2$-), 14.1 (-$\boldsymbol{C}$H3). FT-IR (cm^{-1}): 726 (s, C-H), 894 (w, C-H), 1149 (s, C-O), 1736 (s, -COO-), 2861 (m, C-H), 2930 (m, C-H), HRMS (ESITOF) m/z: [M + H] Calculated for [$C_{15}H_{28}O_4$] 273.2067. Found 273.2066.

Poly (2-Hydroxyethyl Methacrylate (PHEMA) (M_n = 211000 g/mol) was synthesized using free radical polymerization of 2-hydroxyethyl Methacrylate utilizing 1 mol% AIBN initiator following reported procedure.[266]

3.3.4 Synthesis of polyester networks based on PHEMA & DEM (PHEMA-DEM-x)

A typical synthesis of polyester based networks is described below. PHEMA (Mn = 211000 g/mol, 1 g, 7.7 mmol with respect to OH group) was dissolved in methanol. To it DEM (0.4 g, 2.5 mmol) was added and mixed thoroughly using a magnetic stirrer. The mixture was then transferred into Teflon Petri dish. The methanol was evaporated and the solution was heated at 150 °C for 3 h. Using a similar process, four different networks were synthesized by varying the molar ratio of [OH] to [COOEt] groups in the crosslinking mixture.

3.3.5 Synthesis of PHEMA-DEM-xC

A set of polyester networks were prepared by adding $Sn(Oct)_2$ to the mixture of PHEMA and DEM before crosslinking. The mixture of PHEMA (2.0 g, 15.4 mmol with respect to OH group), DEM (0.8 g, 5 mmol) and $Sn(Oct)_2$ (0.1 g, 0.25 mmol) were prepared at 25 °C in methanol. The mixture was stirred for 5 min and the methanol was evaporated under ambient conditions. The resulting mixture was dried at 100 °C for 4 h in heating oven. The nomenclature of the networks is PHEMA-DEM-x (catalyst free) or PHEMA-DEM-xC (possesses 5 mol% of $Sn(Oct)_2$ with respect to DEM), where x = [OH]/[COOEt] in the reaction mixture, [OH] and [COOEt] are the molar concentrations of each functionality in the initial reaction mixture (Table S1).

3.3.6 Calculation of Crosslinking Density (d_c)

Crosslinking density was calculated by the following standard procedure available in literature.[267, 268]

$$d_c = E'/RT \tag{3.1}$$

where E′ is rubbery or Plateau Modulus (storage modulus) at 170 °C, "R" = Gas constant in J/ mol °K and T is the temperature in °K.

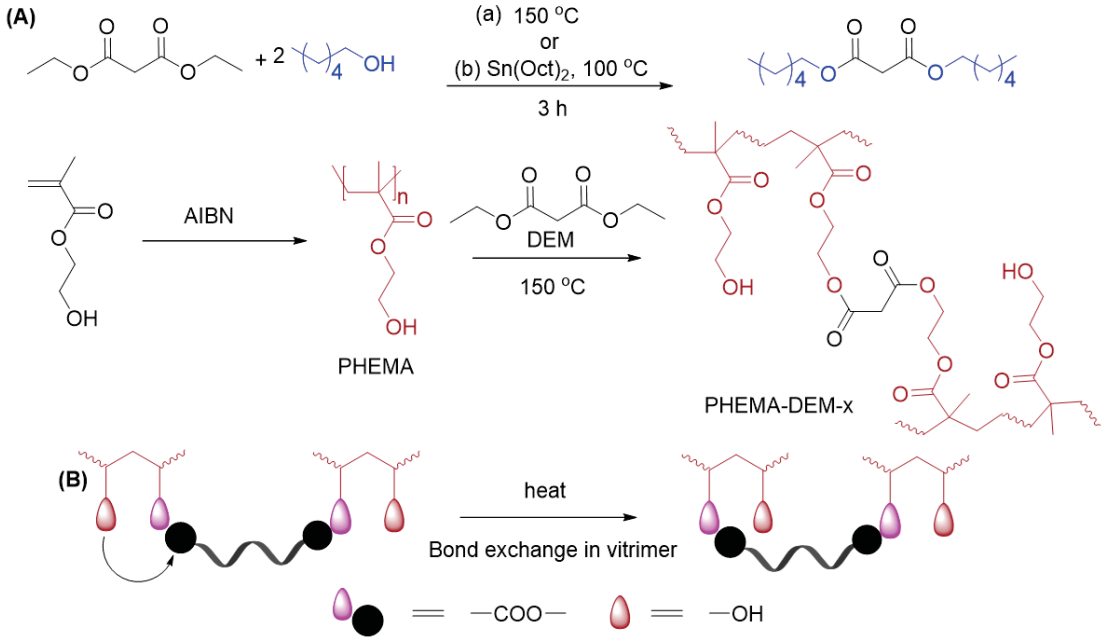

Scheme 3.1: (A) Trans-esterification of model compounds and the synthesis of PHEMADEM- x vitrimers, (B) the schematic shows the exchange of ester bond under thermal conditions.

3.4 Results and Discussions

DEM was selected as the β-activated ester for this purpose, since both the ester functionalities present in DEM possess a -C=O group at the β-position. The reaction of DEM with n-hexanol was performed under solvent free and stoichiometric ([DEM]:[n-hexanol] $\approx$ 1:4, mol:mol) conditions under temperatures in the range of 120 to 150 °C (Scheme3.1). The progress of the trans-esterification was observed by ^{1}H NMR spectroscopy (Figure3.1A). A new triplet at 4.1 ppm responsible to -CH_2CH_2OCO- and multiplet at 1.6 ppm for -$CH_2CH_2CH_2O$- in ^{1}H NMR spectrum supported the formation of trans-esterified product. Similarly, disappearance of peak at 7 61.4 ppm for -OCH_2CH_3 and appearance of peak at 65.8 ppm for -OCH_2CH_2- in ^{13}C NMR spectra suggested successful reaction (Figure3.2). The HRMS data showed the most abundant peak at 273.2066 amu for the M+H peak of dihexyl malonate further supporting the trans-esterification. Ethanol evolved from the trans-esterification reaction continuously evaporated from the reaction mixture due to the volatile nature and shifted the equilibrium towards the product. The conversion versus reaction time plots were built at different reaction temperatures to understand the rate of the reaction (Figure3.1B). The trans-esterification reached equilibrium within 150 min at 150 °C. The rate constant values were plotted against temperature and the activation energy (Ea) was derived

from the slope of the Arrhenius plot (Figure3.1C). The Ea value for the catalyst free reaction was observed to be 110.9 kJ/mol. Similarly, the above trans-esterification was carried out in presence of 5 mol% $Sn(Oct)_2$ at reaction temperatures between 70 to 100 °C. The reaction reached equilibrium within 180 min in presence of $Sn(Oct)_2$ at 100 °C (Figure3.3).

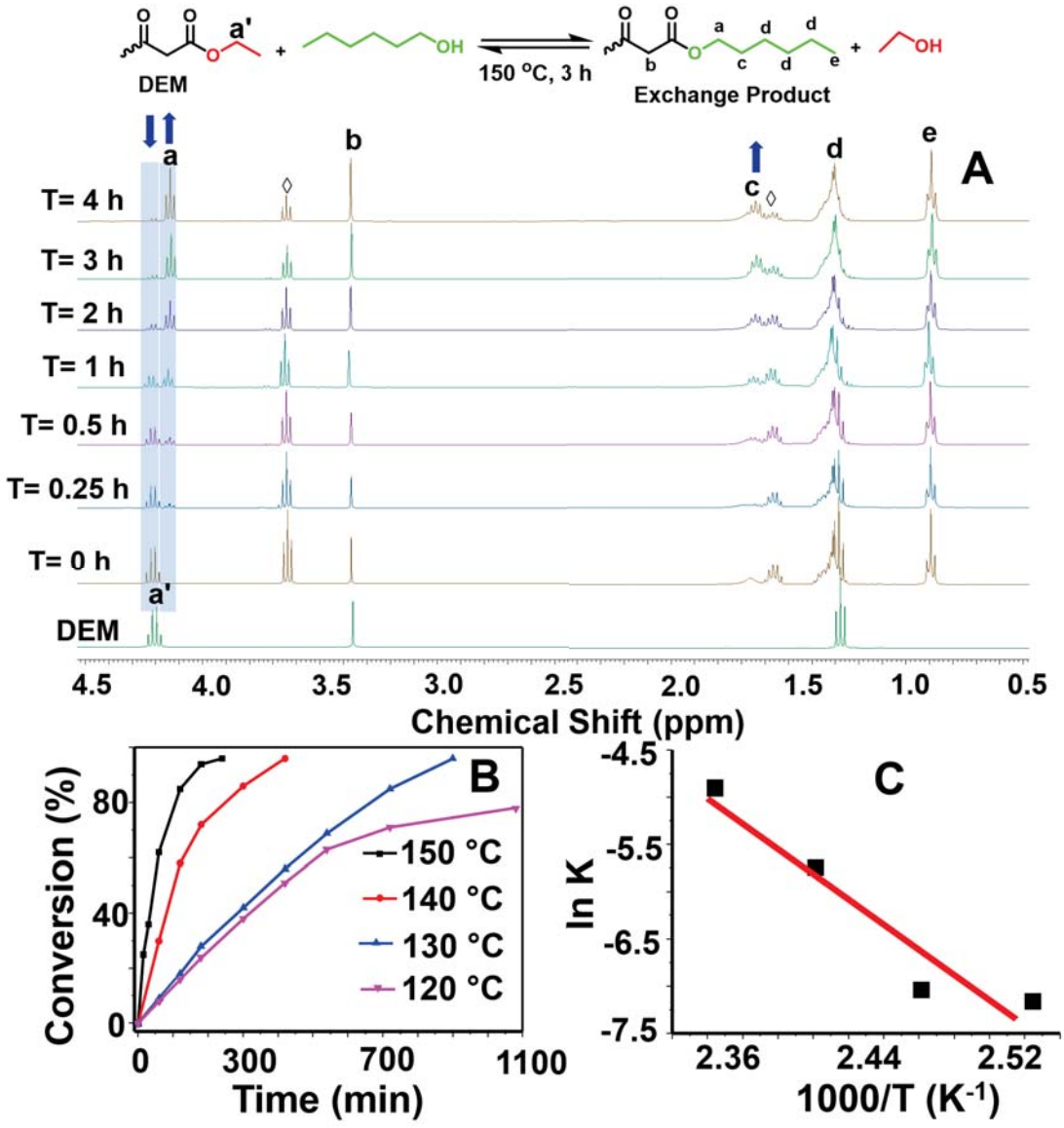

Figure 3.1: (A)^{1}H NMR spectra of DEM and trans-esterified product with n-hexanol after different time interval, (B) the time versus conversion profile of the DEM and n-hexanol trans-esterification under different reaction temperatures, (C) the Arrhenius plot of the trans-esterification reaction. "♢" the peaks assigned to unreacted n-hexanol present in reaction mixture.

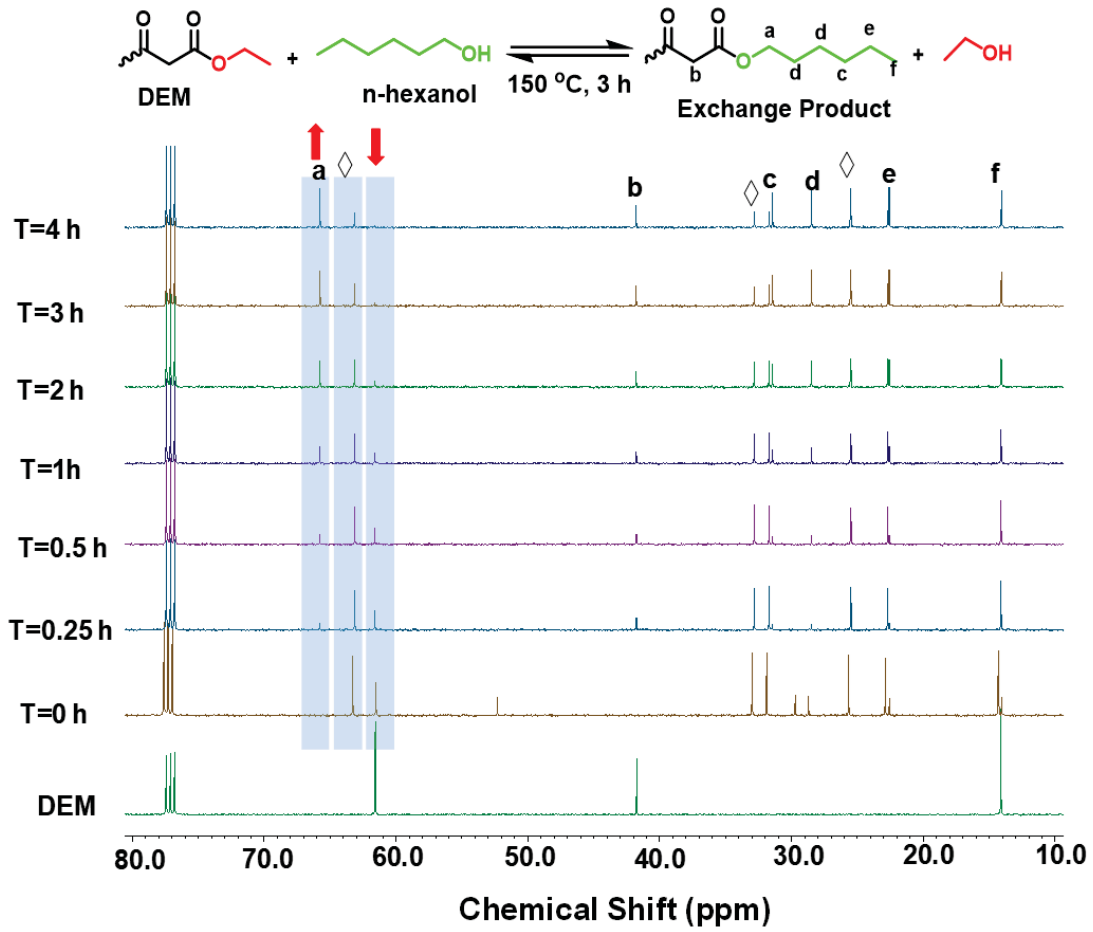

Figure 3.2: ^{13}C NMR spectra of Diethylmalonate and n-hexanol without catalyst at different time interval at 150 °C for kinetics study.

Presumably, the Ea value (79.3 kJ/mol) of the trans-esterification in presence of $Sn(Oct)_2$ was lower compared to that of the catalyst free reaction (Figure3.4). The model compound study shown that the trans-esterification of β,β'-diesters are swift at 150 °C under catalyst free conditions and the temperature may be further decreased to 100 °C if $Sn(Oct)_2$ in small mol% is added to the reaction mixture. A comparatively short reaction time of ∼2-3 h also suggested that the resulting vitrimers based on the above ester linkage may be easily processed at ∼150 and 110 °C in absence and presence of $Sn(Oct)_2$ respectively. A set of catalyst free polyester networks were prepared by using PHEMA as the hydroxyl precursor and DEM as the crosslinking agent (Scheme3.1B). The molar ratio between -OH (PHEMA) and -COOEt (DEM) functionality was varied between 1.5 to 6 (mol/mol) to synthesize four vitrimers. Another set of vitrimers were prepared by maintaining the above molar ratio between -OH and -COOEt and adding 5 mol% of $Sn(Oct)_2$ with respect to DEM to the crosslinking mixture.

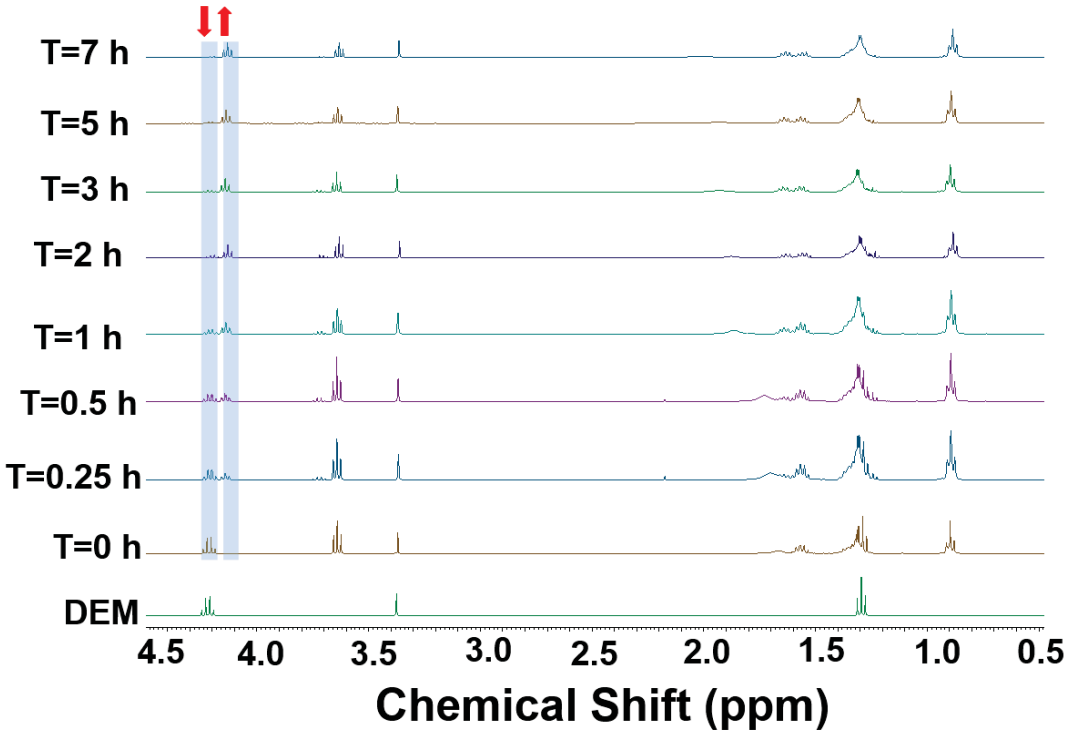

Figure 3.3: ^{1}H NMR spectra of Diethylmalonate and n-hexanol at different time interval at 100 °C for kinetics study in presence of 5 mol% $Sn(Oct)_2$ with respect to DEM.

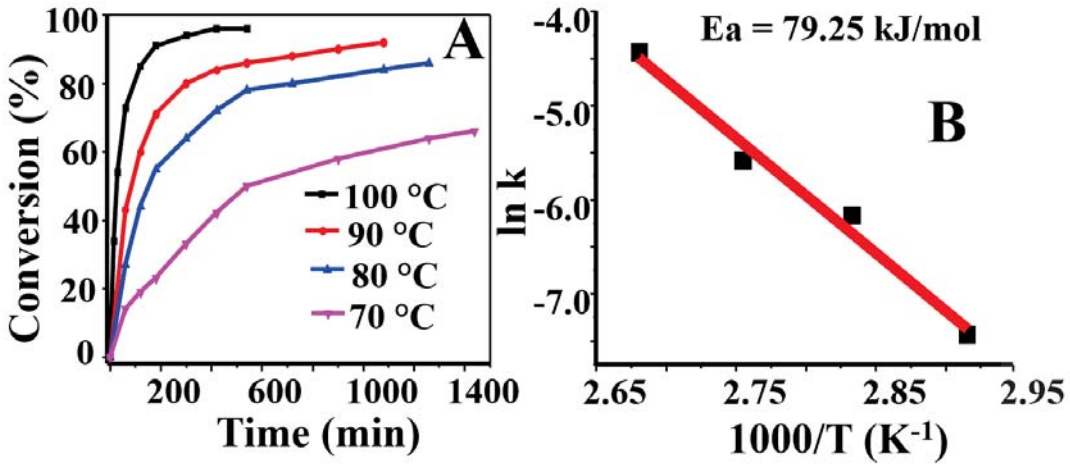

Figure 3.4: The conversion plots of the trans esterification of DEM with n-hexanol at 100 °C, 90 °C, 80 °C and 70 °C in presence of 5 mol% $Sn(Oct)_2$. The ratio between diethylmalonate with n-hexanol at 1:2 (mol:mol) for the transesterification reaction, (B) The Arrhenius plots of transesterification of various temperatures.

Table 3.1: The mechanical properties data of the synthesized vitrimers in presence and absence of catalyst

Sample Code	[OH]/[ester] (mol/mol)	UTS (MPa)	ε (%)	E (MPa)	E' (MPa)	d_c* x 10^3 (mol/cm^3)
Catalyst Free Vitrimers						
PHEMA-DEM-1.5	1.5	33.0 ±1.4	81 ± 3	609 ± 21	1112 ± 11	2.4 ± 0.3
PHEMA-DEM-2	2.0	25.4 ± 0.6	127 ±7	513 ± 7	1000 ± 6	1.0 ± 0.1
PHEMA-DEM-3	3.0	19.2 ±1.8	206 ±13	467 ±14	855 ± 23	0.6 ± 0.1
PHEMA-DEM-6	6.0	11.3 ±1.3	290 ± 13	183 ± 13	317 ± 9	0.2 ± 0.03
Vitrimers possessing $Sn(Oct)_2$						
PHEMA-DEM-1.5C	1.5	30.2 ± 1.5	76 ± 5	602 ± 24	1060 ± 34	1.1 ± 0.2
PHEMA-DEM-2C	2.0	23.3 ± 1.1	112 ± 8	499 ± 9	977 ± 19	0.6 ± 0.1
PHEMA-DEM-3C	3.0	17.0 ± 1.0	205 ± 14	417 ± 15	726 ± 21	0.3 ± 0.1
PHEMA-DEM-6C	6.0	10.5 ± 0.8	284 ± 14	133 ± 13	300 ± 10	0.2 ± 0.05

*the value was determined form the DMTA data by considering the rubbery plateau modulus values at 170 °C, the UTS, elongation at break (ε) and E values were determined from tensile analysis at room temperature conditions, the E' value was determined from DMA analysis.

The resulting networks were dipped in methanol for 12 h at 30 °C to remove the soluble fraction. The mass loss was restricted to $\leq$ 5 wt% only, suggesting the crosslinking is efficient in these systems. The networks were dried under reduced pressure condition and subsequently the mechanical properties on thin films were recorded. The ε (76-284 %) and E values (133-602 MPa) of the catalyzed networks were also comparable to those of the catalyst free networks (ε=81-290%, E=183-609 MPa) suggesting networks with similar mechanical properties may be prepared using catalyzed or catalyst free conditions (Table3.1). The modulus versus frequency scans of the catalyst free vitrimers revealed that the storage modulus (E') values (317-1112 MPa) are substantially higher compared to that of the loss modulus (E') (90-200 MPa) (Figure3.5C). This supported that the network samples are crosslinked in nature.[269]

The E' versus temperature and the Tan δ traces for the vitrimers were got from the DMTA analysis (Figure3.5B). The onset of the Tan δ peak shown the relaxation temperatures of these networks. The PHEMA control displayed a broad transition with the onset of Tan δ peak at $\sim$ 65 °C and the peak maximum at 107 °C. The onset values shifted to higher temperature after crosslinking and the values for the catalyst free networks were observed at $\sim$95-115 °C and the corresponding Tan δ peaks were obtained in the range of 120-130 °C (Figure3.5B). The crosslink density (d_c) values were calculated from the plateau modulus data at 170 °C (Table3.1). Presumably, the network (PHEMA-DEM-1.5) synthesized using maximum DEM displayed highest d_c value (2.4 x 10^{-3} mol/cm^3). The d_c values gradually

decreased to 0.2 x 10^{-3} mol/cm^3 on increasing the molar ratio of OH:COOEt in the networks (Table3.1).

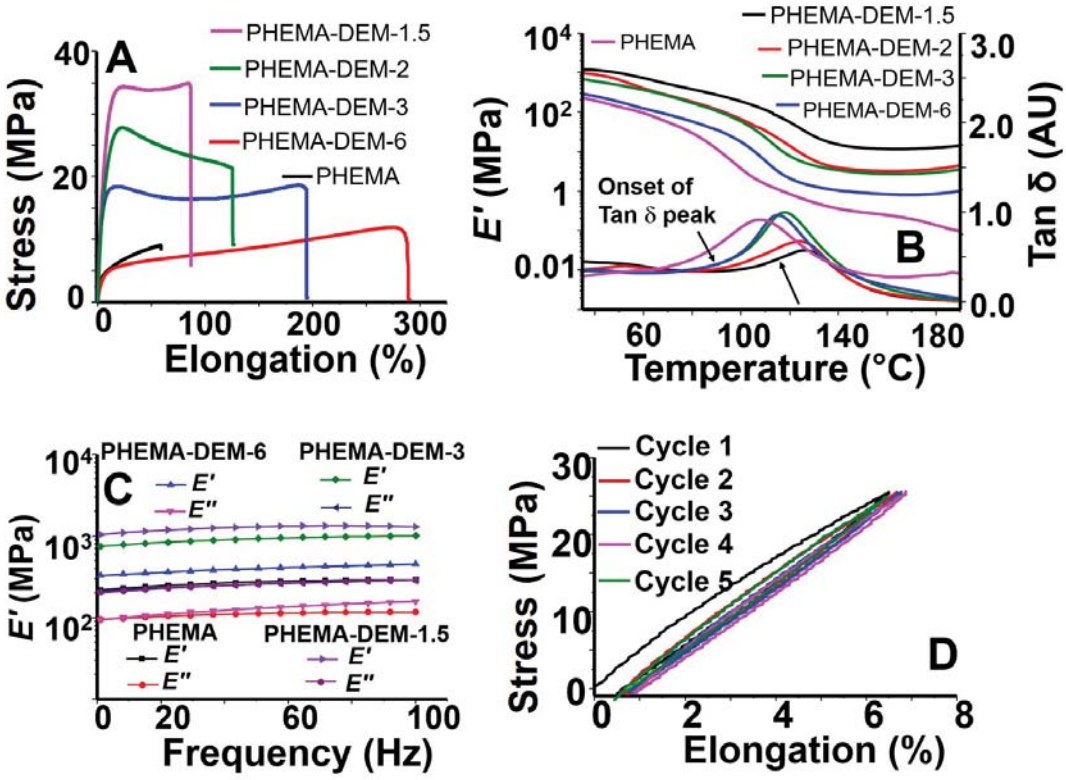

Figure 3.5: (A) The tensile, (B) E' versus temperature and Tan δ versus temperature, (C) E' versus frequency plots of PHEMA-DEM-x networks, (D) the tensile hysteresis data of PHEMA-DEM-1.5 under constant stress mode.

The networks showed vitrimer behavior and exhibited stress relaxation ability at high temperature. The stress-relaxation plots were found for PHEMA-DEM-1.5 in the temperature range of 130 to 170 °C and the Arrhenius plot was created from the time corresponding to the G/G_0 value of 0.37 for each temperature scan (Figure3.7A-B). The Ea value (112.0 kJ/mol) got from the stress relaxation data was comparable to that of the model compound study (110.9 kJ/mol). Similar trend for vitrimers is already reported in literature.[270] The stress relaxation data of other catalyst free compositions (PHEMA-DEM-2 and PHEMA-DEM-3) were also recorded and the Arrhenius plots were created to determine the values of Ea. Overall, the Ea values of catalyst free networks were observed in the range of 108.1 to 106.3 kJ/mol (Figure3.8 & Figure3.9). resumably, the onset of Tan δ peaks for the networks based on $Sn(Oct)_2$ were obtained at lower temperatures ($\sim$ 85 °C) compared to that of the catalyst free networks (95-115 °C) (Figure3.6B).

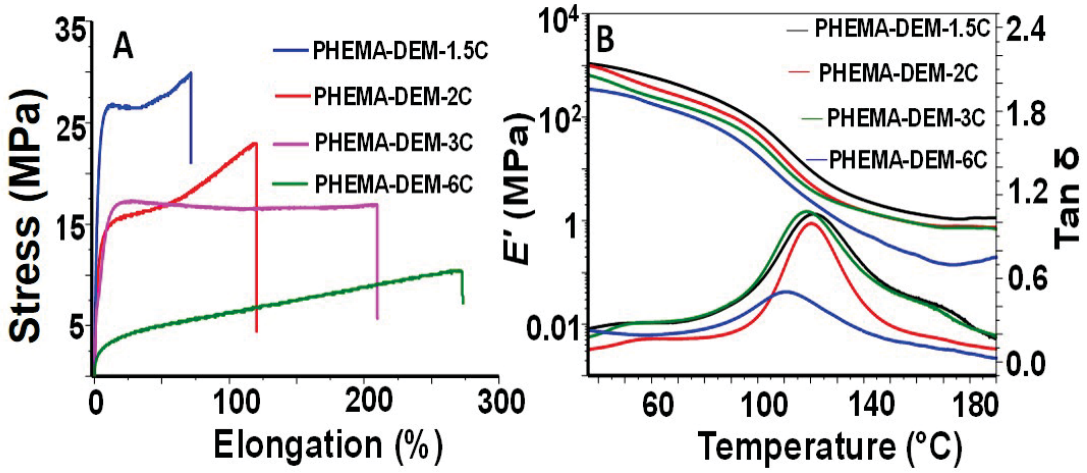

Figure 3.6: (A) Tensile and (B) E' versus temperature and Tan δ versus temperature traces of vitrimers synthesized in presence of 5 mol% of $Sn(Oct)_2$ with respect to DEM.

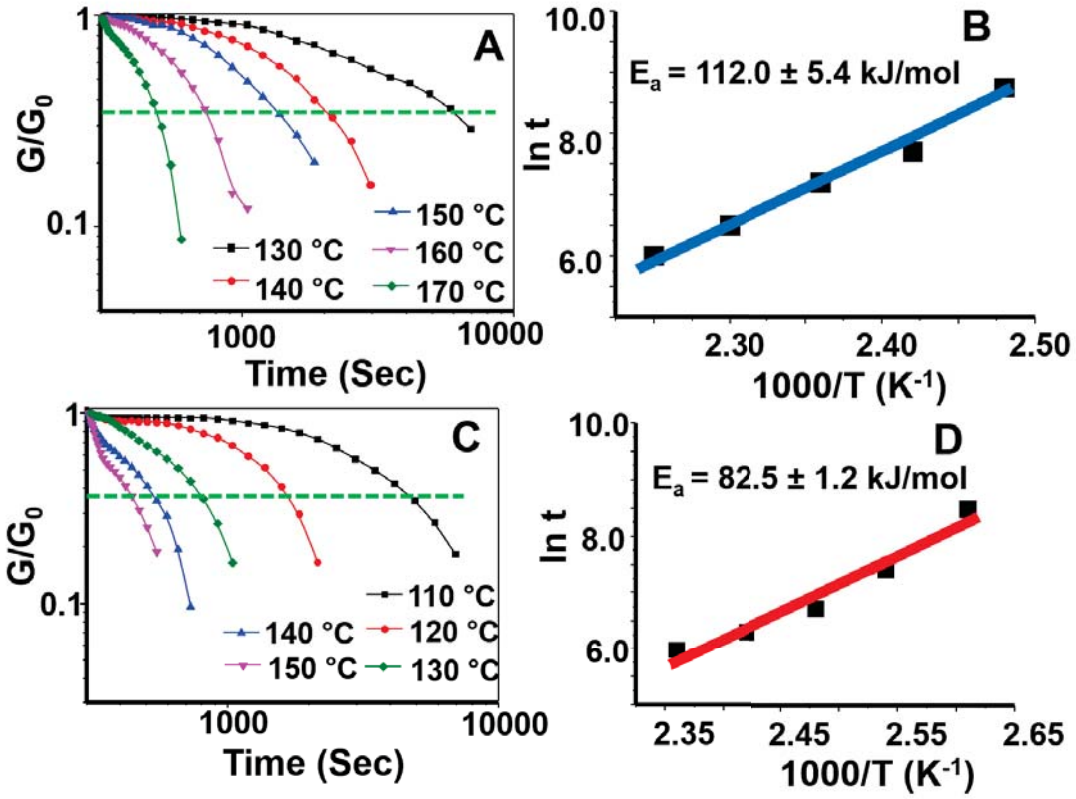

Figure 3.7: (A) The stress relaxation plots of (A) PHEMA-DEM-1.5 and (C) PHEMA-DEM-1.5C under different temperature conditions, the Arrhenius plots for (B) PHEMA-DEM-1.5 and (D) PHEMA-DEM-1.5C constructed from stress-relaxation data.

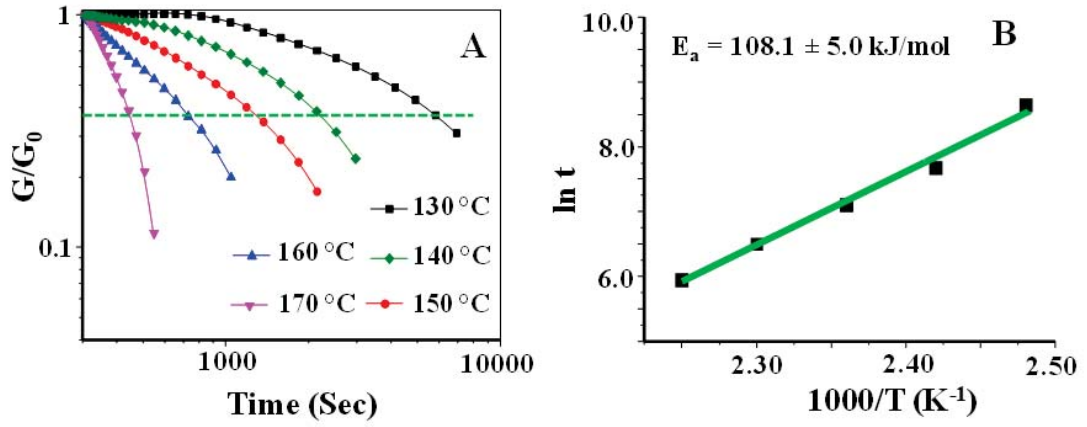

Figure 3.8: (A) The stress relaxation plots of PHEMA-DEM-2 under different temperature conditions, and (B) the Arrhenius plot constructed from stress-relaxation data.

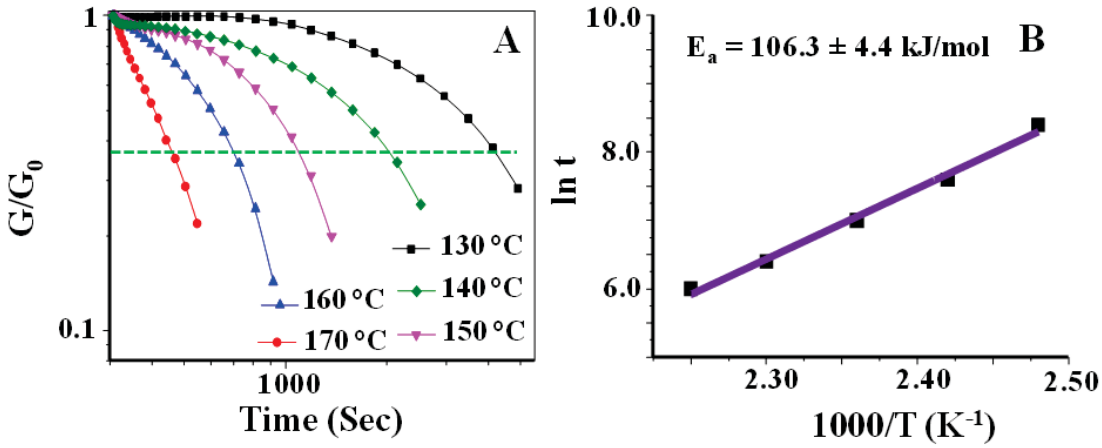

Figure 3.9: (A) The stress relaxation plots of PHEMA-DEM-3 under different temperature conditions, and (B) the Arrhenius plot constructed from stress-relaxation data.

The Tanδ peak maxima (110-121 °C) of catalyzed networks were also lower compared to that of the catalyst free networks (120-130 °C). Interestingly, the d_c values of catalyzed networks (1.1 to 0.2 x 10^{-3} mol/cm^3) were somewhat lower compared to that of the catalyst free networks (2.4 to 0.2 x 10^{-3} mol/cm^3) (Table3.1), which may be attributed to the lower crosslinking temperature in case of the former. The stress relaxation plots of catalyst based network (PHEMA-DEM-1.5C) were recorded in the temperature range of 110 to 150 °C. The sample relaxed under low temperature conditions compared to that of the catalyst free samples (Figure3.7A-C). The Arrhenius plot was built to obtain the Ea values (82.5 kJ/mol) (Figure3.7D). The value was in agreement with that of the model compound study (79.2 kJ/mol) in presence of catalyst and lower compared to that of the catalyst free sample (112.0

kJ/mol). The above data suggested the model compound study and recommended that the networks possessing $Sn(Oct)_2$ may be processed at lower temperature compared to that of the catalyst free samples.

The self-healing capability of the vitrimers under thermal conditions were accessed by laterally overlapping two thin strips of PHEMA-DEM-1.5 and heating the sample at 150 °C for 4 h under 10 kg load. The UTS value of the healed strips (29 MPa) recovered up to 91% compared to that of the original film (32 MPa) telling efficient healing (Figure3.10B). The E' versus temperature traces and the E' versus frequency scans of the original and healed films were also similar further supporting the above (Figure3.10C-D). The crack healing of the samples was checked under microscope at 150 °C.

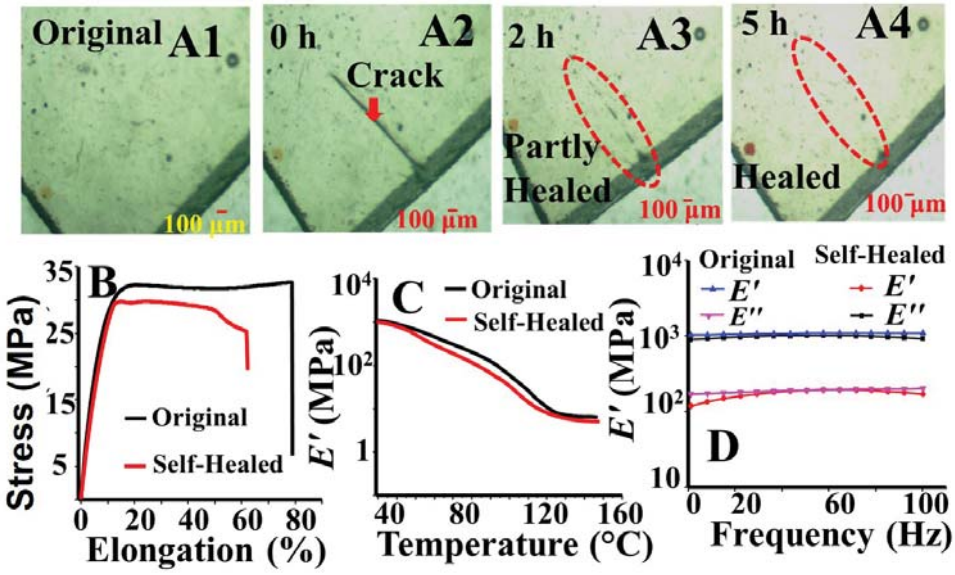

Figure 3.10: Initial PHEMA-DEM-1.5 film, (A2) Cut made by razor blade on A1 surface, (A3) A2 after 2 h of self-healing, (A4) A2 after 5 h of self-healing, (B) tensile data, (C) DMTA data, and (D) Frequency sweep data of original and self-healed PHEMA-DEM-1.5 film.

A thin cut made on a uniform film of PHEMA-DEM-1.5 using a razor blade gradually healed with time under a temperature of 150 °C and the cracked spot was unrecognizable after 5 h (Figure3.10A1-A4).

The topology changes and reprocessability of these vitrimers was accessed under thermal conditions. Small pieces of PHEMA-DEM-1.5 were assembled and compressed under 40 kg load at 150 °C for 5 h. The pieces reintegrated and made a continuous film (Figure3.11A1-A3). The reprocessed films recovered up to 90% of the original UTS value and the E' value ($\sim$ 1000 MPa) became similar to that of the original sample (Figure3.11C-D).

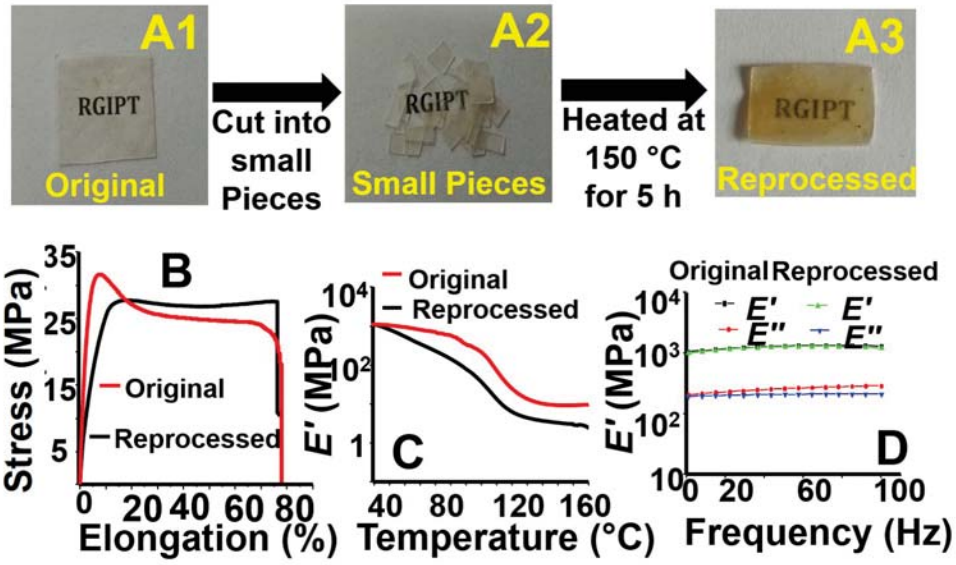

Figure 3.11: (A1) Original PHEMA-DEM-1.5 film, (A2) A1 cut into small pieces, (A3) A2 after 150 °C for 5 h under 40 kg load, (B) tensile traces, (C) DMTA plots, and (D) frequency sweep data of original and reprocessed film.

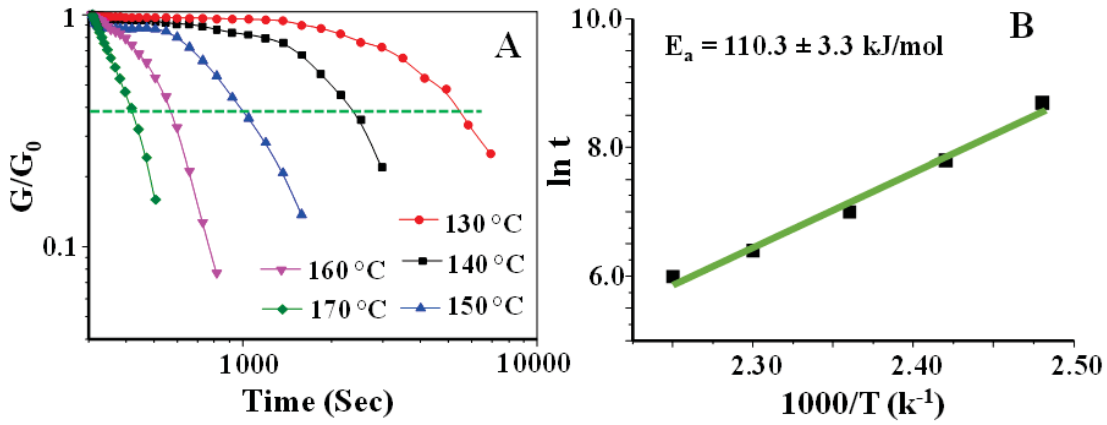

Figure 3.12: (A) The stress relaxation plots of reprocessed PHEMA-DEM-1.5 under different temperature conditions, and (B) the Arrhenius plot constructed from stress-relaxation data.

However, the crosslink density value (1.0 x 10^{-3} mol/cm^3) of the reprocessed films was lower compared to that of the original sample, which may be attributed to the inefficient way of reprocessing the sample by simply pressing the small pieces under load. Using appropriate tools, the crosslink density of reprocessed films may be better-quality further. Overall, the study supported that these vitrimers may be efficiently reprocessed and self-healed at 150 °C with retention of mechanical properties.

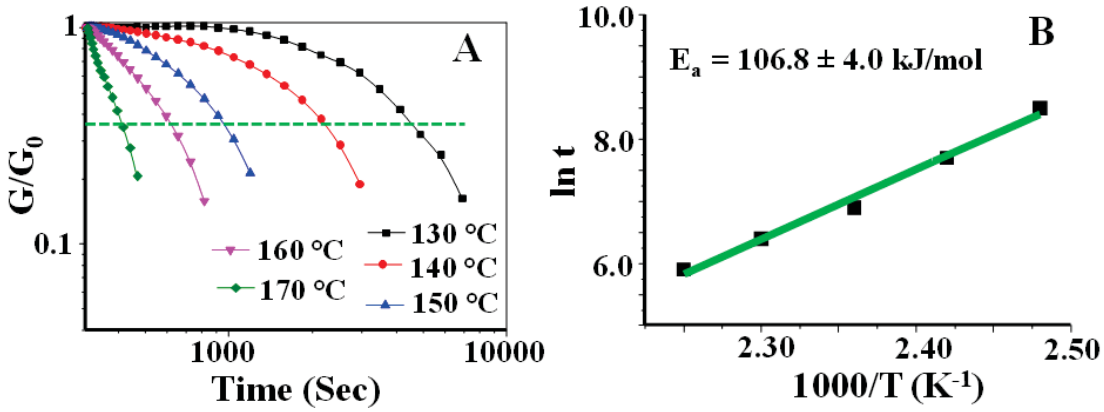

Figure 3.13: (A) The stress relaxation plots of reprocessed PHEMA-DEM-2 under different temperature conditions, and (B) the Arrhenius plot constructed from stress-relaxation data.

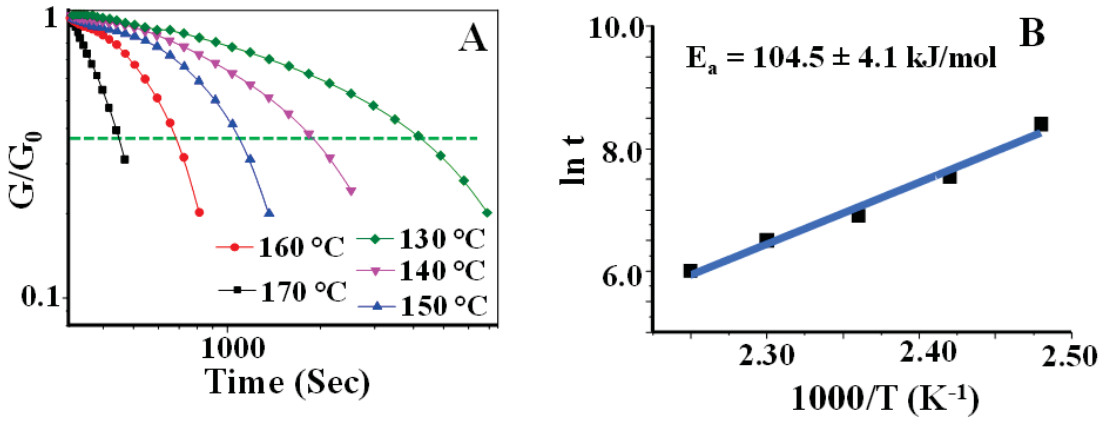

Figure 3.14: (A) The stress relaxation plots of reprocessed PHEMA-DEM-3 under different temperature conditions, and (B) the Arrhenius plot constructed from stress-relaxation data.

The reprocessed samples also showed stress relaxation behavior under high temperature condition. The Ea values of the reprocessed catalyst free networks were in the range of 110.3 to 104.5 kJ/mol(Figure3.12,3.13 &3.14). Similarly, the vitrimers (PHEMA-DEM-1.5C) possessing $Sn(Oct)_2$ was cut into small pieces and pressed under 40 kg load at 110 °C for 4 h. The pieces joined together to form a continuous film. The tensile and DMA data of the reprocessed films were compared to that of the original samples. The UTS and E' values recovered up to ∼95 and 97% respectively after reprocessing. This suggested that the catalyzed vitrimers are successfully reprocessable at relatively low temperature (110 °C). Overall, the study exposed that DEM is an effective crosslinker for synthesis of polyester vitrimers based on PHEMA. In absence of catalyst, the processing temperature is ∼150 °C and the temperature can be brought down to 110 °C by adding $Sn(Oct)_2$ in small mole fraction. In both the cases, the reprocessing is efficient and the mechanical properties are

regained in the reprocessed samples.

3.5 Conclusion

Trans-esterification of β-activated esters is swift under catalyst free conditions at 150 °C. The rate may further be increased and the trans-esterification temperature can be decreased to 100 °C by using $Sn(Oct)_2$ as the catalyst in small amount (5 mol%). The trans-esterification chemistry based on β activated esters may be applied to synthesize catalyst free vitrimers. These vitrimers are readily reprocessable and self-healable under thermal conditions with retaining of mechanical properties. In presence of a small amount of $Sn(Oct)_2$, the processability temperature may be further decreased to 110 °C. Both catalyzed and catalyst free procedures may be applied to synthesize vitrimers with comparable mechanical properties. The hydroxyl precursors may be altered and a range of catalyst free vitrimers may be synthesized using DEM as the crosslinking agent for future uses. In future, the polymeric precursor, i.e. PHEMA may be substituted with a small molecular weight multihydroxy precursor to develop fully degradable and recyclable vitrimers. The usefulness of these developed vitrimers may be explored in the area of coatings, adhesives, hydrogels, synthetic fabrics and biomaterials in future.

This page was intentionally left blank.

Chapter 4

Solvent Processable and Recyclable Covalent Adaptive Organogels Based on Dynamic Trans-Esterification Chemistry: Separation of Toluene from Azeotropic Mixtures

4.1 Abstract

New covalent adaptive networks (CAN) holding processability and recyclability to monomer are desirable, as an alternative to traditional plastics to address the issues related to the plastic waste. Moreover, the conventional polymeric networks are usually insoluble in organic solvents. Herewith, we report a set of CANs those can be dissolved in an alcoholic solvent via reactive depolymerization and fully recycled to the monomer. In this study, we have used trans-esterification of α-substituted β,β'-diesters with multi-hydroxy compounds under moderate temperature conditions (110-140 °C) to develop a set of polyester based CANs. The synthesized CANs showed ultimate tensile strength (UTS) and elongation at break value up to $\sim$1.1 MPa and $\sim$595% respectively. The CANs displayed thermal stability

up to 215 °C. The films were stable under acidic as well as basic conditions. These CANs readily depolymerized and dissolved in an alcoholic solvent at ∼120 °C within 15 h through competitive trans-esterification with the solvent. The films restructured on evaporation of the solvent followed by curing at 140 °C. The reprocessed CANs showed UTS (∼1.0 MPa) and Young's modulus (∼1.8 MPa) comparable to that of the original samples. Due to the simplicity of synthesis, solvent processability, recyclability, economically reliable starting material and moderate processing temperature, these polyester CANs may be appropriate for various commercial applications. The CANs rapidly and selectively absorbed aromatic compounds compared to that of the other organic solvents and swelled by ∼750 wt% in toluene within 90 min. This property was used to efficiently separate aromatics from various azeotropic mixtures involving toluene, methanol and water.

4.2 Introduction

Crosslinked polymeric networks having dynamic covalent linkages capable of undergoing a reversible exchange reaction in presence of external stimuli is an important area of research in materials science.[271, 272] These covalent adaptable networks (CAN) or dynamic covalent networks are able to match the mechanical properties,[273] thermal stability,[274] solvent resistance[275] and overcome the concern of nonprocessability[276] associated with the conventional thermosets. The dynamic covalent linkages present in these CANs undergo rapid exchange reaction when triggered by external stimuli such as temperature,[277] light,[278] solvent[279, 280] and reagent.[281] This permits the change in topology of CANs and reprocessability of the samples under specific conditions.[282] Therefore, the CANs are favorable candidates for a range of applications with recyclable commodity plastics, [283] self-healing materials, shape memory polymers,[284, 285] reversible adhesives,[286] actuators,[287] and coatings.[288] Several functional linkages including Diels-Alder adduct, [289] imine,[290] Michael adduct,[291] amides,[292] hydrazones,[293, 294] urethane,[295, 296] disulfide linkages,[297] vinylogous urethanes,[298] carbonates,[299] and boronate esters [300] are successfully studied as the dynamic linkages in CANs. Some of the CANs have also shown the capability to recycle back to the monomers under specific conditions.[301] Recyclability permits swift degradation of the CANs via depolymerization to the corresponding monomeric precursors.

Hydrogels and organogels based on dynamic covalent linkages are an important class of materials.[302, 303] Such gel systems have showed self-healing ability,[304] responsiveness, [305] and dynamic control of morphology[306] and are studied for potential use in drug delivery matrix,[307] scaffold for polymerization,[308] stem cell culture,[309] in-

jectable hydrogels,[310] strain sensors,[311] and burn wound healing.[312] Efforts have been made to tailor the stiffness of the hydrogels via control of the crosslink using light as the stimulus.[313, 314] Recently, small molecule based stimuli responsive reversible hydrogels were established based on amine-formaldehyde chemistry.[315] Therefore, design of new organogel systems based on dynamic covalent linkages are necessary for various material applications.

Among the several reported CANs, dynamic polyesters with a wide range of mechanical properties are one of the widely studied class of CANs due to their potential applications in numerous areas.[316, 317] Typically, a trans-esterification catalyst such as $Zn(acac)_2$,[318] $Sn(Oct)_2$,[319] or Bronsted acid[320] is used to improve the efficiency of exchange reaction in these CANs. A range of precursors are designed and applied for development of dynamic ester based networks in literature.[321, 322] Recently, we have used the β,β'-diesters as the activated precursors to develop catalyst free polyester vitrimers.[323] The β,β'-diesters having no substituents in the α position reached trans-esterification equilibrium within 3 h at 100 °C in presence of 5 mol% $Sn(Oct)_2$. However, substituents at α position is essential to increase the number of ester functionalities and enhance the versatility of the precursor. Furthermore, multi-functional ester precursor will permit the use of low molecular weight hydroxyl precursors and development of completely recyclable polyester CANs. In this report, we have discussed the effect of α substitution on the rate of trans-esterification of β, β'-diesters using α alkyl substituted β,β'-diesters as the model compounds using $Sn(Oct)_2$ as the trans-esterification catalyst under moderate temperature conditions. Subsequently, several CANs are designed and prepared applying the above trans-esterification reaction as the key reaction. The thermal and mechanical properties of the resulting CANs are studied. The solvent processability and recyclability of these CANs are evaluated. The swellability of these CANs in different organic solvents is assessed and subsequently, the CANs are used to separate aromatics from azeotropic mixtures under ambient conditions.

4.3 Experimental

4.3.1 Materials

α-Butyl diethylmalonate (BEM, TCI Chemicals, >99.0%), n-Hexanol (Alfa Aesar, 98.0%), Tin(II) 2-Ethylhexanoate $Sn(Oct)_2$, TCI Chemicals, >85.0%), 1,6-Dibromohexane (Avra Synthesis, 98.0%), Diethyl malonate (DEM, s-d fine chem., 98.0%), Potassium carbonate

anhydrous (Fisher Scientific, 99.0%), Acetonitrile (Merck, 99.0%), Ethyl acetate (Fischer Scientific, 98.0%), Sodium sulphate anhydrous (Finar Chemicals, 99.0%), Triethanolamine (TEA, s-d fine chem., 99.0%), Pentaerythritol (PTE, Himedia Laboratories, >98.0%), Poly (tetramethylene oxide) diol (PTMO, Sigma Aldrich, $M_n \sim$ 2900), n-Butanol (Nice Chemicals, 99.0%), Deionized water collected from Pure Lab-ALGA water purifier, N,N-Dimethylformamide (DMF, Spectrochem, 99.0%), Dimethyl sulphoxide (DMSO, Fisher Scientific, 98.0%), Toluene (Fisher Scientific, 99.5%), Octanol (Merck, 99.0%), Methanol (s-d fine chem., 99.0%), Acetone (Molychem, 99.0%), $CDCl_3$ (Sigma Aldrich, 99.8 atom % D) are used as received unless otherwise stated.

4.3.2 Characterization

The JEOL-400 YH NMR spectrometer was used to record ^{1}H and ^{13}C NMR spectra at 25 °C probe temperature. The FTIR spectra were performed in a Perkin Elmer Spectrum Two with PIKE MIRacle single reflection horizontal ATR accessory. Agilent Accurate-Mass Q-TOF LC/MS 6520 was used for recording the ESI-HRMS mass spectra and peaks were assigned as m/z values (% of base peak). The ultimate tensile strength (UTS) of polymer films were measured by H5KL, Tinius Olsen machine under Generic Tensile mode using rectangular film specimens of width ∼5 mm and thickness ∼0.8 mm. The tensile data was recorded at ∼25 °C under 5.0 mm/min machine speed. For representing the data, we have taken the average of three measurements. The Young's moduli (E) were calculated from the linear region of the tensile traces. The dynamic mechanical analyzer (DMA) was performed on DMA Q-800 TA instrument using tension mode and 50 ASTM D4065-01 procedure. The stress relaxation experiments were performed at constant strain value of 0.5% under compression mode and the data was collected after 10 min of the equilibrium. After normalization of the modulus, the activation energy was calculated. The width and thickness of the specimen rectangular samples were ∼5 and ∼0.8 mm respectively. Thermal gravimetric analysis (TGA) was carried out in TGA PT 1000, Linseis under N_2 atmosphere. For TGA, 15 mg of powdered samples were heated up to 700 °C at 10 °C/min ramp. DSC 4000 Perkin Elmer instrument was used for the recording of differential scanning calorimetry (DSC) data under N_2 atmosphere (50 mL/min). During measurement, finely powdered sample was taken in an aluminum foil and heated from 0 °C to 180 °C at a rate of 10 °C/min. After cooling to 0 °C, the sample was again heated to 180 °C to find glass transition temperature (T_g) values. For recording the Ultraviolet-visible (UV-Vis) spectra, UV-VIS 3200 instrument (Lab India) was used and the data were collected at 1 nm/min scan rate.

4.3.3 Synthesis of tetraethyl octane-1, 1, 8, 8-tetracarboxylate (TEOC)

Diethyl malonate (20.0 g, 125.0 mmol), 1,6-dibromohexane (7.6 g, 31.3 mmol) and anhydrous potassium carbonate (25.8 g, 186.9 mmol) were added to 150 mL acetonitrile and the mixture was allowed to reflux for 18 h. The reaction mixture was cooled to room temperature, the solvent was evaporated and the residue was poured in to water. The product was extracted with ethyl acetate. The organic fraction was washed with water for two times and dried over anhydrous sodium sulphate. The excess diethyl malonate was removed under low pressure conditions at 140 °C. ^{1}H NMR (400 MHz, $CDCl_3$) δ (ppm): 4.2 (q, 8H, -OC$\boldsymbol{H}_2-CH_3$), 3.3 (t, 2H, -C$\boldsymbol{H}(COO)_2$-), 1.8 (m, 4H, -$CH_2-C\boldsymbol{H}_2$-), 1.3 (m, 4H, -$CH_2-C\boldsymbol{H}_2-CH_2$), 1.1 (t, 12H, -C$\boldsymbol{H}_3$).^{13}C NMR (100 MHz, $CDCl_3$ δ (ppm): 169.8(-*C*OO-), 61.3 (-O$-\boldsymbol{C}H_2$), 52.3 (-$\boldsymbol{C}H-(COO-)_2$), 29.0 (-$\boldsymbol{C}H_2$-), 27.4 (-$\boldsymbol{C}H_2$-), 13.9 (-$\boldsymbol{C}H_3$). FTIR (cm^{-1}): 786 (m, C-H), 860 (s, C-H), 1175 (s, C-O), 1729 (s, -COO-), 2860 (m, C-H), 2935 (m, C-H).

4.3.4 Synthesis of butyl hexylmalonate (BHM)

α-Butyl diethylmalonate (BEM, 0.5 g, 2.3 mmol) and n-hexanol (0.9 g, 9.2 mmol) were taken in a round-bottomed flask and 5 mol% of $Sn(Oct)_2$ (46.8 mg, 0.11 mmol) with respect to BEM was added to the above mixture at 140 °C. The reaction was carried out under solvent free conditions for 5 h. The product was directly used for characterization without any further purification. ^{1}H NMR (400 MHz, $CDCl_3$) δ (ppm): 4.1 (q, 4H, -COOC$\boldsymbol{H}_2CH_2$-), 3.3 (t, 2H, -C$\boldsymbol{H}(COO)_2$-), 1.9 (m, 6H, -$CH_2-C\boldsymbol{H}_2-CH$-), 1.6 (m, 12H, -$COO-CH_2-C\boldsymbol{H}_2$-), 1.3 (m, 4H, -$C\boldsymbol{H}_2-C\boldsymbol{H}_2-CH_2$), 0.9 (t, 9H, -C$\boldsymbol{H}_3$).^{13}C NMR (100 MHz, $CDCl_3$) δ (ppm): 169.8 (-$\boldsymbol{C}$OO-), 65.6 (-$(COO)_2-\boldsymbol{C}H_2-CH_2$), 52.2 (-$\boldsymbol{C}H-(COO-)_2$), 31.40 (-$\boldsymbol{C}H_2-\boldsymbol{C}H_2$-), 28.6 (-$\boldsymbol{C}H_2-\boldsymbol{C}H_2$-), 25.7 (-$\boldsymbol{C}H_2-\boldsymbol{C}H_2$-), 22.4 (-$\boldsymbol{C}H_2-CH_3$), 13.9 (-$\boldsymbol{C}H_3$). FTIR ($cm^{-1}$): 796 (s, C-H), 890 (s, C-H), 1157 (s, C-O), 1734 (s, -COO-), 2860 (m, C-H), 2931 (m, C-H), HRMS (ESI-TOF) m/z: [M + H] Calculated for [$C_{19}H_{36}O_4$] = 329.2693. Found 329.2681.

4.3.5 Synthesis of TEOC based CANs

TEOC (2.0 g, 5.0 mmol), PTE (0.8 g, 6.0 mmol) and $Sn(Oct)_2$ (0.2 g, 10 mol% with respect to TEOC) were taken in a R.B flask and heated at 140 °C for 8 h. Then the mixture was poured into a Teflon petri dish and kept for 12 h in vacuum oven at 140 °C for curing purposes.

Table 4.1: The mechanical properties data of the synthesized vitrimers in presence and absence of catalyst

Code[#]	Multi-ol	TEOC (mmol)	Multi-ol (mmol)
TEOC-PTE	PTE	4.97	5.96
TEOC-TEA	TEA	4.97	5.97
TEOC-PTMO	PTMO	4.97	2.76
TEOC-PTMO-PTE*	PTMO/PTE	4.97	6.00

*PTMO:PTE = 1.2:4.8 (mmol:mmol), [#]10 mol% of $Sn(Oct)_2$ with respect to TEOC was used in all the cases and the reaction temperature was 140 °C.

4.3.6 Degradation and reprocessing of the CANs

Small pieces of the CANs (5.0 g) were taken in a round bottom flask with n-butanol (20 mL) and refluxed at 120 °C for 15 h. The strips dissolved and a homogeneous solution was obtained. Subsequently, the solvent was evaporated and the mass was incubated at 140 °C for 12 h in vacuum oven to reform the networks.

4.3.7 Swelling ratio of the samples

Different CAN (TEOC-PTE, TEOC-TEA, TEOC-PTMO, TEOC-PTMO-PTE) films (100 mg) were occupied in organic solvents, e.g. toluene, octanol, acetone, DMF and methanol and water. The weight gain was measured after different time intervals by gravimetric method till saturation. The swelling ratio was calculated using the following equation;

$$Weight\ Swelling\ Ratio = \frac{Final\ Weight - Initial\ Weight}{Initial\ Weight} \times 100\% \tag{4.1}$$

4.3.8 Separation of toluene from azeotropic mixtures by CANs

The binary (toluene:methanol = 1.15:0.38, vol:vol) and ternary azeotropes (toluene:methanol: water = 1.15:0.19:0.06, vol:vol) were prepared following reported procedures.[324, 325]

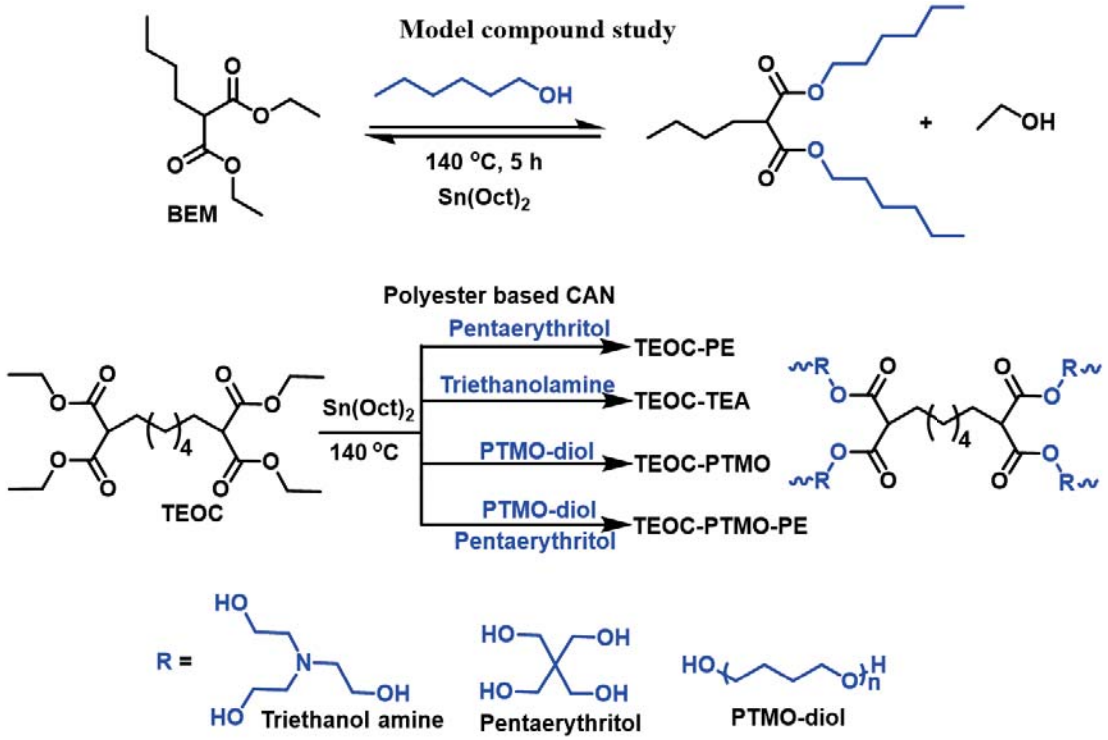

Scheme 4.1: Trans-esterification of model compound and synthesis of polyester based CANs using TEOC and different multi-ols

TEOC-PTMO-PTE strip (200 mg) was dipped in the above azeotropic mixtures. The strip was removed after regular time intervals and the absorbance of the peak at 260 nm in UV-Vis spectra of the azeotropic mixture was examined to determine the concentration of toluene. To check reusability of the CAN film, the soaked TEOC-PTMO-PTE film was heated at 110 °C for 1 h to evaporate the solvent. The dry TEOC-PTMO-PTE film was again dipped in a fresh azeotropic mixture and the toluene absorption efficiency was monitored. The above process was carried out for five consecutive cycles of soaking and drying.

4.4 Results and Discussion

4.4.1 Study of model compounds

BEM possessing structural similarity to that of the polymerizable tetraester (TEOC) was chosen as the model compound.

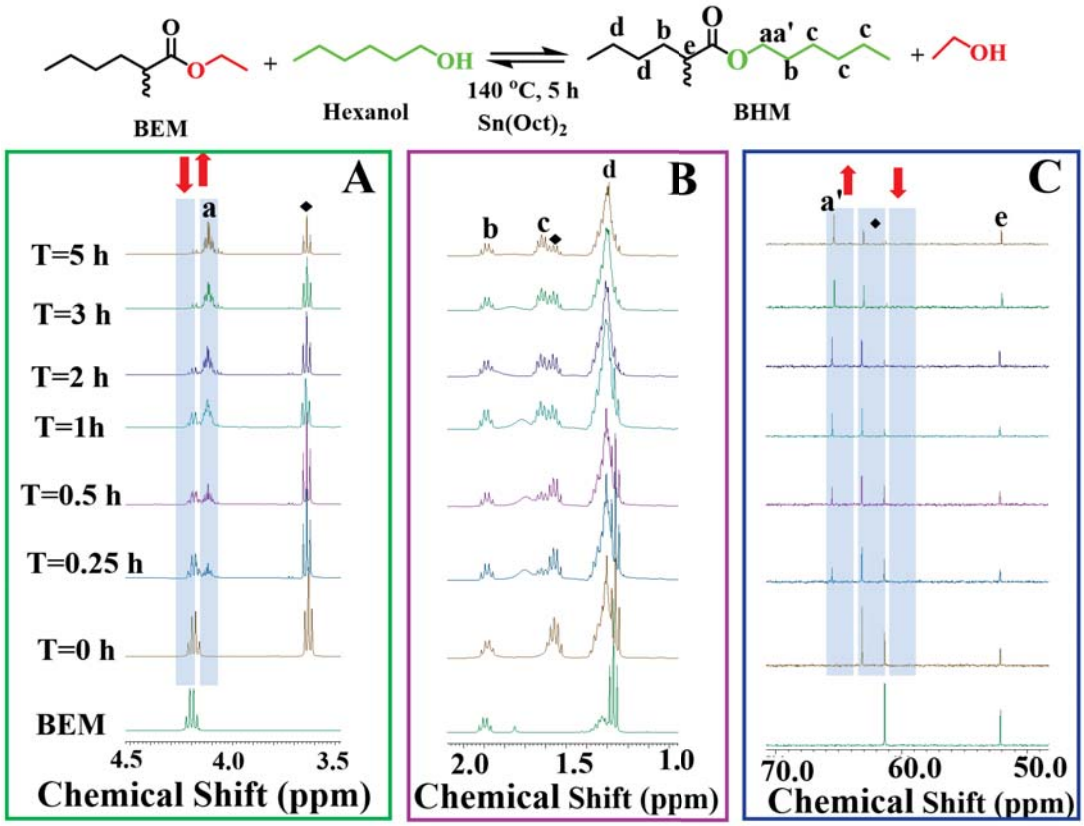

Figure 4.1: (A-B) ^{1}H NMR and (C) ^{13}C NMR spectra of the precursor and reaction mixture recorded at different time intervals, the reaction of BEM and n-hexanol was conducted in presence of $Sn(Oct)_2$ at 140 °C, the peak marked with "◇" represents the amount of n-hexanol present in the reaction mixture. The schematic on top of the figure displays the exchange of ethoxy moiety with n-hexyloxy group in the ester.

The rate of trans-esterification with n-hexanol was studied in presence of $Sn(Oct)_2$ (Scheme4.1). At 140 °C, the trans-esterification reaction appeared equilibrium within 2 h in presence of 5 mol% $Sn(Oct)_2$ under solvent free conditions. In ^{1}H NMR spectra, the intensity of quartet at 4.2 ppm for -$COOCH_2CH_3$ slowly decreased and new multiplets at 4.1 and 1.6 ppm accountable to -$COOCH_2CH_2$- and -$COOCH_2CH_2$- of the product appeared suggesting successful exchange of ethoxy moiety with n-hexyloxy group in BEM (Figure4.1A-B). Similarly, a new peak at 65.6 ppm responsible to -$COOCH_2CH_2$- appeared and the peak at 61 ppm for -$COOCH_2CH_3$ in BEM disappeared supporting the conversion (Figure4.1C). The principal peak at 329.2681 (M+H) accountable to the exchanged product (BHM) was observed in HRMS spectra. The conversion of the above trans-esterification was observed under different temperature conditions (110-140 °C) till equilibrium. The half-lives ($t_{1/2}$) of the reactions were used to control the rate constant (k) using second order rate equation.

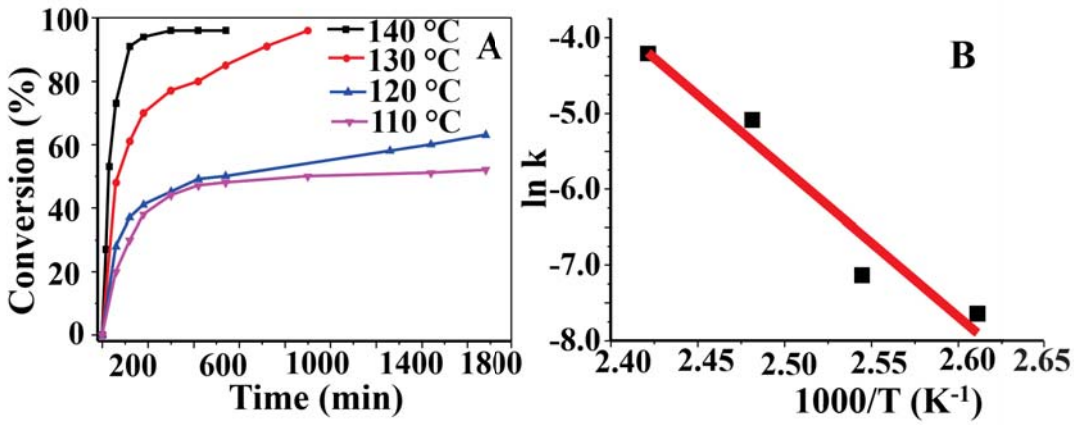

Figure 4.2: (A) The conversion plots of the trans-esterification of BEM with n-hexanol at 140 °C, 130 °C, 120 °C and 110 °C. The ratio between BEM and n-hexanol was 1:4 (mol:mol) for the trans-esterification reaction, (B) The Arrhenius plot of the trans-esterification reaction was constructed by plotting the $t_{1/2}$ values under different temperature conditions using second order kinetics.

The k values were subsequently plotted against the temperature to construct the Arrhenius plot and determine the activation energy (Ea) of the reaction (Figure4.2). The Ea value of the trans-esterification reaction between α-alkyl substituted β-β'-diesters and primary alcohols was around 157.8 ± 4.8 kJ/mol.

4.4.2 Synthesis of polyester based CANs

On the basis of model compound study, the CANs were prepared at 140 °C with adequate $Sn(Oct)_2$ (10 mol% with respect to TEOC) loading. Four different CANs were synthesized using TEOC and three different multi-ols. The molar composition of TEOC and multi-ols were optimized based on their tensile properties. The molar ratio of TEOC:PTE = 5:6 (mol:mol) was used to synthesis the TEOC-PTE CAN. Similarly, the other CANs were synthesised using appropriate molar ratio of TEOC to multi-ol (Table4.1). The CANs were colored and mostly transparent in nature (Figure4.3B).

The mechanical and thermal properties of the CANs were measured (Table4.2). The UTS and *E* values were found in the range of 0.1 to 1.1 MPa and 0.7 to 1.8 MPa respectively. The CAN synthsized using the mixture of PTMO and PTE showed UTS value of 1.1 MPa and elongation at break(ε) value up to 301%. The CAN based on PTMO and TEOC exhibited maximum ε value (595%).

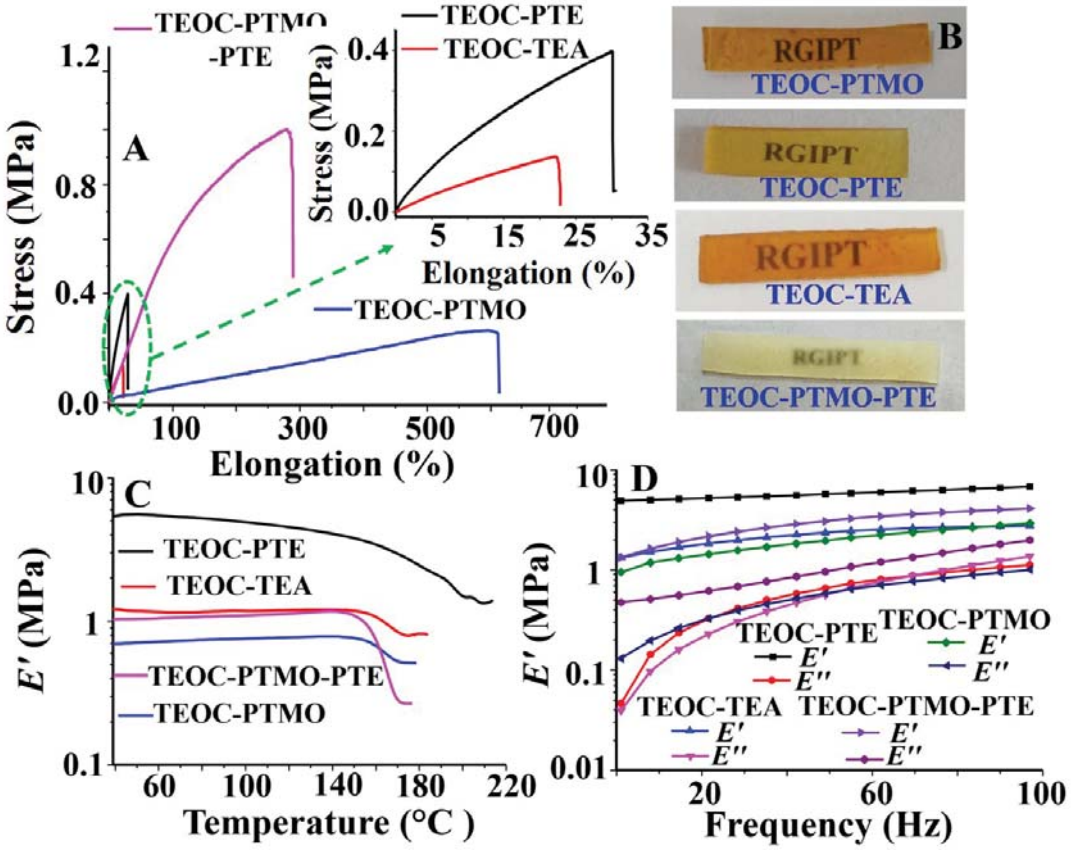

Figure 4.3: (A) Tensile plots of the CANs, (B) Photographs of different films of CANs, (C) DMTA traces and (D) the frequency sweep plots of the CANs.

Table 4.2: Mechanical and thermal properties of the CANs

CANs	UTS* (MPa)	ε* (%)	E* (MPa)	TGA† (°C)	$E'^{\#}$ (MPa)	d_c x 10^3 (mol/cm^3)
TEOC-PTE	0.5 ± 0.06	30.0 ± 3.0	1.8 ± 0.04	215	4.9 ± 0.4	0.13 ± 0.06
TEOC-TEA	0.1 ± 0.01	23.0 ± 3.0	1.1 ± 0.01	205	1.2 ± 0.1	0.07 ± 0.04
TEOC-PTMO	0.3 ± 0.06	595.0 ± 15.0	0.8 ± 0.01	200	0.8 ± 0.1	0.05 ± 0.02
TEOC-PTMO-PTE	1.1 ± 0.03	301.3 ± 22.0	0.7 ± 0.03	210	1.1 ± 0.1	0.03 ± 0.01

*From tensile analysis, the UTS, elongation at break (ε) and E values were calculated. $^{\#}$the values were observed from DMTA analysis. †represents the onset of decomposition in TGA measurement.

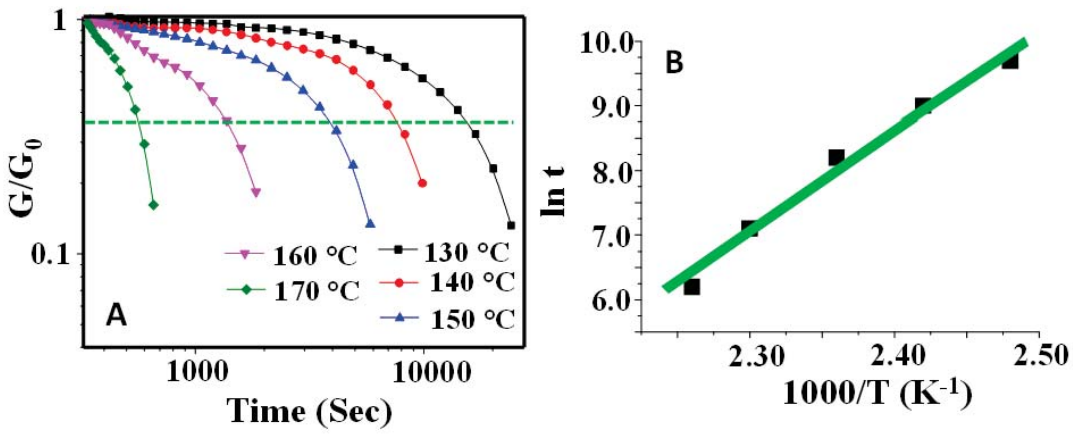

Figure 4.4: (A) The Stress relaxation plot and (B) Arrhenius plot for TEOC-PTMO-PTE film.

The storage modulus *(E′)* values of the CANs were found in the range of 0.8 to 4.9 MPa. The E'values were higher than that of the loss modulus E'' values in all the cases supporting the crosslinked nature of the sample (Figure4.3D).[326] The DMTA plots of the CANs shown that the E' values were retained up to 140 °C under thermo mechanical condition. A sharp decay in the E' value occurred on increasing the temperature beyond 140 °C suggesting the onset of relaxation of the CANs. Interestingly, a small exothermic hump was observed in the DSC spectra in the range of 120-140 °C (Figure4.5B). Both the DMA and DSC data suggested that the relaxation temperature of the CANs may be in the range of 120 to 140 °C. The crosslink density (d_c) values of the CANs were determined from the plateu modulus data at temperatures in the range of 168 to 201 °C . The values were found in the range of 0.03 x 10-3 mol/cm^3 to 0.13 x 10^{-3} mol/cm^3. Only the CAN (TEOC-PTMO-PTE) synthesized using PTMO and PTE showed stress relaxation behavior and the Ea value (145.0 kJ/mol) calculated from the corresponding Arrhenious plot was similar to that of the model compound study. However, the other networks failed to show stress relaxaton characteristics, which may be attributed to the unavailability of free -OH groups in these CANs and absence of possible trans-esterification exchange reaction.

The CANs exhibited thermal stability above 200 °C and the onset of weight loss in TGA traces was observed at ∼215 °C (Table4.2 & Figure4.5A). Maximum weight loss occurred between 300 to 420 °C. Polyesters are known to degrade above 300 °C in the literature.[327] The stability of these CANs were checked in acidic as well as basic solutions. The CAN films were dipped in acidic and basic medium for 12 h at room temperature. The films were subsiquently removed, dried and subjected to tensile measurement. The tensile plots of recovered films were comparable to that of the pristine films (Figure4.6A).

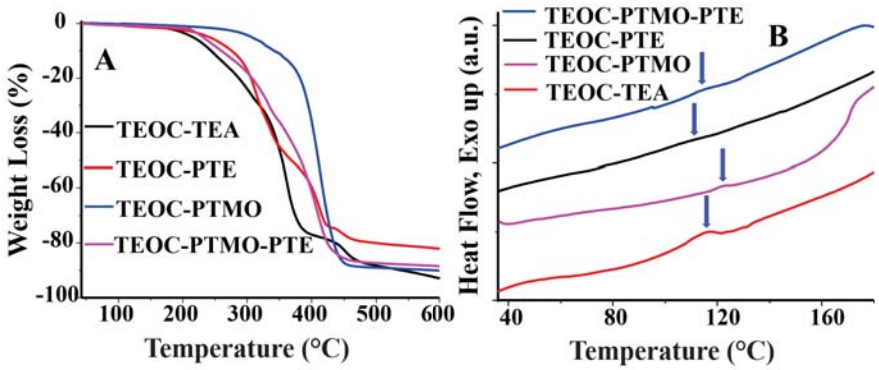

Figure 4.5: (A) TGA traces of different DCNs, (B) The second heating DSC traces of different CANs recorded under N_2 atmosphere.

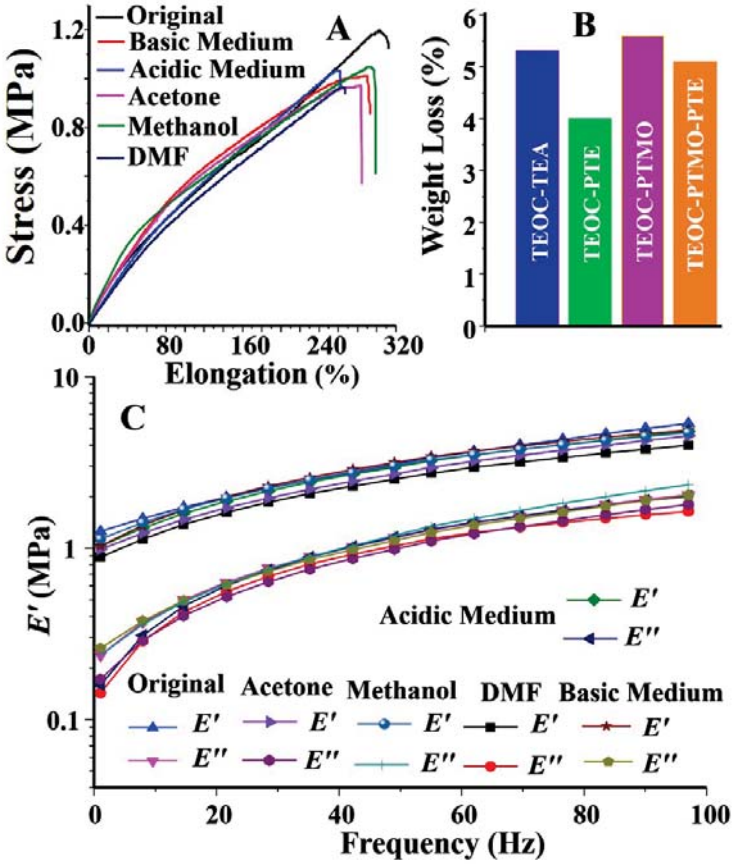

Figure 4.6: (A)Tensile data of original sample and samples after removing from acidic and basic solution, acetone, methanol, and DMF after 12 h, (B) weight loss data of different CANs in DMF solvent, (C) frequency sweep data of original sample and the samples after removal from acidic and basic solution, acetone, methanol and DMF after 12 h.

Similarly, the E' versus frequency plots were similar to that of the original CAN films. The E' values of acid and base treated films were observed in the range of 1.0 to 1.2 MPa (Figure4.6C). The weight loss of different CANs in DMF was below 6% after 12 h of dipping under ambient conditions (Figure4.6B). In other solvents such as acetone, THF and methanol, the weight loss was restricted to 4% only. The UTS values of the solvent processed samples were in the range of 0.9 to 1.1 MPa. The above data suggested that these CAN samples possess adecuate solvent tolerance.

4.4.3 Solution reprocessibility of the CANs

These CANs were estimated to depolymerize in alcoholic solvents via competitive transesterification reaction under moderate temperature conditions. Small pieces of the TEOC-PTMO-PTE were taken in a round-bottomed flask and the mixture was refluxed at 120 °C in n-butanol for 15 h. The films readily dissolved in the solvent suggesting depolymerisation of the sample (Figure4.7A2-B2). The samples retained in other non-alcoholic solvent remained intact under similar conditions after 15 h (Figure4.8). The homogeneous solution of TEOC-PTMO-PTE found in n-butanol was placed at 140 °C under reduced pressure condition to gradually evaporate the solvent and initiate the crosslinking process. The samples reformed after 12 h under above conditions. The UTS = ($\sim$1.0 MPa) and E= ($\sim$0.61 MPa) values of 1^{st} reprocessed sample of TEOC-PTMO-PTE were comparable to that of the original sample (UTS $\sim$ 1.1 MPa and E $\sim$ 0.7 MPa). The tensile properties of the 2^{nd} reprocessed sample (UTS = $\sim$0.9 MPa and E = $\sim$0.5 MPa) also retained up to 90% of the original properties suggesting that the solution processability of these CANs via reactive depolymerisation is effective (Figure4.7C).

4.4.4 Separation of aromatics from azeotropic mixture

Polyether based networks are known to absorb various organic solvents and display organogel characteristics.[328] Therefore, CANs were synthesized by adding PTMO along with PTE to induce organogel ability in the CANs. The capability of these CANs to absorb organic solvents were evaluated by dipping a thin strip of TEOC-PTMO-PTE in different organic solvents under ambient conditions. Interestingly, the CAN selectively absorbed toluene compared to a range of other organic solvents (Figure4.9A). The weight swelling ratio value of TEOC-PTMO-PTE was 750% in toluene, whereas the values were less than 120% in other organic solvents.

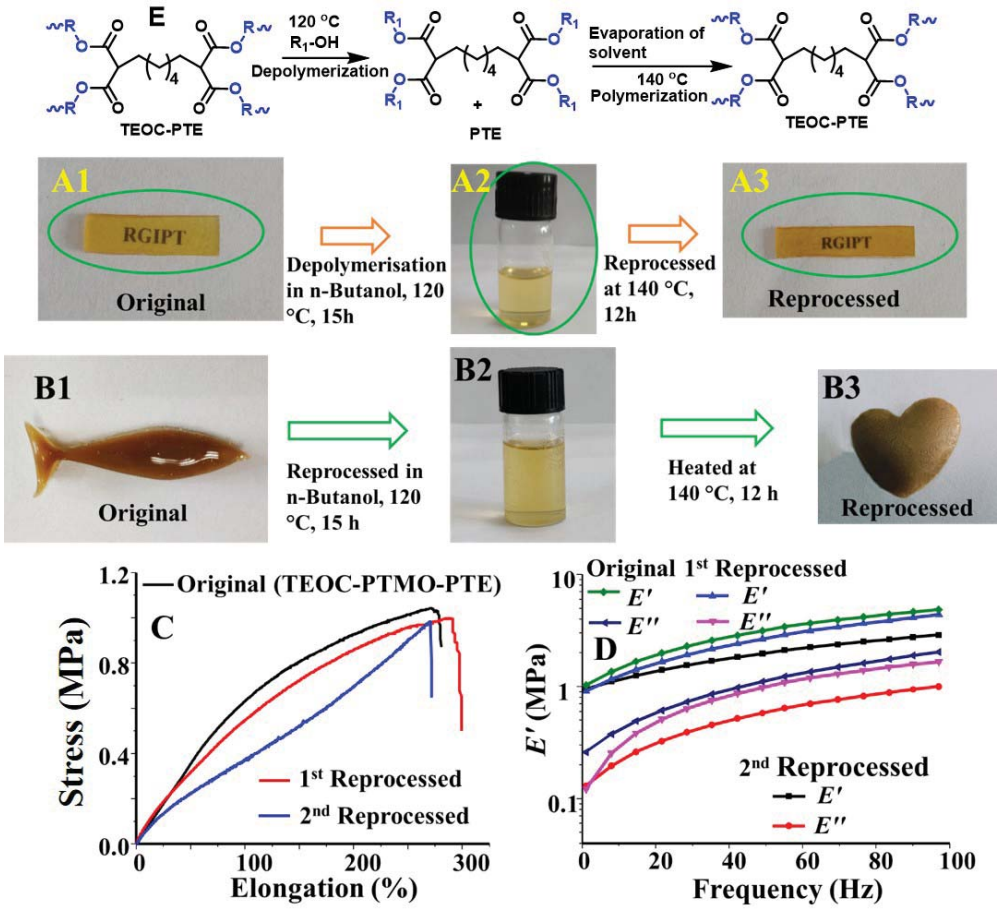

Figure 4.7: (A1) As prepared film of TEOC-PTE, (A2) homogeneous solution in n-butanol after depolymerization, (A3) reformed TEOC-PTE from the depolymerized solution, (B1) photograph of original TEOC-PTMO-PTE, (B2) sample after depolymerization, (B3) reprocessed sample of TEOC-PTMO-PTE, (C) tensile plots of original, 1^{st} and 2^{nd} reprocessed samples and (D) frequency sweep plots of the as-prepared, 1^{st} and 2^{nd} reprocessed samples, (E) the scheme above shows the degradation of TEOC-PTE via competitive transesterification with the solvent and reformation on evaporation of the solvent.

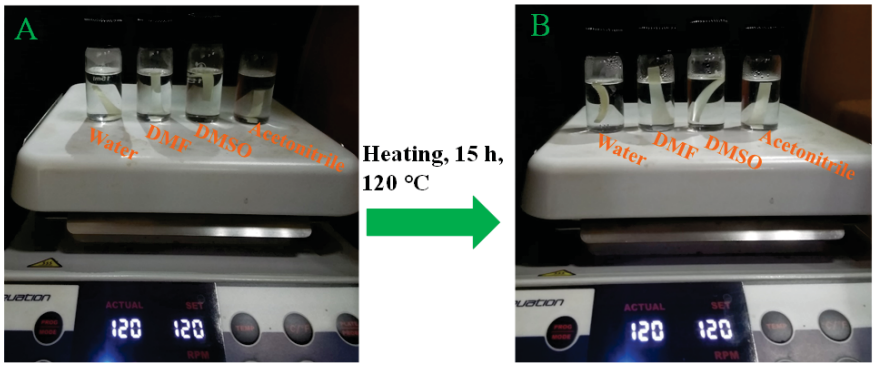

Figure 4.8: TEOC-PTMO–PTE CAN sample kept in non-alcoholic solvent for heating at 120 °C for 15 h.

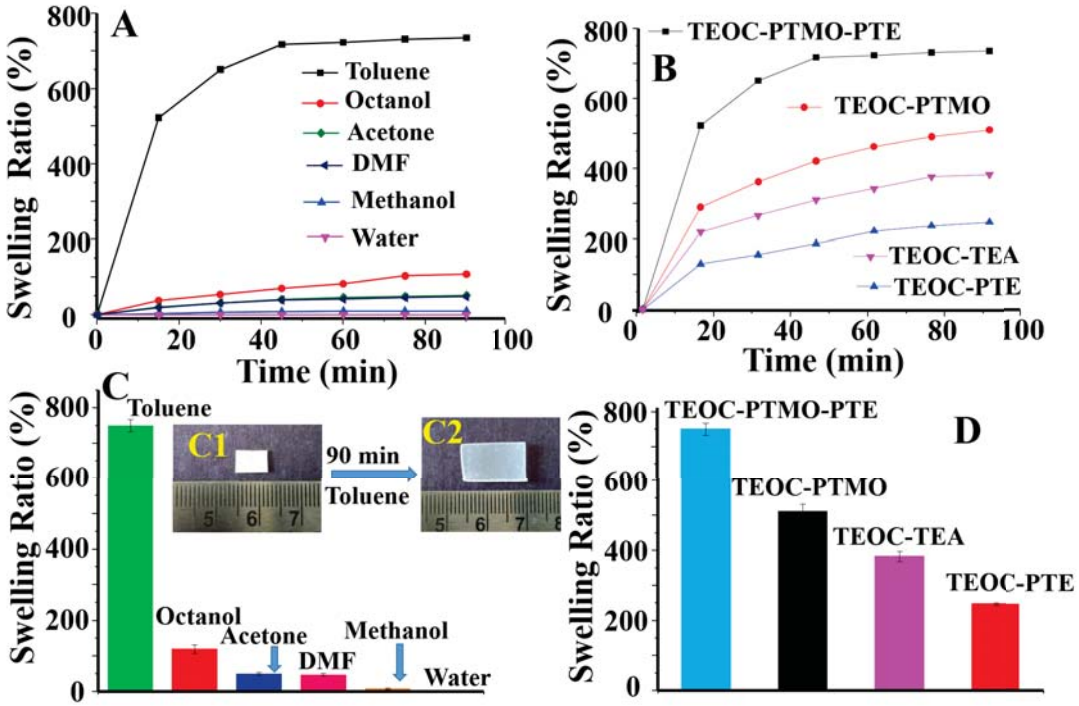

Figure 4.9: (A) Swelling ratio of TEOC-PTMO-PTE in various organic solvents and water after regular time intervals, (B) swelling ratio of different CANs in toluene after regular time intervals, (C) maximum swelling ratios of TEOC-PTMO-PTE in different solvents and (D) maximum swelling ratio of different CANs in toluene. The inset in (C) shows a dry and toluene soaked TEOC-PTMO-PTE after 90 min in toluene.

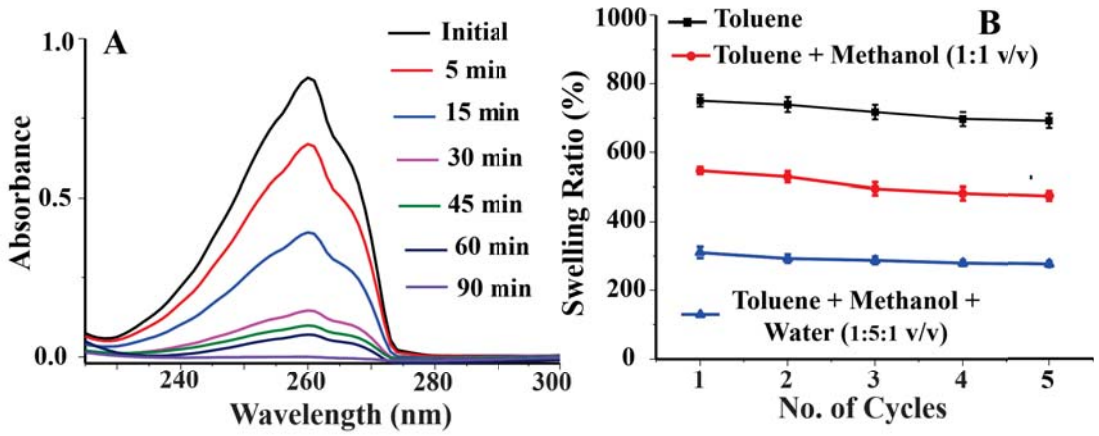

Figure 4.10: (A) Removal of toluene from methanol-toluene azeotrope (1.15:0.38, vol:vol) by TEOC-PTMO-PTE, (B) swelling ratio of TEOC-PTMO-PTE in toluene, toluene:methanol (1:1, vol/vol) and toluene:methanol:water (1:5:1, vol/vol) in repetitive cycles.

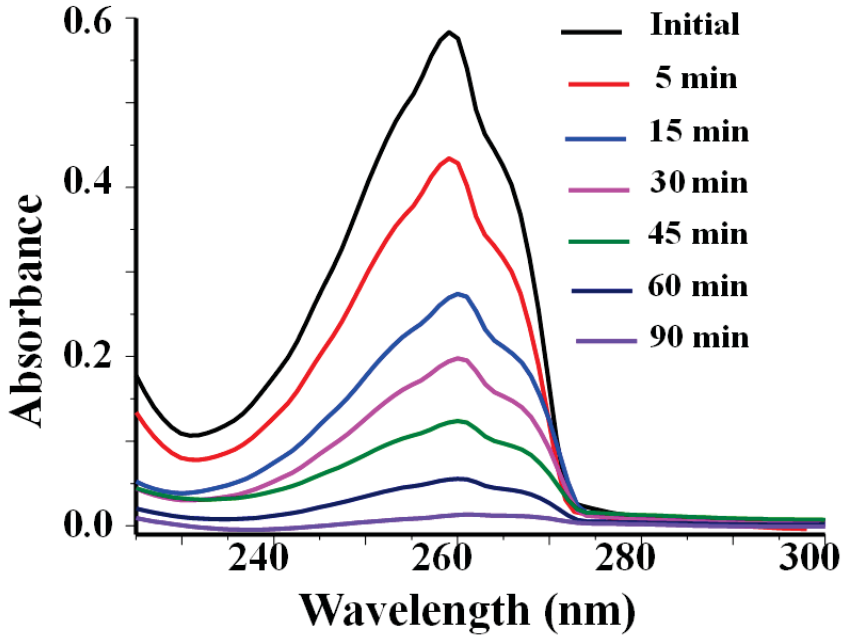

Figure 4.11: Monitoring the removal of toluene from toluene-methanol-water azeotrope (1.15:0.19:0.06, vol:vol) by TEOC-PTMO-PTE film through UV-Vis spectroscopy.

However, the swelling ratio values of other CANs were $\leqslant$500% in toluene (4.9B). The swelling was comparatively fast and equilibrium was reached within 1 h of dipping in the solvent (Figure4.9B). The above data suggested that the CANs may be utilized to separate toluene from different organic and azeotropic mixtures. Separation of azeotropic mixture is an important problem in industries and needs cumbersome process units such as pressure-swing distillation, extractive distillation and critical temperature and pressure conditions.[329, 330] Binary (toluene:methanol = 1.15:0.38, vol:vol) and ternary (toluene : methanol : water = 1.15:0.19:0.06, vol:vol) azeotropes were prepared and the efficiency of TEOC-PTMO-PTE to remove toluene from the above azeotropic mixtures were accessed. Strips of TEOC-PTMO-PTE were dipped in the above azeotropic mixture for a fixed time period. The strips were removed and UV-Visible spectra of the mixture was recorded after specific time intervals. The peak at 260 nm assigned to the toluene slowly decreased with the immersion time. The peak disappeared within 90 min suggesting maximum removal of toluene from the mixture (Figure4.10A & Figure4.11).

The reusability of these CANs were accessed by frequently using a set of TEOC-PTMO-PTE strips for five continuous absorption-desorption cycles in toluene and different solvent mixtures. The sample retained up to 90% swelling ratio till 5^{th} cycle (Figure4.10B). The fast absorption and reusability of the samples suggested that these CANs may be a cost effective and suitable alternative to be used in large scale fixed beds for continuous separation of azeotropic mixture.

4.5 Conclusions

The α-substituted β,β'-diesters undergo trans-esterification reaction under moderate temperature conditions (110 to 140 °C) in presence of a minor amount of $Sn(Oct)_2$. This trans-esterification chemistry is appropriate to synthesize solution processable and recyclable CANs. Typical volatile alcohols promptly depolymerize the CANs via competitive trans-esterification. Evaporation of solvent and subsequent heating is sufficient to reform the CANs with comparable properties to that of the original samples. Overall, the synthesis and reprocessability of these CANs is suitable and cost effective. Organogels can be planned and synthesized by incorporating suitable polyether diols into the CANs. The PTMO based CANs are capable of selectively absorbing aromatics among several organic solvents and separating toluene from various azeotropic mixtures. These CANs hold promise of being applied in fixed bed columns for continuous separation of aromatics form azeotropic mixtures in future.

This page was intentionally left blank.

Chapter 5

Reprocessable and Self Healable Segmented Polyurethane Vitrimers Displaying Creep Resistance Behavior and Triple Shape Memory Ability

5.1 Abstract

In spite of vast use of conventional polyurethane foams as polymer materials, the lack of reprocessability and creep resistance ability limits their further commercial growth. Imparting recyclability, self healing and creep resilience ability to segmented PU networks (PUN) is needed to further enhance their commercial utility and address the concern related to polymer waste accumulation. In this article, we apply the strategy of incorporating a dynamic carboxylate linkage in the main chain of polytetramethylene oxide (PTMO) based segmented PUNs to achieve the above. The resulting PUNs exhibited adequate tensile properties (tensile strength $\approx$ 8-33 MPa, elongation at break $\approx$ 345-680% and Young's modulus $\approx$ 19-270 MPa). The samples showed typical vitrimer behavior and stress relaxed in the temperature range of 140 to 180 °C. The PUNs thermally reprocessed at 150 °C, recovered up to 70-85% of the original tensile strength. Importantly, these vitrimers showed improved creep resistant

behavior at elevated temperature, which has been a concern with the conventional vitrimer materials. The PUNs showed triple shape memory abilities at inflection temperatures of 60 and 130 °C respectively. The samples also possessed effective self healing and self welding ability. Overall, these PUNs with versatile properties are potential candidates for various applications.

5.2 Introduction

Polyurethane networks (PUN) are one of the extensively commercialized polymeric materials due to their promising mechanical,[331] thermal and insulating properties[332] along with oxidative and hydrolytic stability.[333] These class of materials have been applied in biomedical devices,[334] electronics,[335] adhesives,[336] blends,[337] commodity applications, automobile industries and insulation.[338] The segmented PUs have been especially attractive, as their tensile strength, elongation, and modulus values are adjustable over a wide range via moderation of the ratio between soft and hard segments in the polymer.[339, 340] Moreover, these materials due to their microphase segregated morphology, display multiple thermal transitions and shape memory behavior.[341, 342] Mainly, polymeric diols or diamines such as α,ω-bishydroxy endcapped polytetramethylene oxides (PTMO), polyisobutylene, polydimethyl siloxanes are used as the soft segment to synthesize the segmented PUs using diisocyanate or dicarbonates as the chain extenders. In the isocyanate pathway, the combination of diisocyanate and butanediol or ethanediol forms the hard segment. The ratio between the hard segment and soft segment in PUs determines the mechanical properties and forms the basis of structure-property relationship.[343] Along with versatile thermal and mechanical properties, these materials are known to have biocompatibility and biodegradability.[344, 345]

In spite of the above promising properties, the commercial implementation of conventional PUs is somewhat restricted due to their recyclability and processability concerns. Therefore, attention has done to induce reprocessability and self-healing ability of PUNs by stimulating the chemical linkages in the polymer.[346] Basically, two routes are followed in literature to induce thermal reprocessability in PUNs. In the first approach, the dynamic characteristics were induced to the urethane linkage by adapting the electronic environment of the functional group. As an example, N,N′-diaryl substitution induced reversibility to the urethane-urea linkage at 100 °C.[347] Likewise, N-alkyl hydroxyl urethanes were swiftly remolded at 160 °C under catalyst free conditions.[348] In some cases, to thermally reprocess the samples catalyst such as dibutyltin dilaurate was added to the PU systems.[349] Stoichiometric imbalance was also used as a tool to impart thermal reversibility to PUNs and

excess of hydroxyl functional groups in the matrix helped the samples to quantitatively recover original crosslink density after reprocessing at 140 °C.[350] Use of phenolic hydroxyl groups also showed quick thermal reversibility at ∼100 °C to the urethane linkage due to the electron withdrawing nature of the moiety.[351] Attachment of C=N functionality to the "O" of urethane linkage activated the linkage and the resulting oxime based PUs also exhibited prompt reprocessibility at 120 °C.[352]

The other approach was to incorporate a suitable dynamic chemical linkage in the polymer chain to render the PUNs self healability and reprocessability.[353, 354] For example, disulfide linkages were introduced into the main chain of the PUNs to impart thermal processability and the resulting materials showed swift relaxation time of 30 s at 150 °C.[355, 356] Photoactive hexa aryl biimidazole moieties were introduced into the PUNs to achieve light mediated processability of the PUs and the materials displayed actuating properties.[357] Integration of stimuli responsive Diels-Alder linkages rendered the PUNs to reprocess at 130 °C.[358] Hydrogen bond forming moieties such as diazolidinyl urea was introduced in the PU chains to rapidly self heal the materials at 90 °C.[359] PU based on double-decker silsesquioxane showed self healing ability via reversible physical crosslinking between the inorganic domain and urethane linkage.[360] PUs derived based on polyester segments such as polycaprolactone and polylactide showed recyclability due to the degradable nature of the ester segment.[361, 362] Currently, silica nano particles were dispersed in the PUN samples to promote reprocessability.[363] The thermally reprocessed samples recovered original mechanical properties. Triazolinedione chemistry was also used to reprocess the PUNs at 120 °C. The samples quantitatively self healed within 30 min exposure to 120 °C.[364]

So far, dynamic carboxylate linkage has not been utilized to develop reprocessable and self healable PUNs in literature to the best of our knowledge. Carboxylate linkages are known to have thermal stability, solvent resistance, biocompatibility and functional group tolerance and therefore are desirable to be utilized in PUs to induce reprocessability. Recently, several carboxylate systems having thermal reversibility is reported in literature. For example, the ethyl vinylacetate linkage underwent ester exchange reaction in presence of 1,5,7- triazabicyclo[4.4.0]dec-5-ene at 120 °C.[365] Exchangeable β-hydroxyl ester linkages were recently used to develop recyclable polymer network that showed soft actuating properties.[366] Similarly, carboxylate linkages based on epoxy-anhydride reaction were reprocessable at 180 °C.[367] Neighboring carboxylic acids and sulphonic acids intramolecular catalyzed the ester exchange reaction to synthesize dynamic covalent polyesters.[368, 369] Brønsted acids catalyzing the ester exchange in polyester vitrimers under moderate temperature conditions is also available in literature.[370] We have recently reported a thermally reversible β-carbonyl carboxylate system that undergoes associative ester bond exchange

under moderate temperature conditions expedited by the neighboring group effect of the carbonyl moiety.[371, 372] The dynamic ester linkages underwent associative bond exchange below 100 °C in presence of $Sn(Oct)_2$ as catalyst.

Considering the above, we have introduced introduce the above dynamic β-carbonyl carboxylate linkages in the PUNs to render these materials reprocessability and self healability. Typically, segmented PUNs will be made consisting of PTMO as the soft segment and combination of pentaerythrotol (PETL) and methyl diphenyl diisocyanate (MDI) as the hard segment. The PETL units will also support in crosslinking of the PU chains. The dynamic carboxylate moiety will be integrated to the PTMO diol. A set of PU networks by changing the ratio between hard and soft segment will be synthesized and their mechanical proeprties and reprocessability will be evaluated. The self healing as well as shape memory abilities will be studied to propose the viability of these class of materials.

5.3 Experimental

5.3.1 Materials and Methods

Diethyl malonate (DEM, SD Fine Chem., 98.0%), Tin (II) 2-Ethylhexanoate ($Sn(Oct)_2$, >85.0%), PTMO-diol (Sigma-Aldrich, M_n ~2900), MDI (Sigma-Aldrich, 98%), PETL (Himedia Laboratories, >98.0%), toluene (Fisher Scientific, 99.5%), THF (Qualigens, 99.0%), methanol (SD Fine Chem., 99.0%), acetone (Molychem, 99.0%), N,N-dimethylformamide (DMF, Spectrochem, 99.0%), dimethyl sulphoxide (DMSO, Fisher Scientific, 98.0%) and deionized water.

5.3.2 Characterization

We used JEOL-400 YH for the ^1H and ^{13}C NMR study using $CDCl_3$ as the solvent at 25 °C. We used Tinius Olsen (H5KL UTM) machine to measure the ultimate tensile strength (UTS) at ramp rate of 5.0 mm/min. Samples of ~4 mm width and ~0.5 mm thickness were used for measurement and average of three experimental data is described. We got the Young's moduli (E) data from the linear region of UTS plot (Hookean zone). Temperature sweep experiment was achieved under tension mode in DMA Q-800 TA instrument following 50 ASTM D4065-01 norm. Sample dimension for the above was as follows; width ~ 4.0 mm

and thickness $\sim$ 0.5 mm. The stress relaxation behavior of the samples (width $\sim$8 mm and thickness $\sim$2 mm) was checked under compression mode. We used 0.1% constant strain and 10 min temperature equilibrium under compressed mode for measuring stress relaxation behavior. We calculated the activation energy (Ea) after normalizing the relaxation modulus. The DMA Q-800 was used to measure the shape memory performance of the materials. For double shape memory performance; first we equilibrated the sample at 60 °C at 0.001 N force for 10 min. Subsequently the force was increased to 3.0 N under 0.2 N ramp and the sample was kept under isothermal condition for 10 min. Then the sample was cooled and kept 0 °C for 15 min. After that, the applied force was released to 0.001N and kept for 15 min. The temperature was gradually increased to 60 °C and kept it for 15 min for the last step. For cyclic double shape memory performance, the same experiment was repeated for three times. For triple shape memory performance first the sample was equilibrated at 130 °C for 20 min and 0.55 N force was applied. The isothermal step was kept for 20 min for the first shape fixing. Subsequently, the temperature was decreased to 60 °C and the isothermal step was continued for 10 min. The force was increased to 1.6 N for the second shape fixing. The temperature was released to 0 °C and the condition was maintained for 15 min. The force was released to 0.001N and the sample was maintained isothermal for 15 min. The temperature was increased to 60 °C and continued for 15 min for the first recovery of the sample. The temperature was increased to 130 °C and maintained for 20 min for the second recovery. We repeated the same experiment for cyclic triple shape memory experiment. DMA Q-800 instrument was used for Creep experiment. The samples (width $\sim$4.0 mm and thickness $\sim$0.4 mm) were stretched under different constant stress (4, 6, 8, 12, 16, 18 and 20 MPa) for 10 min followed by 20 min recovery time. Creep experiment also conducted at different temperatures (30, 40, 50, 80, 100, 120 and 140 °C) under constant stress (6 MPa). Differential Scanning Calorimetry experiment (DSC) was performed in Mettler Toledo 832 instrument at 10 °C/min rate under N_2 atmosphere. The glass transition temperature (T_g) and melt temperature (T_m) determined from first heating traces was presented. The T_g was taken as the mid-point of the transition. Atomic Force Microscopy (AFM) imaging was performed in a Bruker Dimension FastScan model using RTESP-300 cantilever. The experiment was done at room temperature under tapping mode. Waters 2414 RI Detector attached with Waters 1515 Isocratic Pump was used for the determination of molecular weight of the samples. THF was used as eluent with injection volume of 10 μl.

5.3.3 Synthesis of DEM-PTMO$_2$

The mixture of DEM (1.0 g, 6.25 mmol) and PTMO-diol (39.87 g, 13.74 mmol) was heated in presence of Sn(Oct)$_2$ (126.0 mg, 5 mol% with respect to DEM) at 100 °C under sol-

vent free conditions for 24 h. The reaction mixture was cooled to room temperature and used for further analysis without purification.^{1}H NMR ($CDCl_3$, 400 MHz) δ (ppm): 4.1 (t, -COOC$\boldsymbol{H}_2$CH$_2$-, 4H), 3.4 (t, -CH$_2-$C$\boldsymbol{H}_2-$O-, 4H), 3.3 (s, -C$\boldsymbol{H}_2$(COO)$_2$-, 2H), 1.6 (m, -CH$_2-$C$\boldsymbol{H}_2-$C$\boldsymbol{H}_2-$CH$_2$-, 8H). ^{13}C NMR ($CDCl_3$, 100 MHz) δ (ppm): 166.7 (-$\boldsymbol{C}$OO-), 70.6 (-O$-\boldsymbol{C}$H$_2$), 62.7 (-O$-\boldsymbol{C}$H$_2$), 41.5 (-$\boldsymbol{C}$H$_2-$(COO$-)_2$), 30.4 (-$\boldsymbol{C}$H$_2-$CH$_2$-), 26.7 (-$\boldsymbol{C}$H$_2-$CH$_2$). GPC (THF solvent): number average molecular weight (M_n) = 6500 g/mol, polydispersity index (PDI) = M_w/M_n = 1.02.

5.3.4 Synthesis of Polyurethanes

Azeotropic distillation of DEM-PTMO$_2$ (1.09 g, 0.37 mmol) and Sn(Oct)$_2$ (2.8 mg, 0.007 mmol) mixture was carried out by using dry toluene (10 mL) at 50 °C for 6 h under vacuum. To the above mixture dry toluene (20 mL) was added and a homogenous solution was prepared. The mixture was kept at 80 °C under dry nitrogen atmosphere for 15 min. To it, MDI (0.58 g, 2.33 mmol) was added and stirred for 30 min. To the above mixture, PETL (0.23 g, 1.7 mmol) was added. Then the mixture was heated at 80 °C for further 3 h to found a highly viscos polymeric material. The material was poured into Teflon petri dish and allowed to cure for 24 h under ambient conditions to evaporate the toluene. Subsequently, the material was dried in vacuum oven at 50 °C for 12 h. Five different compositions were synthesized following the above procedure by varying the molar ratio of PETL and MDI. The amount of MDI and PETL together was considered as hard segment and the amount of DEM-PTMO$_2$ was taken as the soft segment in the PUNs. The nomenclature of the samples was given as follows PUNn, where "n" is the amount of hard segment in the samples. The molar compositions of the precursors in the samples were as follows; PUN43 (PETL=1.7 mmol, MDI=2.33 mmol), PUN40 (PETL=1.0 mmol, MDI=2.33 mmol), PUN32 (PETL=0.66 mmol, MDI=1.68 mmol), PUN24 (PETL=0.66 mmol, MDI=1.03 mmol), PUN21 (PETL=0.33 mmol, MDI=1.03 mmol). All the above composition possessed same amount of DEM-PTMO$_2$ (0.37 mmol).

5.3.5 Determination of Cross-Linking Density (d_c)

The d_c values of the PUNn samples were determined from the following Equation;

$$d_c = E'/RT \tag{5.1}$$

where E' is plateau modulus (storage modulus) at 250 °C, and T is the temperature in °K, R is the gas constant in J $mol^{-1}K^{-1}$.

5.3.6 Ratio of Shape Fixity (R_f) and Ratio of Shape Recovery (R_r) Determination

Ratio of shape fixity (R_f) and ratio of shape recovery (R_r) were calculated using below equations;

$$R_f(\%) = \frac{\varepsilon_u(N)}{\varepsilon_i(N)} \times 100 \tag{5.2}$$

$$R_r(\%) = \frac{\varepsilon_u(N) - \varepsilon_f(N)}{\varepsilon_i(N) - \varepsilon_f(N-1)} \times 100 \tag{5.3}$$

Where, ε_u = Strain value recorded after releasing of the applied load, ε_i = Initial strain value before release of the load, ε_f = train value after heating without applied load, N = No. of cycles.

5.4 Results and Discussion

The DEM-$PTMO_2$ having two units of β-carbonyl carboxylate linkage in the centre was synthesized by reacting DEM with PTMO-diol under solvent free conditions as shown in Scheme5.1 and used as the soft segment in the PUN synthesis. The ^{1}H NMR quartet at 4.22 ppm for the -OCH_2- and triplet at 1.40 ppm for -CH_3 present in DEM.

The substantially decreased and a new triplet at 4.16 ppm for -OCH_2CH_2- in product seemed supporting the formation of DEM-$PTMO_2$ (Figure5.1A). Similarly, in ^{13}C NMR spectra new peak at 62.7 ppm responsible to -OCH_2- of DEM-$PTMO_2$ and disappearance of peak at 18 ppm for the -CH_3 of DEM supported the trans-esterification (Figure5.1B). The integration of ^{1}H NMR signal at 4.22 ppm was compared to that of the 4.16 ppm to estimate the extent of PTMO functionalization on DEM, which was determined to be >94%. The M_n value (6500 g/mol) obtained from the GPC analysis was close to the theoretical molecular weight of the product (5960 g/mol) and the PDI value was narrow, which supported the

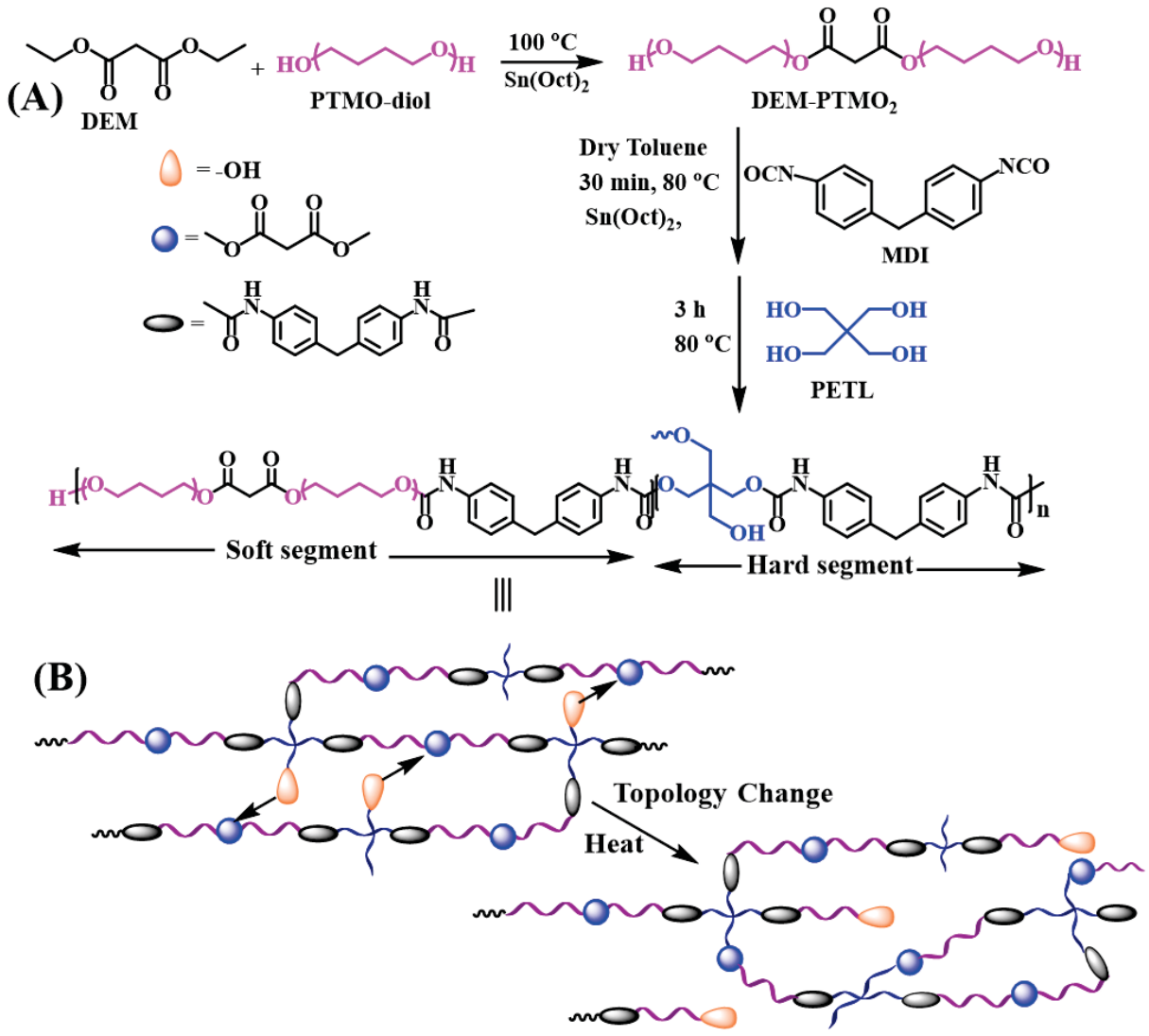

Scheme 5.1: (A) The synthetic scheme for the PTMO based segmented PUNs, (B) the schematics display the topology change of the network under thermal condition though exchange of the -OH group in dynamic carboxylate linkage.

Table 5.1: The amount of hard segment, mechanical properties and cross-linking density of PUNs possessing β-CO carboxylate moiety

Sample Code	HS* (wt%)	UTS (MPa)	ε (%)	$E^{\#}$ (MPa)	$E'^{\&}$ (MPa)	d_c x 10^3 (mol/cm^3)
PUN43	43	33.0 ± 2.1	345 ± 14	270.0 ±13.5	750.0 ± 21.3	18.5 ± 0.9
PUN40	40	30.0 ± 2.0	360 ± 14	210.0 ± 12.0	580.0 ± 18.5	13.6 ± 0.7
PUN32	32	22.0 ± 1.1	400 ± 15	150.0 ± 5.0	390.0 ± 17.6	10.3 ± 0.5
PUN24	24	14.0 ±1.0	515 ± 20	40.0 ± 1.2	185.0 ± 15.8	1.0 ± 0.05
PUN21	21	8.0 ± 0.6	680 ± 22	19.0 ± 0.5	105.0 ± 12.4	0.8 ± 0.03

*the combination of MDI and PETL constituted the hard segment (HS) and DEM-PTMO$_2$ constituted the soft segment, $^{\#}E$ value was calculated from the tensile plot, and $^{\&}E'$ was determined from the DMTA trace.

formation of DEM-PTMO$_2$ and absence of possible side products. The DEM-PTMO$_2$ and MDI were reacted together in the first step in presence of Sn(Oct)$_2$ (0.3 mol% with respect to MDI) to form the soft segments and the networking was carried out in the second step by adding PETL as the chain extender and crosslinker (Scheme5.1). A series of PUNs were synthesized by varying the ratio between soft segment and hard segment (Table5.1). The synthesized networks were dipped in THF for 24 h to estimate the gel fraction. In all the cases, the mass loss was obtained between 3 to 5 wt%, suggesting effective crosslinking in the networks.

The mechanical properties of the PUNs were assessed using tensile and DMA analysis. The samples showed UTS values in the range of 8 to 33 MPa (Table5.1). Presumably, the value increased with the amount of hard segment in the networks (Figure5.2A-C). The ε value decreased from 680 to 345% on increasing the %age of hard segment from 21 to 43 in the sample. The E values were found in the range of 19 to 270 MPa suggesting networks of varying flexibility may be synthesized by tailoring the ratio between hard and soft segments in the samples.Importantly, the E value almost linearly increased with the hard segment content in the PUN (Figure5.2F). This suggested that the hard segment domain content and distribution controlled the modulus of the samples. The hysteresis of the samples was monitored under tensile mode by using thin film of PUN43.

The hysteresis was performed under a constant high UTS value of 20 MPa to understand the load bearing ability (Figure5.2B). The first cycle exhibited a residual strain of 10% and was related with an energy dissipation value of 660 kJ/m^3. However, the subsequent cycles displayed improved recovery and the deformation lag decreased to 2% in 2^{nd} cycle. The notable decrease of dissipation energy from the 1^{st} to subsequent cycles are are also depicted in literature, which may be assigned to the possible morphology change in the vitrimer system.[373, 374] The energy dissipation value in the 2^{nd} to 5^{th} cycle was calculated between 9 kJ/m^3 to 2 kJ/m^3. The repetitive recovery of the sample from a high stress value of

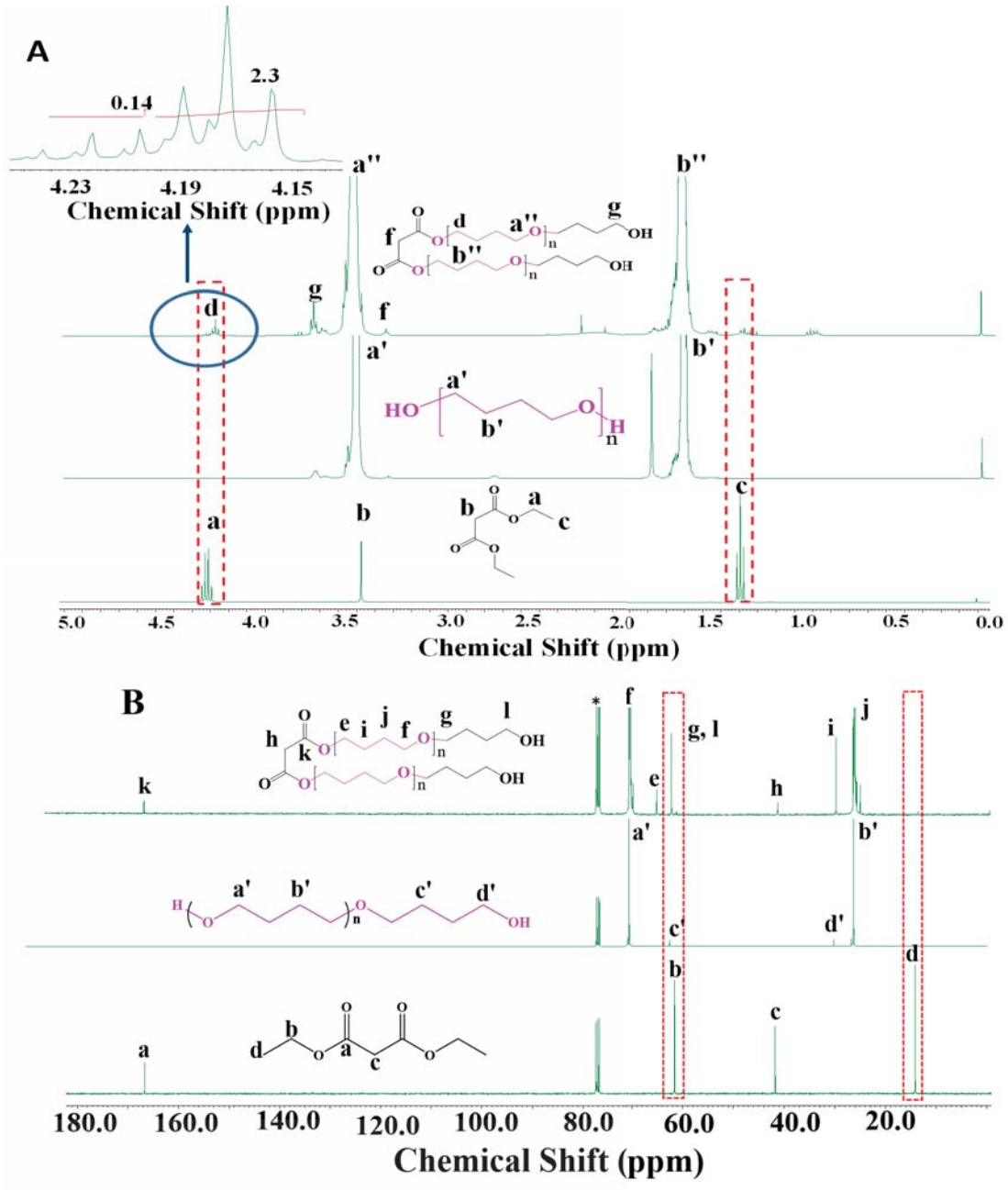

Figure 5.1: (A) ^{1}H NMR spectra of precursors and DEM-PTMO$_2$. The inset shows the magnified signals between 4.0 to 4.3 ppm with integration, (B) the ^{13}C NMR spectra of the precursors and the substituted product (DEM-PTMO$_2$).

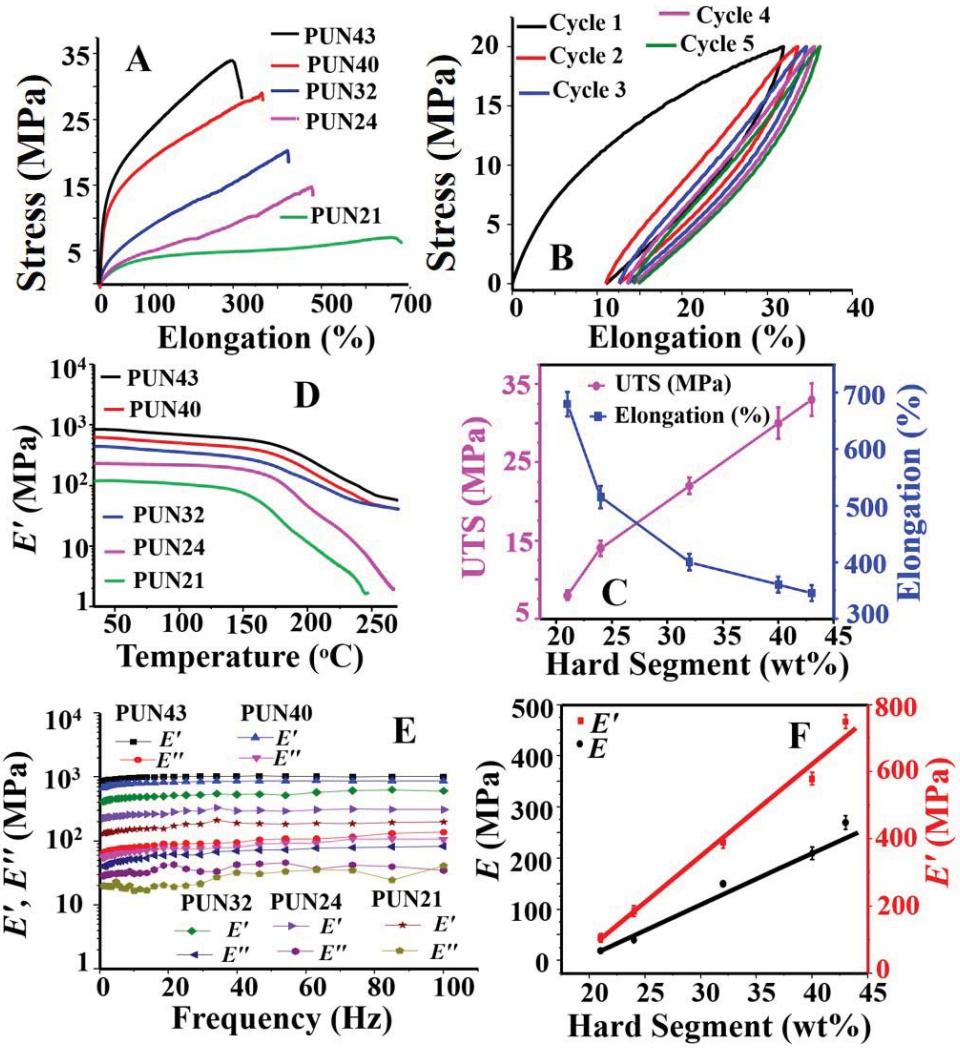

Figure 5.2: (A)Tensile plots of the PUNs, (B) hysteresis curves of PUN43, (C) effect of HS wt% on the UTS and elongation of resulting PUNs, (D) DMTA traces of the PUNs, (E) DMA frequency sweep data and (F) effect of HS wt% on the E and E' values.

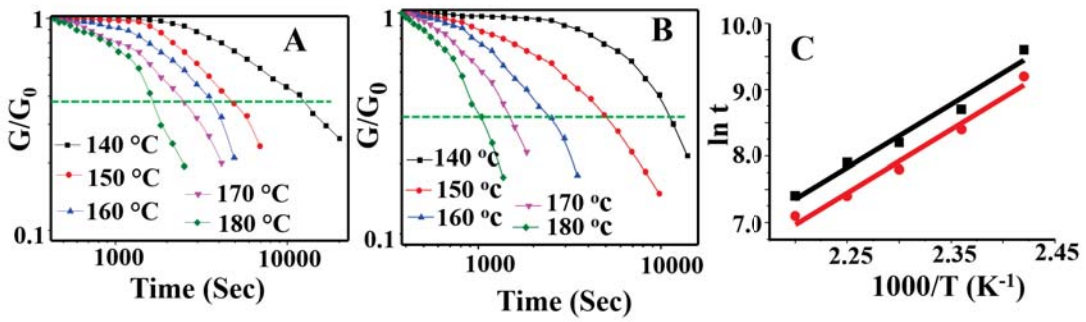

Figure 5.3: Stress relaxation traces of (A) PUN43 and (B) PUN40 under different temperature conditions and (C) Arrhenius plots of PUN43 and PUN40.

20 MPa with low energy dissipation value suggested that these networks possess satisfactory load bearing ability. The DMTA traces of the samples were recorded by heating the thin films from 30 to 270 °C at a frequency of 1 Hz. The major transition in E' values were observed beyond 150 °C suggesting the PUNs are suitable for applications in temperature range below 150 °C. The rubbery plateau zone for PUN43, PUN40 and PUN32 was detected beyond 250 °C. However, in case of PUN24 and PUN21, the E' values constantly decreased without showing a plateau (Figure5.2D). This could be attributed to the low degree of crosslinking in the samples. The d_c values of the PUNn were calculated from the E' value at 250 °C. As anticipated, the sample (PUN43) having maximum PETL amount exhibited d_c value of 18.5x10^{-3} mol/cm^3, which gradually decreased to 0.8x10^{-3} mol/cm^3 with the decrease in PETL amount (Table5.1).

Similarly, the difference between E' and E'' values was maximum for PUN43 telling strong degree of crosslinking in the sample. Overall, the E' value was higher compared to that of the E'' in all the samples suggesting the crosslinked nature of the PUNs (Figure5.2E). The β-carbonyl carboxylate linkages present in these PUNs were presumed to undergo associative bond exchange in presence of free -OH groups in the temperature range of 130 to 170 °C. Therefore, the vitrimer behavior of the samples were evaluated by performing the stress relaxation analysis of PUN43 and PUN40 (Figure5.3A-B). The samples stress relaxed in the temperature range of 140 to 180 °C. The time taken to reach a G/G_0 value of 0.37 was considered as the half life of the samples and the values were plotted against the temperatures to determine the Ea value of the exchange reaction of free -OH with β-CO carboxylate exchange reaction in PU matrix. The values were calculated to be 80 and 75 kJ/mol for PUN43 and PUN40 (Figure5.3C).[375] The data show that, these PUNs display vitrimer behavior in the temperature range above 140 °C. The stress relaxation data at 120 °C showed negligible change in G/G_0 value up to 10000 sec suggesting the exchange reaction in these PUNs are extremely slow in the temperature range of 120 °C or below.

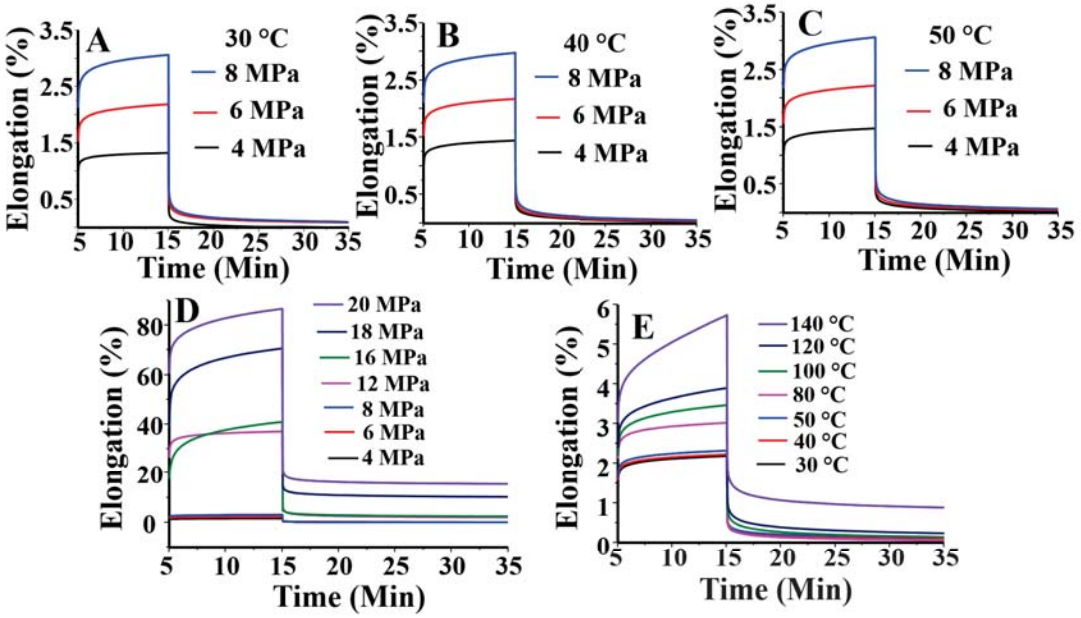

Figure 5.4: Creep resistance studies of PUN43 at (A) 30, (B) 40 and (C) 50 °C under applied stress value of 4, 6 and 8 MPa, (D) the extent of recovery of PUN43 under different stress values at room temperature conditions, (E) the extent of recovery of PUN43 under different temperature conditions at an applied stress of 6 MPa.

Creep recovery ability of the materials, especially at high temperature is another desirable property from the perspective of practical applications.[376, 377] Importantly, the number of reports on PUNs possessing improved creep behavior is limited in literature. Especially, vitrimers are known to show weak creep resistance behavior due to the thermosensitivity of the dynamic linkage.[378] Crosslinking is one of the approach adopted to improve the creep resistant properties in materials.[379] Since, in this work, the covalent crosslinking (-NHCOO-) and dynamic covalent linkages ($COCH_2COO$-) are different, we have showed that the PUNs exhibit improved creep behavior till the stress relaxation temperature. The creep resistance ability of these PUNs were investigated. Preliminarily, thin films of PUNs were evaluated for possible creep recovery ability. The samples were analyzed under multiple stress (4, 6 and 8 MPa) and temperature (30, 40 and 50 °C) conditions. All the samples reached strain equilibrium under application of the above stress values following a viscoelastic pattern and the strain quantitatively recovered on release of stress suggesting satisfactory creep resistance behavior (Figure5.4 & 5.5). To investigate the creep resistance ability under high stress, PUN43 was permitted to relax from a reasonably high load up to 20 MPa and the recovery was monitored. Till 16 MPa load, the sample strain quantitatively recovered on release of stress suggesting excellent creep resistance ability in these materials.

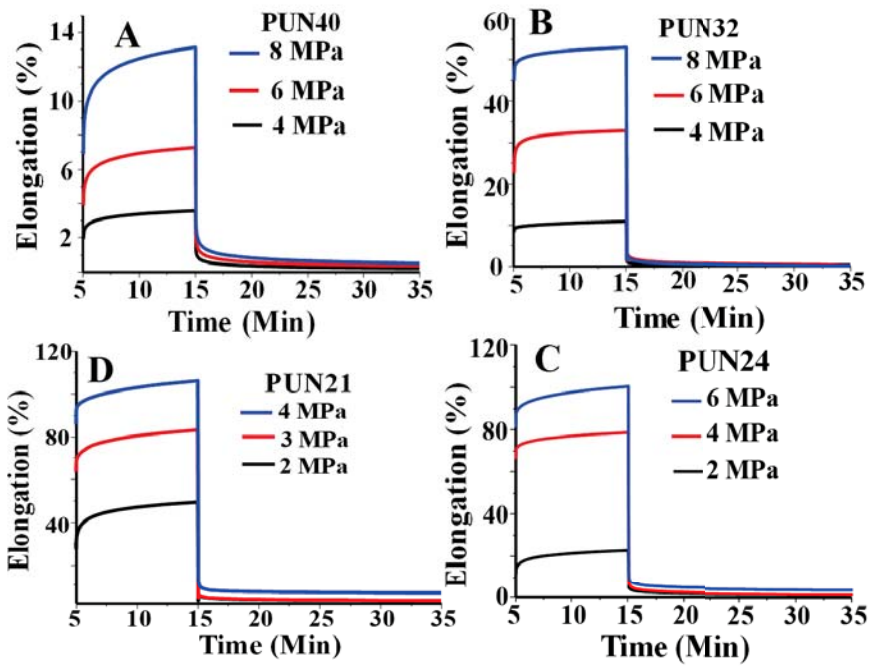

Figure 5.5: Creep resistance studies of the film (A) PUN40, (B) PUN32, (C) PUN 24 and (D) PUN21 under applied stress value of 2, 3, 4, 6 and 8 MPa.

On further increasing the load up to 20 MPa, the recovery was limited to 86% only, this could be due to the partial damage of the network arrangement at such high stress. Similarly, the PUN43 sample was performed under different temperature conditions from 30 to 140 °C at 6 MPa stress. Till 120 °C, the sample quantitatively recovered with no negligible residual strain signifying adequate creep recovery ability at high temperature conditions. At 140 °C, the strain recovery was up to 88%, which may be attributed to the cleavage of dynamic linkage at this temperature and rearrangement of the network structure. The creep resistance ability of these PUNs were found to superior compared to that of the several vitrimer materials reported in literature.[380, 381]

Subsequently, the thermal processability of the PUNs were studied at 150 °C. The films of PUN43 and PUN40 were cut into small pieces and pressed with 90 kg load at 150 °C to perform the reprocessing efficiency.

The pieces joined together to form a continuous film within 5 h (Figure5.6A1-A3). However, the color of the samples turned somewhat dark, which could be attributed to the thermo-sensitive urethane linkages existing in the sample. Similar observation is already observed in the literature for thermally processed PUs.[382] The UTS and E' values of the reprocessed PUN43 recovered up to 70 and 87.5% respectively of the original samples supporting the reprocessability efficiency (Figure5.6B-D & 5.7).

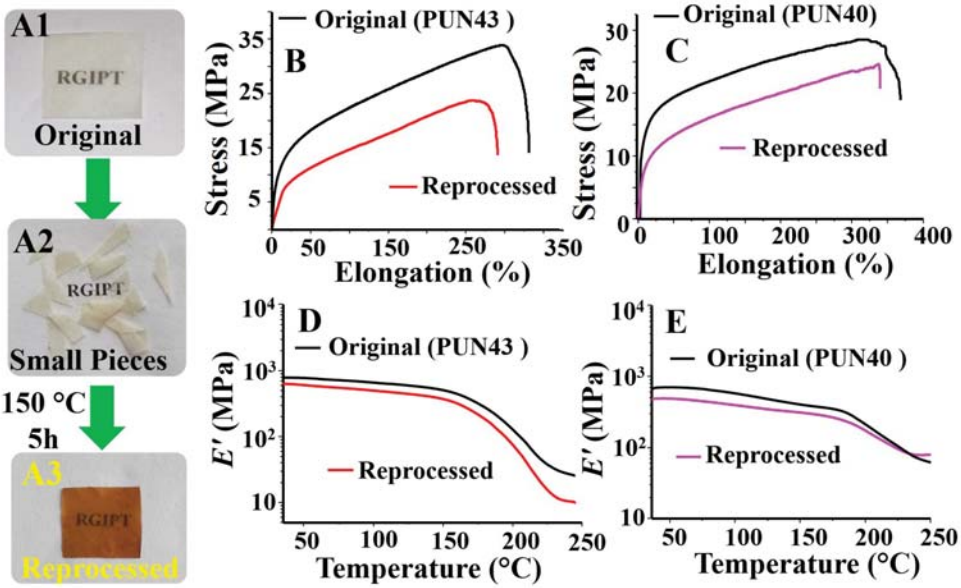

Figure 5.6: (A1) Original, (A2) small cut pieces (A3) reprocessed PU film, (B) tensile plots of original and reprocessed film of PUN43, (C) tensile plots of original and reprocessed film of PUN40, (D) DMTA traces of original and reprocessed film of PUN43, (E) DMTA traces of original and reprocessed film of PUN40.

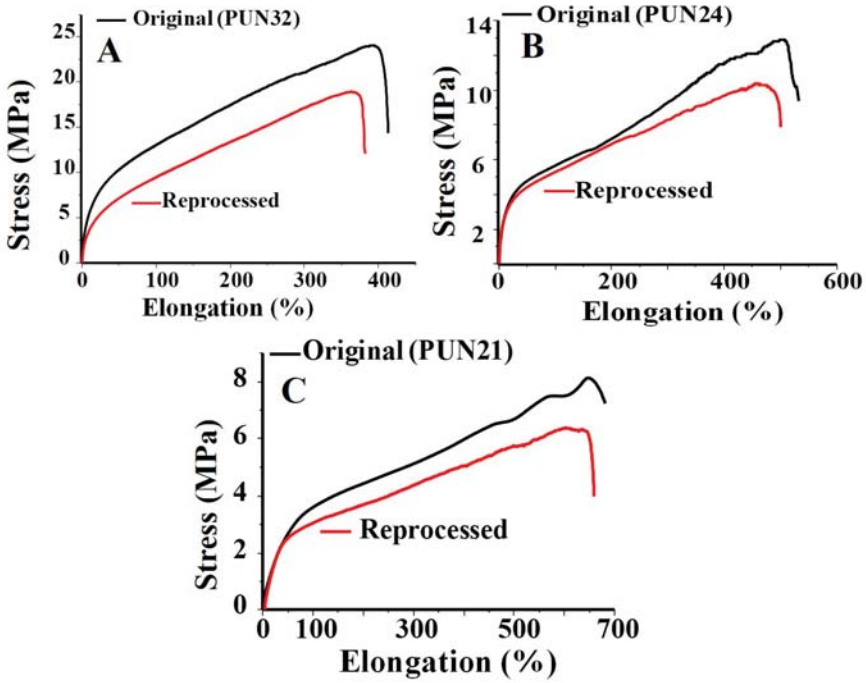

Figure 5.7: Tensile plots of original and reprocessed film of (A) PUN32, (B) PUN24, & PUN21

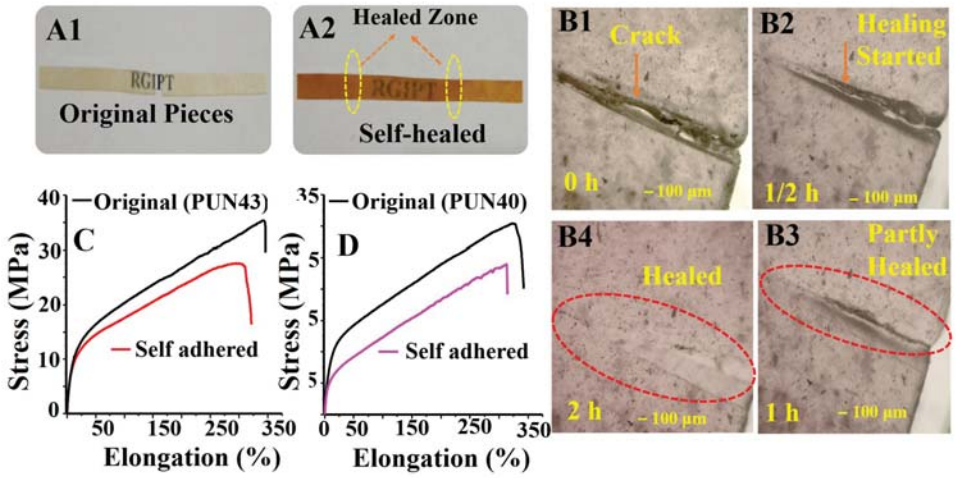

Figure 5.8: (A1) Original, (A2) self-adhered PUN43 films, (B1) thin film of PUN21 with a cut made by razor blade, self-healing after (B2) 30 min, (B3) 1 h and (B4) 2 h, tensile plots of original and self adhered films of (C) PUN43 and (D) PUN40.

The tensile plots of the original and reprocessed samples of the thin films of all the PUNs are provided for clarity. The recovery effectiveness of the UTS values for all the PUNs were calculated to be in the range of 70 to 80% after thermal reprocessing at 150 °C.Subsequently, the self adhering ability of the samples were monitored by overlapping the ends of two pieces of PUN43 and allowing the sample to weld at 150 °C under 90 kg load. The pieces adhered to each other successfully and the UTS value of the adhered sample was 72% of the native sample (Figure5.8A-C & 5.9). Similarly, the self adhered PUN40 exhibited 73% UTS value of the pristine sample (Figure 5.8D). The other PUNs displayed 76-82% and 82-88% recovery in the UTS and E value respectively suggesting adequate self welding ability. The somewhat lower recovery of the tensile properties of the reprocessed and welded films could be attributed to the amount and distribution of β-CO carboxylate dynamic linkages in the samples. Possibly, the hard segment zones in the PU networks failed to soften at 150 °C, which prohibited quantitative healing of the samples. The issue may be suitably addressed by adjusting the composition and type of isocyanate crosslinkers used in the samples.

The crack healing of the samples was monitored by making a thin cut on a PUN21 thin film and permitting the cut to heal by heating the cracked specimen at 150 °C. The crack gradually healed and the cut point was unrecognizable after 2h suggesting PUN21 films are capable of self healing under thermal conditions (Figure5.8B1-B4). It is important to note that the T_m of PUN21 was observed at 190 °C (Figure5.12C). Therefore, the self healing in the sample may be ascribed to the topology change aided by the exchange of dynamic carboxylate linkage.

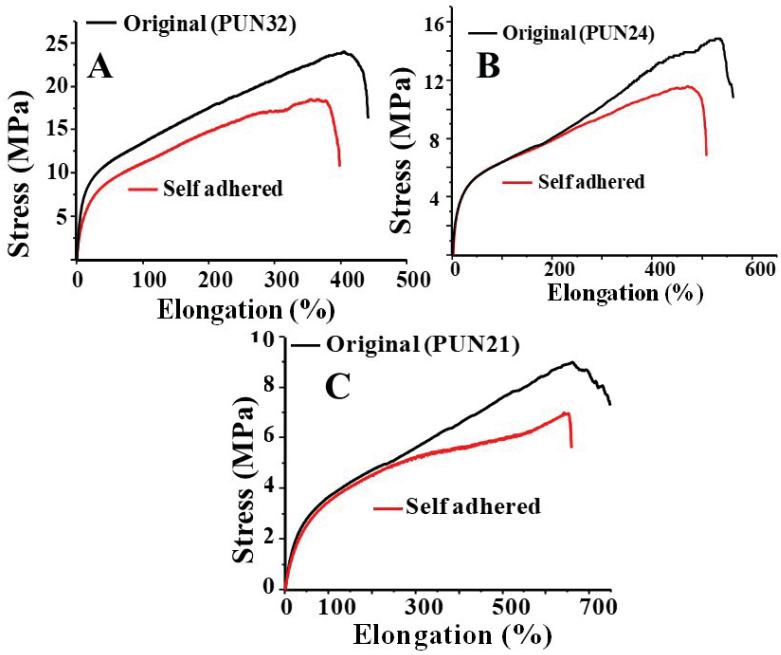

Figure 5.9: Tensile plots of original and self adhered film of (A) PUN32, (B) PUN24, & PUN21

These PUNs are segmented structures having PTMO based soft segment and PETL and MDI based hard segment domains. These segments are known to phase segregate in PU samples and the phase segregation pattern is dependent on the ratio of hard to soft segment in the samples.[383] The AFM phase images recorded under tapping mode exhibited distinct phases in the samples possessing hard segment amount of 65 wt% and above. The PUN40 displayed discrete spherical hard segment zones in the continuous soft segment phase (Figure5.10B). The 3D version of the AFM images are also included for effective visualization of the segregated hard domains (Figure5.11). The PUN43 possessing maximum hard segment content (43 wt%) showed bulk phase segregation with irregular patches of both hard and soft segment domains throughout the film surface (Figure5.10A). However, AFM analysis of the PUN films having hard segment content of 32 wt% or below failed to expose any distinct segregation pattern though odd hard segment phases were noticeable in the phase images (Figures 5.10C-D). The phase segregation in these PUNs raised the possibility of these samples to show efficient shape memory ability as reported in literature for other segmented PUs.[384] The trigger temperature for shape fixing and recovery of the samples were determined from the DMA and DSC analysis. All the samples showed a small hump around 58-62 °C in the Tan δ trace suggesting the glass transition and softening of the PTMO soft segment domains (Figure5.12B).

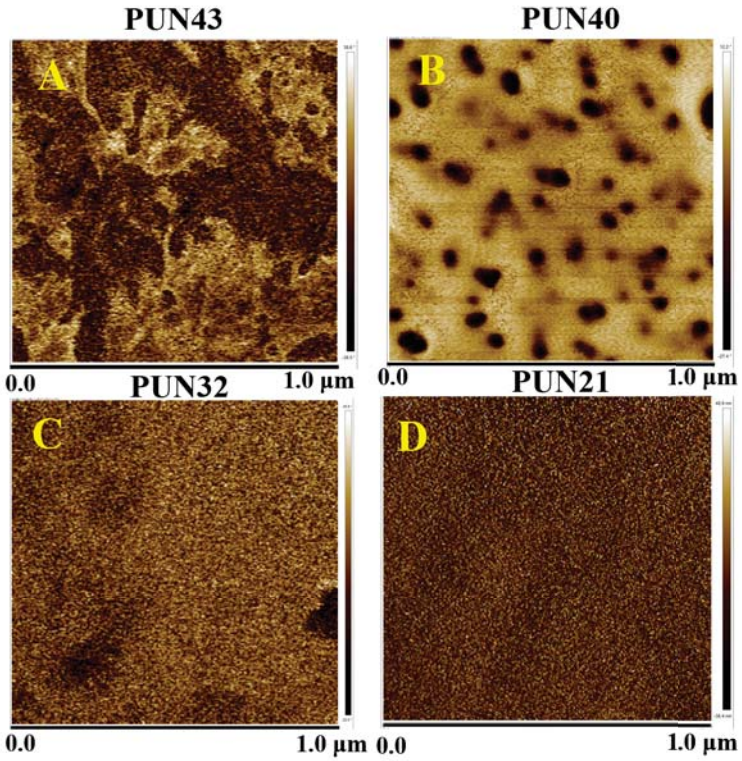

Figure 5.10: AFM tapping mode phase images of (A) PUN43, (B) PUN40, (C) PUN32 and (D) PUN21 recorded under non-contact mode and ambient conditions.

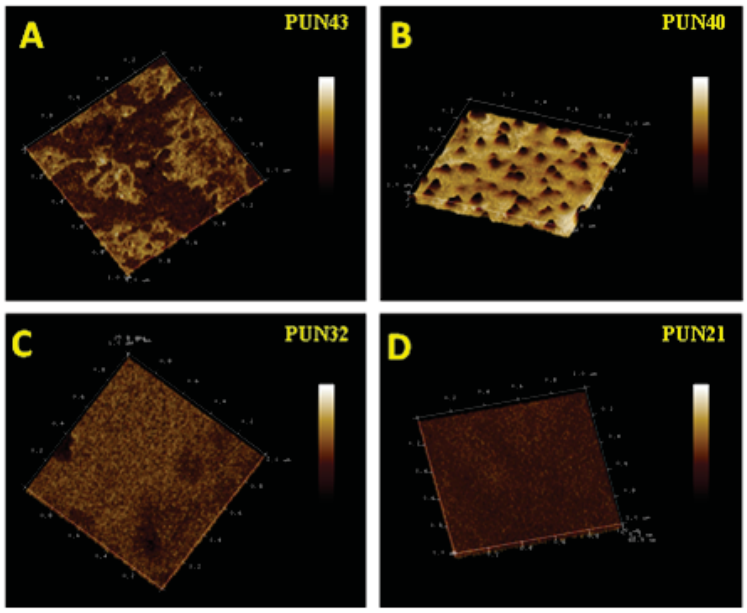

Figure 5.11: AFM phase images of different PUNs recorded under tapping mode in 3D format.

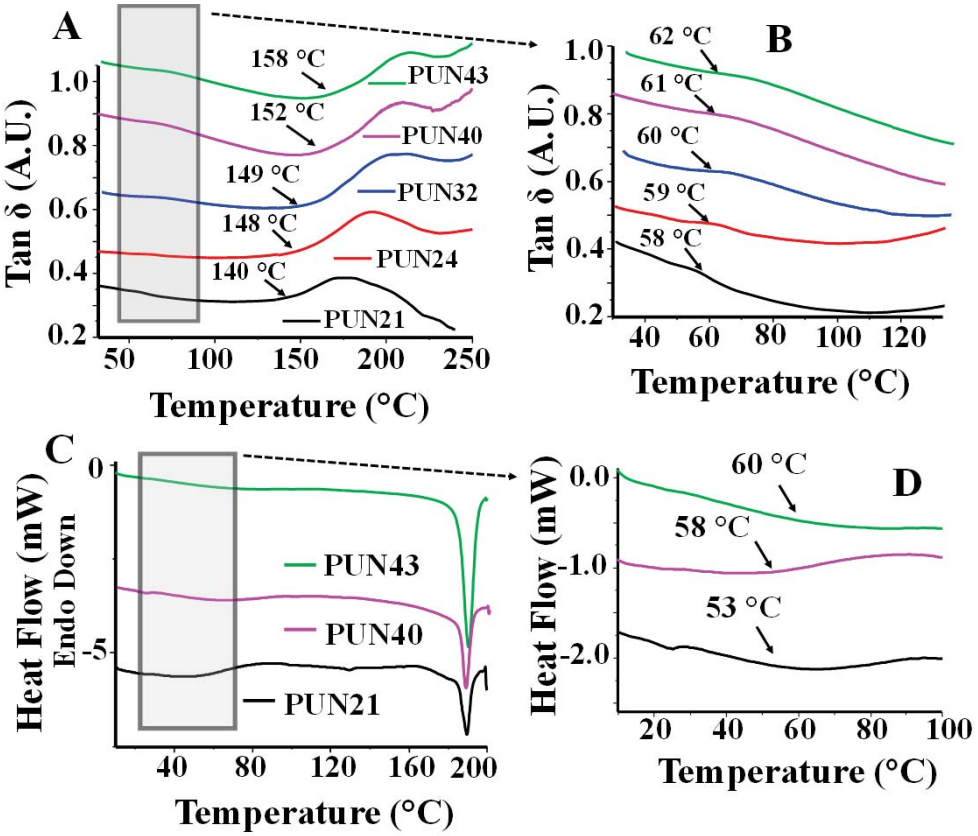

Figure 5.12: (A) Tan δ traces of PUNs derived from DMTA traces, (B) the zoomed section of "A" in the range of 30 to 130 °C, (C) DSC heating traces of PUNs showing the thermal transitions and (D) the zoomed section of "C" in the temperature range of 10 to 100 °C.

The E' values of all the PUNn samples also decreased by 10-30% further suggesting softening of the samples. The DSC analysis also supported the above and the T_g of the PUNs in the DSC heating traces were detected in the range of 53 to 60 °C (Figure5.12C-D). The above suggestions favored that, temperature around 60 °C can be used as the first inflection temperature to measure the shape memory ability. The onsets of the major tan δ peak in these PUNs were obtained in the range of 140 to 158 °C (Figure5.12A). Interestingly, no thermal transition corresponding to the temperature region was observed in the DSC analysis and the T_m was observed at $\sim$190 °C (Figure5.12C). This suggested that the above tan δ peak may be assigned to the initiation of exchange reaction of the dynamic carboxylate linkage present in the samples. This raised the possibility of utilizing $\sim$140 °C as the second inflection temperature to assess the triple shape memory ability of the sample. The double shape memory ability of PUN21 was measured by stretching the specimen up to 80% and recording the fixity and recoverability for continuous three double shape memory cycles to realize the repeatability and programmability efficiency (Figure5.13A-B).

Table 5.2: Double shape memory data of three cycles of PUN21

Sample No.	R_f (%)	R_r (%)	Maximum Strain (%)
1^{st} Cycle	97.0	95.0	74.4
2^{nd} Cycle	95.4	98.4	78.6
3^{rd} Cycle	95.7	99.3	81.8

Table 5.3: Double shape memory data of different PUNs

Sample No.	R_f (%)	R_r (%)	Maximum Strain (%)
PUN43	74.0	88.0	25.0
PUN40	95.0	93.0	49.5
PUN24	96.0	97.0	85.0
PUN21	97.5	93.0	81.0

The T_g of PTMO segment (60 °C) was applied as the trigger temperature to estimate the R_f and R_r of the sample. The R_f and R_r values for PUN21 were observed to be 97.5 and 93.0% respectively . The R_f and R_r values for three consecutive cycles are tabulated in Table5.2 (Figure5.13B). The R_f values for PUN21 slightly decreased from 97.0 to 95.4% and the R_r value increased from 95.0 to 99.3% after the third cycle suggesting superior double shape memory efficiency. The samples with maximum hard segment amount (PUN43) stretched up to 25% only, whereas the samples with less hard segment content (PUN21 and PUN24) stretched up to 81-85% under the particular stress during the shape fixing. The R_f values for PUN21, PUN24 and PUN40 was found to be in the range of 95.0-97.5% and the corresponding R_r values were detected in the range of 93.0-97.0% .

However, the R_f (74.0%) and R_r values (88.0%) of PUN43 was somewhat lower, which could be attributed to the rigidness of the hard segment domains existing in the films as reflected from the AFM images.The exchangeability of the dynamic β-CO carboxylate linkage at $\sim$130 °C was presumed to be another suitable trigger temperature for these samples. Reversible linkages are projected to overcome the rigidity associated with the permanent crosslinks and facilitate shape memory ability. To further verify this trigger temperature, a PUN21 sample was constantly observed at a fixed force value of 1.0 N by gradually increasing the temperature.

The elongation started to increase and the slope of the curve changed at 130 °C suggesting probable bond exchange of the dynamic linkage and softening of the sample (Figure5.14A). Subsequently, the triple shape memory abilities of the samples were evaluated by using 60 and 130 °C as the two trigger temperatures (Figure5.13C). The overall R_f values for the PUNn samples was detected in the range of 88.3-97.5% and the R_f values corresponding to the shape fixing at 60 °C was calculated to be 83.4-95.3% (Table5.4,Figure5.14B-D).

Table 5.4: Triple shape memory efficiency data of the PUNn at 130 and 60 °C inflection temperatures

Sample Code	R_f[#] (60 °C)	R_f[#] (Overall)	R_r[#] (60 °C)	R_r[#] (130 °C)	R_r[#] (Overall)	Strain 1[*] (%)	Strain 2[*] (%)
PUN43	83.6	90.3	100.0	54.9	86.0	16.1	39.0
PUN40	83.4	88.3	100.0	73.0	93.6	13.4	45.7
PUN24	95.3	96.7	100.0	39.0	82.7	19.8	56.6
PUN21	95.0	97.5	100.0	41.3	76.3	18.5	40.7

[*]Strain 1 and strain 2 correspond to the elongation achieved for shape fixing corresponding to 130 and 60 °C inflection temperature respectively. [#]the % shape fixity and recovery values are presented below.

Presumably, the R_f values in soft samples (PUN21 & PUN24) possessing less amount of hard segment content were relatively higher than that of the hard samples (PUN43 & PUN40).

The R_r values for the shape recovery at 60 °C was establish to be quantitative (100%) in all the cases. However, the R_r values (39-73%) corresponding to 130 °C was somewhat lower. The relatively low R_r value corresponding to the shape recovery at 130 °C could be ascribed to the rate of exchange reaction of the dynamic carboxylate linkage and the deformation of the network structure. The overall R_r values for these PUNn samples were detected in the range of 76.3-93.6% (Table5.4). The samples (PUN21 and PUN24) possessing relatively less amount of hard segment and low d_c value showed effective R_f value (>96%) and marginally weak overall R_r value (<83%) (Table5.4). Both the overall R_f (>88%) and R_r (>86%) values for PUN40 (d_c = 13.6 x 10^{-3} mol/cm^3) and PUN43 (d_c = 18.5 x 10^{-3} mol/cm^3) with high d_c values and different segregated hard segment domains were adequate (Figure5.10, Tables5.1 & 5.4). Possibly, the crosslink density & rigidity offered by the hard segment domains controlled the above shape memory behavior. The crosslink density of networks is known to control the shape memory ability and well-studied in literature. Importantly, all the samples displayed adequate overall R_f (>88%) and R_r values (>76%) suggesting effective triple shape memory ability. The consecutive cycles of triple shape memory cycles of PUN21 are shown in Figure5.13D. The overall R_f (97.5%) value remain unchanged and overall R_r value increased from 81.7 to 93.1% in the second cycle telling reproducible shape memory performance. Marginal improvement in R_r values are known to occur in subsequent shape memory cycles in literature.

For demonstration purposes, a thin film of PUN21 was shape fixed at 60 and 130 °C and steadily the shape recovery was observed on heating the sample till the inflection temperatures. The accurate shape recoveries at 60 °C followed by 130 °C further supported the DMA data and validated the triple shape memory ability of the samples (Figure5.13E).

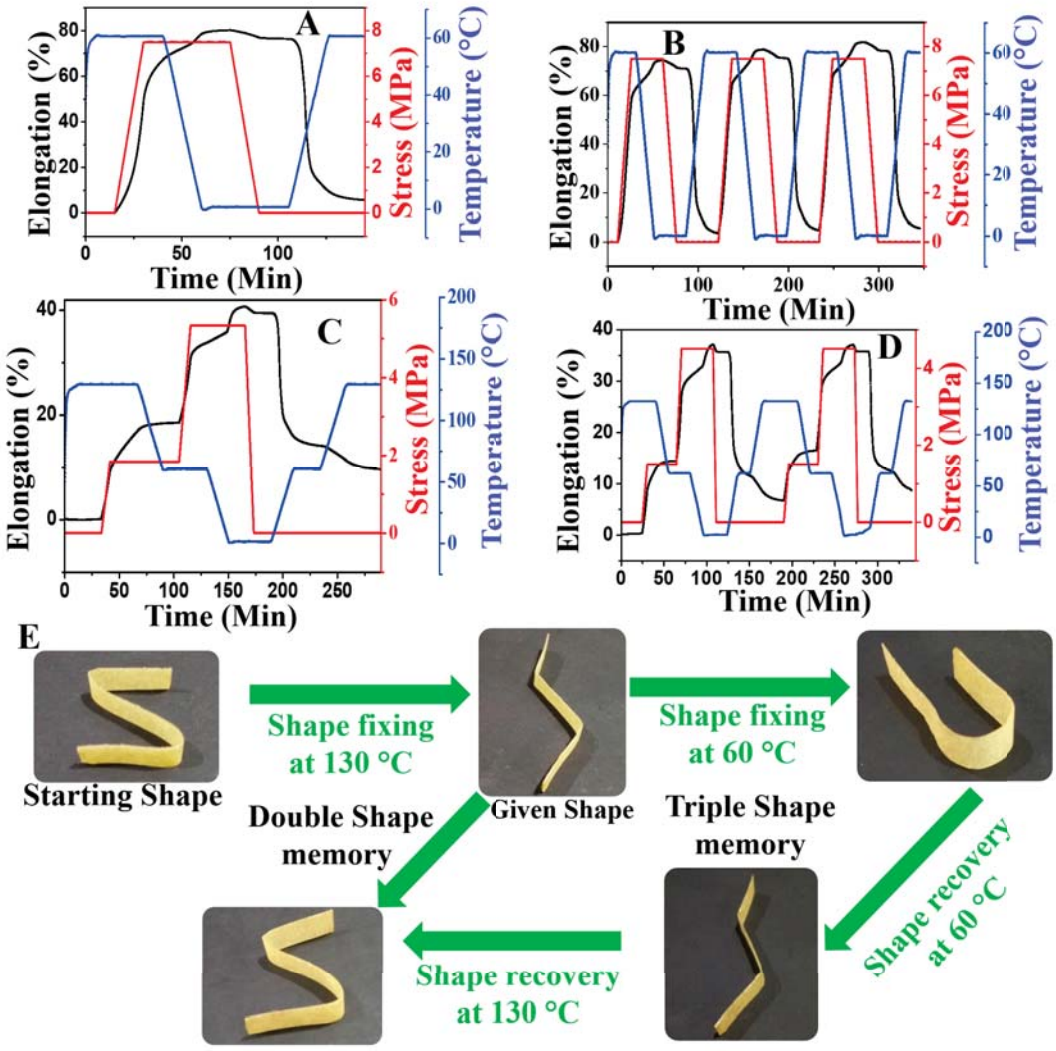

Figure 5.13: (A) Double shape memory performance, (B) three continuous cycles of double shape memory performance, (C) triple shape memory performance, and (D) two continuous cycles of triple shape memory performance of PUN21, (E) demonstration of double and triple shape memory performance with a thin film of PUN21 by fixing and recovering shapes at 130 and 60 °C.

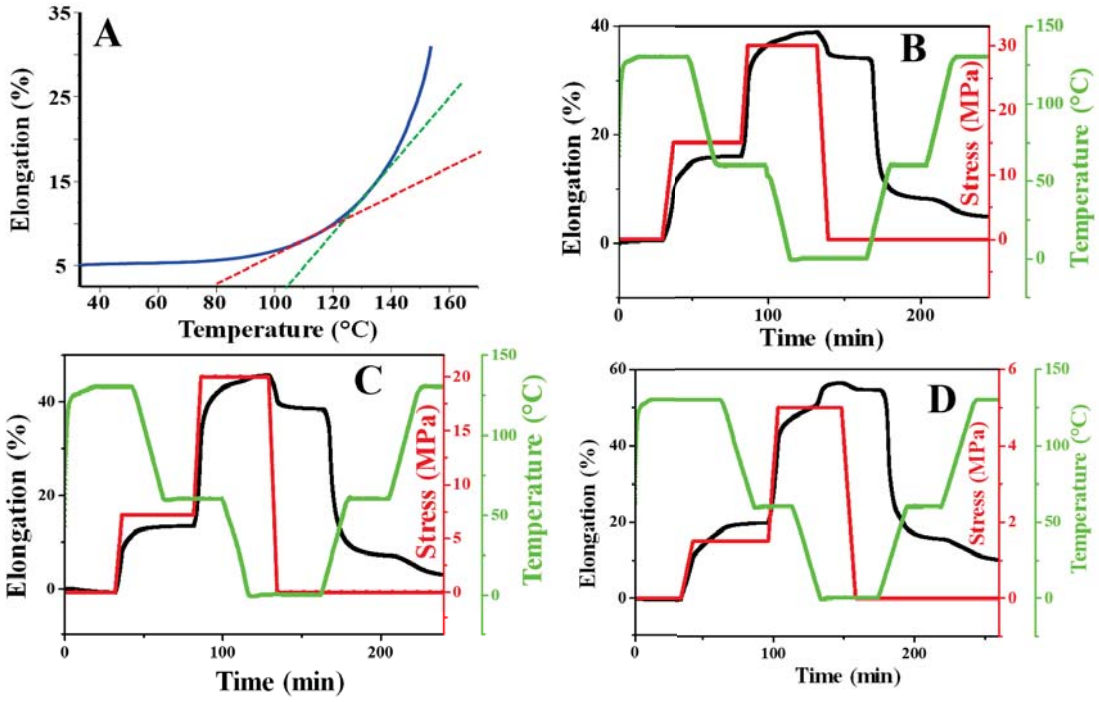

Figure 5.14: (A) Elongation vs temperature plot of PUN21 under constant stress, triple shape memory performance of (B) PUN43, (C) PUN40 & (D) PUN24

Overall, a set of sustainable PUNs were synthesized possessing thermal reprocessability via exchange of the dynamic β-CO carboxylate linkage. Importantly, these samples showed excellent creep resistance ability at high temperature conditions suggesting their potential for various applications. These vitrimers also exhibited useful triple shape memory, self welding and self healing ability.

5.5 Conclusion

In conclusion, dynamic β-carbonyl carboxylate linkages can be incorporated in to the PUN chains to encourage thermal reprocessability in the samples. Multi-functional hydroxyl compounds can be used for chain extension purposes to permit free hydroxyl groups to be present in the matrix, that will initiate exchange reaction with the carboxylate bond in presence of thermal stimuli. The soft and hard segment in these PUNs can be tailored to moderate the tensile properties. These samples possessing inherent covalent crosslinks exhibit superior creep resistance properties under high temperature conditions, which has been an issue with the vitrimer materials. The materials can be self adhered and self healed under thermal con-

ditions with slight loss in mechanical properties. The PUNs display effective triple shape memory ability and the shape memory efficiency is dependent on the amount of hard segment and crosslink density in the networks. The strategy is general and can be explored to other PU systems to induce dynamic properties.

Chapter 6

Summary and Future Directions

The main objective of my research work is to prepare thermosets based on dynamic covalent linkage for high strength, recyclable, self-healable and solvent reprocessable properties. Covalently cross-linked polymers with outstanding recyclability, sustainability, creep resistance, mechanical strength, self healing, malleability, shape-memory, adaptability, responsiveness and thermal stability possess important applications in many fields.

Dynamic covalent chemistry based on Michael addition reaction is cost effective, easy to carry under homogeneous, heterogeneous conditions. This simple chemistry may be utilized for the metathesis between the different michael adducts. This could be the new addition of the dynamic, reversible networks. This chemistry may be extended to develop polymers having dynamic nature for biomedical, sensing, energy storage and controlled drug release applications.

The polymeric precursor, i.e PHEMA in polyester networks may be replaced with some bio-based multihydroxy precusors to develop fully degradable, recyclable ecofriendly materilas. This polyester based vitrimers can be explored in the area of biomaterials, hydrogels, adhesives, coatings and synthetic fabrics etc. We may increase the activity by incorporating neighbouring group in β-activated esters. This highly acivated system may be utilized for the synthesis of catalyst free remoldable organogels in various applications.

The PTMO based CANs can able to absorb aromatics among several organic solvents and seperating toluene from various azeotropic mixtures. This continuous seperation of

toluene from azeotropic mixture can solve the industrial problems. These CANs may be utilized in fixed bed columns for seperation of aromatics fom different azeotropic mixtures.

The beauty of segmented PUs lies in its self healing, reprocessing, creep resistance behavior, tripe shape memory ability and their varied tensile strength, elongation, modulus values over a broad range via adjustment of the ratio between soft and hard segments in the polymer. The PUN synthesis strategy is general and can be extended to other PU systems to induce different dynamic linkages for various commercial applications.

References

[1] Wim Denissen, Martijn Droesbeke, Renaud Nicolaÿ, Ludwik Leibler, Johan M Winne, and Filip E Du Prez, "Chemical control of the viscoelastic properties of vinylogous urethane vitrimers", *Nat. Commun.* **8**(1), pp. 1–7 (2017).

[2] Liming Cao, Jianfeng Fan, Jiarong Huang, and Yukun Chen, "A robust and stretchable cross-linked rubber network with recyclable and self-healable capabilities based on dynamic covalent bonds", *J. Mater. Chem. A* **7**(9), pp. 4922–4933 (2019).

[3] Progyateg Chakma and Dominik Konkolewicz, "Dynamic covalent bonds in polymeric materials", *Angew. Chem.* **58**(29), pp. 9682–9695 (2019).

[4] Marc Guerre, Christian Taplan, Renaud Nicolaÿ, Johan M. Winne, and Filip E. Du Prez, "Fluorinated vitrimer elastomers with a dual temperature response", *J. Am. Chem. Soc.* **140**(41), pp. 13272–13284 (2018).

[5] Xiangxu Chen, Matheus A. Dam, Kanji Ono, Ajit Mal, Hongbin Shen, Steven R. Nutt, Kevin Sheran, and Fred Wudl, "A thermally re-mendable cross-linked polymeric material", *Science* **295**(5560), pp. 1698–1702 (2002).

[6] Fátima García, Janis Pelss, Han Zuilhof, and Maarten M. J. Smulders, "Multi-responsive coordination polymers utilising metal-stabilised, dynamic covalent imine bonds", *Chem. Commun.* **52**(58), pp. 9059–9062 (2016).

[7] Shainaz M. Landge and Ivan Aprahamian, "A ph activated configurational rotary switch: Controlling the e/z isomerization in hydrazones", *J. Am. Chem. Soc.* **131**(51), pp. 18269–18271 (2009).

[8] Hannes A. Houck, Eva Blasco, Filip E. Du Prez, and Christopher Barner-Kowollik, "Light-stabilized dynamic materials", *J. Am. Chem. Soc.* **141**(31), pp. 12329–12337 (2019).

[9] Yang Yang, Zhiqiang Pei, Xiqi Zhang, Lei Tao, Yen Wei, and Yan Ji, "Carbon nanotube–vitrimer composite for facile and efficient photo-welding of epoxy", *Chem. Sci.* **5**(9), pp. 3486–3492 (2014).

[10] Amy M. Peterson, Robert E. Jensen, and Giuseppe R. Palmese, "Room-temperature healing of a thermosetting polymer using the diels-alder reaction", *ACS Appl. Mater. Interfaces* **2**(4), pp. 1141–1149 (2010).

[11] Craig M. Hamel, Xiao Kuang, Kaijuan Chen, and H. Jerry Qi, "Reaction-diffusion model for thermosetting polymer dissolution through exchange reactions assisted by small-molecule solvents", *Macromolecules* **52**(10), pp. 3636–3645 (2019).

[12] Maciej Podgórski, Benjamin D. Fairbanks, Bruce E. Kirkpatrick, Matthew McBride, Alina Martinez, Adam Dobson, Nicholas J. Bongiardina, and Christopher N. Bowman, "Toward stimuli-responsive dynamic thermosets through continuous development and improvements in covalent adaptable networks (cans)", *Adv. Mater.* **32**(20), pp. 1906876 (2020).

[13] Nabarun Roy, Bernd Bruchmann, and Jean-Marie Lehn, "Dynamers: dynamic polymers as self-healing materials", *Chem. Soc. Rev.* **44**(11), pp. 3786–3807 (2015).

[14] Ying Yang and Marek W. Urban, "Self-healing polymeric materials", *Chem. Soc. Rev.* **42**(17), pp. 7446–7467 (2013).

[15] David J. Fortman, Jacob P. Brutman, Christopher J. Cramer, Marc A. Hillmyer, and William R. Dichtel, "Mechanically activated, catalyst-free polyhydroxyurethane vitrimers", *J. Am. Chem. Soc.* **137**(44), pp. 14019–14022 (2015).

[16] Olivia R. Cromwell, Jaeyoon Chung, and Zhibin Guan, "Malleable and self-healing covalent polymer networks through tunable dynamic boronic ester bonds", *J. Am. Chem. Soc.* **137**(20), pp. 6492–6495 (2015).

[17] Jia-Tao Miao, Meiying Ge, Shuqiang Peng, Jie Zhong, Yuewei Li, Zixiang Weng, Lixin Wu, and Longhui Zheng, "Dynamic imine bond-based shape memory polymers with permanent shape reconfigurability for 4d printing", *ACS Appl. Mater. Interfaces* **11**(43), pp. 40642–40651 (2019).

[18] Guogao Zhang, Qian Zhao, Weike Zou, Yingwu Luo, and Tao Xie, "Unusual aspects of supramolecular networks: Plasticity to elasticity, ultrasoft shape memory, and dynamic mechanical properties", *Adv. Func. Mater.* **26**(6), pp. 931–937 (2016).

[19] Christopher N. Bowman and Christopher J. Kloxin, "Covalent adaptable networks: Reversible bond structures incorporated in polymer networks", *Angew. Chem.* **51**(18), pp. 4272–4274 (2012).

[20] Christopher J. Kloxin and Christopher N. Bowman, "Covalent adaptable networks: smart, reconfigurable and responsive network systems", *Chem. Soc. Rev.* **42**, pp. 7161–7173 (2013).

[21] Lutz Greb, Hatice Mutlu, Christopher Barner-Kowollik, and Jean-Marie Lehn, "Photo- and metallo-responsive n-alkyl α-bisimines as orthogonally addressable

main-chain functional groups in metathesis polymers", *J. Am. Chem. Soc.* **138**(4), pp. 1142–1145 (2016).

[22] Maciej Podgórski, Benjamin D. Fairbanks, Bruce E. Kirkpatrick, Matthew McBride, Alina Martinez, Adam Dobson, Nicholas J. Bongiardina, and Christopher N. Bowman, "Toward stimuli-responsive dynamic thermosets through continuous development and improvements in covalent adaptable networks (cans)", *Adv. Mater.* **32**(20), pp. 1906876 (2020).

[23] Rudy J. Wojtecki, Michael A. Meador, and Stuart J. Rowan, "Using the dynamic bond to access macroscopically responsive structurally dynamic polymers", *Nat. Mater.* **10**(1), pp. 14–27 (2011).

[24] Christopher J. Kloxin, Timothy F. Scott, Brian J. Adzima, and Christopher N. Bowman, "Covalent adaptable networks (cans): A unique paradigm in cross-linked polymers", *Macromolecules* **43**(6), pp. 2643–2653 (2010).

[25] Georg M. Scheutz, Jacob J. Lessard, Michael B. Sims, and Brent S. Sumerlin, "Adaptable crosslinks in polymeric materials: Resolving the intersection of thermoplastics and thermosets", *J. Am. Chem. Soc.* **141**(41), pp. 16181–16196 (2019).

[26] Johan M. Winne, Ludwik Leibler, and Filip E. Du Prez, "Dynamic covalent chemistry in polymer networks: a mechanistic perspective", *Polym. Chem.* **10**(45), pp. 6091–6108 (2019).

[27] Wim Denissen, Johan M. Winne, and Filip E. Du Prez, "Vitrimers: permanent organic networks with glass-like fluidity", *Chem. Sci.* **7**(1), pp. 30–38 (2016).

[28] Damien Montarnal, Mathieu Capelot, François Tournilhac, and Ludwik Leibler, "Silica-like malleable materials from permanent organic networks", *Science* **334**(6058), pp. 965–968 (2011).

[29] Mathieu Capelot, Damien Montarnal, François Tournilhac, and Ludwik Leibler, "Metal-catalyzed transesterification for healing and assembling of thermosets", *J. Am. Chem. Soc.* **134**(18), pp. 7664–7667 (2012).

[30] Xiangxu Chen, Matheus A. Dam, Kanji Ono, Ajit Mal, Hongbin Shen, Steven R. Nutt, Kevin Sheran, and Fred Wudl, "A thermally re-mendable cross-linked polymeric material", *Science* **295**(5560), pp. 1698–1702 (2002).

[31] Honghao Hou, Jie Yin, and Xuesong Jiang, "Reversible diels–alder reaction to control wrinkle patterns: from dynamic chemistry to dynamic patterns", *Adv. Mater.* **28**(41), pp. 9126–9132 (2016).

[32] Philip Taynton, Huagang Ni, Chengpu Zhu, Kai Yu, Samuel Loob, Yinghua Jin, H. Jerry Qi, and Wei Zhang, "Repairable woven carbon fiber composites with full recyclability enabled by malleable polyimine networks", *Adv. Mater.* **28**(15), pp. 2904–2909 (2016).

[33] Mareva Fevre, Gavin O. Jones, Musan Zhang, Jeannette M. García, and James L. Hedrick, "Melt-processable dynamic-covalent poly(hemiaminal) organogels as scaffolds for uv-induced polymerization", *Adv. Mater.* **27**(32), pp. 4714–4718 (2015).

[34] Shou Zhao and Mahdi M. Abu-Omar, "Catechol-mediated glycidylation toward epoxy vitrimers/polymers with tunable properties", *Macromolecules* **52**(10), pp. 3646–3654 (2019).

[35] Progyateg Chakma, Luiz Henrique Rodrigues Possarle, Zachary A. Digby, Borui Zhang, Jessica L. Sparks, and Dominik Konkolewicz, "Dual stimuli responsive self-healing and malleable materials based on dynamic thiol-michael chemistry", *Polym. Chem.* **8**(42), pp. 6534–6543 (2017).

[36] Peeyush Kumar Sharma, Sagarika Taneja, and Yashveer Singh, "Hydrazone-linkage-based self-healing and injectable xanthan–poly(ethylene glycol) hydrogels for controlled drug release and 3d cell culture", *ACS Appl. Mater. Interfaces* **10**(37), pp. 30936–30945 (2018).

[37] Seon-Mi Kim, Hyeonyeol Jeon, Sung-Ho Shin, Seul-A Park, Jonggeon Jegal, Sung Yeon Hwang, Dongyeop X. Oh, and Jeyoung Park, "Superior toughness and fast self-healing at room temperature engineered by transparent elastomers", *Adv. Mater.* **30**(1), pp. 1705145 (2018).

[38] Rachel L. Snyder, David J. Fortman, Guilhem X. De Hoe, Marc A. Hillmyer, and William R. Dichtel, "Reprocessable acid-degradable polycarbonate vitrimers", *Macromolecules* **51**(2), pp. 389–397 (2018).

[39] Jian-Cheng Lai, Jin-Feng Mei, Xiao-Yong Jia, Cheng-Hui Li, Xiao-Zeng You, and Zhenan Bao, "A stiff and healable polymer based on dynamic-covalent boroxine bonds", *Adv. Mater.* **28**(37), pp. 8277–8282 (2016).

[40] Max Röttger, Trystan Domenech, Rob van der Weegen, Antoine Breuillac, Renaud Nicolaÿ, and Ludwik Leibler, "High-performance vitrimers from commodity thermoplastics through dioxaborolane metathesis", *Science* **356**(6333), pp. 62–65 (2017).

[41] Chase A. Tretbar, James A. Neal, and Zhibin Guan, "Direct silyl ether metathesis for vitrimers with exceptional thermal stability", *J. Am. Chem. Soc.* **141**(42), pp. 16595–16599 (2019).

[42] Sébastien Delpierre, Bertrand Willocq, Giuseppe Manini, Vincent Lemaur, Jonathan Goole, Pascal Gerbaux, Jérôme Cornil, Philippe Dubois, and Jean-Marie Raquez, "Simple approach for a self-healable and stiff polymer network from iminoboronate-based boroxine chemistry", *Chem. Mater.* **31**(10), pp. 3736–3744 (2019).

[43] Peiwen Zheng and Thomas J. McCarthy, "A surprise from 1954: Siloxane equilibration is a simple, robust, and obvious polymer self-healing mechanism", *J. Am. Chem. Soc.* **134**(4), pp. 2024–2027 (2012).

[44] Ning Zheng, Zizheng Fang, Weike Zou, Qian Zhao, and Tao Xie, "Thermoset shape-memory polyurethane with intrinsic plasticity enabled by transcarbamoylation", *Angew. Chem.* **55**(38), pp. 11421–11425 (2016).

[45] Hanze Ying, Yanfeng Zhang, and Jianjun Cheng, "Dynamic urea bond for the design of reversible and self-healing polymers", *Nat. Commun.* **5**(1), pp. 1–9 (2014).

[46] Mona M. Obadia, Bhanu P. Mudraboyina, Anatoli Serghei, Damien Montarnal, and Eric Drockenmuller, "Reprocessing and recycling of highly cross-linked ion-conducting networks through transalkylation exchanges of c–n bonds", *J. Am. Chem. Soc.* **137**(18), pp. 6078–6083 (2015).

[47] Yi-Xuan Lu and Zhibin Guan, "Olefin metathesis for effective polymer healing via dynamic exchange of strong carbon–carbon double bonds", *J. Am. Chem. Soc.* **134**(34), pp. 14226–14231 (2012).

[48] L. Imbernon, E. K. Oikonomou, S. Norvez, and L. Leibler, "Chemically crosslinked yet reprocessable epoxidized natural rubber via thermo-activated disulfide rearrangements", *Polym. Chem.* **6**(23), pp. 4271–4278 (2015).

[49] Yoshifumi Amamoto, Hideyuki Otsuka, Atsushi Takahara, and Krzysztof Matyjaszewski, "Self-healing of covalently cross-linked polymers by reshuffling thiuram disulfide moieties in air under visible light", *Adv. Mater.* **24**(29), pp. 3975–3980 (2012).

[50] Marc Guerre, Christian Taplan, Renaud Nicolaÿ, Johan M. Winne, and Filip E. Du Prez, "Fluorinated vitrimer elastomers with a dual temperature response", *J. Am. Chem. Soc.* **140**(41), pp. 13272–13284 (2018).

[51] Wim Denissen, Guadalupe Rivero, Renaud Nicolaÿ, Ludwik Leibler, Johan M. Winne, and Filip E. Du Prez, "Vinylogous urethane vitrimers", *Adv. Func. Mater.* **25**(16), pp. 2451–2457 (2015).

[52] Alexander W. Jackson and David A. Fulton, "Dynamic covalent diblock copolymers prepared from raft generated aldehyde and alkoxyamine end-functionalized polymers", *Macromolecules* **43**(2), pp. 1069–1075 (2010).

[53] Hui Song, Zhong-jin Wang, Xiao-dong He, and Jie Duan, "Self-healing of damage inside metals triggered by electropulsing stimuli", *Sci. Rep.* **7**(1), pp. 1–11 (2017).

[54] Yixi Wang, Jiayu Yan, Zhicun Wang, Jianning Wu, Guihua Meng, Zhiyong Liu, and Xuhong Guo, "One-pot fabrication of triple-network structure hydrogels with high-strength and self-healing properties", *Mater. Lett* **207**(15), pp. 53–56 (2017).

[55] Yang Li, Long Li, and Junqi Sun, "Bioinspired self-healing superhydrophobic coatings", *Angew. Chem.* **49**(35), pp. 6129–6133 (2010).

[56] Usama Zulfiqar, Muhammad Awais, Syed Zajif Hussain, Irshad Hussain, S Wilayat Husain, and Tayyab Subhani, "Durable and self-healing superhydrophobic surfaces for building materials", *Mater. Lett* **192**(1), pp. 56–59 (2017).

[57] Yanfeng Zhang, Hanze Ying, Kevin R. Hart, Yuxiao Wu, Aaron J. Hsu, Anthony M. Coppola, Tae Ann Kim, Ke Yang, Nancy R. Sottos, Scott R. White, and Jianjun Cheng, "Malleable and recyclable poly(urea-urethane) thermosets bearing hindered urea bonds", *Adv. Mater.* **28**(35), pp. 7646–7651 (2016).

[58] Wen-Xing Liu, Chi Zhang, Huan Zhang, Ning Zhao, Zhi-Xiang Yu, and Jian Xu, "Oxime-based and catalyst-free dynamic covalent polyurethanes", *J. Am. Chem. Soc.* **139**(25), pp. 8678–8684 (2017).

[59] Philippe Cordier, François Tournilhac, Corinne Soulié-Ziakovic, and Ludwik Leibler, "Self-healing and thermoreversible rubber from supramolecular assembly", *Nature* **451**(7181), pp. 977–980 (2008).

[60] Qiang Chen, Lin Zhu, Hong Chen, Hongli Yan, Lina Huang, Jia Yang, and Jie Zheng, "A novel design strategy for fully physically linked double network hydrogels with tough, fatigue resistant, and self-healing properties", *Adv. Func. Mater.* **25**(10), pp. 1598–1607 (2015).

[61] Tao Wang, Ying Zhang, Qingchang Liu, Wen Cheng, Xinran Wang, Lijia Pan, Baoxing Xu, and Hangxun Xu, "A self-healable, highly stretchable, and solution processable conductive polymer composite for ultrasensitive strain and pressure sensing", *Adv. Func. Mater.* **28**(7), pp. 1705551 (2018).

[62] Fei Zhao, Ye Shi, Lijia Pan, and Guihua Yu, "Multifunctional nanostructured conductive polymer gels: synthesis, properties, and applications", *Acc. Chem. Res.* **50**(7), pp. 1734–1743 (2017).

[63] Weiguo Huang, Kalpana Besar, Yong Zhang, Shyuan Yang, Gregory Wiedman, Yu Liu, Wenmin Guo, Jian Song, Kevin Hemker, Kalina Hristova, et al., "A high-capacitance salt-free dielectric for self-healable, printable, and flexible organic field effect transistors and chemical sensor", *Adv. Func. Mater.* **25**(24), pp. 3745–3755 (2015).

[64] Jin Young Oh, Simon Rondeau-Gagné, Yu-Cheng Chiu, Alex Chortos, Franziska Lissel, Ging-Ji Nathan Wang, Bob C Schroeder, Tadanori Kurosawa, Jeffrey Lopez, Toru Katsumata, et al., "Intrinsically stretchable and healable semiconducting polymer for organic transistors", *Nature* **539**(7629), pp. 411–415 (2016).

[65] Yan Qian, Xinwen Zhang, Linghai Xie, Dianpeng Qi, Bevita K Chandran, Xiaodong Chen, and Wei Huang, "Stretchable organic semiconductor devices", *Adv. Mater.* **28**(42), pp. 9243–9265 (2016).

[66] Olivia R. Cromwell, Jaeyoon Chung, and Zhibin Guan, "Malleable and self-healing covalent polymer networks through tunable dynamic boronic ester bonds", *J. Am. Chem. Soc.* **137**(20), pp. 6492–6495 (2015).

[67] Sihong Wang, Jin Young Oh, Jie Xu, Helen Tran, and Zhenan Bao, "Skin-inspired electronics: An emerging paradigm", *Acc. Chem. Res.* **51**(5), pp. 1033–1045 (2018).

[68] Jian Hua Xu, Sheng Ye, Chen Di Ding, Ling Hua Tan, and Jia Jun Fu, "Autonomous self-healing supramolecular elastomer reinforced and toughened by graphitic carbon nitride nanosheets tailored for smart anticorrosion coating applications", *J. Mater. Chem. A* **6**(14), pp. 5887–5898 (2018).

[69] Brian T. Michal, Emily J. Spencer, and Stuart J. Rowan, "Stimuli-responsive reversible two-level adhesion from a structurally dynamic shape-memory polymer", *ACS Appl. Mater. Interfaces* **8**(17), pp. 11041–11049 (2016).

[70] Binjie Jin, Huijie Song, Ruiqi Jiang, Jizhou Song, Qian Zhao, and Tao Xie, "Programming a crystalline shape memory polymer network with thermo-and photo-reversible bonds toward a single-component soft robot", *Sci. Adv.* **4**(1), pp. eaao3865 (2018).

[71] Yonglin He, Shenglong Liao, Hanyu Jia, Yuanyuan Cao, Zhenning Wang, and Yapei Wang, "A self-healing electronic sensor based on thermal-sensitive fluids", *Adv. Mater.* **27**(31), pp. 4622–4627 (2015).

[72] Jie Cao, Canhui Lu, Jian Zhuang, Manxiao Liu, Xinxing Zhang, Yanmei Yu, and Qingchuan Tao, "Multiple hydrogen bonding enables the self-healing of sensors for human–machine interactions", *Angew. Chem.* **56**(30), pp. 8795–8800 (2017).

[73] Yan Huang, Ming Zhong, Yang Huang, Minshen Zhu, Zengxia Pei, Zifeng Wang, Qi Xue, Xuming Xie, and Chunyi Zhi, "A self-healable and highly stretchable supercapacitor based on a dual crosslinked polyelectrolyte", *Nat. Commun.* **6**(1), pp. 1–8 (2015).

[74] Christopher J. Kloxin and Christopher N. Bowman, "Covalent adaptable networks: smart, reconfigurable and responsive network systems", *Chem. Soc. Rev.* **42**(17), pp. 7161–7173 (2013).

[75] Arpan Biswas, Vinod K. Aswal, P. U. Sastry, Dipak Rana, and Pralay Maiti, "Reversible bidirectional shape memory effect in polyurethanes through molecular flipping", *Macromolecules* **49**(13), pp. 4889–4897 (2016).

[76] Tao Xie, "Tunable polymer multi-shape memory effect", *Nature* **464**(7286), pp. 267–270 (2010).

[77] Andreas Lendlein, Hongyan Jiang, Oliver Jünger, and Robert Langer, "Light-induced shape-memory polymers", *Nature* **434**(7035), pp. 879–882 (2005).

[78] Julie Mendez, Pratheep K. Annamalai, Stephen J. Eichhorn, Rafeadah Rusli, Stuart J. Rowan, E. Johan Foster, and Christoph Weder, "Bioinspired mechanically adaptive polymer nanocomposites with water-activated shape-memory effect", *Macromolecules* **44**(17), pp. 6827–6835 (2011).

[79] Hongmei Chen, Ying Li, Ye Liu, Tao Gong, Lin Wang, and Shaobing Zhou, "Highly pH-sensitive polyurethane exhibiting shape memory and drug release", *Polym. Chem.* **5**(17), pp. 5168–5174 (2014).

[80] Yong Chae Jung, Hye Jin Yoo, Yoong Ahm Kim, Jae Whan Cho, and Morinobu Endo, "Electroactive shape memory performance of polyurethane composite having homogeneously dispersed and covalently crosslinked carbon nanotubes", *Carbon* **48**(5), pp. 1598–1603 (2010).

[81] Muhammad Yasar Razzaq, Marc Behl, Ulrich Nöchel, and Andreas Lendlein, "Magnetically controlled shape-memory effects of hybrid nanocomposites from oligo (ω-pentadecalactone) and covalently integrated magnetite nanoparticles", *Polymer* **55**(23), pp. 5953–5960 (2014).

[82] Christian Ohm, Christophe Serra, and Rudolf Zentel, "A continuous flow synthesis of micrometer-sized actuators from liquid crystalline elastomers", *Adv. Mater.* **21**(47), pp. 4859–4862 (2009).

[83] Taekwoong Chung, Angel Romo-Uribe, and Patrick T. Mather, "Two-way reversible shape memory in a semicrystalline network", *Macromolecules* **41**(1), pp. 184–192 (2008).

[84] S Pandini, F Baldi, KATIA Paderni, Massimo Messori, M Toselli, Francesco Pilati, A Gianoncelli, M Brisotto, E Bontempi, and T Riccò, "One-way and two-way shape memory behaviour of semi-crystalline networks based on sol–gel cross-linked poly (ε-caprolactone)", *Polymer* **54**(16), pp. 4253–4265 (2013).

[85] Marc Behl, Karl Kratz, Ulrich Noechel, Tilman Sauter, and Andreas Lendlein, "Temperature-memory polymer actuators", *Proceedings of the National Academy of Sciences* **110**(31), pp. 12555–12559 (2013).

[86] Igor Kolesov, Oleksandr Dolynchuk, Dieter Jehnichen, Uta Reuter, Manfred Stamm, and Hans-Joachim Radusch, "Changes of crystal structure and morphology during two-way shape-memory cycles in cross-linked linear and short-chain branched polyethylenes", *Macromolecules* **48**(13), pp. 4438–4450 (2015).

[87] Suk-kyun Ahn, Prashant Deshmukh, and Rajeswari M. Kasi, "Shape memory behavior of side-chain liquid crystalline polymer networks triggered by dual transition temperatures", *Macromolecules* **43**(17), pp. 7330–7340 (2010).

[88] Taylor Ware, Keith Hearon, Alexander Lonnecker, Karen L. Wooley, Duncan J. Maitland, and Walter Voit, "Triple-shape memory polymers based on self-complementary hydrogen bonding", *Macromolecules* **45**(2), pp. 1062–1069 (2012).

[89] Thomas Defize, Raphaël Riva, Jean-Michel Thomassin, Michaël Alexandre, Niels Van Herck, Filip Du Prez, and Christine Jérôme, "Reversible tad chemistry as a convenient tool for the design of (re)processable pcl-based shape-memory materials", *Macromol. Rapid Commun.* **38**(1), pp. 1600517 (2017).

[90] Qian Zhao, Weike Zou, Yingwu Luo, and Tao Xie, "Shape memory polymer network with thermally distinct elasticity and plasticity", *Sci. Adv.* **2**(1) (2016).

[91] Guogao Zhang, Qian Zhao, Lipeng Yang, Weike Zou, Xiangyi Xi, and Tao Xie, "Exploring dynamic equilibrium of diels-alder reaction for solid state plasticity in remoldable shape memory polymer network", *ACS Macro Lett.* **5**(7), pp. 805–808 (2016).

[92] Ning Zheng, Zizheng Fang, Weike Zou, Qian Zhao, and Tao Xie, "Thermoset shape-memory polyurethane with intrinsic plasticity enabled by transcarbamoylation", *Angew. Chem.* **55**(38), pp. 11421–11425 (2016).

[93] Binjie Jin, Huijie Song, Ruiqi Jiang, Jizhou Song, Qian Zhao, and Tao Xie, "Programming a crystalline shape memory polymer network with thermo- and photo-reversible bonds toward a single-component soft robot", *Sci. Adv.* **4**(1) (2018).

[94] Andreas Lendlein, Marc Behl, Bernhard Hiebl, and Christian Wischke, "Shape-memory polymers as a technology platform for biomedical applications", *Expert Rev. Med. Devices* **7**(3), pp. 357–379 (2010).

[95] Yin Huang, Ning Zheng, Zhiqiang Cheng, Ying Chen, Bingwei Lu, Tao Xie, and Xue Feng, "Direct laser writing-based programmable transfer printing via bioinspired shape memory reversible adhesive", *ACS Appl. Mater. Interfaces* **8**(51), pp. 35628–35633 (2016).

[96] YJ Liu, HY Du, LW Liu, and JS Leng, "Shape memory polymer composites and their applications in aerospace: a review", *Smart Mater. Struct* **23**(2), pp. 023001 (2014).

[97] Ben L. Feringa, "The art of building small: From molecular switches to motors (nobel lecture)", *Angew. Chem.* **56**(37), pp. 11060–11078 (2017).

[98] Nopporn Ruangsupapichat, Michael M Pollard, Syuzanna R Harutyunyan, and Ben L Feringa, "Reversing the direction in a light-driven rotary molecular motor", *Nat. Chem* **3**(1), pp. 53–60 (2011).

[99] Michael M Lerch, Mickel J Hansen, Willem A Velema, Wiktor Szymanski, and Ben L Feringa, "Orthogonal photoswitching in a multifunctional molecular system", *Nat. Commun.* **7**(1), pp. 1–10 (2016).

[100] Rafal Klajn, "Spiropyran-based dynamic materials", *Chem. Soc. Rev.* **43**(1), pp. 148–184 (2014).

[101] Harikrishnan Vijayamohanan, Edmund F. Palermo, and Chaitanya K. Ullal, "Spirothiopyran-based reversibly saturable photoresist", *Chem. Mater.* **29**(11), pp. 4754–4760 (2017).

[102] IRIE MASAHIRO, "Diarylethenesformemoriesandswitches", *Chem. Rev* **100**(5), pp. 1685–1716 (2000).

[103] Shou-Zhi Pu, Qi Sun, Cong-Bin Fan, Ren-Jie Wang, and Gang Liu, "Recent advances in diarylethene-based multi-responsive molecular switches", *J. Mater. Chem. C* **4**(15), pp. 3075–3093 (2016).

[104] Erandimala U. Kulawardana, Thilini Kuruwita-Mudiyanselage, and Douglas C. Neckers, "Dual responsive poly(n-isopropylacrylamide) hydrogels having spironaphthoxazines as pendant groups", *J Polym Sci A Polym Chem* **47**(13), pp. 3318–3325 (2009).

[105] Sameh Helmy, Frank A. Leibfarth, Saemi Oh, Justin E. Poelma, Craig J. Hawker, and Javier Read de Alaniz, "Photoswitching using visible light: A new class of organic photochromic molecules", *J. Am. Chem. Soc.* **136**(23), pp. 8169–8172 (2014).

[106] Kazuki Matsubara, Masayoshi Watanabe, and Yukikazu Takeoka, "A thermally adjustable multicolor photochromic hydrogel", *Angew. Chem.* **46**(10), pp. 1688–1692 (2007).

[107] Yuwei Gu, Eric A Alt, Heng Wang, Xiaopeng Li, Adam P Willard, and Jeremiah A Johnson, "Photoswitching topology in polymer networks with metal–organic cages as crosslinks", *Nature* **560**(7716), pp. 65–69 (2018).

[108] Joseph V. Accardo and Julia A. Kalow, "Reversibly tuning hydrogel stiffness through photocontrolled dynamic covalent crosslinks", *Chem. Sci.* **9**, pp. 5987–5993 (2018).

[109] Hongwei Zhou, Changguo Xue, Philipp Weis, Yasuhito Suzuki, Shilin Huang, Kaloian Koynov, Günter K Auernhammer, Rüdiger Berger, Hans-Jürgen Butt, and Si Wu, "Photoswitching of glass transition temperatures of azobenzene-containing polymers induces reversible solid-to-liquid transitions", *Nat. Chem* **9**(2), pp. 145–151 (2017).

[110] Damien Montarnal, Mathieu Capelot, François Tournilhac, and Ludwik Leibler, "Silica-like malleable materials from permanent organic networks", *Science* **334**(6058), pp. 965–968 (2011).

[111] Zhanhua Wang, Esther van Andel, Sidharam P. Pujari, Huanhuan Feng, Joshua A. Dijksman, Maarten M. J. Smulders, and Han Zuilhof, "Water-repairable zwitterionic polymer coatings for anti-biofouling surfaces", *J. Mater. Chem. B* **5**(33), pp. 6728–6733 (2017).

[112] Jun Kamada, Kaloian Koynov, Cathrin Corten, Azhar Juhari, Jeong Ae Yoon, Marek W. Urban, Anna C. Balazs, and Krzysztof Matyjaszewski, "Redox responsive behavior of thiol/disulfide-functionalized star polymers synthesized via atom transfer radical polymerization", *Macromolecules* **43**(9), pp. 4133–4139 (2010).

[113] V. R. Sastri and G. C. Tesoro, "Reversible crosslinking in epoxy resins. ii. new approaches", *J. Appl. Polym. Sci* **39**(7), pp. 1439–1457 (1990).

[114] L. Imbernon, E. K. Oikonomou, S. Norvez, and L. Leibler, "Chemically crosslinked yet reprocessable epoxidized natural rubber via thermo-activated disulfide rearrangements", *Polym. Chem.* **6**(23), pp. 4271–4278 (2015).

[115] Akira Takahashi, Tomoyuki Ohishi, Raita Goseki, and Hideyuki Otsuka, "Degradable epoxy resins prepared from diepoxide monomer with dynamic covalent disulfide linkage", *Polymer* **82**(15), pp. 319–326 (2016).

[116] Brian T. Michal, Colin A. Jaye, Emily J. Spencer, and Stuart J. Rowan, "Inherently photohealable and thermal shape-memory polydisulfide networks", *ACS Macro Lett.* **2**(8), pp. 694–699 (2013).

[117] Jeong Ae Yoon, Jun Kamada, Kaloian Koynov, Jake Mohin, Renaud Nicolaÿ, Yaozhong Zhang, Anna C. Balazs, Tomasz Kowalewski, and Krzysztof Matyjaszewski, "Self-healing polymer films based on thiol–disulfide exchange reactions and self-healing kinetics measured using atomic force microscopy", *Macromolecules* **45**(1), pp. 142–149 (2012).

[118] Benjamin D. Fairbanks, Samir P. Singh, Christopher N. Bowman, and Kristi S. Anseth, "Photodegradable, photoadaptable hydrogels via radical-mediated disulfide fragmentation reaction", *Macromolecules* **44**(8), pp. 2444–2450 (2011).

[119] Timothy F. Scott, Andrew D. Schneider, Wayne D. Cook, and Christopher N. Bowman, "Photoinduced plasticity in cross-linked polymers", *Science* **308**(5728), pp. 1615–1617 (2005).

[120] Yoshifumi Amamoto, Jun Kamada, Hideyuki Otsuka, Atsushi Takahara, and Krzysztof Matyjaszewski, "Repeatable photoinduced self-healing of covalently cross-linked polymers through reshuffling of trithiocarbonate units", *Angew. Chem.* **50**(7), pp. 1660–1663 (2011).

[121] K. C. Nicolaou, Scott A. Snyder, Tamsyn Montagnon, and Georgios Vassilikogiannakis, "The diels-alder reaction in total synthesis", *Angew. Chem.* **41**(10), pp. 1668–1698 (2002).

[122] Malcolm P. Stevens and Aubrey D. Jenkins, "Crosslinking of polystyrene via pendant maleimide groups", *J Polymer Sci Polymer Chem Ed* **17**(11), pp. 3675–3685 (1979).

[123] Joseph P. Kennedy and Kenneth F. Castner, "Thermally reversible polymer systems by cyclopentadienylation. i. a model for termination by cyclopentadienylation of olefin polymerization", *J Polymer Sci Polymer Chem Ed* **17**(7), pp. 2039–2054 (1979).

[124] J. C. Salamone, Y. Chung, S. B. Clough, and A. C. Watterson, "Thermally reversible, covalently crosslinked polyphosphazenes", *J Polym Sci A Polym Chem* **26**(11), pp. 2923–2939 (1988).

[125] Yoshiki Chujo, Kazuki Sada, and Takeo Saegusa, "Reversible gelation of polyoxazoline by means of diels-alder reaction", *Macromolecules* **23**(10), pp. 2636–2641 (1990).

[126] Rana Gheneim, Catalina Perez-Berumen, and Alessandro Gandini, "Diels-alder reactions with novel polymeric dienes and dienophiles: Synthesis of reversibly crosslinked elastomers", *Macromolecules* **35**(19), pp. 7246–7253 (2002).

[127] Shen Yu, Rongchun Zhang, Qiang Wu, Tiehong Chen, and Pingchuan Sun, "Bioinspired high-performance and recyclable cross-linked polymers", *Adv. Mater.* **25**(35), pp. 4912–4917 (2013).

[128] Qiao Tian, Yan Chao Yuan, Min Zhi Rong, and Ming Qiu Zhang, "A thermally remendable epoxy resin", *J. Mater. Chem.* **19**(9), pp. 1289–1296 (2009).

[129] Qiao Tian, Min Zhi Rong, Ming Qiu Zhang, and Yan Chao Yuan, "Synthesis and characterization of epoxy with improved thermal remendability based on diels-alder reaction", *Polym. Int* **59**(10), pp. 1339–1345 (2010).

[130] Ying-Ling Liu and Yi-Wen Chen, "Thermally reversible cross-linked polyamides with high toughness and self-repairing ability from maleimide- and furan-functionalized aromatic polyamides", *Macromol. Chem. Phys.* **208**(2), pp. 224–232 (2007).

[131] Youchun Zhang, Antonius A. Broekhuis, and Francesco Picchioni, "Thermally self-healing polymeric materials: The next step to recycling thermoset polymers?", *Macromolecules* **42**(6), pp. 1906–1912 (2009).

[132] L. M. Polgar, M. van Duin, A. A. Broekhuis, and F. Picchioni, "Use of diels-alder chemistry for thermoreversible cross-linking of rubbers: The next step toward recycling of rubber products?", *Macromolecules* **48**(19), pp. 7096–7105 (2015).

[133] Kazuhiko Inoue, Midori Yamashiro, and Masatoshi Iji, "Recyclable shape-memory polymer: Poly(lactic acid) crosslinked by a thermoreversible diels-alder reaction", *J. Appl. Polym. Sci* **112**(2), pp. 876–885 (2009).

[134] Thomas Defize, Raphaël Riva, Jean-Marie Raquez, Philippe Dubois, Christine Jérôme, and Michaël Alexandre, "Thermoreversibly crosslinked poly(ε-caprolactone) as recyclable shape-memory polymer network", *Macromol. Rapid Commun.* **32**(16), pp. 1264–1269 (2011).

[135] Wei Hu, Zhi Ren, Junpeng Li, Erin Askounis, Zhixin Xie, and Qibing Pei, "New dielectric elastomers with variable moduli", *Adv. Func. Mater.* **25**(30), pp. 4827–4836 (2015).

[136] Stijn Billiet, Kevin De Bruycker, Frank Driessen, Hannelore Goossens, Veronique Van Speybroeck, Johan M Winne, and Filip E Du Prez, "Triazolinediones enable ultrafast and reversible click chemistry for the design of dynamic polymer systems", *Nat. Chem* **6**(9), pp. 815–821 (2014).

[137] Farzad Seidi, Ratchapol Jenjob, and Daniel Crespy, "Designing smart polymer conjugates for controlled release of payloads", *Chem. Rev.* **118**(7), pp. 3965–4036 (2018).

[138] Oscar Valerio, Manjusri Misra, and Amar K. Mohanty, "Poly(glycerol-co-diacids) polyesters: From glycerol biorefinery to sustainable engineering applications, a review", *ACS Sustain. Chem. Eng.* **6**(5), pp. 5681–5693 (2018).

[139] Fangwei Ling, Zhenwei Liu, Mokun Chen, Hao Wang, Yong Zhu, Changshu Ma, Jinrong Wu, and Guangsu Huang, "Compatibility driven self-strengthening during the radical-responsive remolding process of poly-isoprene vitrimers", *J. Mater. Chem. A* **7**, pp. 25324–25332 (2019).

[140] Yingjun Liu, Zhenghai Tang, Yi Chen, Chengfeng Zhang, and Baochun Guo, "Engineering of β-hydroxyl esters into elastomer–nanoparticle interface toward malleable, robust, and reprocessable vitrimer composites", *ACS Appl. Mater. Interfaces* **10**(3), pp. 2992–3001 (2018).

[141] Kelechukwu N. Onwukamike, Stéphane Grelier, Etienne Grau, Henri Cramail, and Michael A. R. Meier, "Sustainable transesterification of cellulose with high oleic sunflower oil in a dbu-co2 switchable solvent", *ACS Sustain. Chem. Eng.* **6**(7), pp. 8826–8835 (2018).

[142] Wei Zhao, Zihao Feng, Zhenhua Liang, Yanfeng Lv, Fukang Xiang, Chuanyin Xiong, Chao Duan, Lei Dai, and Yonghao Ni, "Vitrimer-cellulose paper composites: A new class of strong, smart, green, and sustainable materials", *ACS Appl. Mater. Interfaces* **11**(39), pp. 36090–36099 (2019).

[143] Suman Debnath, Swaraj Kaushal, and Umaprasana Ojha, "Catalyst-free partially bio-based polyester vitrimers", *ACS Appl. Polym. Mater.* **2**(2), pp. 1006–1013 (2020).

[144] Suman Debnath, Swaraj Kaushal, Subhankar Mandal, and Umaprasana Ojha, "Solvent processable and recyclable covalent adaptable organogels based on dynamic trans-esterification chemistry: separation of toluene from azeotropic mixtures", *Polym. Chem.* **11**(8), pp. 1471–1480 (2020).

[145] Guohua Deng, Chuanmei Tang, Fuya Li, Huanfeng Jiang, and Yongming Chen, "Covalent cross-linked polymer gels with reversible sol-gel transition and self-healing properties", *Macromolecules* **43**(3), pp. 1191–1194 (2010).

[146] Philip Taynton, Kai Yu, Richard K. Shoemaker, Yinghua Jin, H. Jerry Qi, and Wei Zhang, "Heat- or water-driven malleability in a highly recyclable covalent network polymer", *Adv. Mater.* **26**(23), pp. 3938–3942 (2014).

[147] Albert Chao, Ioan Negulescu, and Donghui Zhang, "Dynamic covalent polymer networks based on degenerative imine bond exchange: the malleability and self-healing properties by solvent", *Macromolecules* **49**(17), pp. 6277–6284 (2016).

[148] Joydev K Laha, KS Satyanarayana Tummalapalli, and Krupal P Jethava, "Implications of dynamic imine chemistry for the sustainable synthesis of nitrogen heterocycles via transimination followed by intramolecular cyclisation", *Org. Biomol. Chem.* **14**(8), pp. 2473–2479 (2016).

[149] Yi-Xuan Lu, François Tournilhac, Ludwik Leibler, and Zhibin Guan, "Making insoluble polymer networks malleable via olefin metathesis", *J. Am. Chem. Soc.* **134**(20), pp. 8424–8427 (2012).

[150] James A. Neal, Davoud Mozhdehi, and Zhibin Guan, "Enhancing mechanical performance of a covalent self-healing material by sacrificial noncovalent bonds", *J. Am. Chem. Soc.* **137**(14), pp. 4846–4850 (2015).

[151] Zhiyong Liu, Chunyang Yu, Changxu Zhang, Zixing Shi, and Jie Yin, "Revisiting acetoacetyl chemistry to build malleable cross-linked polymer networks via transamidation", *ACS Macro Lett.* **8**(3), pp. 233–238 (2019).

[152] Mona M. Obadia, Bhanu P. Mudraboyina, Anatoli Serghei, Damien Montarnal, and Eric Drockenmuller, "Reprocessing and recycling of highly cross-linked ion-conducting networks through transalkylation exchanges of C–N bonds", *J. Am. Chem. Soc.* **137**(18), pp. 6078–6083 (2015).

[153] Benjamin Hendriks, Jelle Waelkens, Johan M. Winne, and Filip E. Du Prez, "Poly(thioether) vitrimers via transalkylation of trialkylsulfonium salts", *ACS Macro Lett.* **6**(9), pp. 930–934 (2017).

[154] Zhenghai Tang, Yingjun Liu, Qingyi Huang, Jinshan Zhao, Baochun Guo, and Liqun Zhang, "A real recycling loop of sulfur-cured rubber through transalkylation exchange of C–S bonds", *Green Chem.* **20**(24), pp. 5454–5458 (2018).

[155] Siwu Wu, Zhijun Yang, Shifeng Fang, Zhenghai Tang, Fang Liu, and Baochun Guo, "Malleable organic/inorganic thermosetting hybrids enabled by exchangeable silyl ether interfaces", *J. Mater. Chem. A* **7**(4), pp. 1459–1467 (2019).

[156] Zhenjie Ding, Li Yuan, Guozheng Liang, and Aijuan Gu, "Thermally resistant thermadapt shape memory crosslinked polymers based on silyl ether dynamic covalent linkages for self-folding and self-deployable smart 3d structures", *J. Mater. Chem. A* **7**(16), pp. 9736–9747 (2019).

[157] Yoshio Nishimura, Jaeyoon Chung, Hurik Muradyan, and Zhibin Guan, "Silyl ether as a robust and thermally stable dynamic covalent motif for malleable polymer design", *J. Am. Chem. Soc.* **139**(42), pp. 14881–14884 (2017).

[158] Chase A. Tretbar, James A. Neal, and Zhibin Guan, "Direct silyl ether metathesis for vitrimers with exceptional thermal stability", *J. Am. Chem. Soc.* **141**(42), pp. 16595–16599 (2019).

[159] Progyateg Chakma, Luiz Henrique Rodrigues Possarle, Zachary A. Digby, Borui Zhang, Jessica L. Sparks, and Dominik Konkolewicz, "Dual stimuli responsive self-healing and malleable materials based on dynamic thiol-michael chemistry", *Polym. Chem.* **8**(42), pp. 6534–6543 (2017).

[160] Samantha P Daymon and Kevin M Miller, "Probing the dynamic and rehealing behavior of crosslinked polyester networks containing thermoreversible thiol-michael bonds", *Polymer* **145**(15), pp. 286–293 (2018).

[161] Yu-chong Zhang, Xiao-xia Le, Wei Lu, Yu-kun Jian, Jia-wei Zhang, and Tao Chen, "An "off-the-shelf" shape memory hydrogel based on the dynamic borax-diol ester bonds", *Macromol Mater Eng* **303**(7), pp. 1800144 (2018).

[162] Chaehoon Kim, Hirotaka Ejima, and Naoko Yoshie, "Non-swellable self-healing polymer with long-term stability under seawater", *RSC Adv.* **7**(31), pp. 19288–19295 (2017).

[163] Tamiris Figueiredo, Jing Jing, Isabelle Jeacomine, Johan Olsson, Thibaud Gerfaud, Jean-Guy Boiteau, Claire Rome, Craig Harris, and Rachel Auzély-Velty, "Injectable self-healing hydrogels based on boronate ester formation between hyaluronic acid partners modified with benzoxaborin derivatives and saccharides", *Macromol Mater Eng* **21**(1), pp. 230–239 (2020).

[164] Olivia R. Cromwell, Jaeyoon Chung, and Zhibin Guan, "Malleable and self-healing covalent polymer networks through tunable dynamic boronic ester bonds", *J. Am. Chem. Soc.* **137**(20), pp. 6492–6495 (2015).

[165] Yi Chen, Zhenghai Tang, Xuhui Zhang, Yingjun Liu, Siwu Wu, and Baochun Guo, "Covalently cross-linked elastomers with self-healing and malleable abilities enabled

by boronic ester bonds", *ACS Appl. Mater. Interfaces* **10**(28), pp. 24224–24231 (2018).

[166] Christopher P. Kabb, Christopher S. O'Bryan, Christopher C. Deng, Thomas E. Angelini, and Brent S. Sumerlin, "Photoreversible covalent hydrogels for soft-matter additive manufacturing", *ACS Appl. Mater. Interfaces* **10**(19), pp. 16793–16801 (2018).

[167] Mustafa Arslan, Baris Kiskan, and Yusuf Yagci, "Benzoxazine-based thermoset with autonomous self-healing and shape recovery", *Macromolecules* **51**(24), pp. 10095–10103 (2018).

[168] Wim Denissen, Martijn Droesbeke, Renaud Nicolaÿ, Ludwik Leibler, Johan M Winne, and Filip E Du Prez, "Chemical control of the viscoelastic properties of vinylogous urethane vitrimers", *Nat. Commun.* **8**(1), pp. 1–7 (2017).

[169] Jian-Bo Zhu, Eli M. Watson, Jing Tang, and Eugene Y.-X. Chen, "A synthetic polymer system with repeatable chemical recyclability", *Science* **360**(6387), pp. 398–403 (2018).

[170] Adrianne M Rosales and Kristi S Anseth, "The design of reversible hydrogels to capture extracellular matrix dynamics", *Nat. Rev. Mater.* **1**(2), pp. 1–15 (2016).

[171] Yoshio Nishimura, Jaeyoon Chung, Hurik Muradyan, and Zhibin Guan, "Silyl ether as a robust and thermally stable dynamic covalent motif for malleable polymer design", *J. Am. Chem. Soc.* **139**(42), pp. 14881–14884 (2017).

[172] Longhe Zhang and Stuart J. Rowan, "Effect of sterics and degree of cross-linking on the mechanical properties of dynamic poly(alkylurea–urethane) networks", *Macromolecules* **50**(13), pp. 5051–5060 (2017).

[173] Weike Zou, Jiante Dong, Yingwu Luo, Qian Zhao, and Tao Xie, "Dynamic covalent polymer networks: from old chemistry to modern day innovations", *Adv. Mater.* **29**(14), pp. 1606100 (2017).

[174] Wim Denissen, Johan M. Winne, and Filip E. Du Prez, "Vitrimers: permanent organic networks with glass-like fluidity", *Chem. Sci.* **7**(1), pp. 30–38 (2016).

[175] Max Röttger, Trystan Domenech, Rob van der Weegen, Antoine Breuillac, Renaud Nicolaÿ, and Ludwik Leibler, "High-performance vitrimers from commodity thermoplastics through dioxaborolane metathesis", *Science* **356**(6333), pp. 62–65 (2017).

[176] Anne Fuhrmann, Robert Göstl, Robert Wendt, Julia Kötteritzsch, Martin D Hager, Ulrich S Schubert, Kerstin Brademann-Jock, Andreas F Thünemann, Ulrich Nöchel,

Marc Behl, et al., "Conditional repair by locally switching the thermal healing capability of dynamic covalent polymers with light", *Nat. Commun.* **7**(1), pp. 1–7 (2016).

[177] Santiago Lascano, Kang-Da Zhang, Robin Wehlauch, Karl Gademann, Naomi Sakai, and Stefan Matile, "The third orthogonal dynamic covalent bond", *Chem. Sci.* **7**(7), pp. 4720–4724 (2016).

[178] Wen-Xing Liu, Chi Zhang, Huan Zhang, Ning Zhao, Zhi-Xiang Yu, and Jian Xu, "Oxime-based and catalyst-free dynamic covalent polyurethanes", *J. Am. Chem. Soc.* **139**(25), pp. 8678–8684 (2017).

[179] L. M. Polgar, M. van Duin, A. A. Broekhuis, and F. Picchioni, "Use of diels-alder chemistry for thermoreversible cross-linking of rubbers: The next step toward recycling of rubber products?", *Macromolecules* **48**(19), pp. 7096–7105 (2015).

[180] Daniel D. McKinnon, Dylan W. Domaille, Jennifer N. Cha, and Kristi S. Anseth, "Bis-aliphatic hydrazone-linked hydrogels form most rapidly at physiological ph: Identifying the origin of hydrogel properties with small molecule kinetic studies", *Chem. Mater.* **26**(7), pp. 2382–2387 (2014).

[181] Albert Chao, Ioan Negulescu, and Donghui Zhang, "Dynamic covalent polymer networks based on degenerative imine bond exchange: Tuning the malleability and self-healing properties by solvent", *Macromolecules* **49**(17), pp. 6277–6284 (2016).

[182] D Montarnal and M Capelot, "Silica-like malleable materials from permanent organic networks", *Science* **334**(6058), pp. 965–968 (2011).

[183] David J. Fortman, Jacob P. Brutman, Christopher J. Cramer, Marc A. Hillmyer, and William R. Dichtel, "Mechanically activated, catalyst-free polyhydroxyurethane vitrimers", *J. Am. Chem. Soc.* **137**(44), pp. 14019–14022 (2015).

[184] Olivia R. Cromwell, Jaeyoon Chung, and Zhibin Guan, "Malleable and self-healing covalent polymer networks through tunable dynamic boronic ester bonds", *J. Am. Chem. Soc.* **137**(20), pp. 6492–6495 (2015).

[185] Wim Denissen, Ives De Baere, Wim Van Paepegem, Ludwik Leibler, Johan Winne, and Filip E. Du Prez, "Vinylogous urea vitrimers and their application in fiber reinforced composites", *Macromolecules* **51**(5), pp. 2054–2064 (2018).

[186] Shujuan Wang, Xiaolong Xing, Xiaoting Zhang, Xiao Wang, and Xinli Jing, "Room-temperature fully recyclable carbon fibre reinforced phenolic composites through dynamic covalent boronic ester bonds", *J. Mater. Chem. A* **6**(23), pp. 10868–10878 (2018).

[187] Alaitz Rekondo, Roberto Martin, Alaitz Ruiz de Luzuriaga, Germán Cabañero, Hans J. Grande, and Ibon Odriozola, "Catalyst-free room-temperature self-healing elastomers based on aromatic disulfide metathesis", *Mater. Horiz.* **1**(2), pp. 237–240 (2014).

[188] Yanfeng Zhang, Hanze Ying, Kevin R. Hart, Yuxiao Wu, Aaron J. Hsu, Anthony M. Coppola, Tae Ann Kim, Ke Yang, Nancy R. Sottos, Scott R. White, and Jianjun Cheng, "Malleable and recyclable poly(urea-urethane) thermosets bearing hindered urea bonds", *Adv. Mater.* **28**(35), pp. 7646–7651 (2016).

[189] Rudy J. Wojtecki, Gavin O. Jones, Alexander Y. Yuen, Willy Chin, Dylan J. Boday, Alshakim Nelson, Jeannette M. García, Yi Yan Yang, and James L. Hedrick, "Developments in dynamic covalent chemistries from the reaction of thiols with hexahydrotriazines", *J. Am. Chem. Soc.* **137**(45), pp. 14248–14251 (2015).

[190] Wenjin Guo, Xiang Li, Fuchang Xu, Yang Li, and Junqi Sun, "Transparent polymeric films capable of healing millimeter-scale cuts", *ACS Appl. Mater. Interfaces* **10**(15), pp. 13073–13081 (2018).

[191] Raffael C. Wende and Peter R. Schreiner, "Evolution of asymmetric organocatalysis: multi- and retrocatalysis", *Green Chem.* **14**(7), pp. 1821–1849 (2012).

[192] Yong-Feng Cai, Li Li, Meng-Xian Luo, Ke-Fang Yang, Guo-Qiao Lai, Jian-Xiong Jiang, and Li-Wen Xu, "Organocatalytic aza-michael/retro-aza-michael reaction: Pronounced chirality amplification in aza-michael reaction and racemization via retro-aza-michael reaction", *Chirality* **23**(5), pp. 397–403 (2011).

[193] Aaron D. Baldwin and Kristi L. Kiick, "Tunable degradation of maleimide–thiol adducts in reducing environments", *Bioconjug. Chem.* **22**(10), pp. 1946–1953 (2011).

[194] Borui Zhang, Progyateg Chakma, Max P. Shulman, Jun Ke, Zachary A. Digby, and Dominik Konkolewicz, "Probing the mechanism of thermally driven thiol-michael dynamic covalent chemistry", *Org. Biomol. Chem.* **16**(15), pp. 2725–2734 (2018).

[195] IM Serafimova, MA Pufall, S Krishnan, K Duda, MS Cohen, and RL Maglathlin, "Reversible targeting of noncatalytic cysteines with chemically tuned electrophiles", *Nat. Chem. Biol* **8**(5), pp. 471–476 (2012).

[196] Ye Zhong, Yufang Xu, and Eric V. Anslyn, "Studies of reversible conjugate additions", *Eur. J. Org. Chem.* **2013**(23), pp. 5017–5021 (2013).

[197] Ranjana Baruah, Anuj Kumar, Rewati Raman Ujjwal, Soumya Kedia, Amit Ranjan, and Umaprasana Ojha, "Recyclable thermosets based on dynamic amidation and aza-michael addition chemistry", *Macromolecules* **49**(20), pp. 7814–7824 (2016).

[198] Shyam Krishnan, Rand M. Miller, Boxue Tian, R. Dyche Mullins, Matthew P. Jacobson, and Jack Taunton, "Design of reversible, cysteine-targeted michael acceptors guided by kinetic and computational analysis", *J. Am. Chem. Soc.* **136**(36), pp. 12624–12630 (2014).

[199] Jun Jiang, Yunfei Cai, Weiliang Chen, Lili Lin, Xiaohua Liu, and Xiaoming Feng, "Enantioselective aza-michael reaction of hydrazide to chalcones through the nonactivated amine moiety conjugated addition", *Chem. Commun.* **47**(13), pp. 4016–4018 (2011).

[200] Wei Li, Lingfeng Gao, Wenyun Zhuge, Xu Sun, and Gengxiu Zheng, "Catalyst-free synthesis of 3-sulfone nitrile from sulfonyl hydrazides and acrylonitrile in water", *Org. Biomol. Chem.* **15**(37), pp. 7819–7823 (2017).

[201] Min Huang, Sheng-Xue Xie, Ze-Qiang Ma, Qing-Qing Huang, Fa-Jun Nan, and Qi-Zhuang Ye, "Inhibition of monometalated methionine aminopeptidase: inhibitor discovery and crystallographic analysis", *J. Med. Chem.* **50**(23), pp. 5735–5742 (2007).

[202] Emily A. Hoff, Brooks A. Abel, Chase A. Tretbar, Charles L. McCormick, and Derek L. Patton, "Aqueous RAFT at pH zero: enabling controlled polymerization of unprotected acyl hydrazide methacrylamides", *Polym. Chem.* **8**(34), pp. 4978–4982 (2017).

[203] Devatha P. Nair, Maciej Podgórski, Shunsuke Chatani, Tao Gong, Weixian Xi, Christopher R. Fenoli, and Christopher N. Bowman, "The thiol-michael addition click reaction: A powerful and widely used tool in materials chemistry", *Chem. Mater.* **26**(1), pp. 724–744 (2014).

[204] Vyacheslav S. Bryantsev, Mamadou S. Diallo, and William A. Goddard, "pka calculations of aliphatic amines, diamines, and aminoamides via density functional theory with a poisson-boltzmann continuum solvent model", *J. Phys. Chem. A* **111**(20), pp. 4422–4430 (2007).

[205] Stefan Raddatz, Jochen Mueller-Ibeler, Joachim Kluge, Ludger Wab, Gerhard Burdinski, John R. Havens, Tom J. Onofrey, Daguang Wang, and Markus Schweitzer, "Hydrazide oligonucleotides: new chemical modification for chip array attachment and conjugation", *Nucleic Acids Res* **30**(21), pp. 4793–4802 (2002).

[206] Anuj Kumar, Rewati Raman Ujjwal, Apoorva Mittal, Archit Bansal, and Umaprasana Ojha, "Polyacryloyl hydrazide: An efficient, simple, and cost effective precursor to a range of functional materials through hydrazide based click reactions", *ACS Appl. Mater. Interfaces* **6**(3), pp. 1855–1865 (2014).

[207] Michelle M. Smith, William Edwards, and David K. Smith, "Self-organisation effects in dynamic nanoscale gels self-assembled from simple mixtures of commercially available molecular-scale components", *Chem. Sci.* **4**(2), pp. 671–676 (2013).

[208] Gilles B. Desmet, Dagmar R. D'hooge, Pinar Sinem Omurtag, Pieter Espeel, Guy B. Marin, Filip E. Du Prez, and Marie-Françoise Reyniers, "Quantitative first-principles kinetic modeling of the aza-michael addition to acrylates in polar aprotic solvents", *J. Org. Chem.* **81**(24), pp. 12291–12302 (2016).

[209] Michal Bláha, Olga Trhlíková, Jiří Podešva, Sabina Abbrent, Miloš Steinhart, Jiří Dybal, and Miroslava Dušková-Smrčková, "Solvent-free, catalyst-free aza-michael addition of cyclohexylamine to diethyl maleate: reaction mechanism and kinetics", *Tetrahedron* **74**(1), pp. 58–67 (2018).

[210] Umaprasana Ojha, Dingsong Feng, Amol Chandekar, James E. Whitten, and Rudolf Faust, "Peptide surface modification of p(hema-co-mma)-b-pib-b-p(hema-co-mma) block copolymers", *Langmuir* **25**(11), pp. 6319–6327 (2009).

[211] Loren W Hill, "Calculation of crosslink density in short chain networks", *Prog. Org. Coat.* **31**(3), pp. 235–243 (1997).

[212] Rachel L. Snyder, David J. Fortman, Guilhem X. De Hoe, Marc A. Hillmyer, and William R. Dichtel, "Reprocessable acid-degradable polycarbonate vitrimers", *Macromolecules* **51**(2), pp. 389–397 (2018).

[213] Mathieu Capelot, Miriam M. Unterlass, François Tournilhac, and Ludwik Leibler, "Catalytic control of the vitrimer glass transition", *ACS Macro Lett.* **1**(7), pp. 789–792 (2012).

[214] Jacob P. Brutman, Paula A. Delgado, and Marc A. Hillmyer, "Polylactide vitrimers", *ACS Macro Lett.* **3**(7), pp. 607–610 (2014).

[215] William A. Ogden and Zhibin Guan, "Recyclable, strong, and highly malleable thermosets based on boroxine networks", *J. Am. Chem. Soc.* **140**(20), pp. 6217–6220 (2018).

[216] Chunyang Bao, Yi-Jun Jiang, Houyu Zhang, Xingyuan Lu, and Junqi Sun, "Room-temperature self-healing and recyclable tough polymer composites using nitrogen-coordinated boroxines", *Adv. Funct. Mater.* **28**(23), pp. 1800560 (2018).

[217] Donglin Tang, Christopher W. Macosko, and Marc A. Hillmyer, "Thermoplastic polyurethane elastomers from bio-based poly(δ-decalactone) diols", *Polym. Chem.* **5**(9), pp. 3231–3237 (2014).

[218] Renhua Deng, Matthew J. Derry, Charlotte J. Mable, Yin Ning, and Steven P. Armes, "Using dynamic covalent chemistry to drive morphological transitions: Controlled release of encapsulated nanoparticles from block copolymer vesicles", *J. Am. Chem. Soc.* **139**(22), pp. 7616–7623 (2017).

[219] Yangjun Chen, Diana Diaz-Dussan, Di Wu, Wenda Wang, Yi-Yang Peng, Anika Benozir Asha, Dennis G. Hall, Kazuhiko Ishihara, and Ravin Narain, "Bioinspired self-healing hydrogel based on benzoxaborole-catechol dynamic covalent chemistry for 3d cell encapsulation", *ACS Macro Lett.* **7**(8), pp. 904–908 (2018).

[220] Adrián Pérez-San Vicente, Marianna Peroglio, Manuela Ernst, Pablo Casuso, Iraida Loinaz, Hans-Jürgen Grande, Mauro Alini, David Eglin, and Damien Dupin, "Self-healing dynamic hydrogel as injectable shock-absorbing artificial nucleus pulposus", *Biomacromolecules* **18**(8), pp. 2360–2370 (2017).

[221] Xingmao Chang, Zhaolong Wang, Yanyu Qi, Rui Kang, Xinwen Cui, Congdi Shang, Kaiqiang Liu, and Yu Fang, "Dynamic chemistry-based sensing: A molecular system for detection of saccharide, formaldehyde, and the silver ion", *Anal. Chem.* **89**(17), pp. 9360–9367 (2017).

[222] Sampath B. Alahakoon, Christina M. Thompson, Gino Occhialini, and Ronald A. Smaldone, "Design principles for covalent organic frameworks in energy storage applications", *ChemSusChem* **10**(10), pp. 2116–2129 (2017).

[223] Farzad Seidi, Ratchapol Jenjob, and Daniel Crespy, "Designing smart polymer conjugates for controlled release of payloads", *Chem. Rev* **118**(7), pp. 3965–4036 (2018).

[224] Oscar Valerio, Manjusri Misra, and Amar K. Mohanty, "Poly(glycerol-co-diacids) polyesters: From glycerol biorefinery to sustainable engineering applications, a review", *ACS Sustain. Chem. Eng.* **6**(5), pp. 5681–5693 (2018).

[225] Chao Zhao, Andong Liu, Claudia M Santamaria, Andre Shomorony, Tianjiao Ji, Tuo Wei, Akiva Gordon, Hannes Elofsson, Manisha Mehta, Rong Yang, et al., "Polymer-tetrodotoxin conjugates to induce prolonged duration local anesthesia with minimal toxicity", *Nat. Commun.* **10**(1), pp. 1–14 (2019).

[226] Damien Montarnal, Mathieu Capelot, François Tournilhac, and Ludwik Leibler, "Silica-like malleable materials from permanent organic networks", **334**(6058), pp. 965–968 (2011).

[227] Maarten Delahaye, Johan M. Winne, and Filip E. Du Prez, "Internal catalysis in covalent adaptable networks: Phthalate monoester transesterification as a versatile

dynamic cross-linking chemistry", *J. Am. Chem. Soc.* **141**(38), pp. 15277–15287 (2019).

[228] Mathieu Capelot, Damien Montarnal, François Tournilhac, and Ludwik Leibler, "Metal-catalyzed transesterification for healing and assembling of thermosets", *J. Am. Chem. Soc.* **134**(18), pp. 7664–7667 (2012).

[229] Matthew K. McBride, Maciej Podgorski, Shunsuke Chatani, Brady T. Worrell, and Christopher N. Bowman, "Thermoreversible folding as a route to the unique shape-memory character in ductile polymer networks", *ACS Appl. Mater. Interfaces* **10**(26), pp. 22739–22745 (2018).

[230] Jian-Cheng Lai, Lan Li, Da-Peng Wang, Min-Hao Zhang, Sheng-Ran Mo, Xue Wang, Ke-Yu Zeng, Cheng-Hui Li, Qing Jiang, Xiao-Zeng You, et al., "A rigid and healable polymer cross-linked by weak but abundant zn (ii)-carboxylate interactions", *Nat. Commun.* **9**(1), pp. 1–9 (2018).

[231] Wim Denissen, Martijn Droesbeke, Renaud Nicolaÿ, Ludwik Leibler, Johan M Winne, and Filip E Du Prez, "Chemical control of the viscoelastic properties of vinylogous urethane vitrimers", *Nat. Commun.* **8**(1), pp. 1–7 (2017).

[232] Olivia R. Cromwell, Jaeyoon Chung, and Zhibin Guan, "Malleable and self-healing covalent polymer networks through tunable dynamic boronic ester bonds", *J. Am. Chem. Soc.* **137**(20), pp. 6492–6495 (2015).

[233] Chase A. Tretbar, James A. Neal, and Zhibin Guan, "Direct silyl ether metathesis for vitrimers with exceptional thermal stability", *J. Am. Chem. Soc.* **141**(42), pp. 16595–16599 (2019).

[234] Yanfeng Zhang, Hanze Ying, Kevin R. Hart, Yuxiao Wu, Aaron J. Hsu, Anthony M. Coppola, Tae Ann Kim, Ke Yang, Nancy R. Sottos, Scott R. White, and Jianjun Cheng, "Malleable and recyclable poly(urea-urethane) thermosets bearing hindered urea bonds", *Adv. Mater.* **28**(35), pp. 7646–7651 (2016).

[235] Mona M. Obadia, Antoine Jourdain, Philippe Cassagnau, Damien Montarnal, and Eric Drockenmuller, "Tuning the viscosity profile of ionic vitrimers incorporating 1,2,3-triazolium cross-links", *Adv. Funct. Mater.* **27**(45), pp. 1703258 (2017).

[236] Antoine Breuillac, Alexis Kassalias, and Renaud Nicolaÿ, "Polybutadiene vitrimers based on dioxaborolane chemistry and dual networks with static and dynamic cross-links", *Macromolecules* **52**(18), pp. 7102–7113 (2019).

[237] Rachel L. Snyder, David J. Fortman, Guilhem X. De Hoe, Marc A. Hillmyer, and William R. Dichtel, "Reprocessable acid-degradable polycarbonate vitrimers", *Macromolecules* **51**(2), pp. 389–397 (2018).

[238] Wim Denissen, Ives De Baere, Wim Van Paepegem, Ludwik Leibler, Johan Winne, and Filip E. Du Prez, "Vinylogous urea vitrimers and their application in fiber reinforced composites", *Macromolecules* **51**(5), pp. 2054–2064 (2018).

[239] Changfei He, Shaowei Shi, Dong Wang, Brett A. Helms, and Thomas P. Russell, "Poly(oxime–ester) vitrimers with catalyst-free bond exchange", *J. Am. Chem. Soc.* **141**(35), pp. 13753–13757 (2019).

[240] Jacob J. Lessard, Luis F. Garcia, Charles P. Easterling, Michael B. Sims, Kyle C. Bentz, Scarlett Arencibia, Daniel A. Savin, and Brent S. Sumerlin, "Catalyst-free vitrimers from vinyl polymers", *Macromolecules* **52**(5), pp. 2105–2111 (2019).

[241] Georg M. Scheutz, Jacob J. Lessard, Michael B. Sims, and Brent S. Sumerlin, "Adaptable crosslinks in polymeric materials: Resolving the intersection of thermoplastics and thermosets", *J. Am. Chem. Soc.* **141**(41), pp. 16181–16196 (2019).

[242] Johan M. Winne, Ludwik Leibler, and Filip E. Du Prez, "Dynamic covalent chemistry in polymer networks: a mechanistic perspective", *Polym. Chem.* **10**(45), pp. 6091–6108 (2019).

[243] Francisco Lossada, Jiaqi Guo, Dejin Jiao, Saskia Groeer, Elodie Bourgeat-Lami, Damien Montarnal, and Andreas Walther, "Vitrimer chemistry meets cellulose nanofibrils: Bioinspired nanopapers with high water resistance and strong adhesion", *Biomacromolecules* **20**(2), pp. 1045–1055 (2019).

[244] Na Kyung Kim, Eun Jung Cha, Mungyo Jung, Jinseok Kim, Gun-Jae Jeong, Yong Seok Kim, Woo Jin Choi, Byung-Soo Kim, Dong-Gyun Kim, and Jong-Chan Lee, "3D hierarchical scaffolds enabled by a post-patternable, reconfigurable, and biocompatible 2D vitrimer film for tissue engineering applications", *J. Mater. Chem. B* **7**(21), pp. 3341–3345 (2019).

[245] Qiaomei Chen, Xiaojie Qian, Yanshuang Xu, Yang Yang, Yen Wei, and Yan Ji, "Harnessing the day–night rhythm of humidity and sunlight into mechanical work using recyclable and reprogrammable soft actuators", *ACS Appl. Mater. Interfaces* **11**(32), pp. 29290–29297 (2019).

[246] Gayla Berg Lyon, Lewis M. Cox, J. Taylor Goodrich, Austin D. Baranek, Yifu Ding, and Christopher N. Bowman, "Remoldable thiol–ene vitrimers for photopatterning and nanoimprint lithography", *Macromolecules* **49**(23), pp. 8905–8913 (2016).

[247] Cheng Hao, Tuan Liu, Shuai Zhang, Lucas Brown, Ran Li, Junna Xin, Tuhua Zhong, Long Jiang, and Jinwen Zhang, "A high-lignin-content, removable, and glycol-assisted repairable coating based on dynamic covalent bonds", *ChemSusChem* **12**(5), pp. 1049–1058 (2019).

[248] Fangwei Ling, Zhenwei Liu, Mokun Chen, Hao Wang, Yong Zhu, Changshu Ma, Jinrong Wu, and Guangsu Huang, "Compatibility driven self-strengthening during the radical-responsive remolding process of poly-isoprene vitrimers", *J. Mater. Chem. A* **7**(44), pp. 25324–25332 (2019).

[249] Yi Chen, Zhenghai Tang, Xuhui Zhang, Yingjun Liu, Siwu Wu, and Baochun Guo, "Covalently cross-linked elastomers with self-healing and malleable abilities enabled by boronic ester bonds", *ACS Appl. Mater. Interfaces* **10**(28), pp. 24224–24231 (2018).

[250] Kelechukwu N. Onwukamike, Stéphane Grelier, Etienne Grau, Henri Cramail, and Michael A. R. Meier, "Sustainable transesterification of cellulose with high oleic sunflower oil in a dbu-co2 switchable solvent", *ACS Sustain. Chem. Eng.* **6**(7), pp. 8826–8835 (2018).

[251] Wei Zhao, Zihao Feng, Zhenhua Liang, Yanfeng Lv, Fukang Xiang, Chuanyin Xiong, Chao Duan, Lei Dai, and Yonghao Ni, "Vitrimer-cellulose paper composites: A new class of strong, smart, green, and sustainable materials", *ACS Appl. Mater. Interfaces* **11**(39), pp. 36090–36099 (2019).

[252] Cheng Hao, Tuan Liu, Shuai Zhang, Lucas Brown, Ran Li, Junna Xin, Tuhua Zhong, Long Jiang, and Jinwen Zhang, "A high-lignin-content, removable, and glycol-assisted repairable coating based on dynamic covalent bonds", *ChemSusChem* **12**(5), pp. 1049–1058 (2019).

[253] Biao Zhang, Kavin Kowsari, Ahmad Serjouei, Martin L Dunn, and Qi Ge, "Reprocessable thermosets for sustainable three-dimensional printing", *Nat. Commun.* **9**(1), pp. 1–7 (2018).

[254] Jacob P. Brutman, Paula A. Delgado, and Marc A. Hillmyer, "Polylactide vitrimers", *ACS Macro Lett.* **3**(7), pp. 607–610 (2014).

[255] Mathieu Capelot, Damien Montarnal, François Tournilhac, and Ludwik Leibler, "Metal-catalyzed transesterification for healing and assembling of thermosets", *J. Am. Chem. Soc.* **134**(18), pp. 7664–7667 (2012).

[256] Facundo I. Altuna, Valeria Pettarin, and Roberto J. J. Williams, "Self-healable polymer networks based on the cross-linking of epoxidised soybean oil by an aqueous citric acid solution", *Green Chem.* **15**(12), pp. 3360–3366 (2013).

[257] B. P. Bandgar, L. S. Uppalla, and V. S. Sadavarte, "Envirocat epzg and natural clay as efficient catalysts for transesterification of β-keto esters", *Green Chem.* **3**(1), pp. 39–41 (2001).

[258] Phillip Biallas, Janina Heider, and Stefan F. Kirsch, "Functional polyamides with gem-diazido units: synthesis and diversification", *Polym. Chem.* **10**(1), pp. 60–64 (2019).

[259] Phillip Biallas, Tobias M. Mensak, Kevin-Alexander Kunz, and Stefan F. Kirsch, "The deazidoalkoxylation: Sequential nucleophilic substitutions with diazidated diethyl malonate", *J. Org. Chem.* **84**(3), pp. 1654–1663 (2019).

[260] Wei Zhang, Han-Liang Zheng, Yang Liu, Ao Yu, Chen Yang, Xin Li, and Jin-Pei Cheng, "Catalyst-free amination of α-cyanoarylacetates enabled by single-electron transfer", *Org. Chem. Front.* **6**(11), pp. 1900–1904 (2019).

[261] Mei-Na Zhang, Mi-Na Zhao, Ming Chen, Zhi-Hui Ren, Yao-Yu Wang, and Zheng-Hui Guan, "Copper-catalyzed radical coupling of 1,3-dicarbonyl compounds with terminal alkenes for the synthesis of tetracarbonyl compounds", *Chem. Commun.* **52**(36), pp. 6127–6130 (2016).

[262] GB Dharma Rao, BN Acharya, and MP Kaushik, "An efficient synthesis of β-ketoesters via transesterification and its application in biginelli reaction under solvent-free, catalyst-free conditions",*Tetrahedron Lett.* **54**(48), pp. 6644-6647 (2016).

[263] Ranjana Baruah, Anuj Kumar, Rewati Raman Ujjwal, Soumya Kedia, Amit Ranjan, and Umaprasana Ojha, "Recyclable thermosets based on dynamic amidation and aza-michael addition chemistry", *Macromolecules* **49**(20), pp. 7814–7824 (2016).

[264] Santimukul Santra and Anil Kumar, "Facile synthesis of aliphatic hyperbranched polyesters based on diethyl malonate and their irreversible molecular encapsulation", *Chem. Commun.*(18), pp. 2126–2127 (2004).

[265] Mathew D. Rowe, Ersan Eyiler, and Keisha B. Walters, "Bio-based plasticizer and thermoset polyesters: A green polymer chemistry approach", *J. Appl. Polym. Sci.* **133**(45) (2016).

[266] Richard J. Fort and Theodoros M. Polyzoidis, "The unperturbed dimensions of poly(2-hydroxyethyl methacrylate)", *Makromol. Chem* **178**(12), pp. 3229–3235 (1977).

[267] Jin Won Yu, Jin Jung, Yong-Mun Choi, Jae Hun Choi, Jaesang Yu, Jae Kwan Lee, Nam-Ho You, and Munju Goh, "Enhancement of the crosslink density, glass transition temperature, and strength of epoxy resin by using functionalized graphene oxide co-curing agents", *Polym. Chem.* **7**(1), pp. 36–43 (2016).

[268] Jérémy Odent, Sophie Vanderstappen, Antoniya Toncheva, Enzo Pichon, Thomas J. Wallin, Kaiyang Wang, Robert F. Shepherd, Philippe Dubois, and Jean-Marie Raquez, "Hierarchical chemomechanical encoding of multi-responsive hydrogel actuators via 3d printing", *J. Mater. Chem. A* **7**(25), pp. 15395–15403 (2019).

[269] Guilhem X. De Hoe, Michael T. Zumstein, Brandon J. Tiegs, Jacob P. Brutman, Kristopher McNeill, Michael Sander, Geoffrey W. Coates, and Marc A. Hillmyer, "Sustainable polyester elastomers from lactones: Synthesis, properties, and enzymatic hydrolyzability", *J. Am. Chem. Soc.* **140**(3), pp. 963–973 (2018).

[270] Wim Denissen, Guadalupe Rivero, Renaud Nicolaÿ, Ludwik Leibler, Johan M. Winne, and Filip E. Du Prez, "Vinylogous urethane vitrimers", *Adv. Funct. Mater.* **25**(16), pp. 2451–2457 (2015).

[271] Mona M. Obadia, Antoine Jourdain, Philippe Cassagnau, Damien Montarnal, and Eric Drockenmuller, "Tuning the viscosity profile of ionic vitrimers incorporating 1,2,3-triazolium cross-links", *Adv. Funct. Mater.* **27**(45), pp. 1703258 (2017).

[272] Weike Zou, Jiante Dong, Yingwu Luo, Qian Zhao, and Tao Xie, "Dynamic covalent polymer networks: from old chemistry to modern day innovations", *Adv. Mater.* **29**(14), pp. 1606100 (2017).

[273] Zhanhua Wang, Xili Lu, Shaojie Sun, Changjiang Yu, and Hesheng Xia, "Preparation, characterization and properties of intrinsic self-healing elastomers", *J. Mater. Chem. B* **7**(32), pp. 4876–4926 (2019).

[274] Qiong Li, Songqi Ma, Sheng Wang, Wangchao Yuan, Xiwei Xu, Binbo Wang, Kaifeng Huang, and Jin Zhu, "Facile catalyst-free synthesis, exchanging, and hydrolysis of an acetal motif for dynamic covalent networks", *J. Mater. Chem. A* **7**(30), pp. 18039–18049 (2019).

[275] Huan Zhang, Chao Cai, Wenxing Liu, Dongdong Li, Jiawei Zhang, Ning Zhao, and Jian Xu, "Recyclable polydimethylsiloxane network crosslinked by dynamic transesterification reaction", *Sci. Rep.* **7**(1), pp. 1–9 (2017).

[276] Ruibin Mo, Jin Hu, Haowei Huang, Xinxin Sheng, and Xinya Zhang, "Tunable, self-healing and corrosion inhibiting dynamic epoxy–polyimine network built by post-crosslinking", *J. Mater. Chem. A* **7**(7), pp. 3031–3038 (2019).

[277] Marc Guerre, Christian Taplan, Renaud Nicolaÿ, Johan M. Winne, and Filip E. Du Prez, "Fluorinated vitrimer elastomers with a dual temperature response", *J. Am. Chem. Soc.* **140**(41), pp. 13272–13284 (2018).

[278] Hannes A. Houck, Eva Blasco, Filip E. Du Prez, and Christopher Barner-Kowollik, "Light-stabilized dynamic materials", *J. Am. Chem. Soc.* **141**(31), pp. 12329–12337 (2019).

[279] Albert Chao, Ioan Negulescu, and Donghui Zhang, "Dynamic covalent polymer networks based on degenerative imine bond exchange: Tuning the malleability and self-healing properties by solvent", *Macromolecules* **49**(17), pp. 6277–6284 (2016).

[280] Craig M. Hamel, Xiao Kuang, Kaijuan Chen, and H. Jerry Qi, "Reaction-diffusion model for thermosetting polymer dissolution through exchange reactions assisted by small-molecule solvents", *Macromolecules* **52**(10), pp. 3636–3645 (2019).

[281] Progyateg Chakma and Dominik Konkolewicz, "Dynamic covalent bonds in polymeric materials", *Angew. Chem. Int. Ed.* **58**(29), pp. 9682–9695 (2019).

[282] Mona M. Obadia, Bhanu P. Mudraboyina, Anatoli Serghei, Damien Montarnal, and Eric Drockenmuller, "Reprocessing and recycling of highly cross-linked ion-conducting networks through transalkylation exchanges of c–n bonds", *J. Am. Chem. Soc.* **137**(18), pp. 6078–6083 (2015).

[283] Melania Bednarek and Przemysław Kubisa, "Reversible networks of degradable polyesters containing weak covalent bonds", *Polym. Chem.* **10**(15), pp. 1848–1872 (2019).

[284] Wim Denissen, Johan M. Winne, and Filip E. Du Prez, "Vitrimers: permanent organic networks with glass-like fluidity", *Chem. Sci.* **7**(1), pp. 30–38 (2016).

[285] Ning Zheng, Jingjing Hou, Yang Xu, Zizheng Fang, Weike Zou, Qian Zhao, and Tao Xie, "Catalyst-free thermoset polyurethane with permanent shape reconfigurability and highly tunable triple-shape memory performance", *ACS Macro Lett.* **6**(4), pp. 326–330 (2017).

[286] Zhao Wang, Lifeng Guo, Hongyan Xiao, Huan Cong, and Shutao Wang, "A reversible underwater glue based on photo- and thermo-responsive dynamic covalent bonds", *Mater. Horiz.* **7**(1), pp. 282–288 (2020).

[287] Li Liu, Mei-Hua Liu, Lin-Lin Deng, Bao-Ping Lin, and Hong Yang, "Near-infrared chromophore functionalized soft actuator with ultrafast photoresponsive speed and superior mechanical property", *J. Am. Chem. Soc.* **139**(33), pp. 11333–11336 (2017).

[288] R Mafi, SM Mirabedini, MM Attar, and S Moradian, "Cure characterization of epoxy and polyester clear powder coatings using differential scanning calorimetry (dsc) and dynamic mechanical thermal analysis (dmta)", *Prog. Org. Coat.* **54**(3), pp. 164–169 (2005).

[289] L. M. Polgar, M. van Duin, A. A. Broekhuis, and F. Picchioni, "Use of diels–alder chemistry for thermoreversible cross-linking of rubbers: The next step toward recycling of rubber products?", *Macromolecules* **48**(19), pp. 7096–7105 (2015).

[290] Albert Chao, Ioan Negulescu, and Donghui Zhang, "Dynamic covalent polymer networks based on degenerative imine bond exchange: Tuning the malleability and self-healing properties by solvent", *Macromolecules* **49**(17), pp. 6277–6284 (2016).

[291] Debnath, Rewati Raman Ujjwal, and Umaprasana Ojha, "Self-healable and recyclable dynamic covalent networks based on room temperature exchangeable hydrazide michael adduct linkages", *Macromolecules* **51**(23), pp. 9961–9973 (2018).

[292] Ranjana Baruah, Anuj Kumar, Rewati Raman Ujjwal, Soumya Kedia, Amit Ranjan, and Umaprasana Ojha, "Recyclable thermosets based on dynamic amidation and aza-michael addition chemistry", *Macromolecules* **49**(20), pp. 7814–7824 (2016).

[293] Anouk Dirksen, Sjoerd Dirksen, Tilman M. Hackeng, and Philip E. Dawson, "Nucleophilic catalysis of hydrazone formation and transimination: Implications for dynamic covalent chemistry", *J. Am. Chem. Soc.* **128**(49), pp. 15602–15603 (2006).

[294] Kyung-su Kim, Hye Jin Cho, Jookyeong Lee, Seonggyun Ha, Sun Gu Song, Seunghun Kim, Wan Soo Yun, Seong Kyu Kim, Joonsuk Huh, and Changsik Song, "Dynamic covalent hydrazone supramolecular polymers toward multiresponsive self-assembled nanowire system", *Macromolecules* **51**(20), pp. 8278–8285 (2018).

[295] Arpan Biswas, Vinod K. Aswal, P. U. Sastry, Dipak Rana, and Pralay Maiti, "Reversible bidirectional shape memory effect in polyurethanes through molecular flipping", *Macromolecules* **49**(13), pp. 4889–4897 (2016).

[296] Xi Chen, Lingqiao Li, and John M Torkelson, "Recyclable polymer networks containing hydroxyurethane dynamic cross-links: Tuning morphology, cross-link density, and associated properties with chain extenders", *Polymer* **178**(12), pp. 121604 (2019).

[297] Bartosz M. Matysiak, Piotr Nowak, Ivica Cvrtila, Charalampos G. Pappas, Bin Liu, Dávid Komáromy, and Sijbren Otto, "Antiparallel dynamic covalent chemistries", *J. Am. Chem. Soc.* **139**(19), pp. 6744–6751 (2017).

[298] Wim Denissen, Martijn Droesbeke, Renaud Nicolaÿ, Ludwik Leibler, M Winne, and Filip E Du Prez, "Chemical control of the viscoelastic properties of vinylogous urethane vitrimers", *Nat. Commun.* **8**(1), pp. 1–7 (2017).

[299] Rachel L. Snyder, David J. Fortman, Guilhem X. De Hoe, Marc A. Hillmyer, and William R. Dichtel, "Reprocessable acid-degradable polycarbonate vitrimers", *Macromolecules* **51**(2), pp. 389–397 (2018).

[300] Megan F. Dunn, Tao Wei, Ronald N. Zuckermann, and Timothy F. Scott, "Aqueous dynamic covalent assembly of molecular ladders and grids bearing boronate ester rungs", *Polym. Chem.* **10**(18), pp. 2337–2343 (2019).

[301] Peter R Christensen, Angelique M Scheuermann, Kathryn E Loeffler, and Brett A Helms, "Closed-loop recycling of plastics enabled by dynamic covalent diketoenamine bonds", *Nat. Chem.* **11**(5), pp. 442–448 (2019).

[302] Josh E. Richards and Douglas Philp, "A reactive nitrone-based organogel that self-assembles from its constituents in chloroform", *Chem. Commun.* **52**(28), pp. 4995–4998 (2016).

[303] Chihiro Urata, Roland Hönes, Tomoya Sato, Hiroshi Kakiuchida, Yasutaka Matsuo, and Atsushi Hozumi, "Textured organogel films showing unusual thermoresponsive dewetting, icephobic, and optical properties", *Adv. Mater. Interfaces* **6**(2), pp. 1801358 (2019).

[304] Yangjun Chen, Wenda Wang, Di Wu, Hongbo Zeng, Dennis G. Hall, and Ravin Narain, "ponsive and self-healing hydrogel via formation of polymer–nanogel interfacial dynamic benzoxaborole esters at physiological ph", *ACS Appl. Mater. Interfaces* **11**(47), pp. 44742–44750 (2019).

[305] Alexander Sidorenko, Tom Krupenkin, Ashley Taylor, Peter Fratzl, and Joanna Aizenberg, "Reversible switching of hydrogel-actuated nanostructures into complex micropatterns", *Science* **315**(5811), pp. 487–490 (2007).

[306] Tao Yuan, Xinxin Qu, Xinming Cui, and Junqi Sun, "Self-healing and recyclable hydrogels reinforced with in situ-formed organic nanofibrils exhibit simultaneously enhanced mechanical strength and stretchability", *ACS Appl. Mater. Interfaces* **11**(35), pp. 32346–32353 (2019).

[307] Liang Yue, Shan Wang, Verena Wulf, and Itamar Willner, "Stiffness-switchable dna-based constitutional dynamic network hydrogels for self-healing and matrix-guided controlled chemical processes", *Nat. Commun.* **10**(1), pp. 1–10 (2019).

[308] Mareva Fevre, Gavin O. Jones, Musan Zhang, Jeannette M. García, and James L. Hedrick, "Melt-processable dynamic-covalent poly(hemiaminal) organogels as scaffolds for uv-induced polymerization", *Adv. Mater.* **27**(32), pp. 4714–4718 (2015).

[309] Han L. Lim, Jessica C. Chuang, Tuan Tran, Aereas Aung, Gaurav Arya, and Shyni Varghese, "Dynamic electromechanical hydrogel matrices for stem cell culture", *Adv. Funct. Mater.* **21**(1), pp. 55–63 (2011).

[310] Liyang Shi, Yuqin Zeng, Yannan Zhao, Bin Yang, Dmitri Ossipov, Cheuk-Wai Tai, Jianwu Dai, and Changgang Xu, "Biocompatible injectable magnetic hydrogel formed by dynamic coordination network", *ACS Appl. Mater. Interfaces* **11**(49), pp. 46233–46240 (2019).

[311] Shan Xia, Qian Zhang, Shixin Song, Lijie Duan, and Guanghui Gao, "Bioinspired dynamic cross-linking hydrogel sensors with skin-like strain and pressure sensing behaviors", *Chem. Mater.* **31**(22), pp. 9522–9531 (2019).

[312] Ziyi Li, Fei Zhou, Zhiyong Li, Siyu Lin, Lei Chen, Lixin Liu, and Yongming Chen, "Hydrogel cross-linked with dynamic covalent bonding and micellization for promoting burn wound healing", *ACS Appl. Mater. Interfaces* **10**(30), pp. 25194–25202 (2018).

[313] CH Fox, GM ter Hurrne, RJ Wojtecki, GO Jones, HW Horn, EW Meijer, CW Frank, JL Hedrick, and JM García, "Supramolecular motifs in dynamic covalent peg-hemiaminal organogels nat" *Chem. Sci.* **6**(1), pp. 8417 (2015).

[314] Joseph V. Accardo and Julia A. Kalow, "Reversibly tuning hydrogel stiffness through photocontrolled dynamic covalent crosslinks", *Chem. Sci.* **9**(27), pp. 5987–5993 (2018).

[315] Hui Wang and Yiyun Cheng, "All-small-molecule dynamic covalent hydrogels with multistimuli responsiveness", *Mater. Chem. Front.* **3**(3), pp. 472–475 (2019).

[316] Yuan Gao, Weifeng Liu, and Shiping Zhu, "Polyolefin thermoplastics for multiple shape and reversible shape memory", *ACS Appl. Mater. Interfaces* **9**(5), pp. 4882–4889 (2017).

[317] Huijie Song, Zizheng Fang, Binjie Jin, Pengju Pan, Qian Zhao, and Tao Xie, "Synergetic chemical and physical programming for reversible shape memory effect in a dynamic covalent network with two crystalline phases", *ACS Macro Lett.* **8**(6), pp. 682–686 (2019).

[318] Adrien Demongeot, Ramon Groote, Han Goossens, Theo Hoeks, François Tournilhac, and Ludwik Leibler, "Cross-linking of poly(butylene terephthalate) by reactive extrusion using zn(ii) epoxy-vitrimer chemistry", *Macromolecules* **50**(16), pp. 6117–6127 (2017).

[319] Yingchuan Yu, Giuseppe Storti, and Massimo Morbidelli, "Kinetics of ring-opening polymerization of l,l-lactide", *Ind. Eng. Chem. Res.* **50**(13), pp. 7927–7940 (2011).

[320] Jeffrey L. Self, Neil D. Dolinski, Manuel S. Zayas, Javier Read de Alaniz, and Christopher M. Bates, "Brønsted-acid-catalyzed exchange in polyester dynamic covalent networks", *ACS Macro Lett.* **7**(7), pp. 817–821 (2018).

[321] Olivia R. Cromwell, Jaeyoon Chung, and Zhibin Guan, "Malleable and self-healing covalent polymer networks through tunable dynamic boronic ester bonds", *J. Am. Chem. Soc.* **137**(20), pp. 6492–6495 (2015).

[322] Yuzhan Li, Orlando Rios, Jong K. Keum, Jihua Chen, and Michael R. Kessler, "Photoresponsive liquid crystalline epoxy networks with shape memory behavior and dynamic ester bonds", *ACS Appl. Mater. Interfaces* **8**(24), pp. 15750–15757 (2016).

[323] Suman Debnath, Swaraj Kaushal, and Umaprasana Ojha, "Catalyst-free partially bio-based polyester vitrimers", *ACS Appl. Polym. Mater.* **2**(2), pp. 1006–1013 (2020).

[324] Ye Li and Chunjian Xu, "Pressure-swing distillation for separating pressure-insensitive minimum boiling azeotrope methanol/toluene via introducing a light entrainer: Design and control", *Ind. Eng. Chem. Res.* **56**(14), pp. 4017–4037 (2017).

[325] Ao Yang, Renxing Wei, Shirui Sun, Shun'an Wei, Weifeng Shen, and I-Lung Chien, "Energy-saving optimal design and effective control of heat integration-extractive dividing wall column for separating heterogeneous mixture methanol/toluene/water with multiazeotropes", *Ind. Eng. Chem. Res.* **57**(23), pp. 8036–8056 (2018).

[326] Dong Wang, JianHua Xu, JiaoYang Chen, Po Hu, Yang Wang, Wei Jiang, and JiaJun Fu, "Transparent, mechanically strong, extremely tough, self-recoverable, healable supramolecular elastomers facilely fabricated via dynamic hard domains design for multifunctional applications", *Adv. Funct. Mater.* **30**(3), pp. 1907109 (2020).

[327] Smita V. Mankar, Maria Nelly Garcia Gonzalez, Niklas Warlin, Nitin G. Valsange, Nicola Rehnberg, Stefan Lundmark, Patric Jannasch, and Baozhong Zhang, "Synthesis, life cycle assessment, and polymerization of a vanillin-based spirocyclic diol toward polyesters with increased glass-transition temperature", *ACS Sustain. Chem. Eng.* **7**(23), pp. 19090–19103 (2019).

[328] Xu Zhang, Zihua Li, Xuemei Che, Linping Yu, Wangyue Jia, Rui Shen, Jinchun Chen, Yiming Ma, and Guo-Qiang Chen, "Synthesis and characterization of polyhydroxyalkanoate organo/hydrogels", *Biomacromolecules* **20**(9), pp. 3303–3312 (2019).

[329] Weisong Li, Lei Shi, Baoru Yu, Ming Xia, Junwen Luo, Haochun Shi, and Chunjian Xu, "New pressure-swing distillation for separating pressure-insensitive maximum boiling azeotrope via introducing a heavy entrainer: Design and control", *Ind. Eng. Chem. Res.* **52**(23), pp. 7836–7853 (2013).

[330] Jesús A. Jaime, Gerardo Rodríguez, and Iván D. Gil, "Control of an optimal extractive distillation process with mixed-solvents as separating agent", *Ind. Eng. Chem. Res.* **57**(29), pp. 9615–9626 (2018).

[331] Chen-Yu Shi, Qi Zhang, Cheng-Yuan Yu, Si-Jia Rao, Shun Yang, He Tian, and Da-Hui Qu, "An ultrastrong and highly stretchable polyurethane elastomer enabled by a zipper-like ring-sliding effect", *Adv. Mater.* **32**(23), pp. 2000345 (2020).

[332] Qingyu Peng, Yuyang Qin, Xu Zhao, Xianxian Sun, Qiang Chen, Fan Xu, Zaishan Lin, Ye Yuan, Ying Li, Jianjun Li, Weilong Yin, Chao Gao, Fan Zhang, Xiaodong He, and Yibin Li, "Superlight, mechanically flexible, thermally superinsulating, and antifrosting anisotropic nanocomposite foam based on hierarchical graphene oxide assembly", *ACS Appl. Mater. Interfaces* **9**(50), pp. 44010–44017 (2017).

[333] A. C. Weems, J. K. Carrow, A. K. Gaharwar, and D. J. Maitland, "Improving the oxidative stability of shape memory polyurethanes containing tertiary amines by the presence of isocyanurate triols", *Macromolecules* **51**(22), pp. 9078–9087 (2018).

[334] Bingbing Zeng, Ying Li, Lishen Wang, Yu Zheng, Jiabin Shen, and Shaoyun Guo, "Body temperature-triggered shape-memory effect via toughening sustainable poly(propylene carbonate) with thermoplastic polyurethane: toward potential application of biomedical stents", *ACS Sustain. Chem. Eng.* **8**(3), pp. 1538–1547 (2020).

[335] Zihang Yang, Zirui Zhai, Zeming Song, Yingzhu Wu, Jiahao Liang, Yingfa Shan, Jinren Zheng, Haichao Liang, and Hanqing Jiang, "Conductive and elastic 3d helical fibers for use in washable and wearable electronics", *Adv. Mater.* **32**(10), pp. 1907495 (2020).

[336] Yuan Yao, Ziyang Xu, Bo Liu, Meng Xiao, Jianhai Yang, and Wenguang Liu, "Multiple H-bonding chain extender-based ultrastiff thermoplastic polyurethanes with autonomous self-healability, solvent-free adhesiveness, and aie fluorescence", *Adv. Funct. Mater.* **31**(4), pp. 2006944 (2020).

[337] Chenyu Wang, Olga Zolotarskaya, Kayesh M. Ashraf, Xuejun Wen, Dennis E. Ohman, and Kenneth J. Wynne, "Surface characterization, antimicrobial effectiveness, and human cell response for a biomedical grade polyurethane blended with a mixed soft block ptmo-quat/peg copolyoxetane polyurethane", *ACS Appl. Mater. Interfaces* **11**(23), pp. 20699–20714 (2019).

[338] Vivian R. Feig, Helen Tran, and Zhenan Bao, "Biodegradable polymeric materials in degradable electronic devices", *ACS Cent. Sci.* **4**(3), pp. 337–348 (2018).

[339] Seon-Mi Kim, Hyeonyeol Jeon, Sung-Ho Shin, Seul-A Park, Jonggeon Jegal, Sung Yeon Hwang, Dongyeop X. Oh, and Jeyoung Park, "Superior toughness and fast self-healing at room temperature engineered by transparent elastomers", *Adv. Mater.* **30**(1), pp. 1705145 (2018).

[340] Wu Bin Ying, Zhe Yu, Do Hwan Kim, Kyung Jin Lee, Han Hu, Yiwei Liu, Zhengyang Kong, Kai Wang, Jie Shang, Ruoyu Zhang, Jin Zhu, and Run-Wei Li, "Waterproof, highly tough, and fast self-healing polyurethane for durable electronic skin", *ACS Appl. Mater. Interfaces* **12**(9), pp. 11072–11083 (2020).

[341] Yu-chun Chien, Wei-Tsung Chuang, U.-Ser Jeng, and Shan-hui Hsu, "Preparation, characterization, and mechanism for biodegradable and biocompatible polyurethane shape memory elastomers", *ACS Appl. Mater. Interfaces* **9**(6), pp. 5419–5429 (2017).

[342] Hafeez Ur Rehman, Yujie Chen, Mikael S. Hedenqvist, Hua Li, Wenchao Xue, Yunlong Guo, Yiping Guo, Huanan Duan, and Hezhou Liu, "Self-healing shape memory pupcl copolymer with high cycle life", *Adv. Funct. Mater.* **28**(7), pp. 1704109 (2018).

[343] Thuy Thu Truong, Son Hong Thai, Ha Tran Nguyen, Dung Thuy Thi Phung, Loc Tan Nguyen, Hung Quang Pham, and Le-Thu T. Nguyen, "Tailoring the hard–soft interface with dynamic diels–alder linkages in polyurethanes: Toward superior mechanical properties and healability at mild temperature", *Chem. Mater.* **31**(7), pp. 2347–2357 (2019).

[344] Dai Fei Elmer Ker, Dan Wang, Anthony William Behn, Evelyna Tsi Hsin Wang, Xu Zhang, Benjamin Yamin Zhou, Ángel Enrique Mercado-Pagán, Sungwoo Kim, John Kleimeyer, Burhan Gharaibeh, Yaser Shanjani, Drew Nelson, Marc Safran, Emilie Cheung, Phil Campbell, and Yunzhi Peter Yang, "Functionally graded, bone- and tendon-like polyurethane for rotator cuff repair", *Adv. Funct. Mater.* **28**(20), pp. 1707107 (2018).

[345] Tzu-Wei Lin and Shan-hui Hsu, "Self-healing hydrogels and cryogels from biodegradable polyurethane nanoparticle crosslinked chitosan", *Adv. Sci.* **7**(3), pp. 1901388 (2020).

[346] Benjamin R. Elling and William R. Dichtel, "Reprocessable cross-linked polymer networks: Are associative exchange mechanisms desirable?", *ACS Cent. Sci.* **6**(9), pp. 1488–1496 (2020).

[347] Dong Zhang, Hongxiang Chen, Qiaoli Dai, Chuanxi Xiang, Yanjun Li, Xiao Xiong, Yu Zhou, and Jinlong Zhang, "Stimuli-mild, robust, commercializable polyurethane-urea vitrimer elastomer via n,n′-diaryl urea crosslinking", *Macromol Chem Phys* **221**(15), pp. 1900564 (2020).

[348] David J. Fortman, Jacob P. Brutman, Christopher J. Cramer, Marc A. Hillmyer, and William R. Dichtel, "Mechanically activated, catalyst-free polyhydroxyurethane vitrimers", *J. Am. Chem. Soc.* **137**(44), pp. 14019–14022 (2015).

[349] Daylan T. Sheppard, Kailong Jin, Leslie S. Hamachi, William Dean, David J. Fortman, Christopher J. Ellison, and William R. Dichtel, "Reprocessing postconsumer polyurethane foam using carbamate exchange catalysis and twin-screw extrusion", *ACS Cent. Sci.* **6**(6), pp. 921–927 (2020).

[350] Xi Chen, Sumeng Hu, Lingqiao Li, and John M. Torkelson, "Dynamic covalent polyurethane networks with excellent property and cross-link density recovery after recycling and potential for monomer recovery", *ACS Appl. Polym. Mater.* **2**(5), pp. 2093–2101 (2020).

[351] Jiaxin Shi, Tianze Zheng, Yao Zhang, Baohua Guo, and Jun Xu, "Reprocessable cross-linked polyurethane with dynamic and tunable phenol–carbamate network", *ACS Sustain. Chem. Eng.* **8**(2), pp. 1207–1218 (2020).

[352] Wen-Xing Liu, Chi Zhang, Huan Zhang, Ning Zhao, Zhi-Xiang Yu, and Jian Xu, "Oxime-based and catalyst-free dynamic covalent polyurethanes", *J. Am. Chem. Soc.* **139**(25), pp. 8678–8684 (2017).

[353] Sangbaek Park, Gurunathan Thangavel, Kaushik Parida, Shaohui Li, and Pooi See Lee, "A stretchable and self-healing energy storage device based on mechanically and electrically restorative liquid-metal particles and carboxylated polyurethane composites", *Adv. Mater.* **31**(1), pp. 1805536 (2019).

[354] Wuhou Fan, Yong Jin, Liangjie Shi, Rong Zhou, and Weining Du, "Developing visible-light-induced dynamic aromatic schiff base bonds for room-temperature self-healable and reprocessable waterborne polyurethanes with high mechanical properties", *J. Mater. Chem. A* **8**(14), pp. 6757–6767 (2020).

[355] David J. Fortman, Rachel L. Snyder, Daylan T. Sheppard, and William R. Dichtel, "Rapidly reprocessable cross-linked polyhydroxyurethanes based on disulfide exchange", *ACS Macro Lett.* **7**(10), pp. 1226–1231 (2018).

[356] Xinpan Li, Ran Yu, Yangyang He, Ying Zhang, Xin Yang, Xiaojuan Zhao, and Wei Huang, "Self-healing polyurethane elastomers based on a disulfide bond by digital light processing 3d printing", *ACS Macro Lett.* **8**(11), pp. 1511–1516 (2019).

[357] Shi-Li Xiang, Qiong-Xin Hua, Peng-Ju Zhao, Wen-Liang Gong, Chong Li, and Ming-Qiang Zhu, "Photoplastic self-healing polyurethane springs and actuators", *Chem. Mater.* **31**(14), pp. 5081–5088 (2019).

[358] Yuanlai Fang, Xiaosheng Du, Yuxu Jiang, Zongliang Du, Peiting Pan, Xu Cheng, and Haibo Wang, "Thermal-driven self-healing and recyclable waterborne polyurethane films based on reversible covalent interaction", *ACS Sustain. Chem. Eng.* **6**(11), pp. 14490–14500 (2018).

[359] Xingxing Chen, Qianyun Zhong, Chenhui Cui, Li Ma, Shuang Liu, Qiang Zhang, Youshen Wu, Le An, Yilong Cheng, Shibo Ye, Xiaoming Chen, Zhen Dong, Quan Chen, and Yanfeng Zhang, "Extremely tough, puncture-resistant, transparent, and photoluminescent polyurethane elastomers for crack self-diagnose and healing tracking", *ACS Appl. Mater. Interfaces* **12**(27), pp. 30847–30855 (2020).

[360] Bingjie Zhao, Hao Ding, Sen Xu, and Sixun Zheng, "Organic–inorganic linear segmented polyurethanes simultaneously having shape recovery and self-healing properties", *ACS Appl. Polym. Mater.* **1**(11), pp. 3174–3184 (2019).

[361] Yan Zhang, Jianjun Liao, Xiangchen Fang, Fudong Bai, Kai Qiao, and Lingmin Wang, "Renewable high-performance polyurethane bioplastics derived from lignin–poly(ε-caprolactone)", *ACS Sustain. Chem. Eng.* **5**(5), pp. 4276–4284 (2017).

[362] Deborah K. Schneiderman, Marie E. Vanderlaan, Alexander M. Mannion, Tessie R. Panthani, Derek C. Batiste, Jay Z. Wang, Frank S. Bates, Christopher W. Macosko, and Marc A. Hillmyer, " recyclable biobased polyurethanes", *ACS Macro Lett.* **5**(4), pp. 515–518 (2016).

[363] Xi Chen, Lingqiao Li, Tong Wei, David C Venerus, and John M Torkelson, "Reprocessable polyhydroxyurethane network composites: effect of filler surface functionality on cross-link density recovery and stress relaxation", *ACS Appl. Mater. Interfaces* **11**(2), pp. 2398–2407 (2018).

[364] Niels Van Herck and Filip E. Du Prez, "Fast healing of polyurethane thermosets using reversible triazolinedione chemistry and shape-memory", *Macromolecules* **51**(9), pp. 3405–3414 (2018).

[365] Y. Gao, W. Liu, and S. Zhu, "Reversible shape memory polymer from semicrystalline poly(ethylene-co-vinyl acetate) with dynamic covalent polymer networks", *Macromolecules* **51**(21), pp. 8956–8963 (2018).

[366] Yong Zhu, Junqi Zhang, Qi Wu, Mokun Chen, Guangsu Huang, Jing Zheng, and Jinrong Wu, "Three-dimensional programmable, reconfigurable, and recyclable biomass soft actuators enabled by designing an inverse opal-mimetic structure with exchangeable interfacial crosslinks", *ACS Appl. Mater. Interfaces* **12**(13), pp. 15757–15764 (2020).

[367] Tuan Liu, Xiaolong Guo, Wangcheng Liu, Cheng Hao, Liwei Wang, William C. Hiscox, Chengyun Liu, Can Jin, Junna Xin, and Jinwen Zhang, "Selective cleavage of ester linkages of anhydride-cured epoxy using a benign method and reuse of the decomposed polymer in new epoxy preparation", *Green Chem.* **19**(18), pp. 4364–4372 (2017).

[368] Maarten Delahaye, Johan M. Winne, and Filip E. Du Prez, "Internal catalysis in covalent adaptable networks: Phthalate monoester transesterification as a versatile dynamic cross-linking chemistry", *J. Am. Chem. Soc.* **141**(38), pp. 15277–15287 (2019).

[369] Huiyi Zhang, Soumabrata Majumdar, Rolf A. T. M. van Benthem, Rint P. Sijbesma, and Johan P. A. Heuts, "Intramolecularly catalyzed dynamic polyester networks using neighboring carboxylic and sulfonic acid groups", *ACS Macro Lett.* **9**(2), pp. 272–277 (2020).

[370] Jeffrey L. Self, Neil D. Dolinski, Manuel S. Zayas, Javier Read de Alaniz, and Christopher M. Bates, "Brønsted-acid-catalyzed exchange in polyester dynamic covalent networks", *ACS Macro Lett.* **7**(7), pp. 817–821 (2018).

[371] Debnath, Swaraj Kaushal, and Umaprasana Ojha, "Catalyst-free partially bio-based polyester vitrimers", *ACS Appl. Polym. Mater.* **2**(2), pp. 1006–1013 (2020).

[372] Suman Debnath, Swaraj Kaushal, Subhankar Mandal, and Umaprasana Ojha, "Solvent processable and recyclable covalent adaptable organogels based on dynamic trans-esterification chemistry: separation of toluene from azeotropic mixtures", *Polym. Chem.* **11**(8), pp. 1471–1480 (2020).

[373] Donglin Tang, Christopher W. Macosko, and Marc A. Hillmyer, "Thermoplastic polyurethane elastomers from bio-based poly(δ-decalactone) diols", *Polym. Chem.* **5**(9), pp. 3231–3237 (2014).

[374] Fei Yang, Li Pan, Zhe Ma, Yahui Lou, Yuanyuan Li, and Yuesheng Li, "Highly elastic, strong, and reprocessable cross-linked polyolefin elastomers enabled by boronic ester bonds", *Polym. Chem.* **11**(19), pp. 3285–3295 (2020).

[375] Wim Denissen, Martijn Droesbeke, Renaud Nicolaÿ, Ludwik Leibler, Johan M Winne, and Filip E Du Prez, "Chemical control of the viscoelastic properties of vinylogous urethane vitrimers", *Nat. Commun.* **8**(1), pp. 1–7 (2017).

[376] Kyu Hun Kim, Michelle N. Tsui, and Mohammad F. Islam, "Graphene-coated carbon nanotube aerogels remain superelastic while resisting fatigue and creep over -100 to +500 °c", *Chem. Mater.* **29**(7), pp. 2748–2755 (2017).

[377] Sheng Wang, Songqi Ma, Qiong Li, Xiwei Xu, Binbo Wang, Kaifeng Huang, Yanlin liu, and Jin Zhu, "Facile preparation of polyimine vitrimers with enhanced creep resistance and thermal and mechanical properties via metal coordination", *Macromolecules* **53**(8), pp. 2919–2931 (2020).

[378] Wim Denissen, Guadalupe Rivero, Renaud Nicolaÿ, Ludwik Leibler, Johan M. Winne, and Filip E. Du Prez, "Vinylogous urethane vitrimers", *Adv. Funct. Mater.* **25**(16), pp. 2451–2457 (2015).

[379] Lingqiao Li, Xi Chen, Kailong Jin, and John M. Torkelson, "Vitrimers designed both to strongly suppress creep and to recover original cross-link density after reprocessing: Quantitative theory and experiments", *Macromolecules* **51**(15), pp. 5537–5546 (2018).

[380] Jacob J. Lessard, Georg M. Scheutz, Seung Hyun Sung, Kayla A. Lantz, Thomas H. Epps, and Brent S. Sumerlin, "Block copolymer vitrimers", *J. Am. Chem. Soc.* **142**(1), pp. 283–289 (2020).

[381] Yanwu Zhou, Ramon Groote, Johannes G. P. Goossens, Rint P. Sijbesma, and Johan P. A. Heuts, "Tuning PBT vitrimer properties by controlling the dynamics of the adaptable network", *Polym. Chem.* **10**(1), pp. 136–144 (2019).

[382] Muhammad Adeel, Bingjie Zhao, Lei Li, and Sixun Zheng, "Nanocomposites of poly(hydroxyurethane)s with multiwalled carbon nanotubes: Synthesis, shape memory, and reprocessing properties", *ACS Appl. Polym. Mater.* **2**(4), pp. 1711–1721 (2020).

[383] Konstantinos N. Raftopoulos, Stefanos Koutsoumpis, Małgorzata Jancia, James P. Lewicki, Konstantinos Kyriakos, Harris E. Mason, Stephen J. Harley, Edyta Hebda, Christine M. Papadakis, Krzysztof Pielichowski, and Polycarpos Pissis, "Reduced phase separation and slowing of dynamics in polyurethanes with three-dimensional poss-based cross-linking moieties", *Macromolecules* **48**(5), pp. 1429–1441 (2015).

[384] Anuja Shirole, Carlo U. Perotto, Sandor Balog, and Christoph Weder, "Tailoring the shape memory properties of segmented poly(ester urethanes) via blending", *ACS Appl. Mater. Interfaces* **10**(29), pp. 24829–24839 (2018).

This page was intentionally left blank.

List of Publications

Journals

1. Chandan Upadhyay, **Suman Debnath**, Umaprasana Ojha*, “Thiol ester Linkage Based Self-helable and Dynamic Networks ”, (2021), (Manuscript under preparation).

2. **Suman Debnath**, Chandan Upadhyay, Umaprasana Ojha*, “Remoldable, Self healable Dynamic Organogels Based on Trans esterification Chemistry”, (2021), (Manuscript under preparation).

3. **Suman Debnath**, Saurabh K Tiwary , Umaprasana Ojha*, “Dynamic Carboxylate Linkage Based Reprocessable and Self Healable Segmented Polyurethane Vitrimers Displaying Creep Resistance Behavior and Triple Shape Memory Ability ”, *ACS Appl. Polym. Mater.*, **3**, pp. 2166-2177 (2021) (Most read article in April 2021).

4. **Suman Debnath**, Swaraj Kaushal, Subhankar Mandal, Umaprasana Ojha*, “Solvent Processable and Recyclable Covalent Adaptive Organogels Based on Dynamic Transesterification Chemistry: Separation of Toluene from Azeotropic Mixtures ”, *Polym. Chem.*, **11**, pp. 1471-1480 (2020) (Invited article and published as cover art).

5. **Suman Debnath**, Swaraj Kaushal, Umaprasana Ojha*, “Catalyst-Free Partially Bio-Based Polyester Vitrimers ”, *ACS Appl. Polym. Mater.*, **2**, pp. 1006-1013 (2020) (Most read article in February 2020).

6. **Suman Debnath**, Rewati Raman Ujjwal, Umaprasana Ojha*, “Self-Healable and Recyclable Dynamic Covalent Networks Based on Room Temperature Exchangeable Hydrazide Michael Adduct Linkages ”, *Macromolecules*, **51**, pp. 9961-9973 (2018) (Most read Article in 2018)

7. Rewati Raman Ujjwal, Chandan Sona, **Suman Debnath**, Prem Narayan Yadav, Umaprasana Ojha* “Dye Labelled Polyacryloyl Hydrazide-Ag Nanoparticle Fluorescent Probe for Ultra-sensitive and Selective Detection of Au Ion ”, *ACS Omega*, **2**, pp. 4278-4286 (2017).

Conferences

1. **Suman Debnath**, Umaprasana Ojha* "Dynamic polyamides with tailored curing times for real time 3D printing application ", *ACS Meetings and Expositions, April 5-9, 2021*.

2. **Suman Debnath**, Umaprasana Ojha* "Solvent Processable and Recyclable Covalent Adaptive Networks Based on Dynamic Trans-esterification of *beta* keto Esters ", *Rajiv Gandhi Institute of Petroleum Technology (National Symposium October 31-November 1, 2019*.

3. **Suman Debnath**, Umaprasana Ojha* "Self-Healable and Recyclable Dynamic Covalent Networks Based on RoomTemperature Exchangeable Hydrazide Michael Adduct Linkages ", *Rajiv Gandhi Institute of Petroleum Technology (National Symposium April 13, 2019*.

4. **Suman Debnath**, Umaprasana Ojha*, R. M. Tripathi, S.K. Sahoo."Spatial distribution of uranium and associated water quality parameters in Sultanpur district of Uttar Pradesh", *NSE-20, IIT Gandhinagar and Bhabha Atomic Research centre (BARC), IIT Gandhinagar, Gujarat. Dec 13-15, 2018*.

5. **Suman Debnath**, R. R. Ujjwal, Umaprasana Ojha* "Dye-Labeled Polyacryloyl Hydrazide-Ag Nanoparticle Fluorescent Probe for Ultrasensitive and Selective Detection of Au Ion ", *Expanding Frontiers in Chemical Sciences-2018, Indian Academy of Science and ACS Publications, Banaras Hindu University, Banaras. Nov 1, 2018*.

6. **Suman Debnath**, Umaprasana Ojha* "Statistical Analysis of data generated under National Uranium Project ", *Sept. 26-27, 2018, Bhabha Atomic Research Centre (BARC), Mumbai.*.

7. **Suman Debnath**, Umaprasana Ojha* "Dynamic Polyamides with Tailored Curing Times for Real Time 3D Printing Application ", *Rajiv Gandhi Institute of Petroleum Technology (National Symposium March 17-18, 2018*.

8. **Suman Debnath**, Umaprasana Ojha* "Generation of National database on Uranium in drinking water under National Uranium Project ", *Feb. 8-10, 2017, Bhabha Atomic Research Centre (BARC), Mumbai.*.

9. **Suman Debnath**, Ranjana Baruah, Umaprasana Ojha* "Recyclable Thermosets based on dynamic Amidation and Aza-Michael addition reaction ", *Rajiv Gandhi Institute of Petroleum Technology (National Symposium January 4, 2017*.

Conference Proceedings

1. **Suman Debnath**, Umaprasana Ojha*, R. M. Tripathi, S.K. Sahoo."Spatial distribution of uranium and associated water quality parameters in Sultanpur district of Uttar Pradesh", *Proceeding of Twentieth National Symposium on Environment, (NSE-20) IIT Gandhinagar, Gujarat, Dec 13-15, 2018, page 407*.

2. **S**ubhankar Mandal, **Suman Debnath**, Umaprasana Ojha*, R. M. Tripathi, S.K. Sahoo."Spatial distribution of uranium and associated water quality parameters in Faizabad district of Uttar Pradesh ", *Proceeding of Twentieth National Symposium on Environment, (NSE-20) IIT Gandhinagar, Gujarat, Dec 13-15, 2018, page 403*.

3. **N**iharika Pandey, **Suman Debnath**, Umaprasana Ojha*, R. M. Tripathi, S.K. Sahoo."Spatial distribution of uranium and associated water quality parameters in Pratapgarh district of Uttar Pradesh", *Proceeding of Twentieth National Symposium on Environment, (NSE-20) IIT Gandhinagar, Gujarat, Dec 13-15, 2018, page 441*.

Appendix

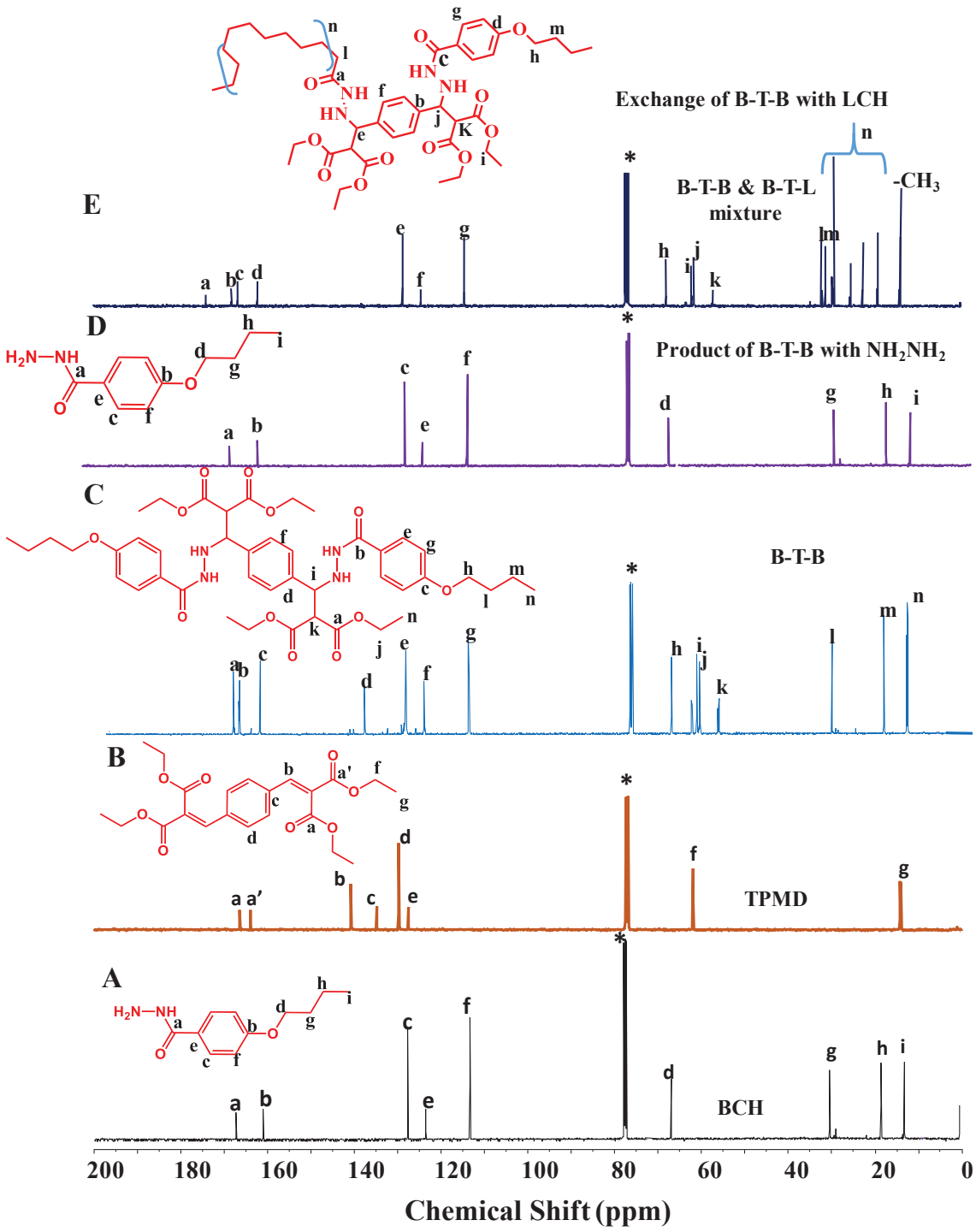

Figure A1: ^{13}C NMR spectra of (A) BCH, (B) TPMD, (C) B-T-B, (D) degraded product of B-T-B with NH_2NH_2 and (E) exchanged product of B-T-B with LCH recorded in $CDCl_3$. The peaks marked with asterisks are assigned to the solvent.

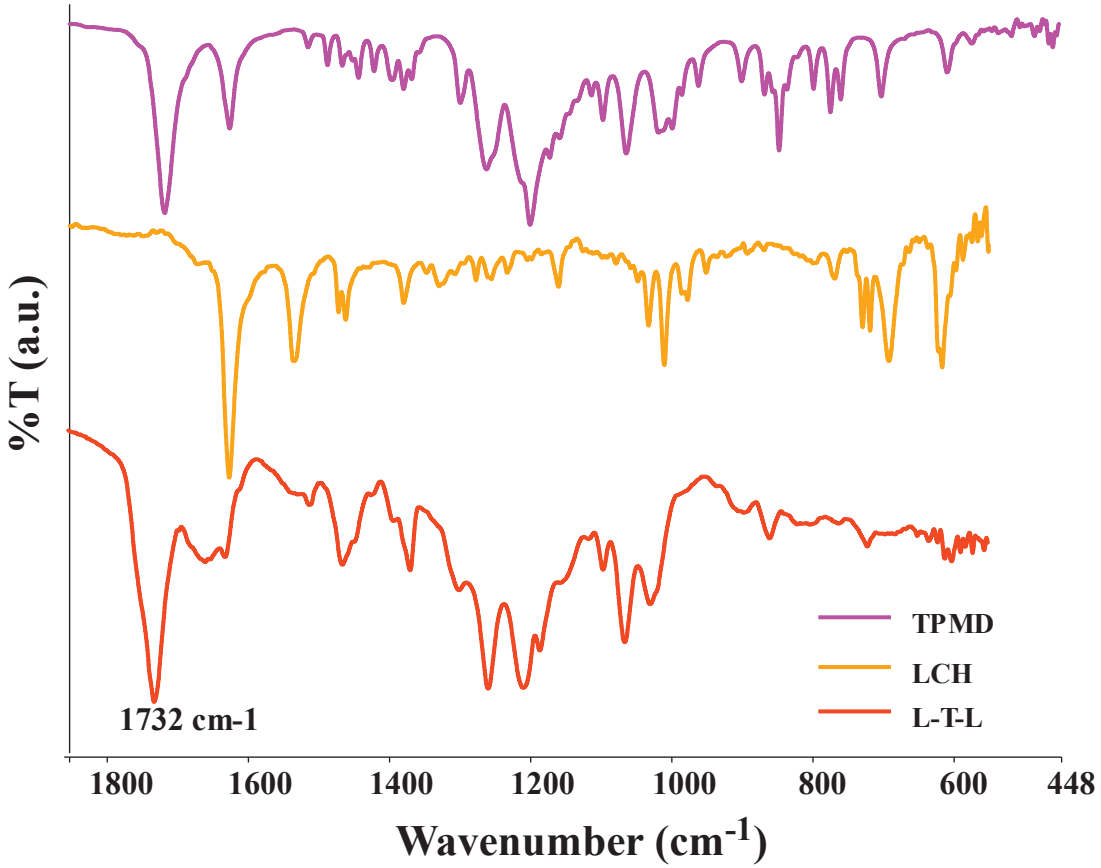

Figure A2: ATR FTIR spectroscopic traces of TPMD, LCH and L-T-L

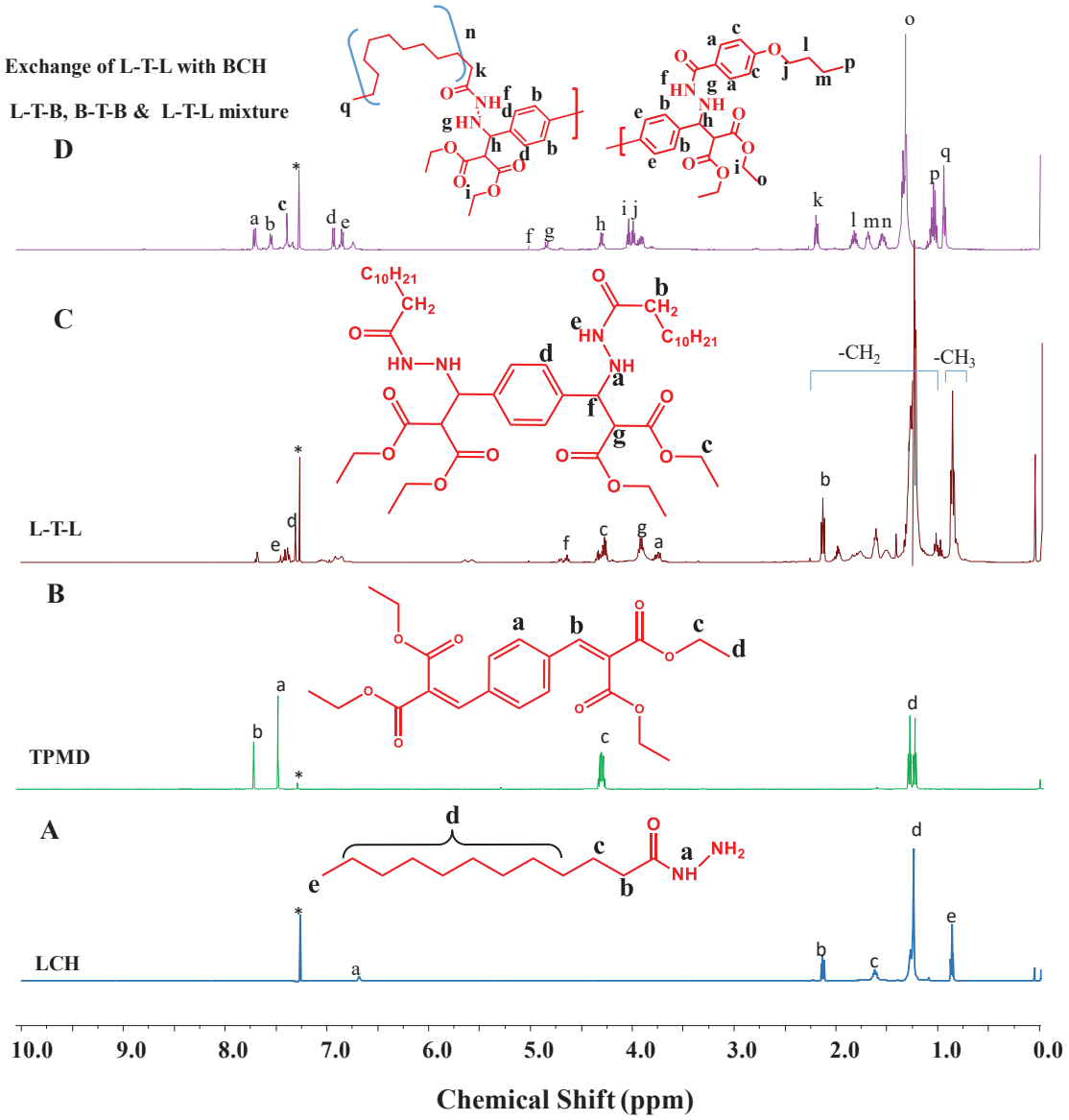

Figure A3: ^{1}H NMR spectra of (A) LCH, (B) TPMD (C) L-T-L and (D) exchanged products of BCH and L-T-L recorded in $CDCl_3$. The peaks marked with asterisks are assigned to the solvent.

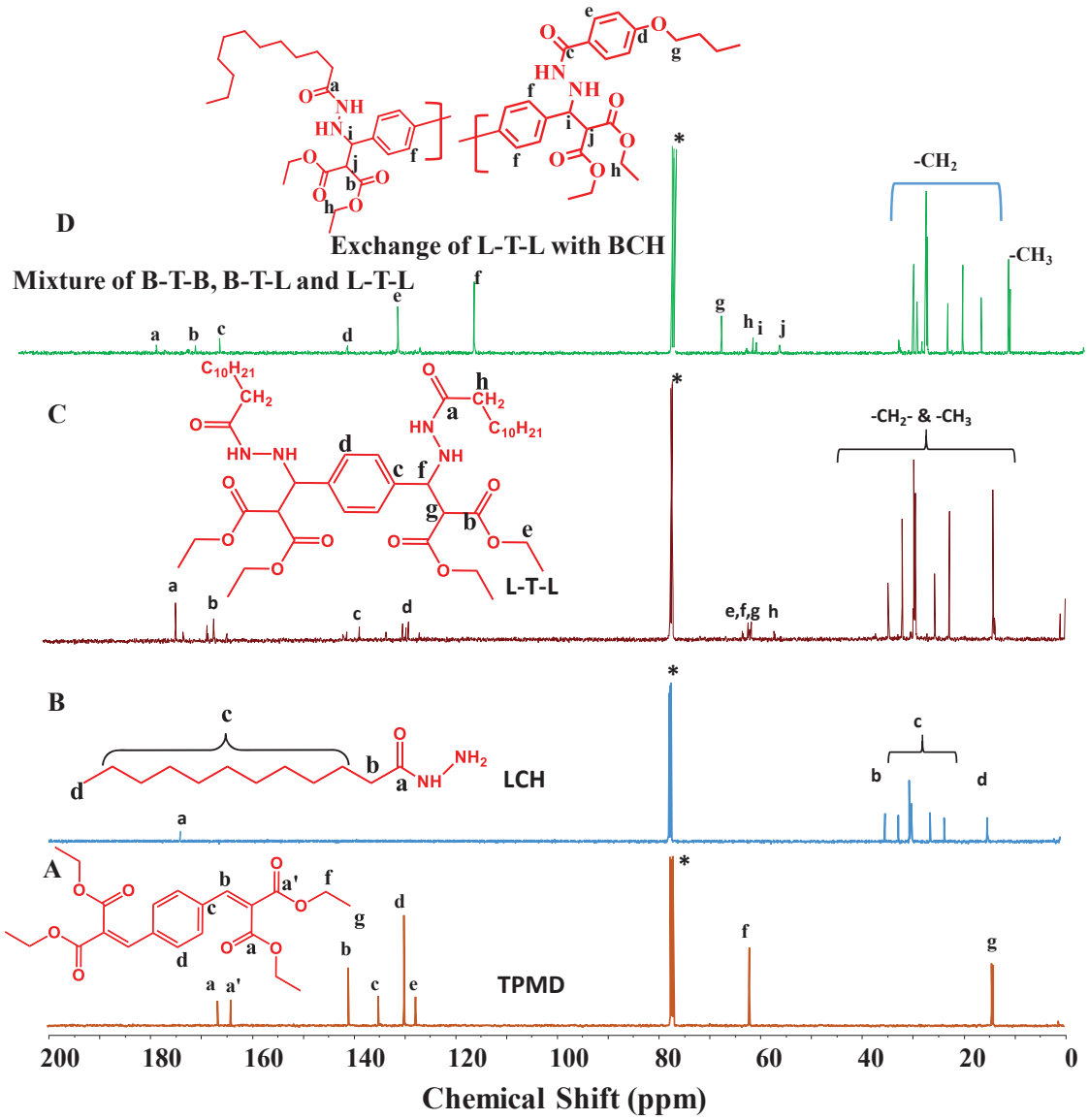

Figure A4: ^{13}C NMR spectra of (A) TPMD, (B) LCH, (C) L-T-L and (D) exchanged products of the reaction between L-T-L and BCH recorded in $CDCl_3$. The peaks marked with asterisks are assigned to the solvent.

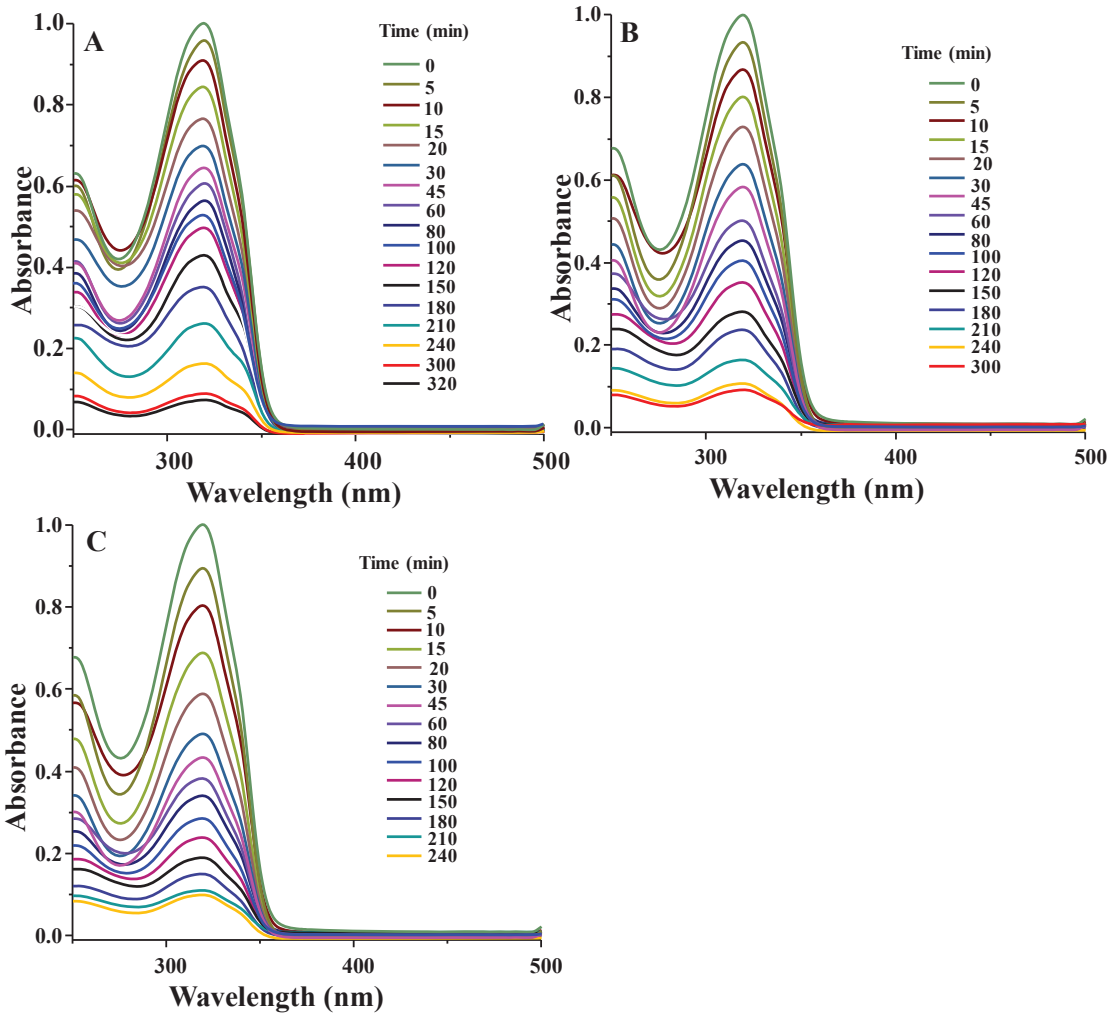

Figure A5: UV-Vis Spectra showing the progress of reaction between TPMD and BCH at (A) 25 °C, (B) 35 °C and (C) 45 °C. Initial concentration: [TPMD] = 0.0078 mol/L, [BCH] = 0.015945 mol/L, At equilibrium, $[TPMD]_{eq}$ = 0.000546 mol/L, $[BCH]_{eq}$ = 0.001092 mol/L and [B-T-B] = 0.007254 mol/L

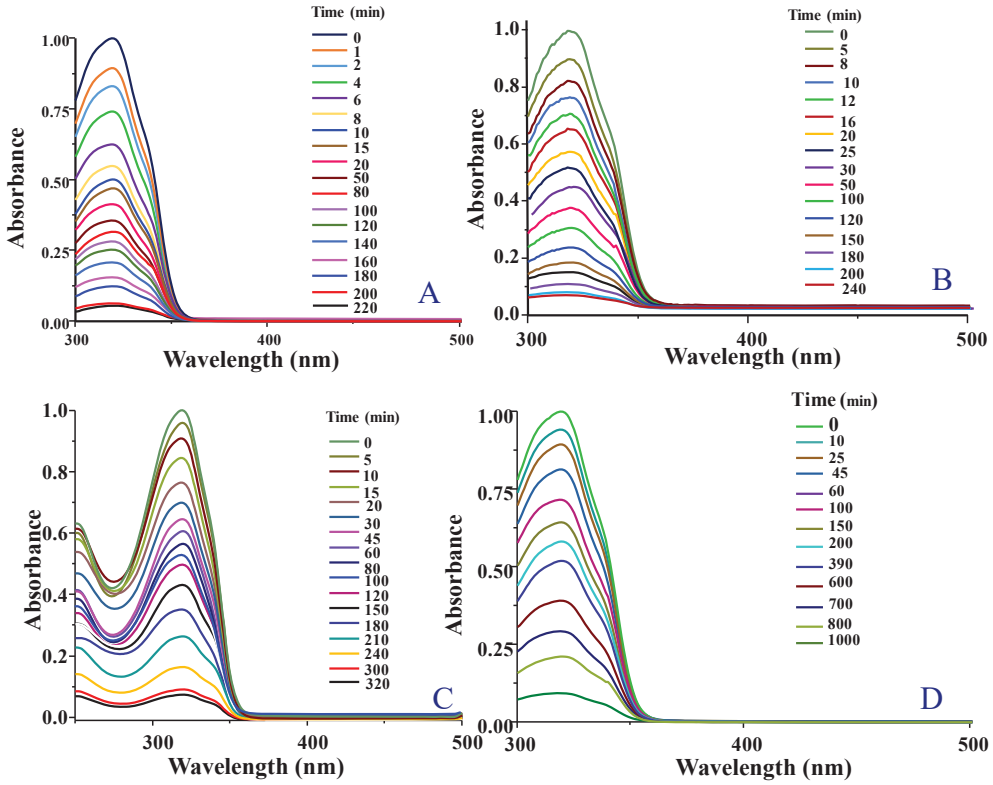

Figure A6: UV-Vis spectroscopic plots recorded at different time intervals for the reaction between TPMD and BCH carried out at different initial concentrations of TPMD (A) 0.03189 mol/L, (B) 0.01595 mol/L, (C) 0.0078 mol/L and (D) 0.00399 mol/L.

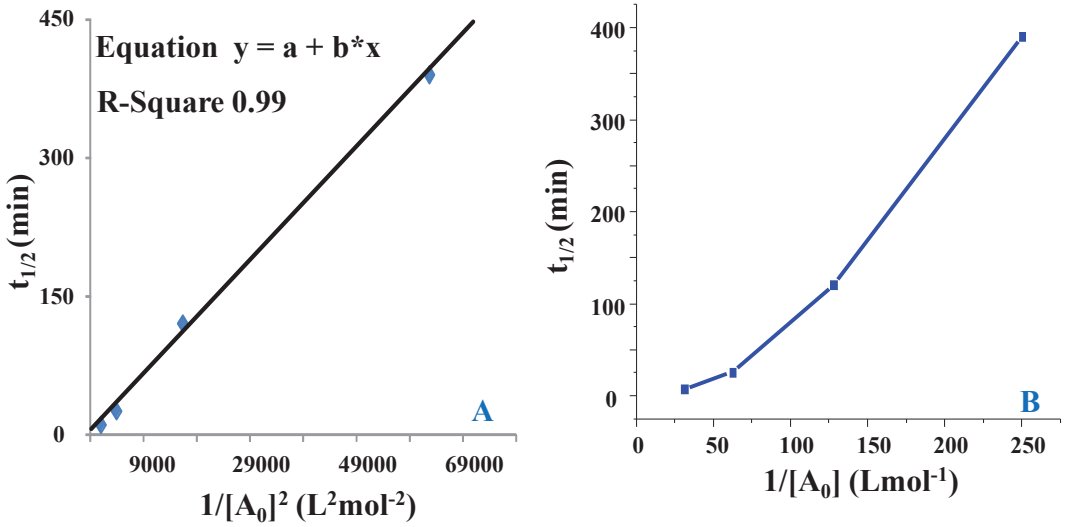

Figure A7: (A) the plots of $t_{1/2}$ versus $1/[A_o]^2$ (third order model) and (B) $t_{1/2}$ versus $1/[A_o]$

(second order model) for the Michael addition between TPMD and BCH carried out at 25 °C.

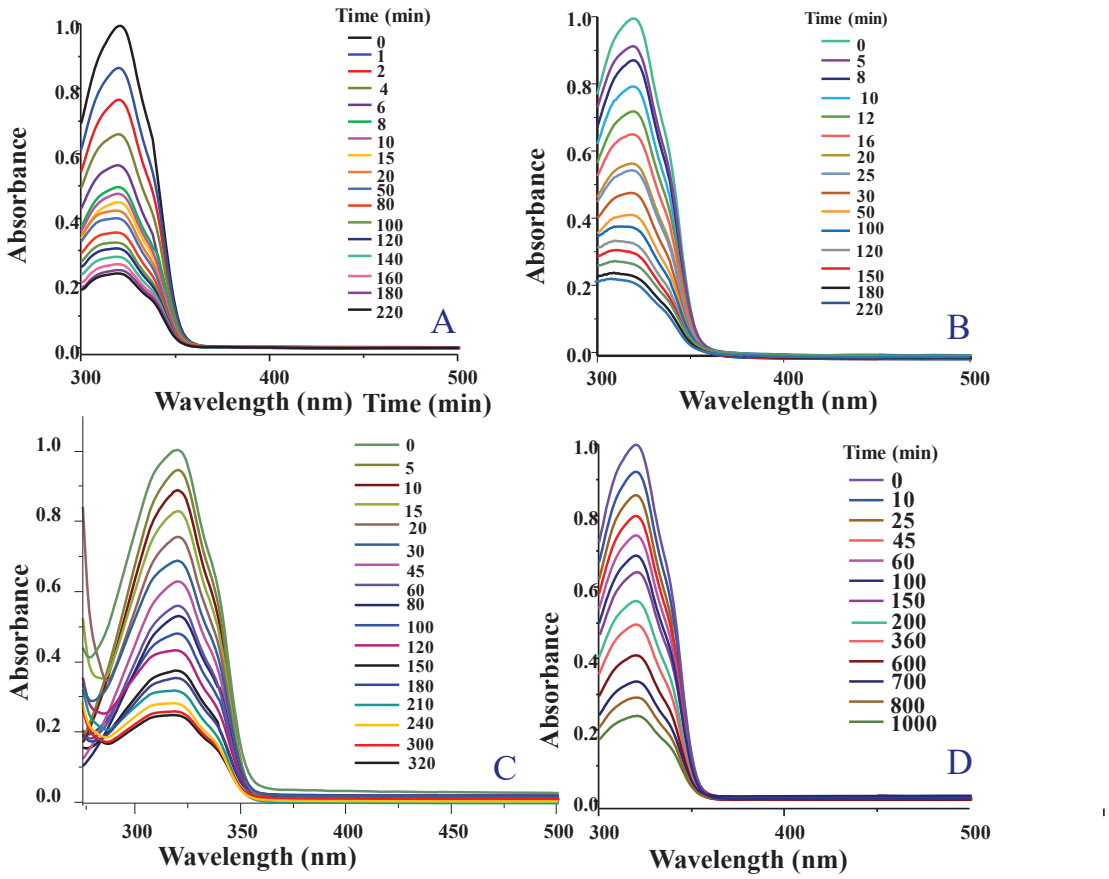

Figure A8: UV-Vis spectroscopic plots recorded at different time intervals for the reaction between TPMD and HCH carried out at different initial concentrations of TPMD (A) 0.03189 mol/L, (B) 0.01595 mol/L (C) 0.0078 mol/L and (D) 0.00399 mol/L

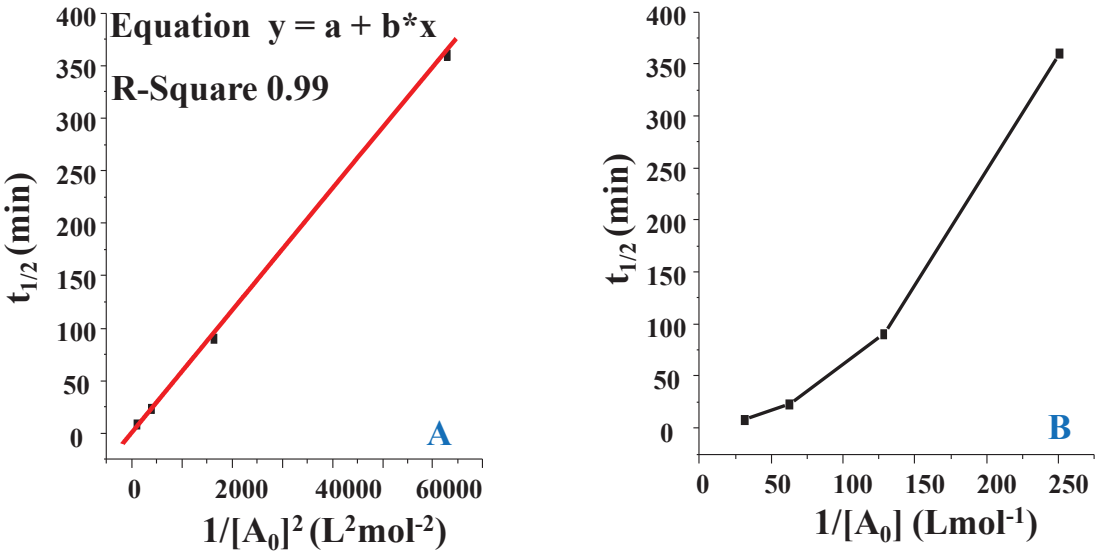

Figure A9: The plots of (A) $t_{1/2}$ versus $1/[A_o]^2$ (third order model), and (B) $t_{1/2}$ versus $1/[A_o]$ (second order model) for the Michael addition between TPMD and HCH carried out at 25 °C.

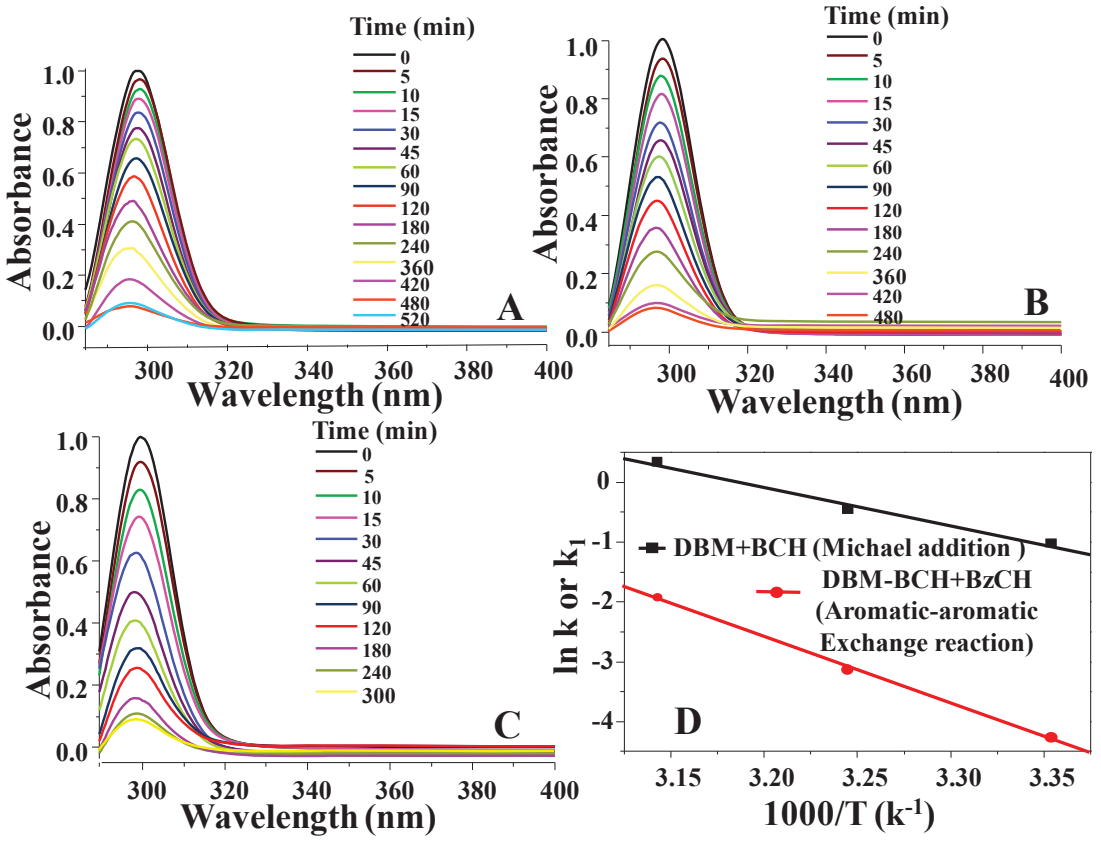

Figure A10: UV-Vis Spectra showing the progress of reaction between DBM and BCH at (A) 25 °C, (B) 35 °C and (C) 45 °C, (D) The Arrhenius plots of the hydrazide Michael addition

between DBM and BCH and trans-Michael (exchange) additions of DBM-BCH with BzCH. For Michael addition; Initial concentration: [DBM]=0.0159 mol/L, [BCH]= 0.0159 mol/L

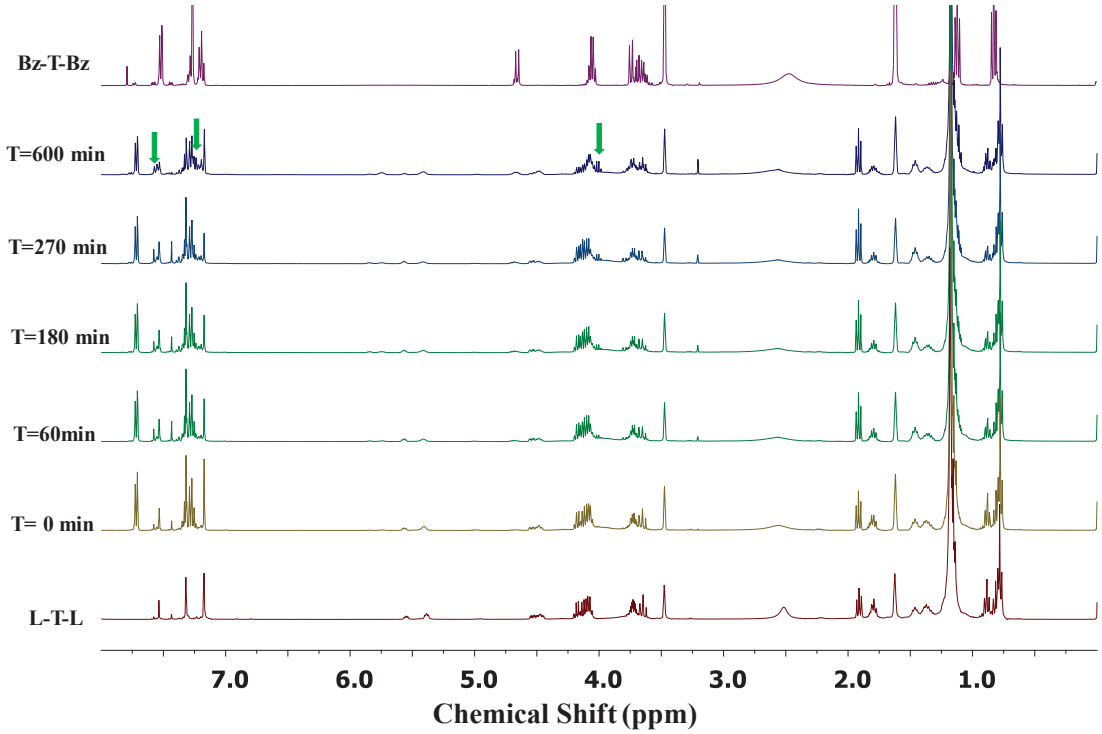

Figure A11: ^{1}H NMR spectra of L-T-L and BzCH in 1:4 molar ratio recorded after different time intervals in THF-D_8 solvent at 25 °C. The peaks marked with "*" is assigned to the solvent. The green arrows support the formation of exchanged adduct (Bz-T-).

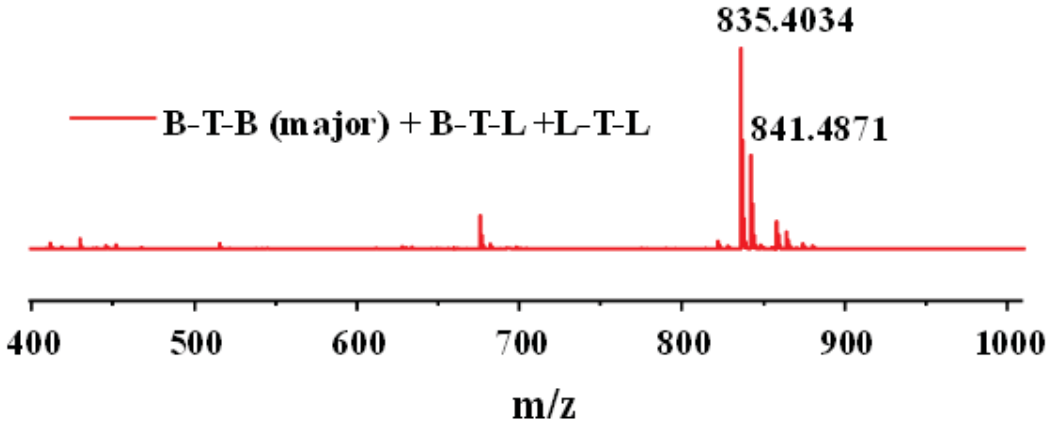

Figure A12: HRMS trace of the products formed after exchange of LCH with BCH in L-T-L, i.e. the products obtained on treatment of BCH with L-T-L at 25 °C.

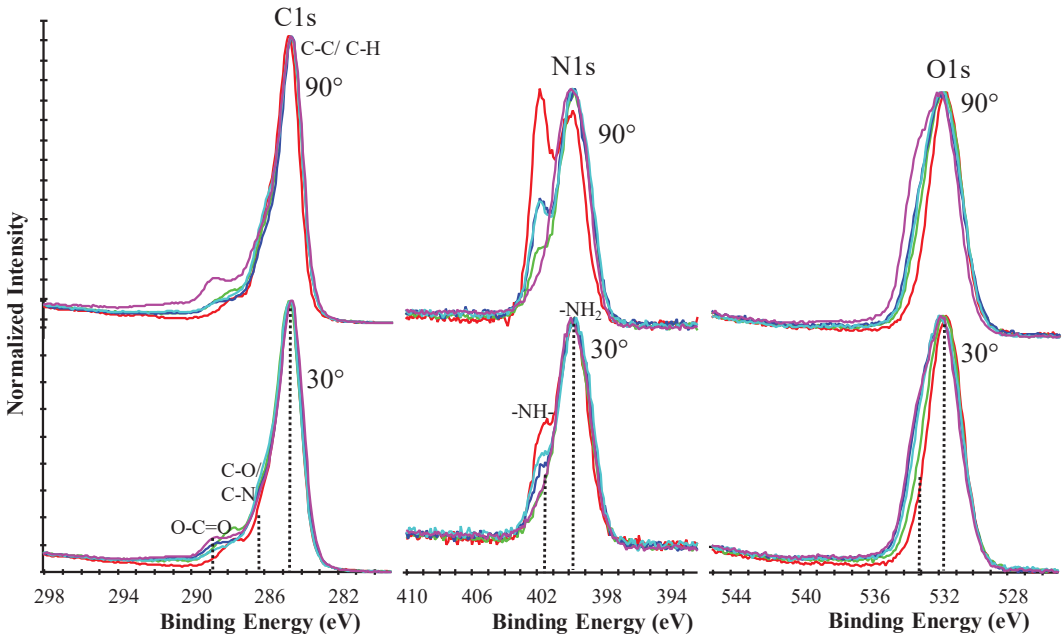

Figure A13: XPS traces showing the effect of crosslinking conditions on the surface atomic ratios; PAHz (red), PAHTD-1 (blue), PAHTD-3 (green) and PAHTD-4 (pink). The data were recorded at 90° and 30° incident angle.

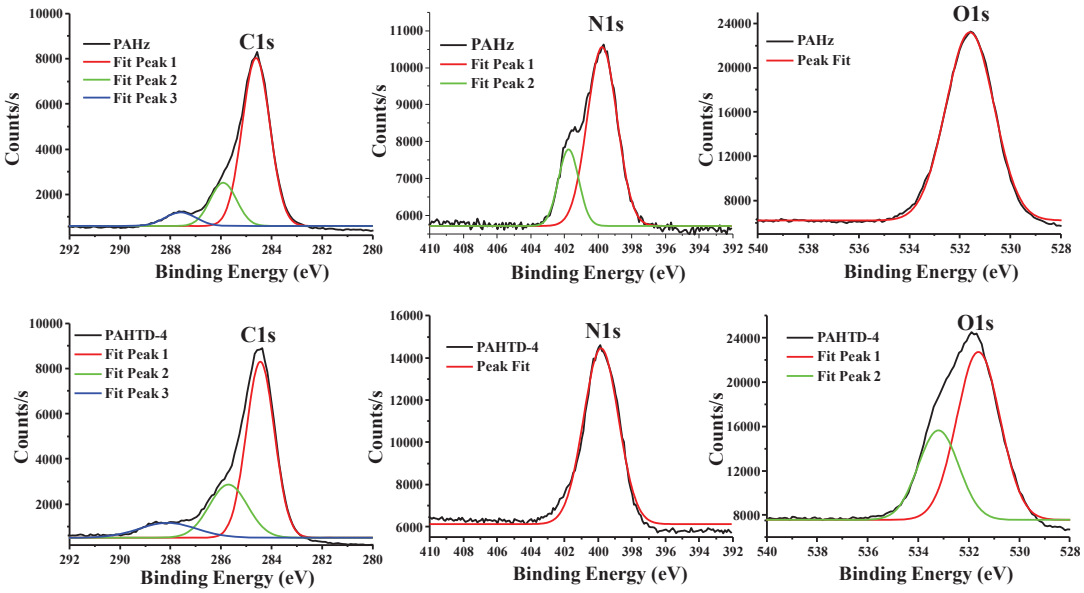

Figure A14: The C1s, N1s and O1s XPS spectra of PAHz and PAHTD-4 films recorded at 30° incident angle.

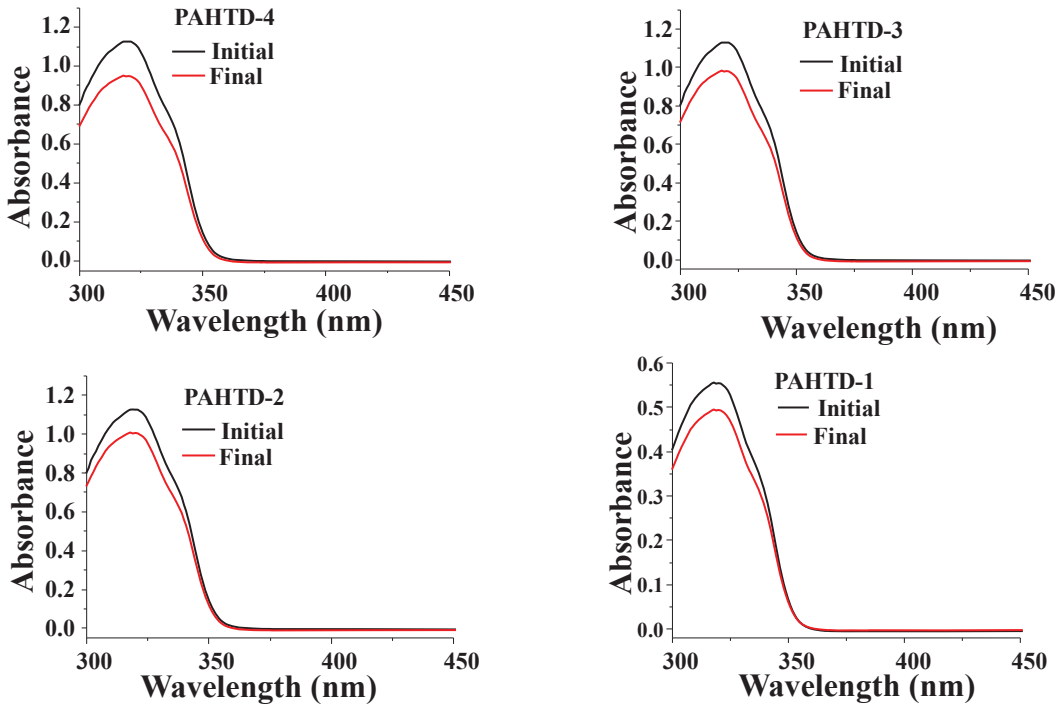

Figure A15: UV-Vis spectroscopic plots for determination of amount of cross-linker in PAHTD films. The black and red spectra in each figure represents the TPMD solution before and after crosslinking.

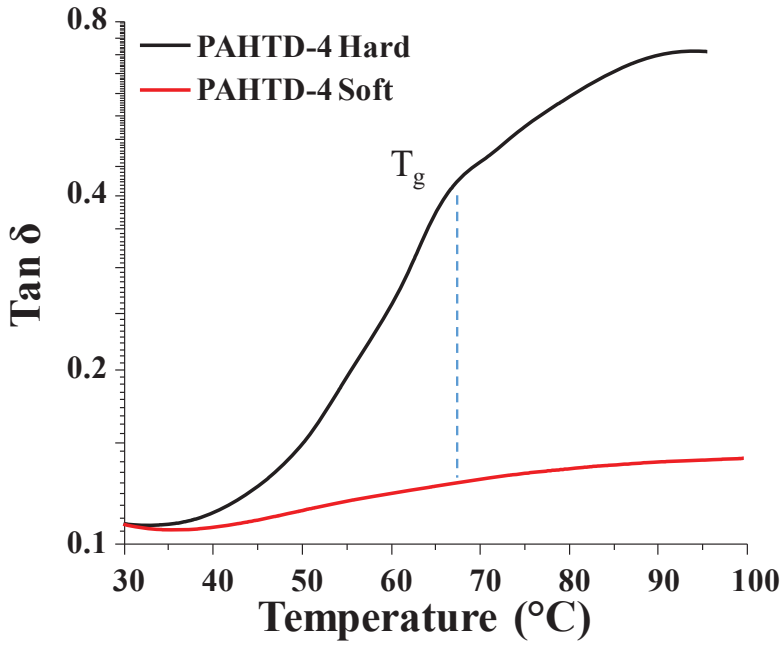

Figure A16: Tan δ versus temperature plot of hard & soft film of PAHTD-4.

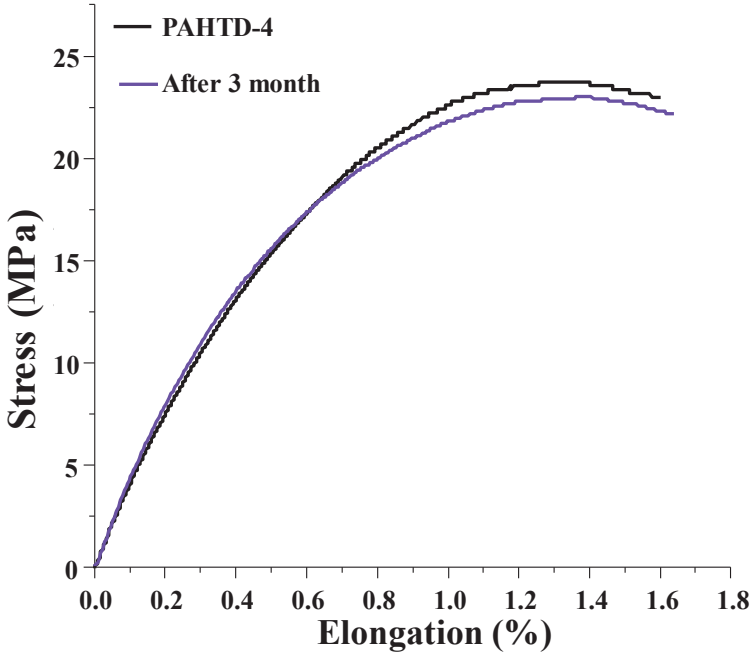

Figure A17: Tensile properties of freshly prepared PAHTD-4 and the sample after 3 months of storage under ambient condition.

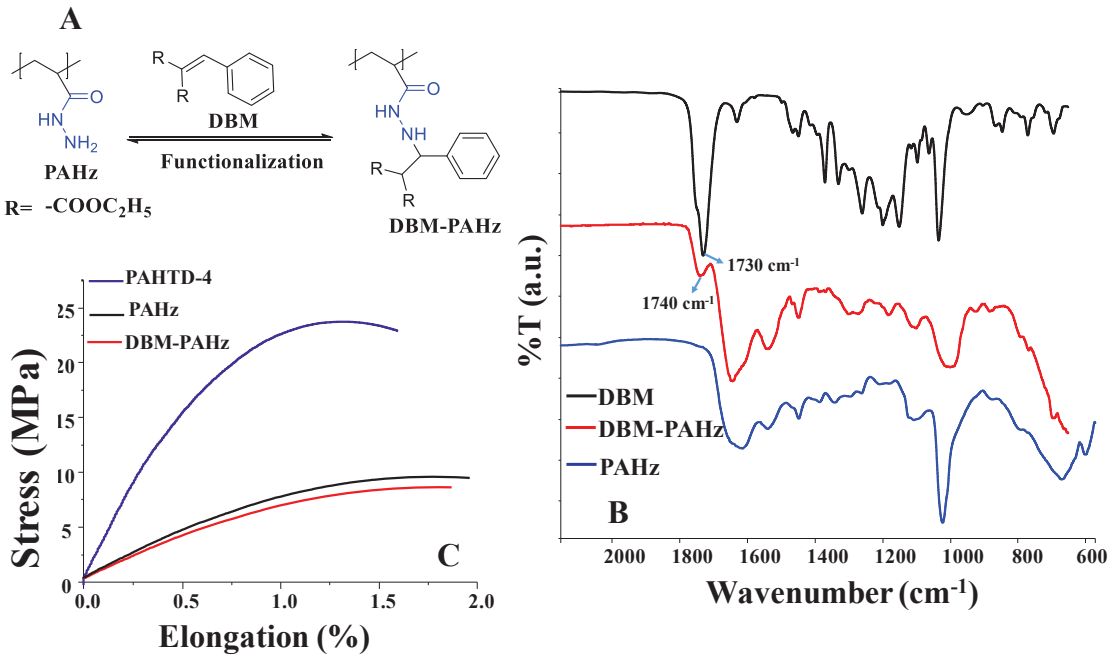

Figure A18: (A) Functionalization of PAHz with DBM, (B) ATR FTIR spectra of DBM, PAHz-DBM and PAHz (C) The tensile properties of PAHz, PAHz-DBM and PAHTD-4.

Table A1: Half-life, activation energy (E_a) data of hydrazide Michael addition and exchange reactions for mono and bi-functional systems.

Reaction	Monofunctional double bond (DBM)		Bifunctional double bond (TPMD)	
	Half-life at 25 °C (min)	E_a (kJ/mol)	Half-life at 25 °C (min)	E_a (kJ/mol)
Michael addition	DBM + BCH*		TPMD + BCH#	
	175	53.4	120	45.2
Exchange Reaction	DBM-BCH + BzCH		B-T-B + BzCH	
	355	91.4	370	93.3

*E_a value was calculated following 2nd order kinetics and #E_a value was calculated following 3rd order kinetics.

Table A2: The atom% data of different elements present on the surfaces of PAHz, PAHTD-1 and PAHTD-4 networks obtained from the XPS traces recorded at 90° and 30° incident angle.

Name		Atomic %		
		90° incident angle		
		PAHz	PAHTD-1	PAHTD-4
C1s		77.3	73.5	70.4
N1s	A	4.9	8.0	9.0
	B	3.1	1.2	2.4
O1s		12.9	15.8	17.3
Si2p		1.8	1.5	0.9
		30° incident angle		
C1s		73.4	69.3	72.2
N1s	A	6.1	10.1	10.2
	B	1.9	0.8	0.6
O1s		16.0	17.8	15.5
Si2p		2.6	2.0	1.5

* the atom% of the N1s peaks at 400.0 and 402.0 eV are assigned as A and B respectively. The atom% values were obtained from the Avantage XPS software.

Calculation, Experimental Section, DFT raw data and Tables:

Activation energy calculation for 3rd order type reaction:

$$A+2B \rightarrow C$$

The activation energy was calculated at three different temperatures (298.15, 308.15, and 318.15 °K). The expression for half-life ($t_{1/2}$) is as followed.

By following the 3rd order reaction kinetics;

$$t_{1/2} = \frac{3}{2K[A_0]^2} \ldots\ldots\ldots (\text{Eq. S1})$$

Where *K*= rate constant of the reaction

$[A_0]$ = initial concentration of the reactant.

The rate constant was obtained by using above equation and the activation energy was obtained.

We know from the Arrhenius Equation

$$K = A\, e^{-Ea/RT} \ldots\ldots\ldots\ldots\ldots\ldots (\text{Eq S2})$$

Where E_a is activation energy of the reaction,

R = Gas constant in J / mol. °K

T = temperature in °K

A = Arrhenius constant

Slope = E_a/R provides the activation energy

Rate of the exchange of donors in hydrazide Michael adduct

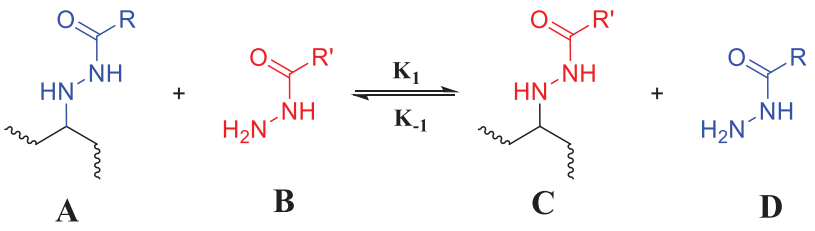

The rate equation for the above pseudo second order reversible reaction may be expressed as follows;

$$\frac{d[C]}{dt} = -\frac{d[A]}{dt} = K_1\,[A][B] - K_{-1}[C][D] \quad \text{(Eq. S3)}$$

If, E_0 is initial concentration of A and B and χ is the fractional conversion of A and B after time t; then

$$[C] = [D] = \chi E_0 \text{ and } [A] = [B] = (1-\chi)E_0$$

Using the above in Eq. S3;

$$\frac{1}{E_0}.\ \frac{d\chi}{dt} = K_1\,(1-\chi)^2 - K_{-1}\,\chi^2 \quad \text{(Eq. S4)}$$

The integrated form of the above equation (Levenspiel) is

$$\ln\left[\frac{\chi_\epsilon - (2\chi_\epsilon - 1)\chi}{\chi_\epsilon - \chi}\right] = 2K_1\left(\frac{1}{\chi_\epsilon} - 1\right) E_0 t \quad \text{(Eq. S5)}$$

Where χ_ϵ is the fractional conversion at equilibrium

The rate constant (K_1) was obtained by using above equation and the activation energy was calculated.

Standard free energy of formation (Δ G°) calculation for hydrazide Michael addition.

$$A + 2B \rightarrow C$$

The Standard free energy was calculated by using below expression.

$$\Delta G° = -2.303RT\ logK_{eq} \quad \text{(Eq S6)}$$

Where, R is gas constant in J/mol. °K, T is the temperature in °K.

The expression for K_{eq} is

$$K_{eq} = \frac{[C]}{[A][B]^2} \text{..... (Eq S7)}$$

By putting K_{eq} in above equation ΔG^0 was calculated.

Calculation of Δ G° value for reversible exchange reactions

$$\mathbf{A + B} \rightleftharpoons \mathbf{C + D}$$

The Standard free energy was calculated by using below expression.

$$\Delta G° = -2.303RT\ log K_{eq}$$

Where, R is gas constant in J/mol. K, T is the temperature in Kelvin.

The expression for K_{eq} is

$$K_{eq} = \frac{[C][D]}{[A][B]} \text{..... (Eq S8)}$$

By putting K_{eq} in above equation $\Delta \mathbf{G^0}$ was calculated.

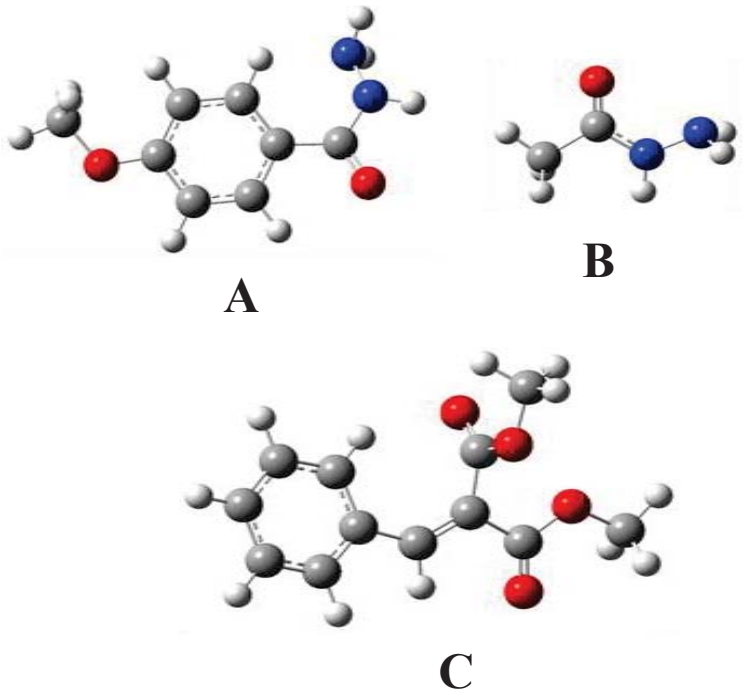

Figure A19: Optimized Structures of (A) BCH fragment, (B) ACH, and (C) TPMD fragment obtained using Gaussian 09.

Table A3: Cartesian coordinates of the optimized geometries for (BCH):

Charge = 0, Multiplicity = 1

Atom	X	Y	Z
C	0.570602	-0.605384	-0.29032
C	1.958742	-0.69805	-0.08061
C	2.76287	0.428766	-0.16399
C	2.201736	1.682748	-0.45053
C	0.821692	1.791083	-0.66713
C	0.028024	0.649402	-0.59548
H	2.405842	-1.65421	0.153359
H	3.835251	0.365985	-0.01165
H	0.36379	2.745683	-0.89651
H	-1.0379	0.712425	-0.7849
O	3.07754	2.724979	-0.49885
C	2.57164	4.018339	-0.79624
H	3.43332	4.687143	-0.78707
H	2.100054	4.049979	-1.78627
H	1.847253	4.352371	-0.04289
C	-0.38802	-1.75178	-0.29961
O	-1.47835	-1.67169	-0.86141
N	-0.05826	-2.96282	0.289897
H	-0.85035	-3.60029	0.263088
N	0.889038	-3.10046	1.319489
H	0.429161	-3.14922	2.227342
H	1.410012	-3.96103	1.175937

Table A4: Cartesian coordinates of the optimized geometries for ACH:

Charge = 0, Multiplicity = 1

Atom	X	Y	Z
C	-4.3052	5.382285	-0.11788
O	-3.17764	5.348354	-0.54575

O	-4.9484	6.504326	0.307205
C	-5.24204	4.197379	-0.01062
H	-5.78212	4.205653	0.939068
H	-5.98242	4.245288	-0.8157
H	-4.66409	3.278909	-0.11212
N	-4.06842	7.703347	0.236066
H	-4.63116	8.299676	0.841618
N	-4.10404	8.194403	-1.06552
H	-4.67362	9.022809	-1.19514
H	-3.15777	8.310873	-1.40395

Table A5: Cartesian coordinates of the optimized geometries for TPMD:

Charge = 0, Multiplicity = 1

Atom	**X**	**Y**	**Z**
C	-1.5277	0.15112	1.07071
C	-0.1585	-0.0271	1.26262
C	0.75874	0.35692	0.26242
C	0.25448	0.94767	-0.915
C	-1.1155	1.11491	-1.1078
C	-2.013	0.71393	-0.1142
H	-2.2191	-0.1407	1.85585
H	0.19798	-0.4289	2.20311
H	0.95031	1.26659	-1.6864
H	-1.4813	1.56316	-2.0268
H	-3.0812	0.85008	-0.2561
C	2.21211	0.20853	0.3668
H	2.78651	0.82486	-0.3233
C	2.97209	-0.5917	1.14667
C	4.45216	-0.5021	0.99176
O	5.03439	0.22284	0.2043
O	5.08752	-1.3256	1.85261

C	2.45395	-1.5781	2.15571
O	2.12362	-1.3044	3.29243
O	2.40433	-2.8197	1.63929
C	1.97895	-3.8626	2.54076
H	2.02249	-4.7818	1.95782
H	2.65126	-3.9143	3.40026
H	0.96074	-3.6727	2.88814
C	6.52624	-1.3082	1.79852
H	6.85212	-2.0171	2.55885
H	6.87223	-1.6145	0.80849
H	6.90152	-0.3058	2.01756

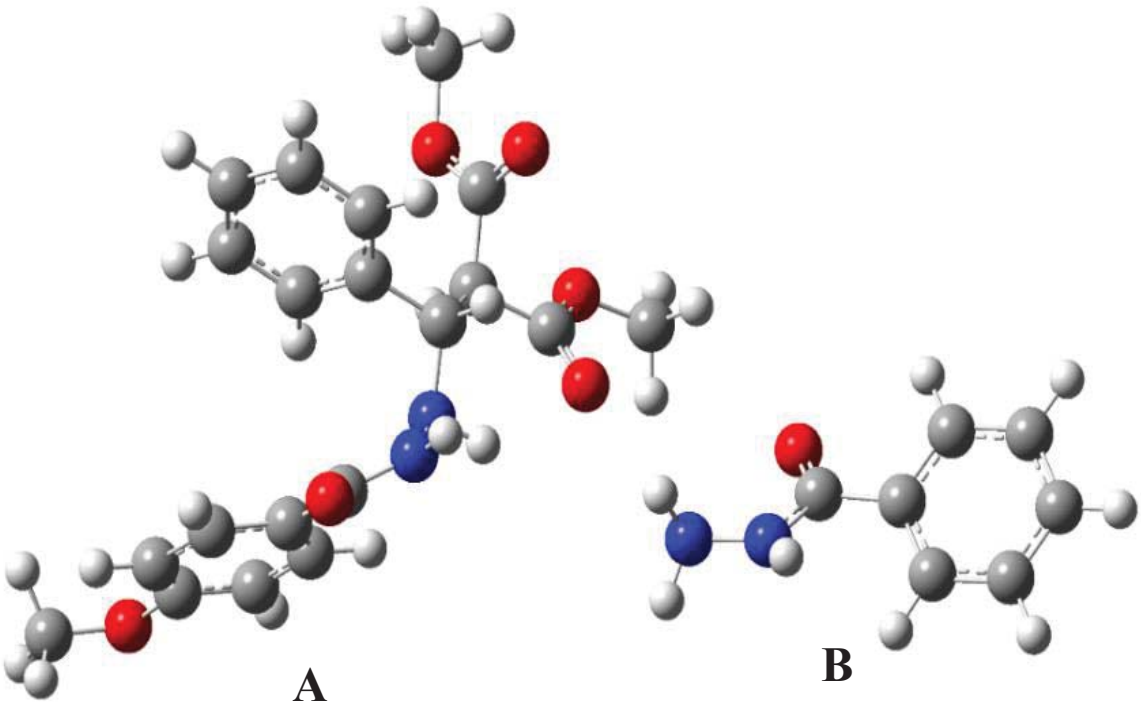

Figure A20: Optimized Structures of A (-B-T) and B (BzCH) mixture obtained using Gaussian 09.

Table A6: Cartesian coordinates of the optimized geometries for A (~B-T) and B (BzCH) mixture:

Charge = 0, Multiplicity = 1

Atom	X	Y	Z
C	-5.49458	2.337975	2.170112
C	-4.173	1.918624	1.992892
C	-3.81248	1.142678	0.884338
C	-4.80035	0.78637	-0.04492
C	-6.12043	1.203926	0.130221
C	-6.47138	1.982633	1.237609
H	-5.75877	2.935276	3.037998
H	-3.41537	2.200529	2.719187
H	-4.53757	0.163565	-0.89427
H	-6.8761	0.914827	-0.59449
H	-7.5001	2.303173	1.375222
C	-2.36328	0.72135	0.685258
H	-1.79802	0.981521	1.594363
C	-1.7131	1.498104	-0.49521
H	-2.22893	1.235574	-1.42463
N	-2.25876	-0.7273	0.39818
H	-1.2774	-0.9298	0.22059
N	-2.65293	-1.5174	1.49469
H	-2.316	-1.25517	2.419831
C	-3.77467	-2.31859	1.547672
O	-4.18968	-2.68135	2.647866
C	-1.85548	3.004276	-0.26901
O	-1.37984	3.588221	0.682977
O	-2.57026	3.589998	-1.2405
C	-0.22538	1.181713	-0.69754
O	0.381728	0.293639	-0.11707
O	0.310906	1.987489	-1.60751
C	-2.7676	5.01418	-1.10645
H	-1.80401	5.528436	-1.10334
H	-3.35969	5.304104	-1.97333

H	-3.30207	5.233678	-0.17981
C	1.730177	1.826104	-1.89798
H	1.942248	2.563743	-2.66932
H	2.312458	2.030768	-0.99885
H	1.946295	0.817732	-2.24831
C	-4.42593	-2.79078	0.280776
C	-3.73143	-3.02973	-0.91425
C	-5.79525	-3.09072	0.349283
C	-4.40119	-3.54994	-2.02418
H	-2.67131	-2.81926	-0.97755
C	-6.46644	-3.59113	-0.76581
H	-6.31528	-2.92991	1.287606
C	-5.77028	-3.82233	-1.95663
H	-3.85225	-3.74345	-2.94142
H	-7.52868	-3.80955	-0.70394
C	8.165114	0.560969	0.322651
C	8.686699	-0.6408	0.823517
C	7.947069	-1.82767	0.695175
C	6.69821	-1.80705	0.087229
C	6.155325	-0.60702	-0.40931
C	6.912154	0.563951	-0.29144
H	8.719983	1.488072	0.401961
H	8.377065	-2.75185	1.066975
H	6.162657	-2.74417	-0.03314
H	6.505743	1.485255	-0.69552
C	4.82131	-0.51507	-1.09038
O	4.558339	0.376287	-1.89178
N	3.927803	-1.50519	-0.73694
H	4.079815	-1.97835	0.146102
N	2.642128	-1.52612	-1.29748
H	2.383369	-2.48317	-1.51119
H	1.955359	-1.08817	-0.68534

O	9.896662	-0.76146	1.438293
C	10.70921	0.399103	1.586145
H	10.20994	1.159498	2.198889
H	11.61474	0.063053	2.092127
H	10.97314	0.827103	0.611483
H	-6.28979	-4.22044	-2.82379

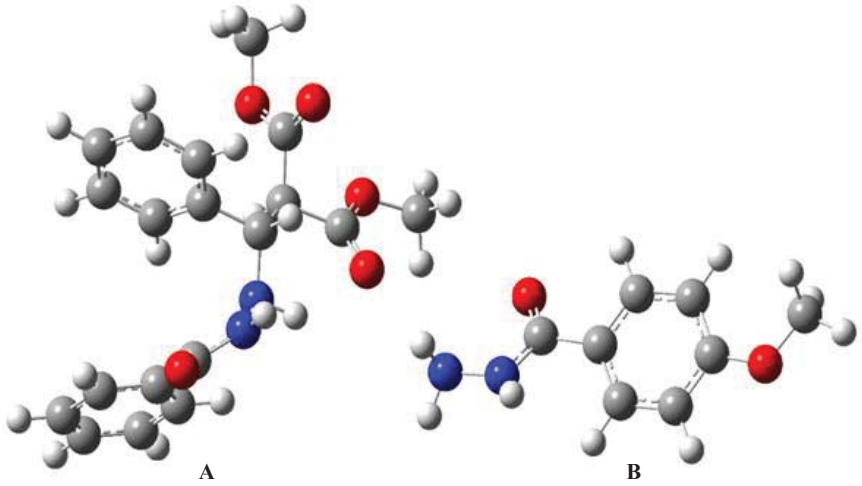

Figure A21: Optimized Structures of A (~Bz-T) and B (BCH) mixture obtained using Gaussian 09.

Table A7: Cartesian coordinates of the optimized geometries for of A (~Bz-T) and B (BCH) mixture:

Charge = 0, Multiplicity = 1

Atom	X	Y	Z
C	-0.000004131	0.000002	0.000004561
C	0.000004695	-0.000004586	0.000004452
C	-0.000000488	0.000001498	-0.000012284
C	-0.000008121	-0.000001524	0.000005195
C	0.000004829	-0.000001366	0.000003624
C	0.000000709	0.000003625	-0.000002237
H	0.000001301	0.000001878	0.000002031
H	-0.000000625	0.000002834	0.000002647

H	-0.000003189	-0.000000182	0.000000952
H	-0.000000559	0.000001114	0.000001284
H	0.00000018	0.000001077	0.000002708
C	0.000006728	-0.000000162	0.00001239
H	-0.000003523	0.000000029	-0.000003845
C	-0.000014684	-0.000007043	-0.000017869
H	0.000001135	0.0000033	0.000002033
N	-0.000004216	0.000016311	0.000023163
H	-0.000008075	-0.000004305	-0.000012124
N	0.000029357	0.000002543	-0.000013547
H	0.000005392	0.000002988	0.000006501
C	-0.00004106	-0.000005004	-0.000014638
O	0.000012627	-0.00000545	0.000021968
C	0.000022004	0.000029004	0.000016075
O	-0.000008818	-0.000008625	0.000006425
O	-0.000000196	-0.000010561	-0.000009256
C	0.000007335	-0.000028271	-0.000058795
O	-0.000039756	0.000001649	0.000039442
O	0.000011377	0.000009406	0.00003914
C	0.000000597	0.000001399	0.000004159
H	0.00000051	-0.000001601	0.000003141
H	0.000000691	-0.00000168	0.000002784
H	0.000000337	-0.000000217	0.000003174
C	0.000012268	-0.000007686	-0.000071593
H	0.000004273	-0.000003579	0.000001261
H	0.000000379	-0.000001965	0.000000852
H	0.000018318	0.000028625	0.000079841
C	0.000015586	0.000007	0.000011181
C	0.000016223	0.0000233	-0.000054847
C	-0.000027111	-0.000020308	0.000027298
C	-0.000022525	-0.000013296	0.00001484
H	0.0000038	-0.000003845	0.00000615

C	0.000011833	0.000023485	-0.000038689
H	-0.000000669	0.000005323	-0.000003361
C	0.00000793	0.000002777	-0.000001135
H	-0.000000853	-0.000001126	-0.000001662
H	-0.000002103	-0.000002127	0.000003598
C	0.00004754	-0.000005722	-0.000014471
C	-0.000034505	-0.000004891	0.000007527
C	0.000019224	0.000010858	-0.000004045
C	0.000007683	-0.00000716	0.000009211
C	-0.000012293	-0.00000555	0.000013569
C	-0.000014216	-0.000005569	-0.000002258
H	-0.000013679	0.00000106	0.000003876
H	-0.000006049	-0.000004301	-0.000002812
H	-0.000005679	0.000000684	-0.000008759
H	0.000003096	-0.000001442	0.000004138
C	0.000012374	0.000054283	-0.000047157
O	-0.000029261	-0.000026931	0.000024884
N	-0.000005496	0.000016853	0.000020349
H	0.00001148	-0.000004005	-0.000003698
N	-0.000047385	-0.000063322	-0.000012305
H	0.000027864	-0.000011705	-0.000035705
H	0.000031745	0.000025598	0.000013139
O	-0.000000603	0.000013898	-0.000026162
C	-0.000009737	-0.000037987	0.000051625
H	-0.000019765	0.000030594	-0.000033588
H	0.000015521	-0.000015424	-0.000004651
H	0.000005401	0.000010812	0.000004102
H	0.000000651	-0.000007283	0.000008107

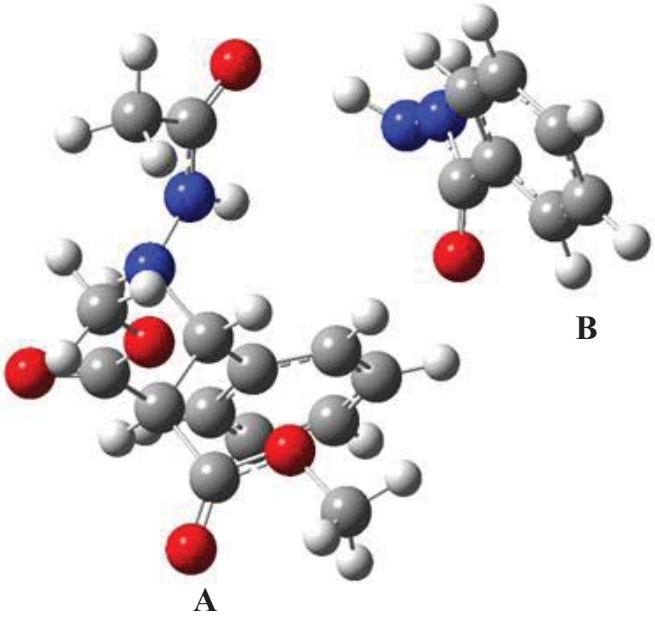

Figure A22: Optimized Structures of A (~L-T) and BzCH mixture obtained using Gaussian 09.

Table A8: Cartesian coordinates of the optimized geometries for of A (~L-T) and BzCH mixture:

Charge = 0, Multiplicity = 1

Atom	X	Y	Z
C	-1.58103	3.471504	-1.26961
C	-1.2651	2.198931	-0.78124
C	-2.27728	1.357928	-0.29628
C	-3.60492	1.818842	-0.30279
C	-3.91788	3.088315	-0.79141
C	-2.90351	3.91909	-1.27841
H	-0.78452	4.109458	-1.64155
H	-0.22832	1.870794	-0.77908
H	-4.40979	1.188113	0.068625
H	-4.95049	3.425476	-0.79567
H	-3.14546	4.906633	-1.66105
C	-1.91779	-0.00898	0.283718

H	-0.86538	-0.21177	0.076637
C	-2.76369	-1.15698	-0.32324
H	-3.83004	-0.9489	-0.21746
C	-2.55338	-2.47739	0.424798
O	-3.40662	-3.02138	1.091199
C	-2.53106	-1.35717	-1.82476
O	-3.37849	-1.80143	-2.5717
O	-1.29496	-1.00797	-2.20435
O	-1.31219	-2.96768	0.241334
C	-0.98313	-1.16435	-3.60346
H	-1.67261	-0.57315	-4.21013
H	0.037896	-0.8008	-3.70904
H	-1.05701	-2.21612	-3.88971
C	-1.03201	-4.22631	0.887784
H	-1.71576	-4.99702	0.5249
H	-0.00315	-4.4651	0.620628
H	-1.14078	-4.12934	1.970467
N	-2.06519	-0.07627	1.759877
H	-3.02019	0.150597	2.034938
N	-1.19174	0.7953	2.425687
H	-1.13073	1.765019	2.120287
C	-0.1892	0.347323	3.238648
O	0.659404	1.137665	3.666931
C	-0.18319	-1.12195	3.594362
H	-1.1576	-1.44704	3.967185
H	0.03585	-1.72098	2.705012
H	0.58761	-1.28483	4.347826
C	4.742602	-0.3978	0.539527
C	5.82018	-1.23156	0.229026
C	6.241622	-1.36818	-1.0958
C	5.572604	-0.67878	-2.11265
C	4.490233	0.145008	-1.80522

C	4.073657	0.303681	-0.47559
H	4.406591	-0.32954	1.570507
H	6.323216	-1.77918	1.020712
H	7.081387	-2.01393	-1.33581
H	5.893087	-0.78656	-3.14486
H	3.949919	0.673237	-2.58383
C	2.889149	1.201449	-0.21862
O	2.001358	1.343737	-1.05635
N	2.907829	1.837538	0.992837
H	3.720957	1.736152	1.586928
N	1.850048	2.656832	1.409727
H	1.495687	2.324643	2.309639
H	2.163619	3.621263	1.477869

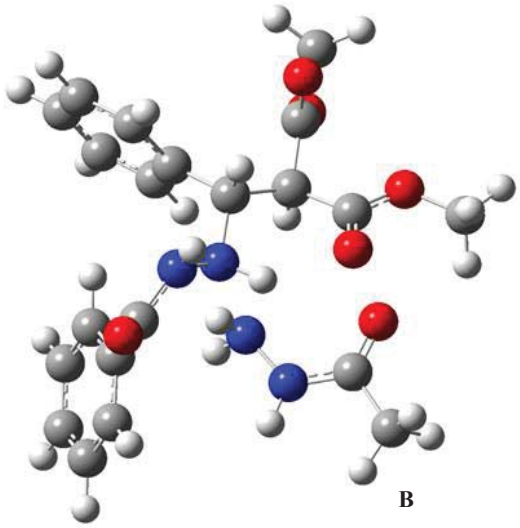

Figure A23: Optimized Structure of A (~Bz-T) and B (ACH) mixture obtained using Gaussian 09.

Table A9: Cartesian coordinates of the optimized geometries for of A (~Bz-T) and B (ACH) mixture:

Charge = 0, Multiplicity = 1

Atom	X	Y	Z
C	-4.16756	547129 0.	342273
C	-0.44947	-3.3272	0.963475
C	-0.48623	-2.13689	0.227323
C	-0.24296	-2.19297	-1.15384
C	0.030986	-3.41086	-1.77975
C	0.073252	-4.59221	-1.03257
H	-0.14016	-5.45881	0.931917
H	-0.64901	-3.30075	2.031177
H	-0.27167	-1.28379	-1.74711
H	0.208346	-3.43725	-2.85137
H	0.288059	-5.53914	-1.51941
C	-0.7774	-0.81751	0.930874
H	-1.15857	-1.05043	1.936625
C	-1.88318	0.002455	0.208204
H	-1.52674	0.349419	-0.76864
N	0.44978	0.016321	1.040353
H	0.138975	0.930146	1.378013
N	1.322038	-0.51517	2.024461
H	0.960915	-0.54738	2.977946
C	2.687946	-0.32085	2.005237
O	3.316321	-0.3303	3.062302
C	-3.12178	-0.87231	0.01561
O	-3.67634	-1.46511	0.918547
O	-3.51634	-0.90812	-1.26661
C	-2.28057	1.279635	0.956114
O	-1.59093	1.840602	1.791152
O	-3.46925	1.722905	0.54972
C	-4.6981	-1.68894	-1.53925
H	-5.54851	-1.29246	-0.97984
H	-4.86317	-1.59492	-2.61185
H	-4.53539	-2.73251	-1.26061

C	-3.8781	3.020816	1.035172
H	-4.89017	3.159535	0.657315
H	-3.86382	3.039061	2.126677
H	-3.20452	3.777196	0.628406
C	3.393031	-0.15082	0.691404
C	3.112299	-0.95142	-0.42427
C	4.44736	0.772429	0.632554
C	3.87577	-0.82305	-1.58704
H	2.313847	-1.68262	-0.3772
C	5.190301	0.91872	-0.54016
H	4.682988	1.357511	1.515846
C	4.907306	0.118826	-1.65246
H	3.668366	-1.46419	-2.43925
H	6.000525	1.641184	-0.58012
H	5.497092	0.218818	-2.55936
C	-0.12779	3.633744	-1.10245
O	-1.29738	3.276136	-1.18208
C	0.253199	5.044918	-0.68118
H	-0.0703	5.20129	0.352245
H	1.324325	5.256014	-0.75213
H	-0.29154	5.752313	-1.31159
N	0.942515	2.820595	-1.3724
H	1.873659	3.155479	-1.15426
N	0.770429	1.472552	-1.72209
H	1.32937	1.269275	-2.5451
H	1.055342	0.871565	-0.94652

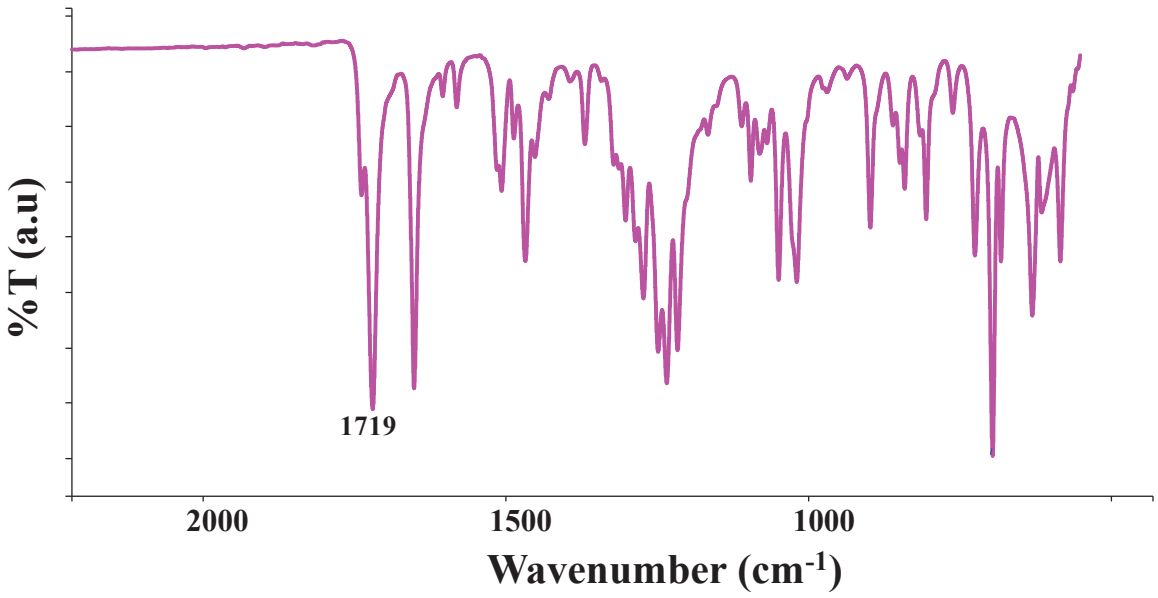

Figure A24: ATR FTIR spectrum of Bz-T-Bz

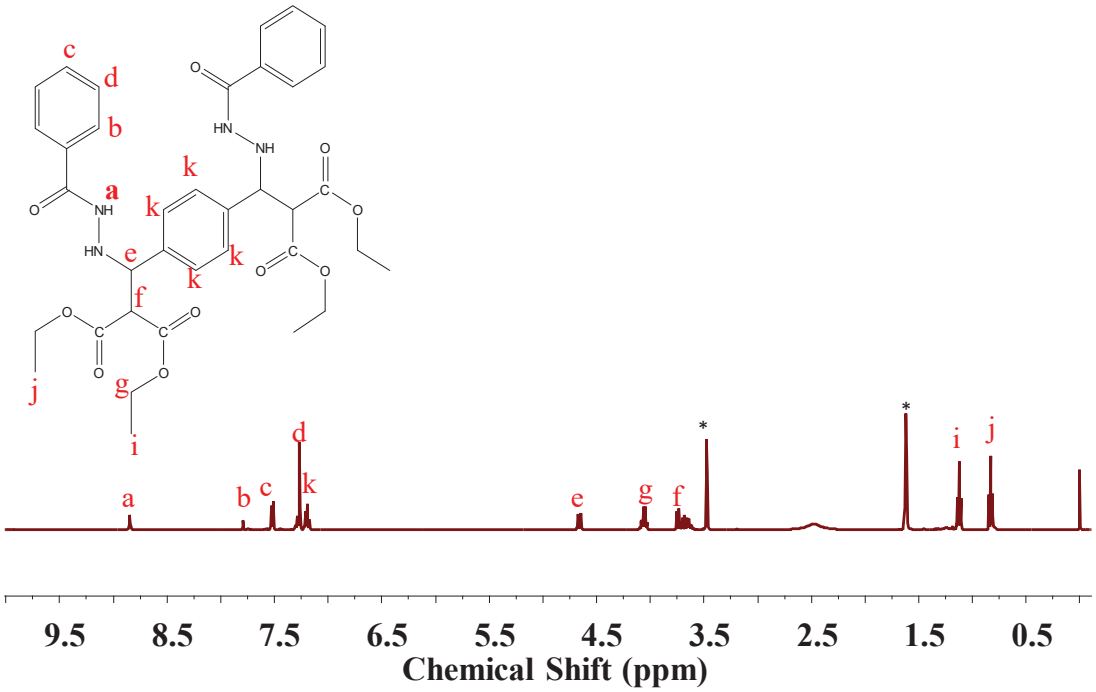

Figure A25: ^{1}H NMR spectrum of Bz-T-Bz recorded in THF-D_8

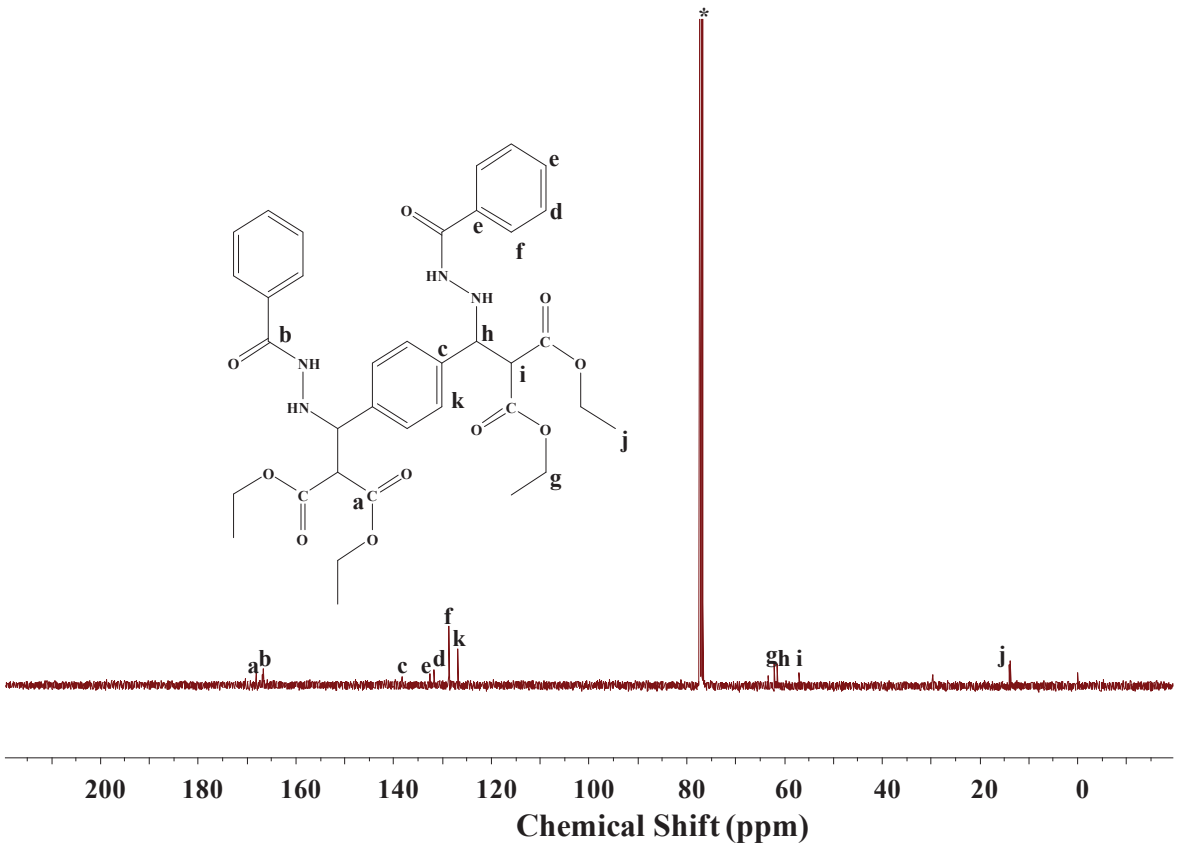

Figure A26: ^{13}C NMR spectrum of Bz-T-Bz recorded in $CDCl_3$

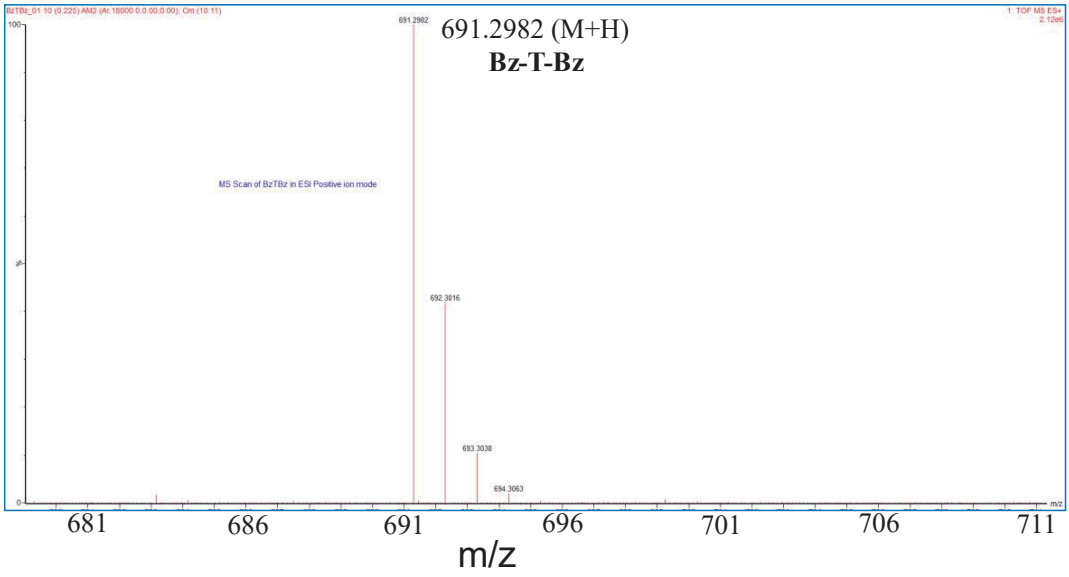

Figure A27: HRMS trace of Bz-T-Bz

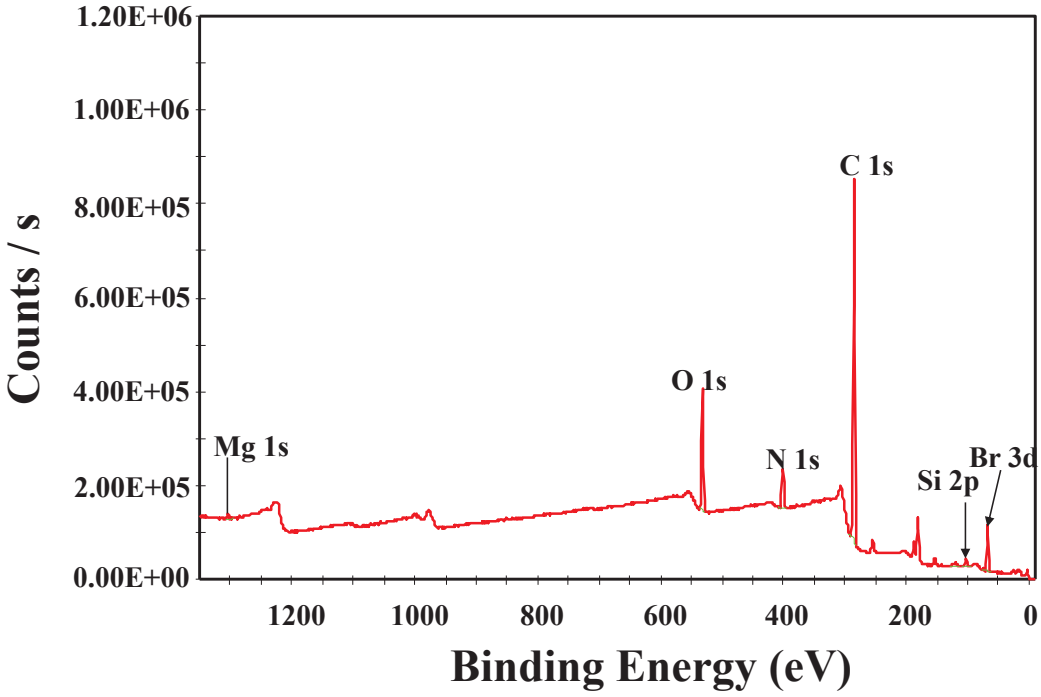

Figure A28: XPS survey spectrum of PAHz

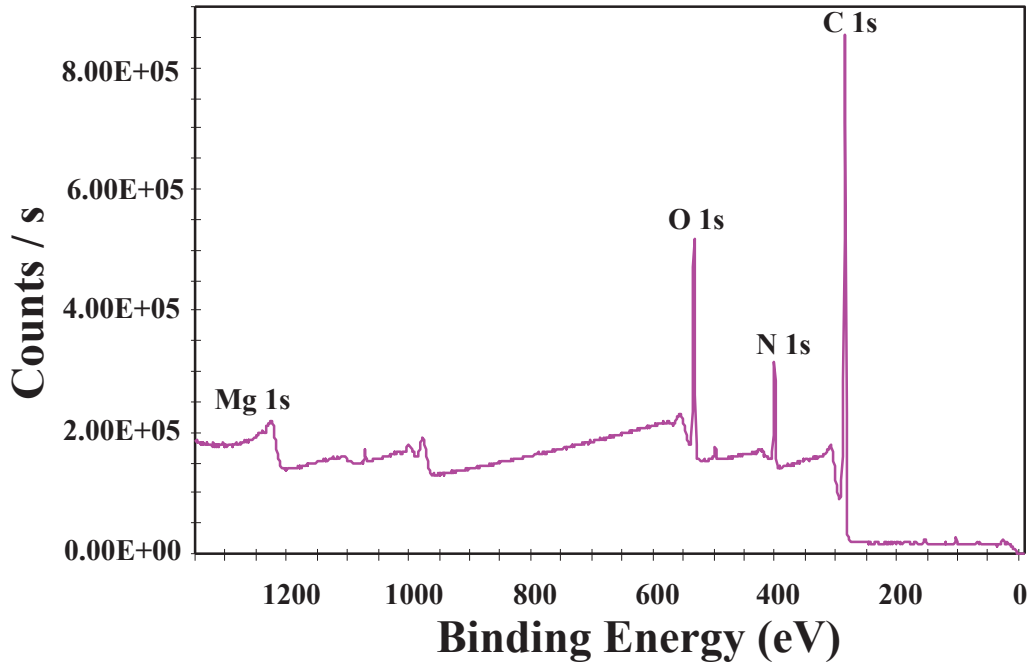

Figure A29: XPS survey spectrum of PAHTD-4

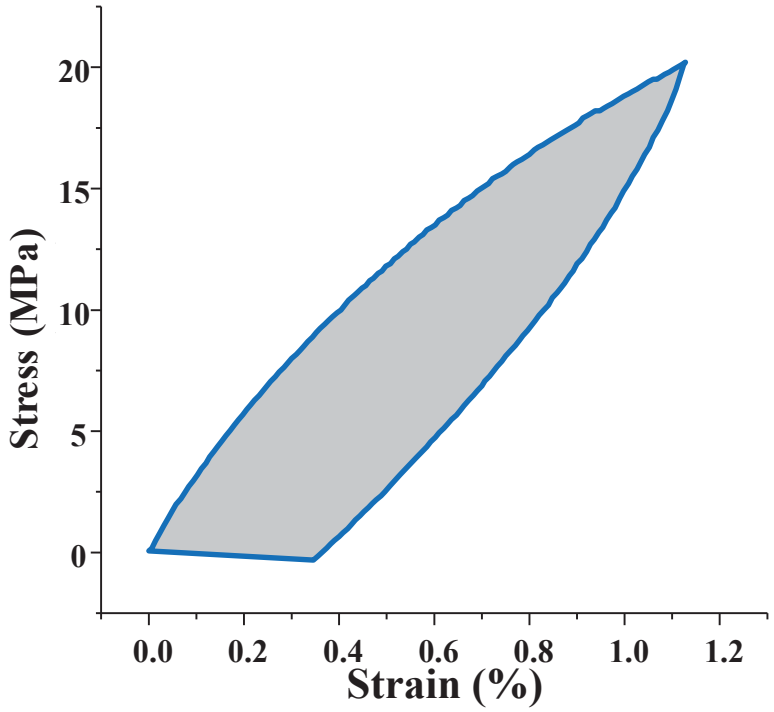

Figure A30: A typical stress versus stain cycle for PAHTD-4. Hysteresis calculation**:** the shaded area between the forward and release curves represented the hysteresis value of the sample.

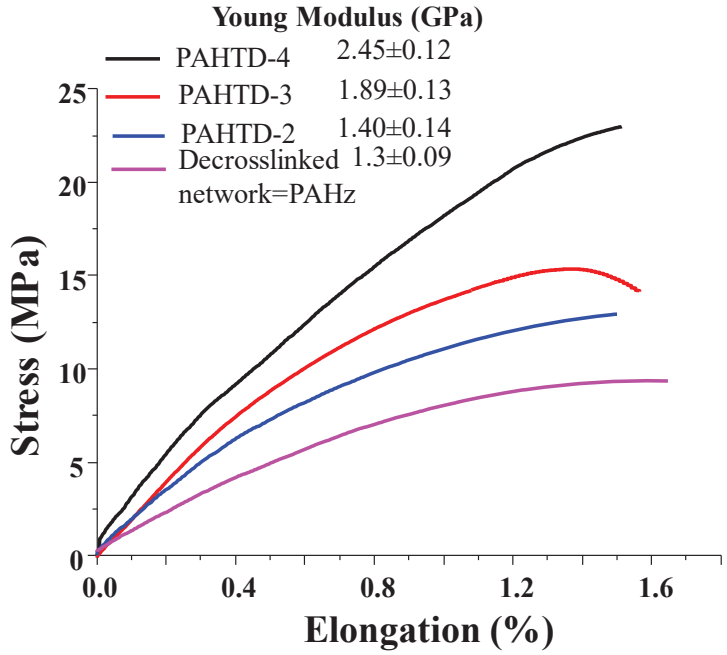

Figure A31: The de-crosslinked network (PAHz) was again crosslinked by dipping in TMPD solution (THF: H_2O). The tensile data of the reformed networks are presented.

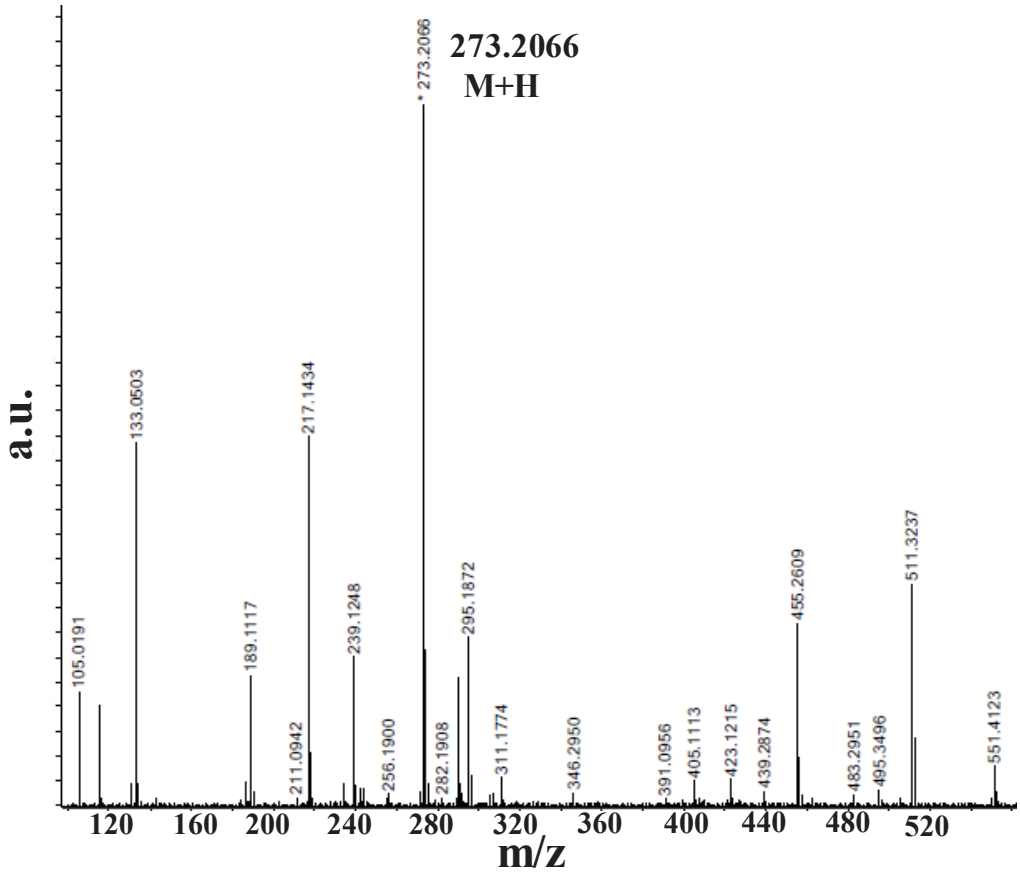

Figure A32: HRMS spectra of exchange reaction product of Diethylmalonate with n-hexanol

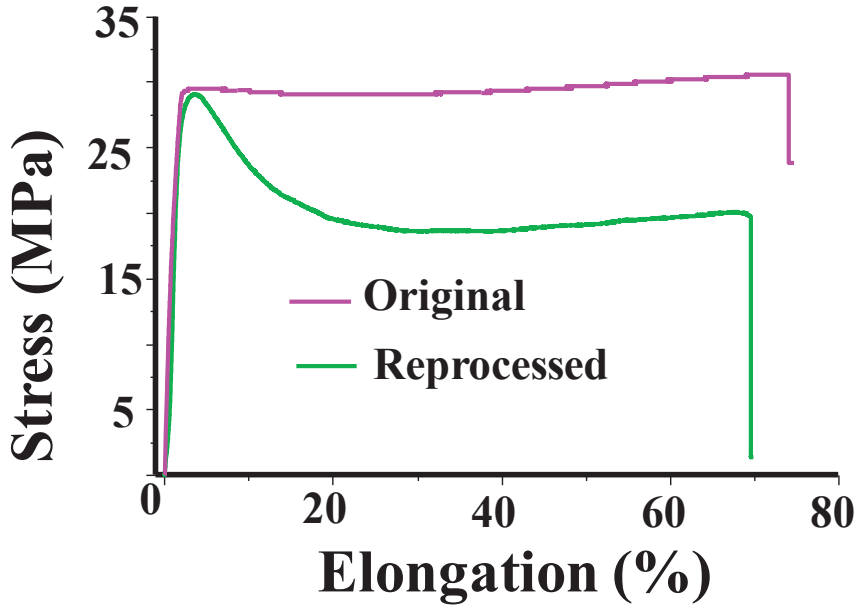

Figure A33: Tensile traces of original & reprocessed film of PHEMA-DEM-1.5C

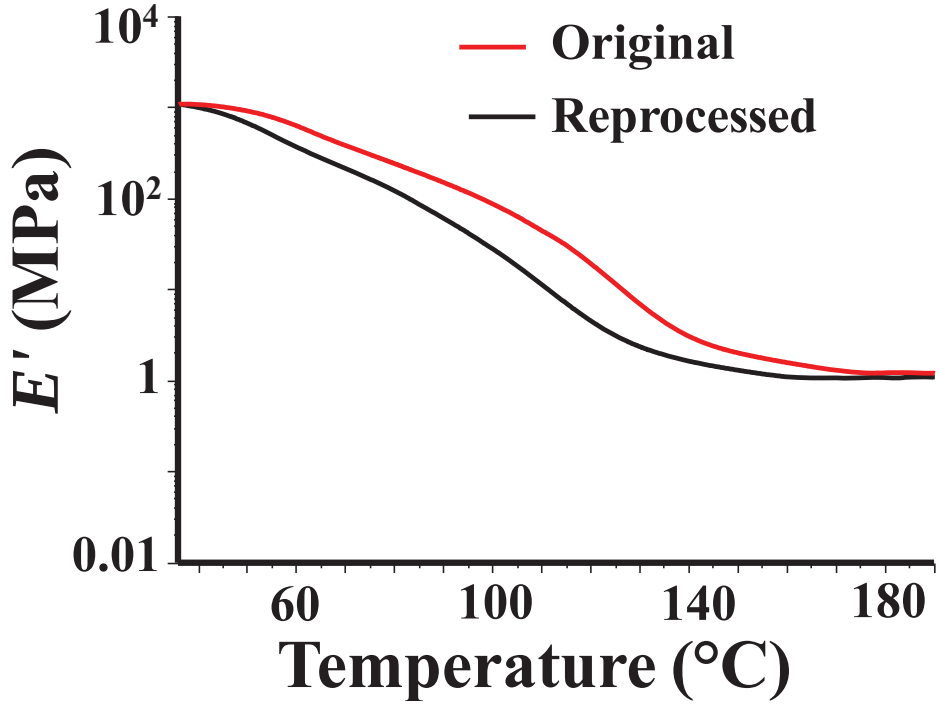

Figure A34: DMTA traces of original & reprocessed film of PHEMA-DEM-1.5C

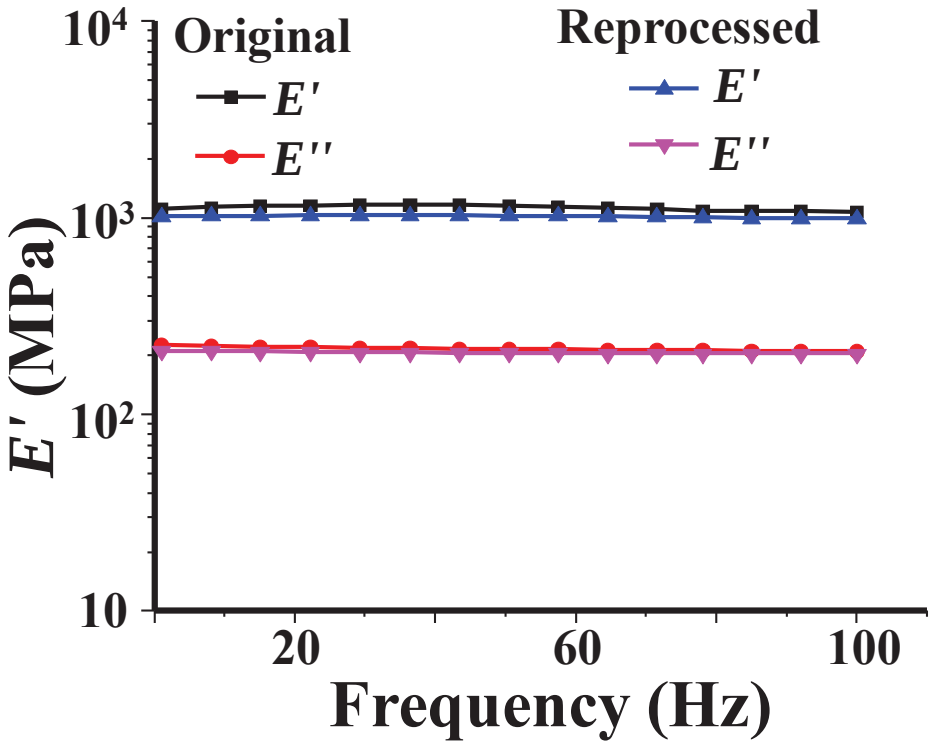

Figure A35: Frequency sweep data of original & reprocessed film of PHEMA-DEM-1.5C

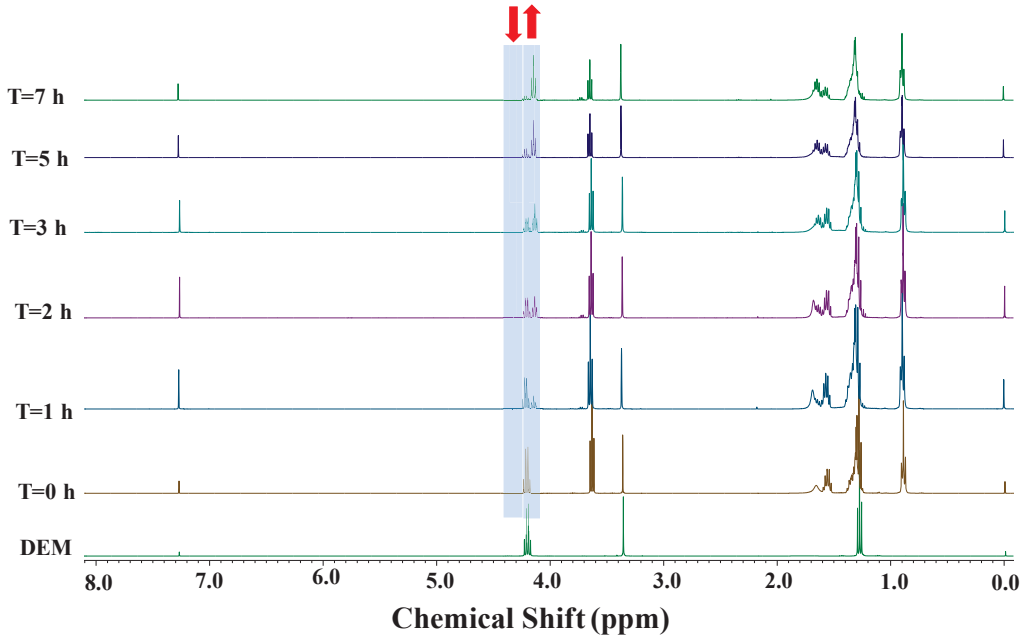

Figure 36: ^{1}H NMR spectra of Diethylmalonate & n-hexanol without catalyst at different time interval at 140 °C for kinetics study.

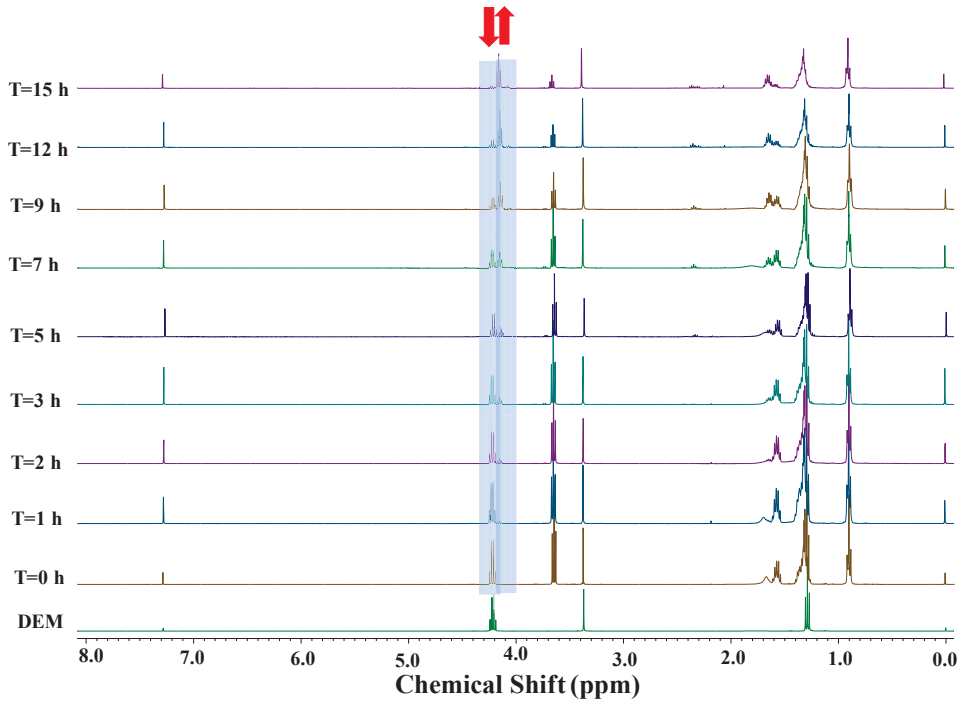

Figure 37: ^{1}H NMR spectra of Diethylmalonate & n-hexanol without catalyst at different time interval at 130 °C for kinetics study.

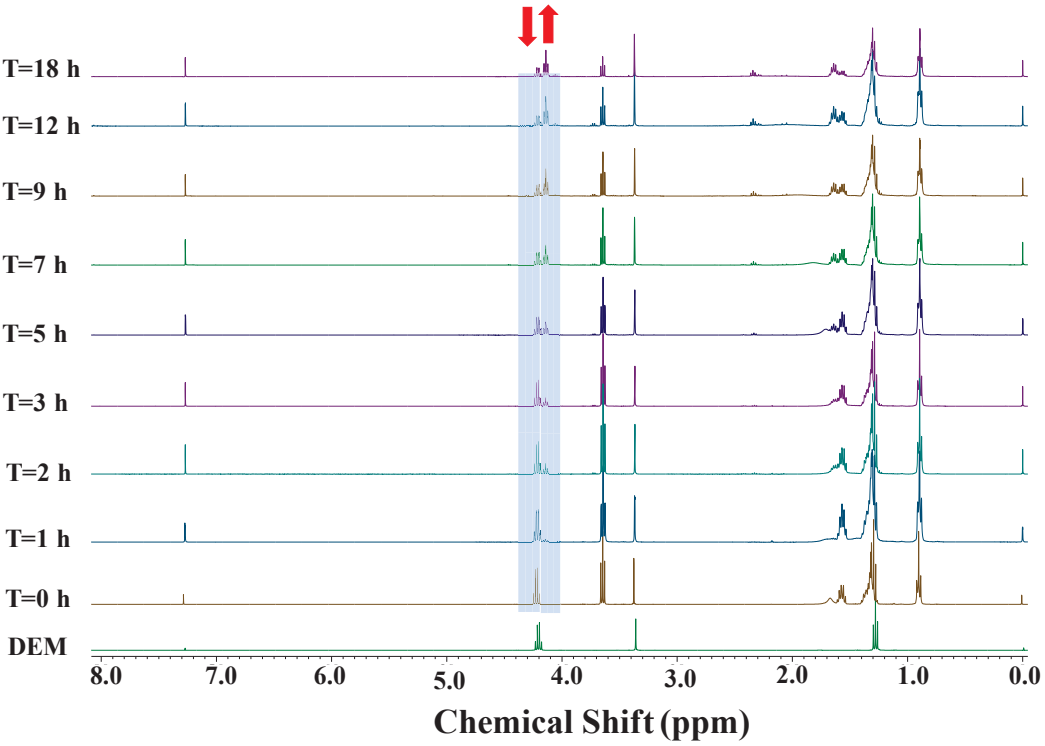

Figure A38: ^{1}H NMR spectra of Diethylmalonate & n-hexanol without catalyst at different time interval at 120 °C for kinetics study.

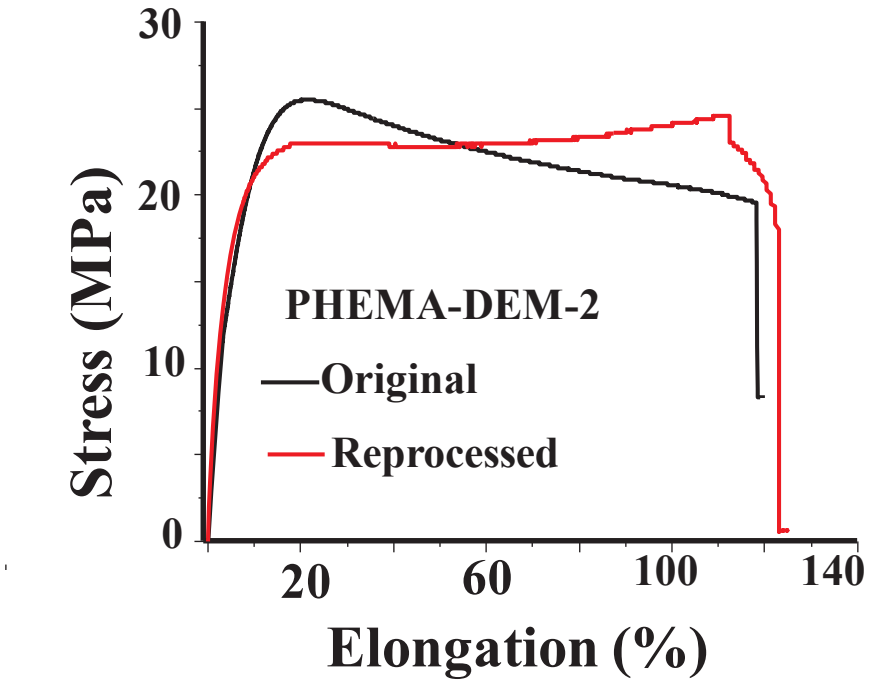

Figure A39: Tensile traces of original & reprocessed film of PHEMA-DEM-2

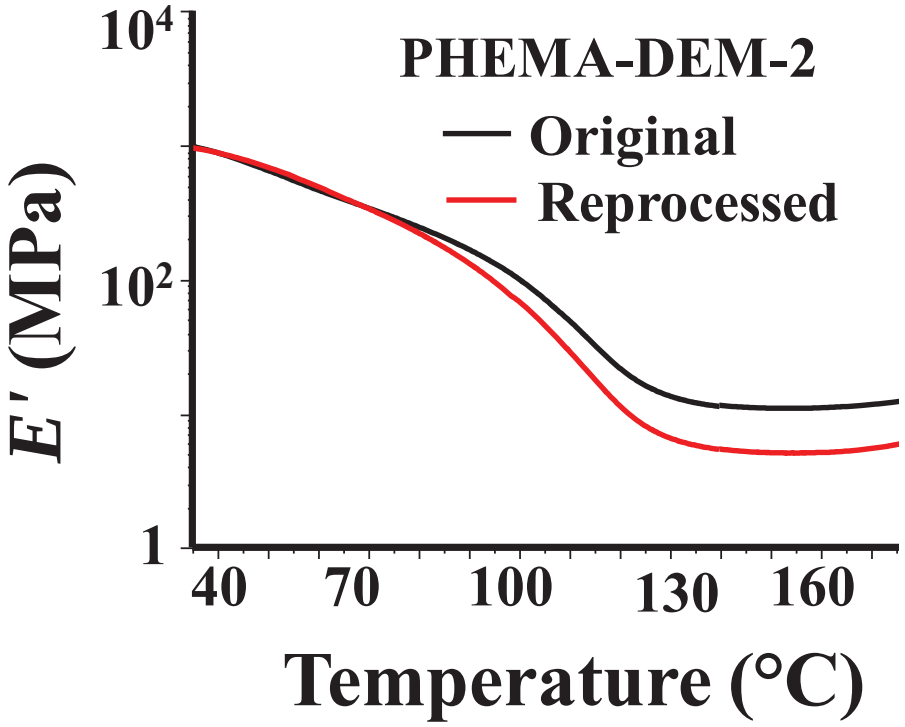

Figure A40: DMTA traces of original & reprocessed film of PHEMA-DEM-2

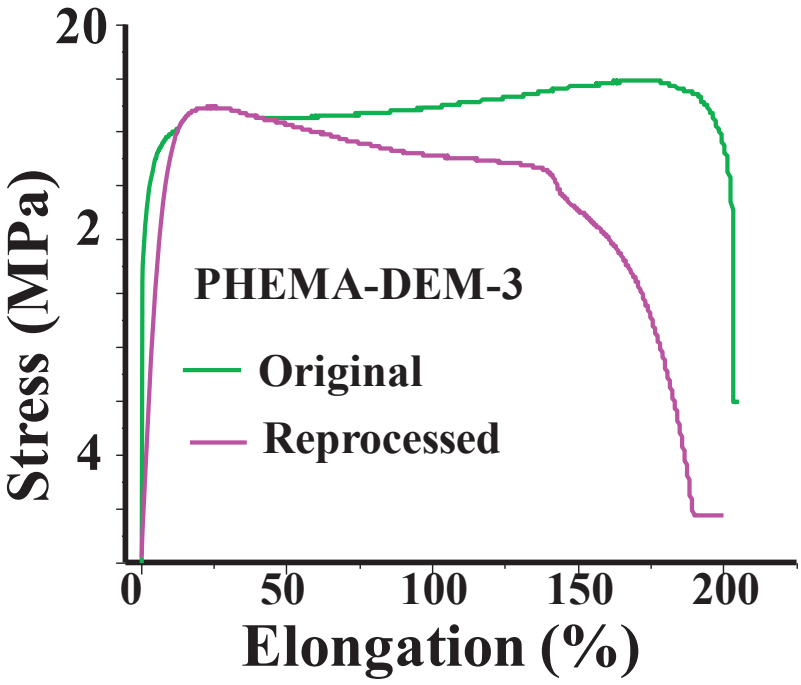

Figure A41: Tensile traces of original & reprocessed film of PHEMA-DEM-3

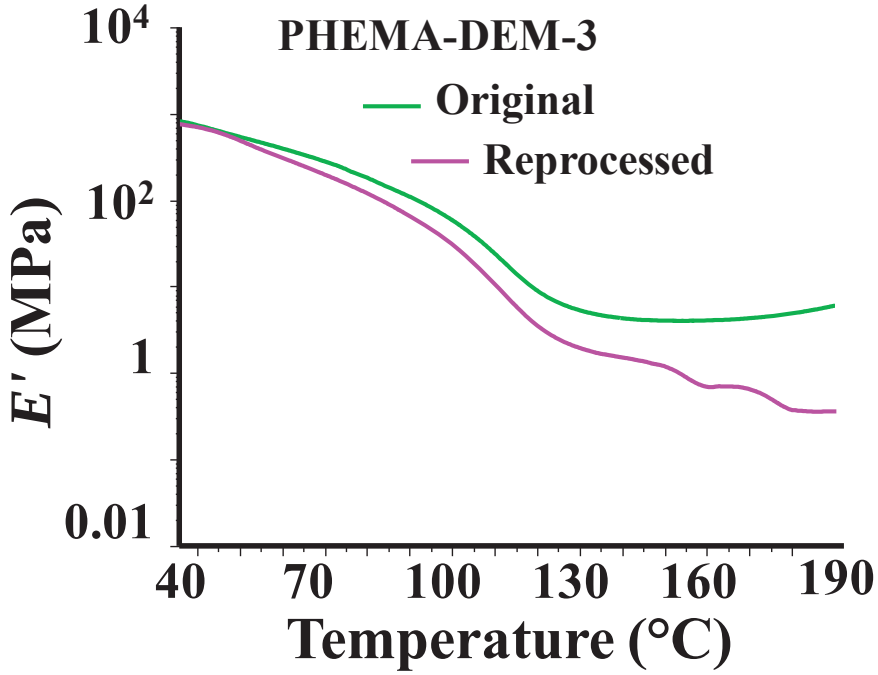

Figure A42: DMTA traces of original & reprocessed film of PHEMA-DEM-3

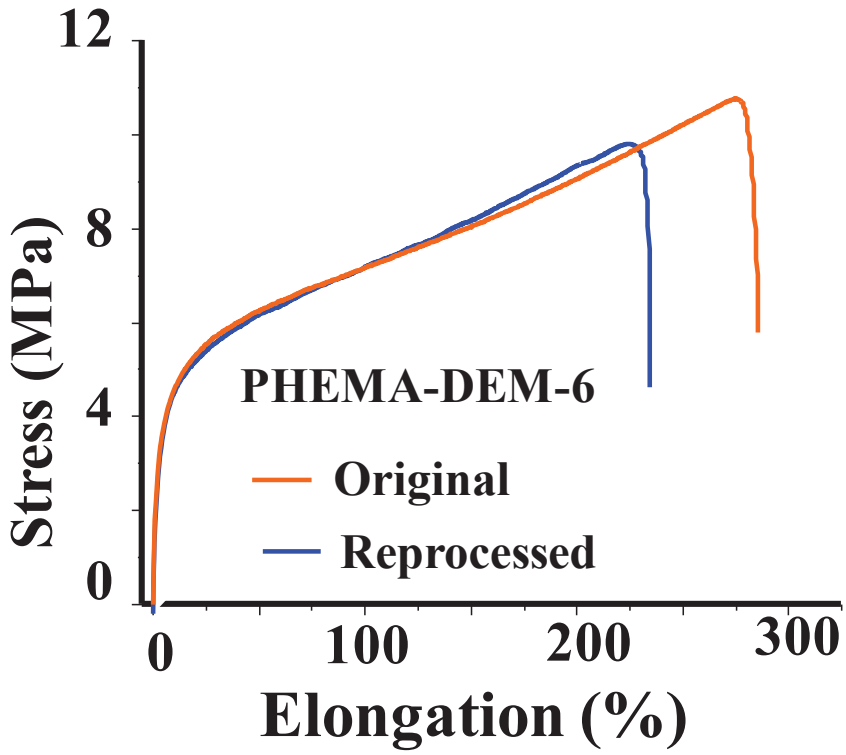

Figure A43: Tensile traces of original & reprocessed film of PHEMA-DEM-6

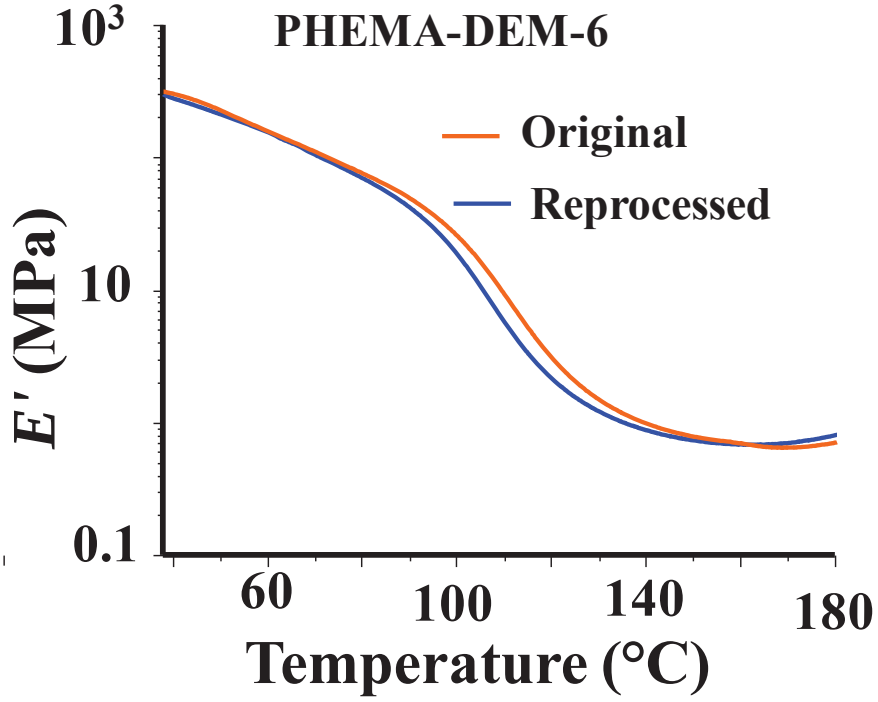

Figure A44: DMTA traces of original & reprocessed film of PHEMA-DEM-6

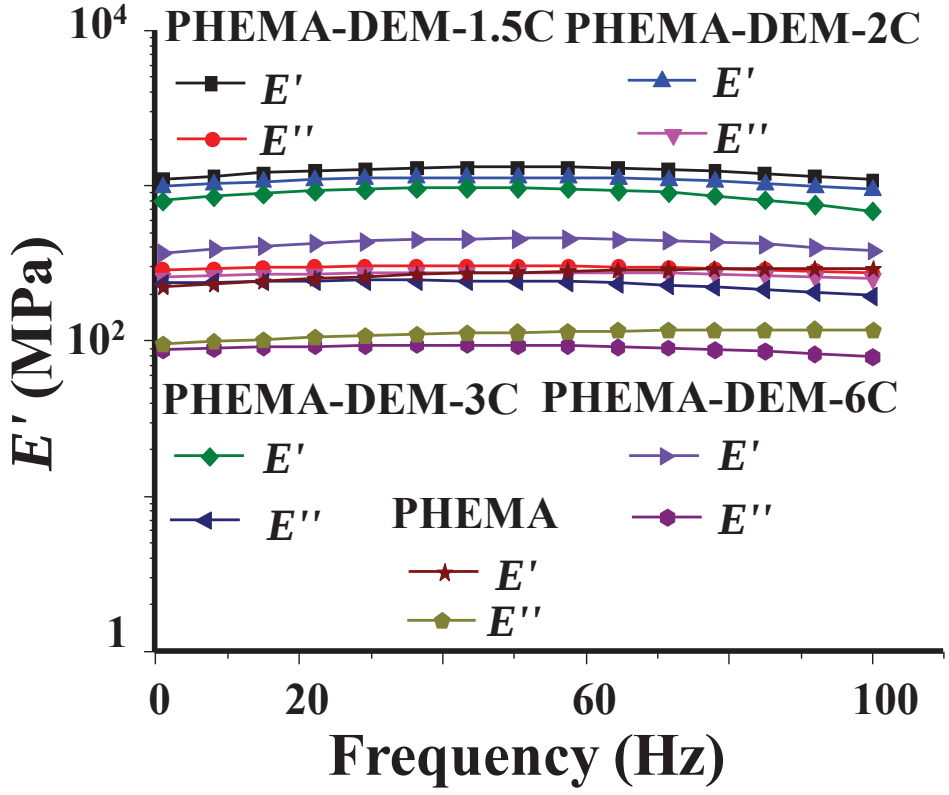

Figure A45: Frequency sweep data of Vitrimers possessing $Sn(Oct)_2$ as catalyst

Synthesis of Poly (2-Hydroxyethyl Methacrylate (PHEMA): We have followed the standard reported procedure for the synthesis of PHEMA. PHEMA was synthesized by the using of 1 mol% α-Azoisobutyronitrile initiator in 20 g (153.8 mmol) 2-hydroxyethyl Methacrylate monomer in 50 ml THF. We have refluxed the resultant mixture for 5h. For purification the PHEMA mixture was dissolved in methanol and precipitated in THF. Yield: 19.0 g (95%). The M_n (211000 g/mol) was determined from viscosity measurements. The intrinsic viscosity value for PHEMA measured in DMF solution is 0.682 dl/g (**Figure A56**). The M_n was calculated using equations.

$$[\eta] = k_m M^a, \text{ where } M = M_n$$

The constant values 'k_m' and 'a' were taken from the literature.

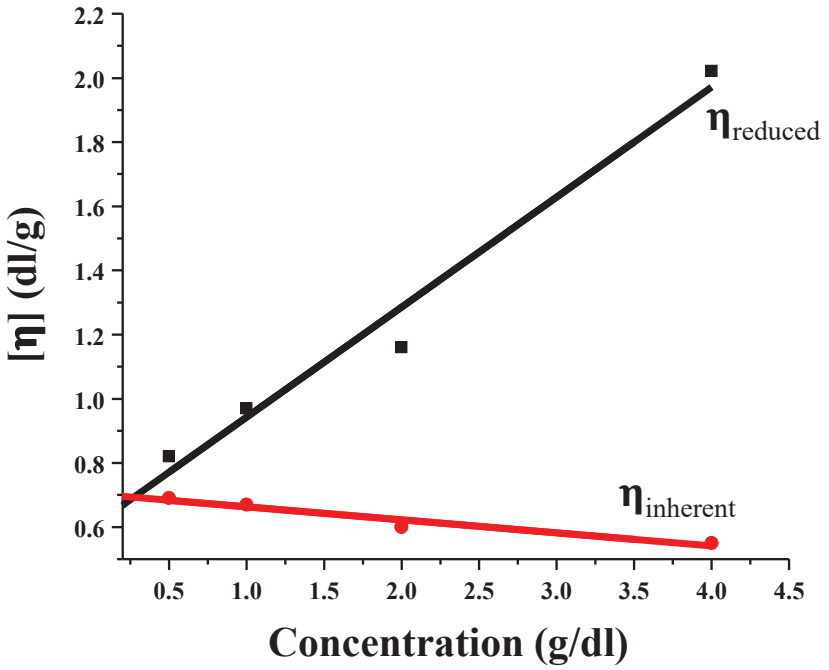

Figure A46: Concentration vs Viscosity graph.

Calculations:

We have calculated the Activation energy from 2nd order reaction kinetics:

$$A+B \rightarrow C+D$$

The equation for half-life ($t_{1/2}$) is as below

$$t_{1/2} = \frac{1}{k[A_0]} \text{ ……...(Eq. S9)}$$

Where *K*= rate constant of the reaction

$[A_0]$ = initial concentration of the reactant.

From the Arrhenius Equation

$$K = A\, e^{-Ea/RT} \text{ …… (Eq S10)}$$

Where *K* = Rate constant of reaction, E_a is the activation energy of the reaction,

R = Gas constant in J / mol. °K

T = temperature in °K

A = Arrhenius constant

Activation energy was calculated from Slope = Ea/R.

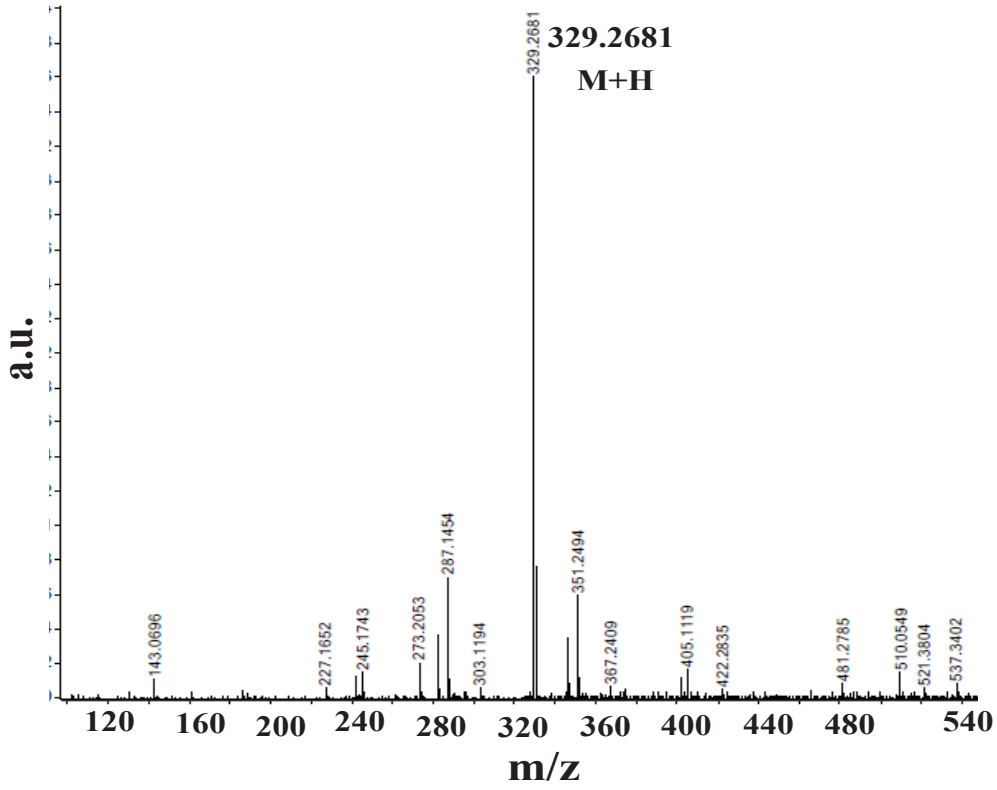

Figure A47: HRMS spectra of exchange reaction product of BEM with n-Hexanol

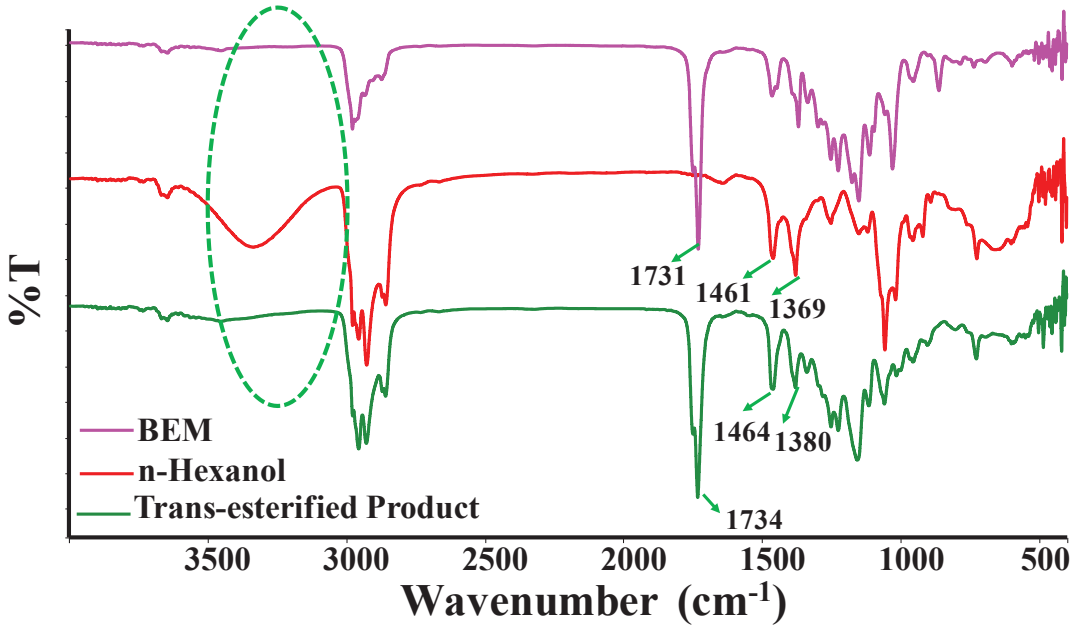

Figure A48: FTIR spectra of BEM, n-Hexanol and exchange product of BEM with n-Hexanol

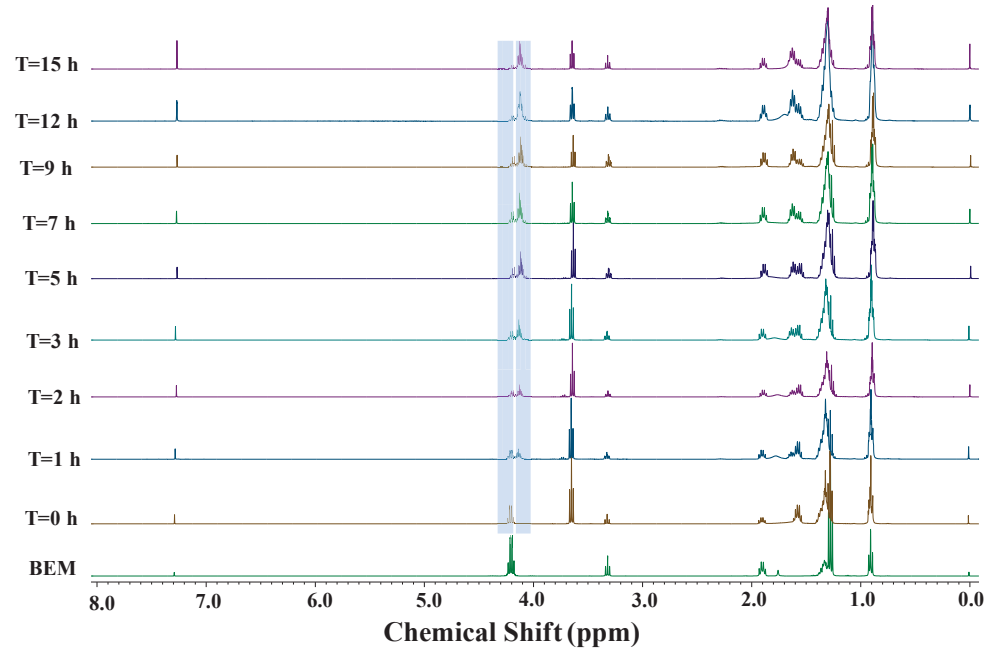

Figure A49: ^{1}H NMR spectra of BEM & n-Hexanol mixture at different time intervals at 130 °C for kinetics study

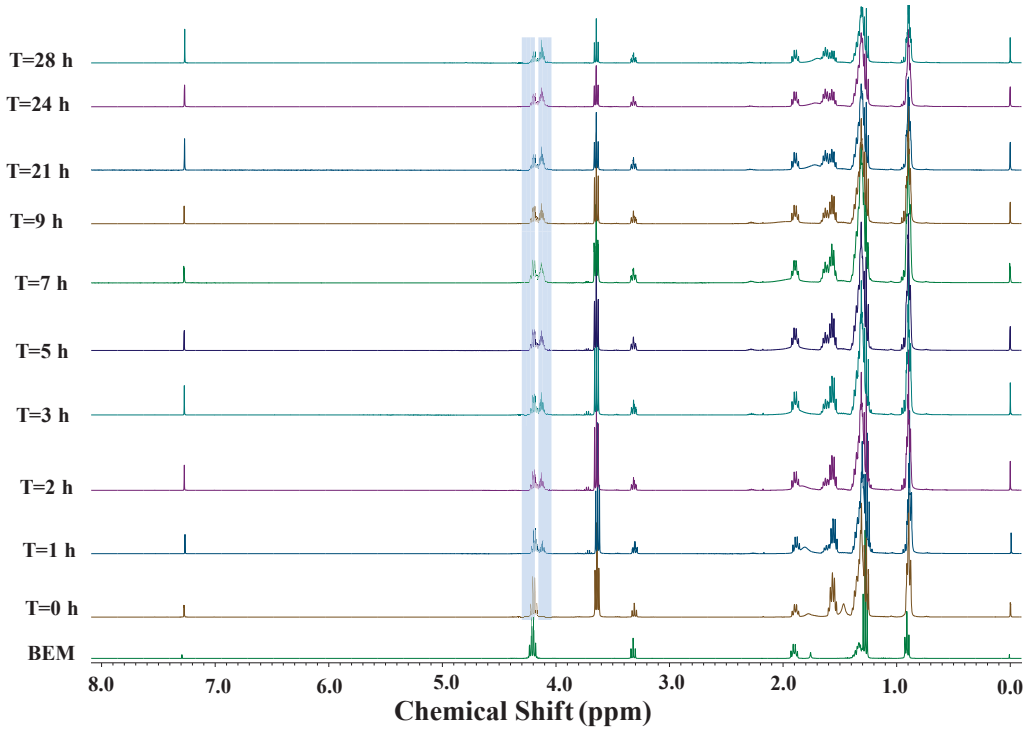

Figure A50: ^{1}H NMR spectra of BEM & n-Hexanol mixture at different time intervals at 120 °C for kinetics study

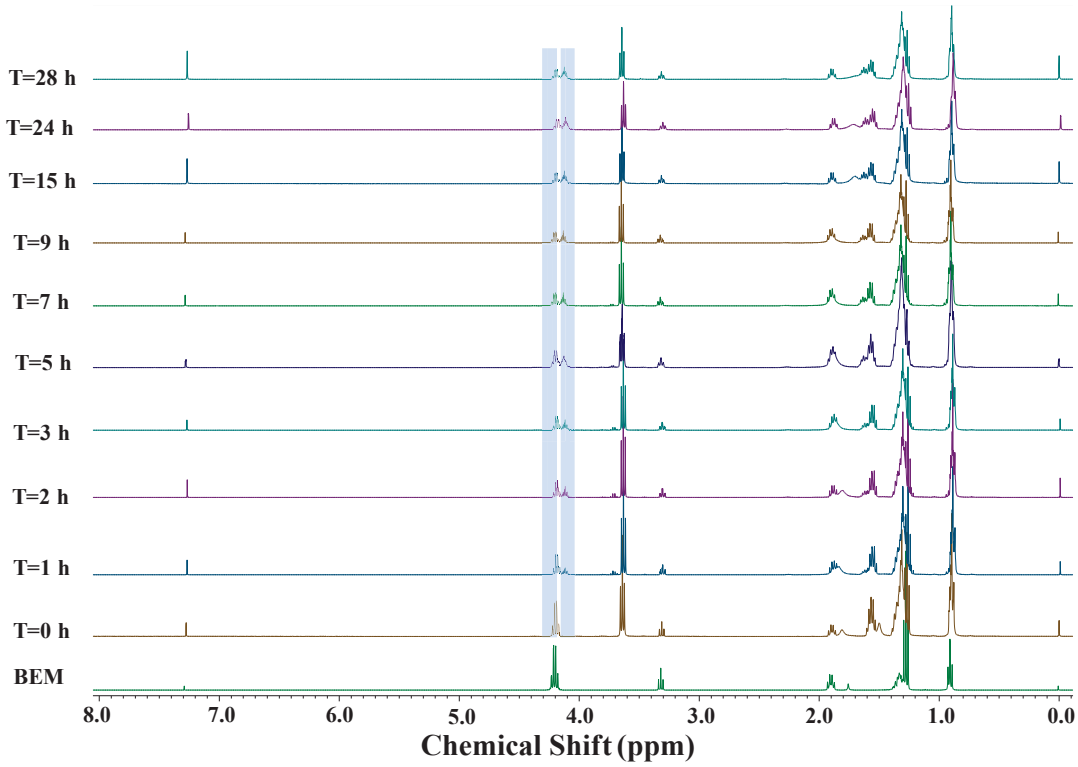

Figure A51: ^{1}H NMR spectra of BEM & n-Hexanol mixture at different time intervals at 110 °C for kinetics study.

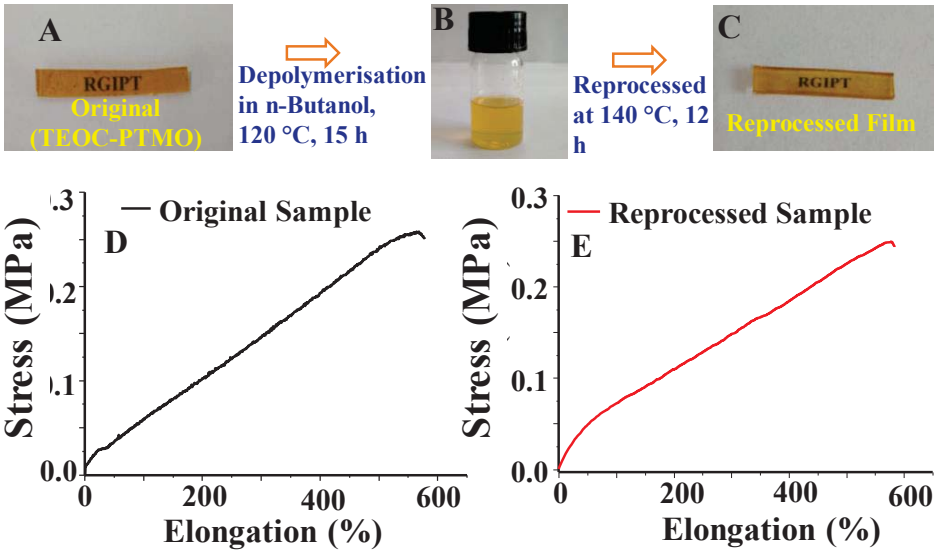

Figure A52: (A) Original sample of TEOC-PTMO, (B) sample after depolymerization, (C) reprocessed sample, (D) tensile data of original and (E) reprocessed sample.

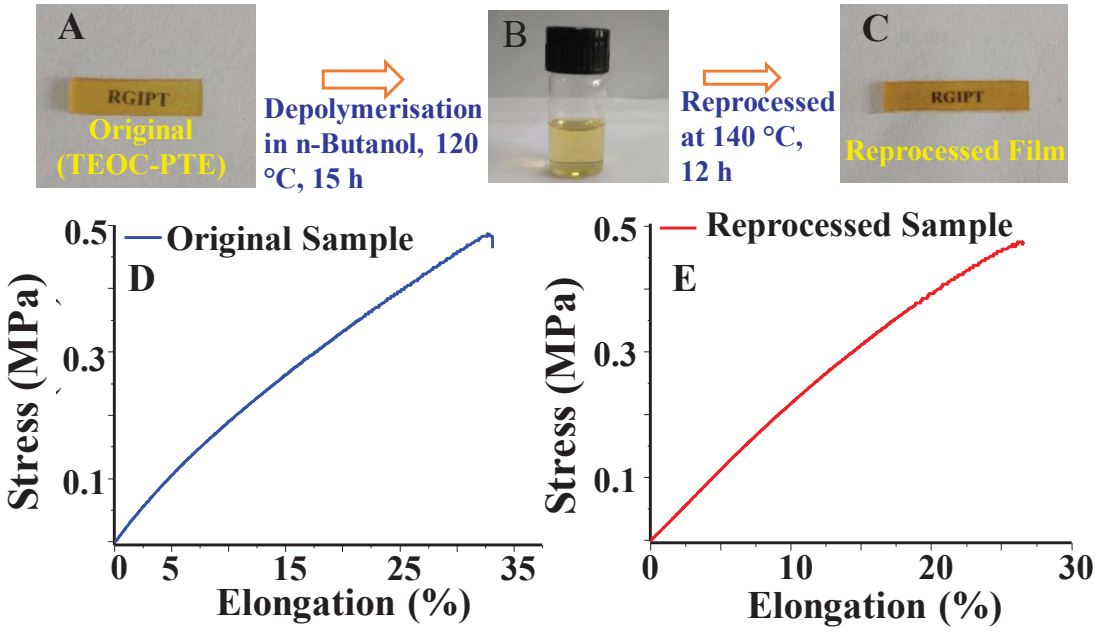

Figure A53: (A) Original sample of TEOC-PTE, (B) sample after depolymerization, (C) reprocessed sample, (D) tensile data of original and (E) reprocessed sample.

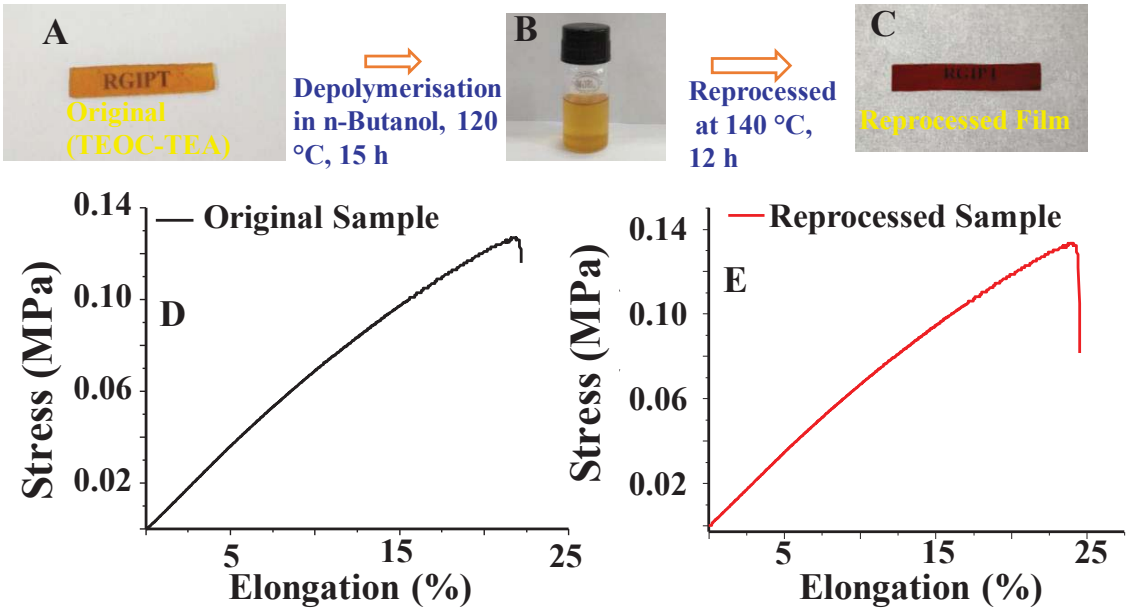

Figure A54: (A) Original sample of TEOC-TEA (B) Sample after depolymerization, (C) reprocessed sample (D) tensile data of original Sample (E) tensile data of reprocessed sample.

Table A10: Molar composition optimization of TEOC and multi-ols in CANs based on their tensile properties

CANs (Code)	Multi-ol	TEOC (mmol)	Multi-ol (mmol)	UTS (MPa)	ε (%)
TEOC-PTE	PTE	4.97	5.96	0.50 ± 0.06	30.0 ± 3.0
TEOC-PTE-1	PTE	4.97	5.46	0.20 ± 0.02	18.0 ± 2.0
TEOC-PTE-2	PTE	4.97	6.46	0.30 ± 0.02	20.0 ± 3.0
TEOC-PTMO-PTE	PTMO/PTE	4.97	6.00	1.10 ± 0.03	283.3 ± 16.0
TEOC-PTMO-PTE-1	PTMO/PTE	4.97	6.23	0.60 ± 0.04	130.0 ± 10.4
TEOC-PTMO-PTE-2	PTMO/PTE	4.97	5.80	0.50 ± 0.03	111.3 ± 9.0

Table A11: Mechanical properties data comparison of original & reprocessed CANs

CANs	UTS (MPa)	ε (%)	*E* (MPa)
TEOC-PTE (Original)	0.51 ± 0.06	30.0 ± 3.0	1.8 ± 0.04
Reprocessed	0.50 ± 0.05	31.0 ± 3.0	1.8 ± 0.03
TEOC-PTMO (Original)	0.30 ± 0.06	595.0 ± 15.0	0.8 ± 0.01
Reprocessed	0.29 ± 0.04	590.0 ± 9.0	0.7 ± 0.01
TEOC-TEA (Original)	0.14 ± 0.01	23.0 ± 2.2	1.1 ± 0.01
Reprocessed	0.12 ± 0.01	20.0 ± 2.0	1.0 ± 0.01
TEOC-PTMO-PTE (Original)	1.12 ± 0.03	301.3 ± 22.0	0.7 ± 0.03
Reprocessed	1.01 ± 0.02	289.0 ± 20.0	0.6 ± 0.02

Calculations:

We calculated activation energy for 2nd order reaction:

$$A+B \rightarrow C+D$$

The activation energy was calculated at three different temperatures (413, 403,393 and 383 °K). The expression for half-life ($t_{1/2}$) is as followed.

By following the 2nd order reaction kinetics;

$$t_{1/2}=\frac{1}{k[A_0]}\ldots\ldots\ldots \text{ (Eq. S11)}$$

Where *k*= rate constant of the reaction

$[A_0]$ = initial concentration of the reactant.

The rate constant was obtained by using above equation and the activation energy was obtained.

We know from the Arrhenius Equation

$$k=A\, e^{-Ea/RT} \ldots\ldots\ldots\ldots\ldots\ldots \text{ (Eq S12)}$$

Where E_a is activation energy of the reaction,

R = Gas constant in J / mol. °K

T = temperature in °K

A = Arrhenius constant

Slope = E_a/R provides the activation energy

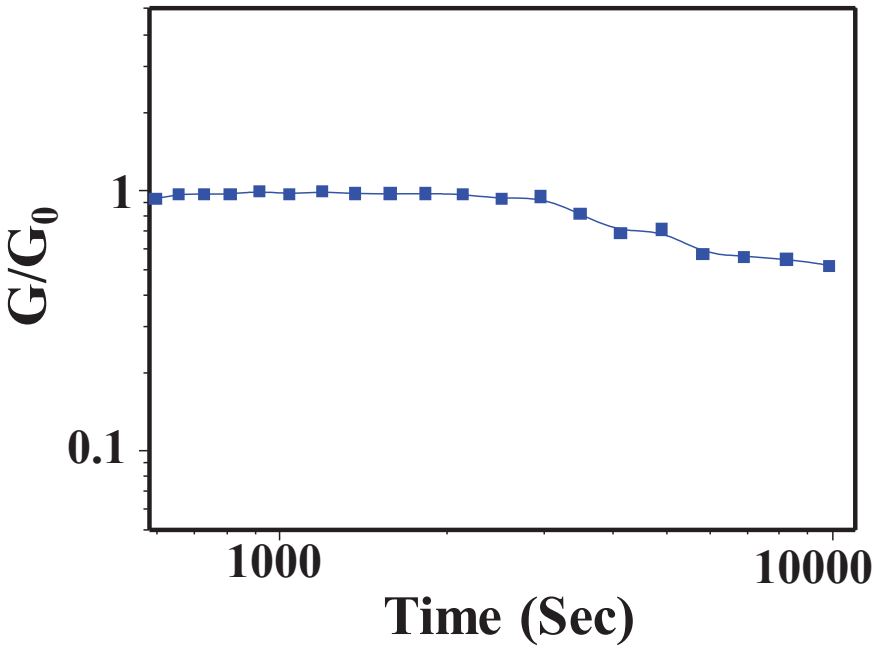

Figure A56: Stress relaxation trace of PUN43 at 120 °C

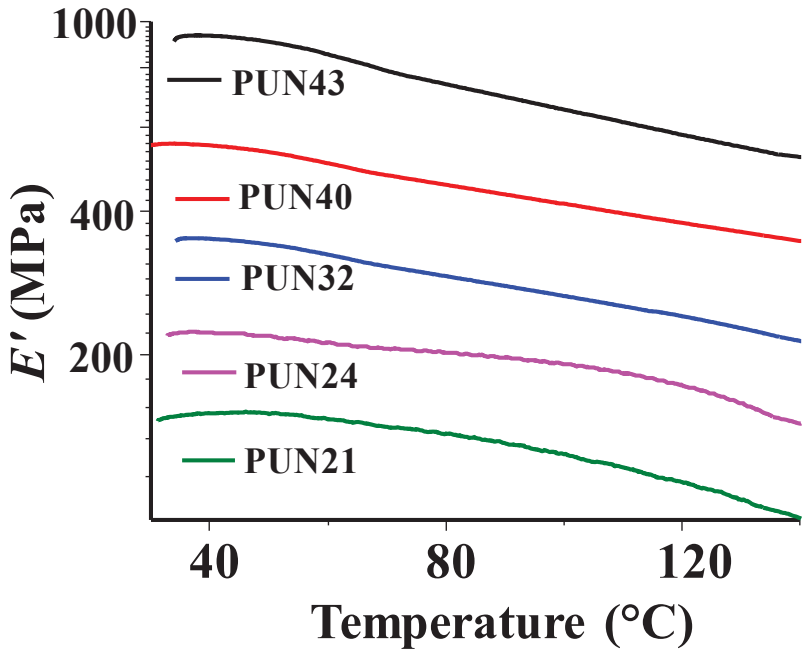

Figure A57: First thermal transition of DMTA traces of different PUN films

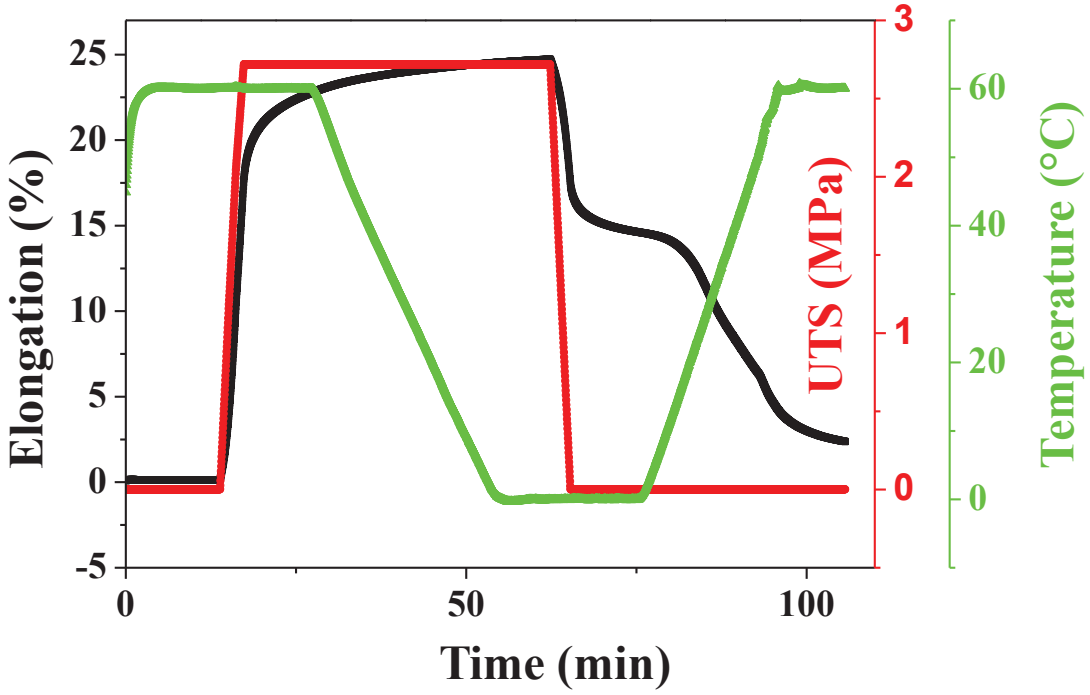

Figure A58: Double shape memory performance of PUN43

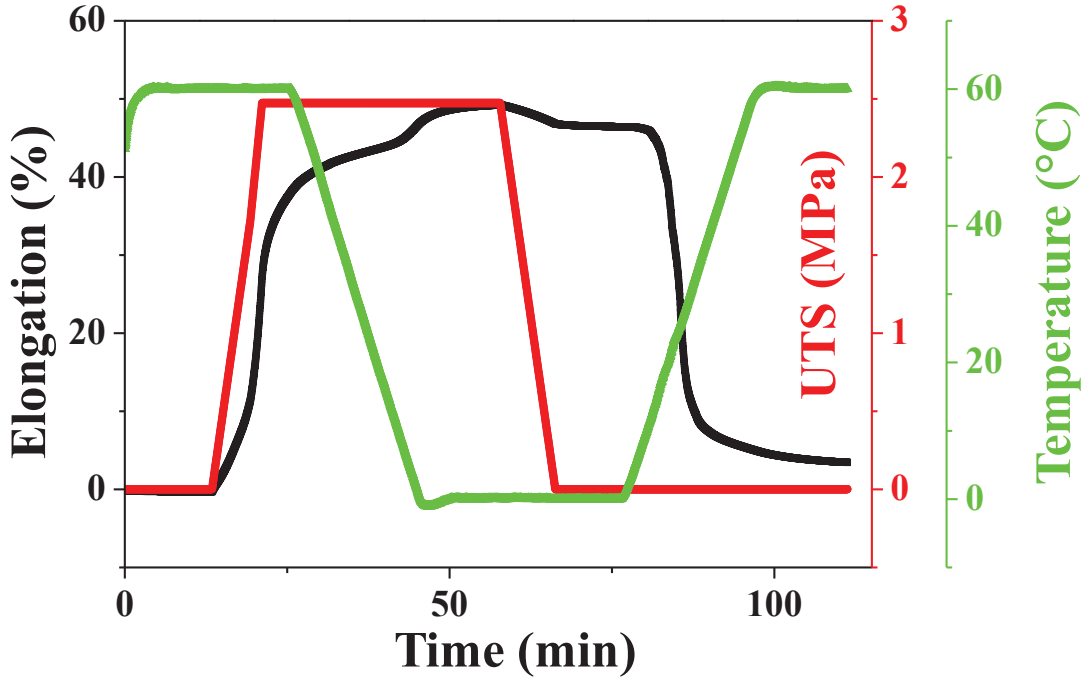

Figure A59: Double shape memory performance of PUN40

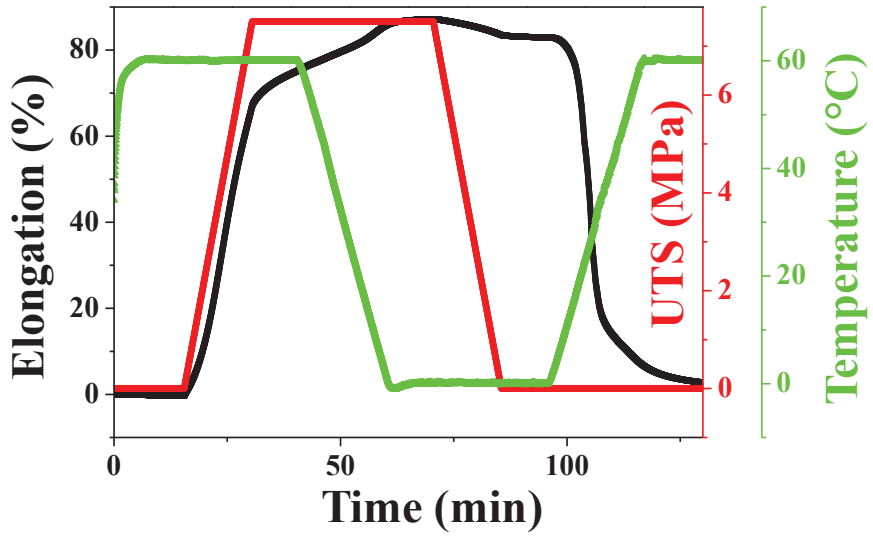

Figure A60: Double shape memory performance of PUN24

Table A12: Mechanical properties data comparison of original & reprocessed PUNs

Sample Code.	UTS (MPa)	Recovery (%)	ε (%)	*E* (MPa)	Recovery (%)
PUN43 (Original)	33.0 ± 2.1	-	345 ± 14	270.0 ±13.5	-
(Reprocessed)	23.1 ± 1.5	70	280 ± 13	192.0 ±12.0	71
PUN40 (Original)	30.0 ± 2.0	-	360 ± 14	210.0 ± 12.0	-
(Reprocessed)	21.6 ± 1.4	72	325 ± 13	155.4 ± 10.0	74
PUN32 (Original)	22.0 ± 1.1	-	400 ± 15	150.0 ± 5.0	-
(Reprocessed)	16.3 ± 1.1	74	350 ± 13	120.0 ± 4.0	80
PUN24 (Original)	14.0 ±1.0	-	515 ± 20	40.0 ± 1.2	-
(Reprocessed)	10.5 ± 1.0	75	490 ± 17	30.6 ± 1.1	85
PUN21 (Original)	8.0 ± 0.6	-	680 ± 22	19.0 ± 0.5	-
(Reprocessed)	6.4 ± 0.5	80	650 ± 20	16.4 ± 0.4	88

Table A13: Mechanical properties data comparison of original & Self adhered PUNs

Sample Code.	UTS (MPa)	Recovery (%)	ε (%)	*E* (MPa)	Recovery (%)
PUN43 (Original)	33.0 ± 2.1	-	345 ± 14	270.0 ±13.5	-
(Self adhered)	23.8 ± 1.6	72	300 ± 13	195.0 ±12.8	72
PUN40 (Original)	30.0 ± 2.0	-	360 ± 14	210.0 ± 12.0	-
(Self adhered)	22.0 ± 1.4	73	330 ± 12	158.0 ± 11.0	75
PUN32 (Original)	22.0 ± 1.1	-	400 ± 15	150.0 ± 5.0	-
(Self adhered)	16.7 ± 1.3	76	360 ± 14	123.0 ± 6.0	82
PUN24 (Original)	14.0 ±1.0	-	515 ± 20	40.0 ± 1.2	-
(Self adhered)	10.9 ± 0.9	78	495 ± 18	31.0 ± 1.1	86
PUN21 (Original)	8.0 ± 0.6	-	680 ± 22	19.0 ± 0.5	-
(Self adhered)	6.6 ± 0.5	82	655 ± 21	16.7 ± 0.5	88

Table A14: Triple shape memory data of two cycles of PUN21

Cycle No	R_f § (60 °C)	R_f § (Overall)	R_r § (60 °C) §	R_r § (130 °C)	R_r § (Overall)	Strain 1* (%)	Strain 2* (%)
First	95.1	97.0	100.0	47.2	81.7	14.5	37.1
Second	96.5	97.1	100.0	56.2	93.1	16.5	37.2

*Strain 1 and strain 2 correspond to the elongation achieved for shape fixing corresponding to 130 and 60 °C inflection temperature respectively. §the % shape fixity and recovery values are tabulated below.